MECHANISTIC STUDIES ON THE GOLD(I)-CATALYZED CYCLIZATION OF N-PROPARGYL BENZAMIDE DERIVATIVES

BY

SKYLAR GLENN NORMAN

A Dissertation Submitted to the Graduate Faculty of

WAKE FOREST UNIVERSITY GRADUATE SCHOOL OF ARTS AND SCIENCES

in Partial Fulfillment of the Requirements

for the Degree of

DOCTOR OF PHILOSPHY

Chemistry

August 2025

Winston-Salem, North Carolina

Approved By:

Amanda C. Jones, Ph.D., Advisor

Kiran K. Solingapuram Sai, Ph.D., Chair

Ulrich Bierbach, Ph.D.

Patricia C. Dos Santos, Ph.D.

Bruce King, Ph.D.

Contents

List of Figures

List of Tables

List of Abbreviations

13C{1H} proton decoupled 13C-NMR

31P{1H} proton decoupled 31P-NMR

Ac acetyl

AcOH acetic acid

br broad

d doublet

DCM dichloromethane

dd doublet of doublets

ddd doublet of doublets of doublets

DMF N,N-dimethylformamide

DME 1,2-dimethoxyethane

Dppm bis(diphenylphosphino)methane

equiv equivalent

Et ethyl

Et2O diethyl ether

EtOAc ethyl acetate

EtOH ethanol

g gram

GC gas chromatography

GC/MS gas chromatography/mass spectrometry

1H proton NMR

hr hour

Hz hertz

k rate constant

M molar

m multiplet

Me methyl

MeOH methanol

mg milligram

MHz megahertz

min minute

mL milliliter

μL microliter

xxii

mmol millimole

mol mole

n-BuLi n-butyl lithium

NEt3 triethylamine

NMR nuclear magnetic resonance

OTf trifluromethanesulfonate

p pentet

Pd(OAc) palladium acetate

Ph phenyl

PPh3 triphenylphosphine

ppm parts per million

q quartet

qd quartet of doublets

s singlet

STAB sodium triacetoxyborohydride

spt septet

t triplet

xxiii

td triplet of doublets

THF tetrahydrofuran

TIC total ion chromatogram

TLC thin layer chromatography

triflate trifluoromethanesulfonate

tt triplet of triplets

XRD X-ray diffraction

Acknowledgements

Above all else, I have to thank my advisor, Professor Amanda Jones. She has always been supportive throughout this entire journey, always keeping an open door whenever I had questions, and always helping me even when those questions were sometimes retroactively embarrassing. If there is anything mournful about the completion of this work, it is that I will no longer be able to work alongside one of my best friends. All you can hope for in a PhD advisor is someone who will guide you towards success and make your time doing the work as enjoyable as possible. In addition to doing all of that, she was so much more, So many of the conversations we had together had little to nothing to do with gold catalysis, instead often focusing on teaching, departmental complaints, tattoos, and my summer vacations across the street from Stephen King's house (I still promise not to give you the address, but I'll try to say hi to him on your behalf).

I would also like to thank my committee members, Professor Uli Bierbach and Professor Bruce King. During defenses, both of you were rigorous with questions, but never unfair. Having your perspective as experts from adjacent fields has been invaluable through this process. Bruce's encyclopedic knowledge of reactions has been an excellent source of expertise in defenses. My thanks as well for your mentorship in your graduate level synthesis course. While it wasn't the only thing I learned, I know now to always check if the product is drawn upside-down. You got me once. Never again.

As for Uli, it's always felt a lot like cheating having him as my "outside" committee member. Someone whose research has necessitated an expertise in

organic synthesis, organometallics, and heteronuclear NMR. Yeah. That's nothing like what I do. I've joked for years that I start from the position that Uli already knows what I'm talking about and I wait for him to indicate otherwise. I thought one of the perks of being a tenured professor was you get to have a niche focus, but I guess not.

My thanks as well to the late additions to my dissertation committee, Professor Patricia Dos Santos and Professor Kiran Sai. I've long thought of Patricia as one of the most brilliant minds in the department, and I'm sure the vast difference in our fields of study will not impede her in the slightest when assessing this work. She and her students have been some of the brightest and most capable people I've encountered in my time at Wake Forest.

I owe an extra debt of gratitude to Kiran. Not only did he agree to join as the committee chair at the final hour, but he also provided me with nearly two years of extra research training and a letter of recommendation prior to joining the program. Analytical chemistry in my own research came easily after running a GC and HPLC under his guidance, though the ones here at Wake are conspicuously lacking Geiger counters. The synthesis of radiotracers is a special kind of magic, just one you have to view through lead glass. Thank you for letting me see that magic, and, as I used to joke about the radiation exposure, letting me "get one step closer to superpowers every day."

I of course must thank my labmates. Dr. Billy Lan, with whom I shared the office and lab for nearly my entire time in the program. In addition to being a knowledgeable chemist, Billy is one of the most hilarious people I've ever met. The

combination of his love of puns, complete lack of a pokerface, and unceasingly loud pants are merely a few of the things which made him a joy to work with.

On the topic of labmates who are easy to get along with, there is Jaden McCane, who joined the group at the start of my fourth year. Jaden was the first graduate student to join the group after me, and watching him learn and improve over the years has been one of the highlights during the second half of my time at Wake. He's also one of the most genuinely kind, easygoing people I've ever met, and I'm confident I'll never again have a labmate so easy to work with, though they may be faster about cleaning NMR tubes. The group is in good hands with Jaden as its most senior member.

Luke Hair and I overlapped for less time, but it was enough time to enjoy countless laughs in the lab and office, as well as to watch him expand his knowledge and skillset. Luke even helped me quite directly in some of the experiments below by figuring out a consistently successful synthetic procedure for JohnphosAuOTs, something which had eluded the group for years. He also quickly got a handle on troubleshooting the NMR, and good timing that he did. I hereby dub him the new "backup Marcus."

I had the tremendous privilege of working with many undergraduates in the lab during my time, all of whom were bright, capable students whose company I greatly enjoyed. My thanks to the undergraduate students I was able to directly mentor: Noah Vasconez, Zhiyu (Clifford) Feng, Sarah Rice, Joe McPherson, Sam Signorelli, Ellie McFarland, and Danny Pham.

One of the people in the department most responsible for my success is undoubtedly Dr. Marcus Wright. Working in an NMR group was so much easier thanks to his expertise and mentorship. In addition to being an invaluable wellspring of expertise, he's one of my favorite people in the world to have a conversation with. You never quite know what topic you're signing up for when you have a conversation with Marcus. It could be organic chemistry, it could be beekeeping, it could be improvised forms of barnyard euthanasia. Much of the work detailed here does not happen without his help in creating the experiments, teaching me the ritual of tricking Topspin into doing what I want, or just giving me an excuse to get out of the lab and laugh for a while.

My thanks as well to other members of Wake Forest's chemistry department. A manuscript detailing much of the work below was published in part thanks to collaboration with Professor Wendu Ding and members of his group. My thanks to him and fellow authors on that paper, Lin Jiao, Leo Liu, and Dr. Jun Yi.

On the teaching side of things, I must thank Professors David Wren, John Tomlinson, and Angela King, who were always cheerleaders for me, writing me letters of recommendation and helping me to secure a TA award. Being one of the first students in the department's history to run the evening skill sessions through the Chem Center has saved me countless time in the future in preparing to one day hopefully teach a full-fledged course.

Other professors who supported me along the way include Christa Colyer, who was always willing to offer advice on navigating the ins and outs of academia (as well as places to visit during a trip to Toronto). Professor Paul Jones, with whom

I shared a lab space and who serendipitously offered his reactive intermediates course in my final semester, perfectly timed to help me prepare for a postdoc studying photochemically-generated carbenes. Professor Cedric Schaack arrived relatively late during my time in the program, but was always available for questions, and was especially valuable as a resource during postdoc applications as someone who more recently went through the process.

I would be remiss if I didn't also thank my undergraduate chemistry professors for their roles in getting me here. The chemistry department at William and Mary is a truly special place, overflowing with professors wholly dedicated to undergraduate education. I didn't appreciate how good I had it while I was there.

Graduate research was a surprisingly easy transition for me, and all the credit for that goes to my undergraduate research advisor, Professor Jonathan Scheerer. The two years I spent in his lab are the bedrock on which my entire future as a scientist are built. I was given incredible freedom as an undergraduate researcher, much more than I felt I deserved, but was simultaneously supported whenever I needed it. For example, when my aldol product kept decomposing on the column, or when I may or may not have nearly detonated a rotovap because, well, I reduced the ozonide with *something* sulfide. (It is not the saints who have patience, but PUI professors.) In addition to being a wonderful research mentor, he was also a magnificent professor in the classroom. I spent a total of three years working with him, the first year as a lecture student in back-to-back semesters, and the following two years in his lab. To this day, I think his practice of giving second semester organic students a class-length orgo 1 final on the first day of lecture is

a stroke of genius, just one some of us maybe didn't appreciate at the time. ("This page… there was some blood spilled on this page," he said, going over the page on the exam dedicated to cyclohexane chairs in a later lecture.) Should I ever have the privilege of teaching a second-semester organic course in the future, I *will* be stealing this trick. His organic synthesis course was my first exposure to high-level coursework and was structured not just to teach us reactions but also to explore the synthetic literature and gain a sense of the discipline's history. Through all of his success, he remains surprisingly humble, as he didn't seem to realize how gifted an educator he is when I had the good fortune of catching up with him during his seminar visit to Wake Forest.

Tremendous thanks is also owed to Professor Elizabeth Harbron. My first lecture on my first day of class at William and Mary was for her first semester organic course. It all starts there. Organic chemistry is an infamously challenging subject, probably known for crushing career aspirations more often than any other college course. The professors who teach it are therefore in a uniquely privileged and difficult position, having to undo this preconceived expectation of failure while also, if they can, demonstrating the beauty of the subject. I suspect few professors have ever met this challenge as well as her. My love for this science begins in her classroom. Students who have been taught by me in the years since don't know how much I'm shamelessly plagiarizing from the Elizabeth Harbron teaching handbook. "Organic chemistry is all about the electron rich getting together with the electron poor," is a phrase I have echoed to new students for the better part of a decade. I've also frequently borrowed her explanation of the geometry of Fischer

projections, which she promised me eleven years ago I would never forget. She was right. The world is a meaningfully better place for her having chosen to become an educator.

Finally, I obviously have to thank Karla Hernandez. Her arrival in the program is the best luck I have ever had. The last few years of this PhD have been made so much easier for her company. Not only is there no one better with whom I could hope to spend my spare time, she has also become one of the most knowledgeable and talented students in the program. She is so much better than she thinks. To lose her daily companionship is the greatest adjustment I will make going into this next chapter (as well as the lost companionship of Agata, Chuletas, Coco, Vecino, but not Pan. Never Pan). My thanks as well to her family for their immense hospitality throughout these last couple of years. Their home was a wonderful place to take shelter from my frigid basement apartment in the winter.

I have never been so eternally grateful for one overly-prolonged hallway conversation and never dreamed a silly game about hiding ducks around the building would turn into what it has. I cannot wait for the day soon when we're no longer apart.

Abstract

The gold(I)-catalyzed cyclization of N-propargyl benzamide has been a popular benchmark reaction for the study of gold catalysis for over two decades. Literature consensus denotes the protodeauration step as rate-limiting, bringing certain assumptions with regards to ligand, anion, and solvent choice. The work described below reveals a solvent-dependent rate-limiting step, calling for a possible recontextualization of this common test reaction and the implications for its continued use. Further work details the study of generated off-cycle degradation products of gold catalysts, the degradation of gold catalysts in the cyclization of carbamate analogues, as well as the synthesis of bisbiphenyl phosphine ligands to limit the formation of these products. Despite the details of its kinetics being more complex than previously understood, the cyclization of N-propargyl benzamide still proves useful in studying the impact of media, substrate, and ligand on the performance of new and old gold catalysts.

Chapter 1: A History of Gold Catalysis of Alkynes

Introduction

In 1995, gold was infamously referred to as “catalytically dead.”[1] Shortly thereafter, the first report of homogenous gold(I) catalysis by Teles et al. for the activation of alkynes towards the addition of methanol was published.[2] By 2000, understanding of gold’s utility as a catalyst had shifted,[3] leading to a now decades-old field of research demonstrating the precious metal’s potency as a Lewis acid.[4–7]

As demonstrated in the initial gold(I) catalysis report by Teles, the foremost role of gold as a catalyst is for the Lewis acidic activation of carbon-carbon π bonds towards nucleophilic attack. The catalytic cycle for this transformation is shown in **Figure 1**.

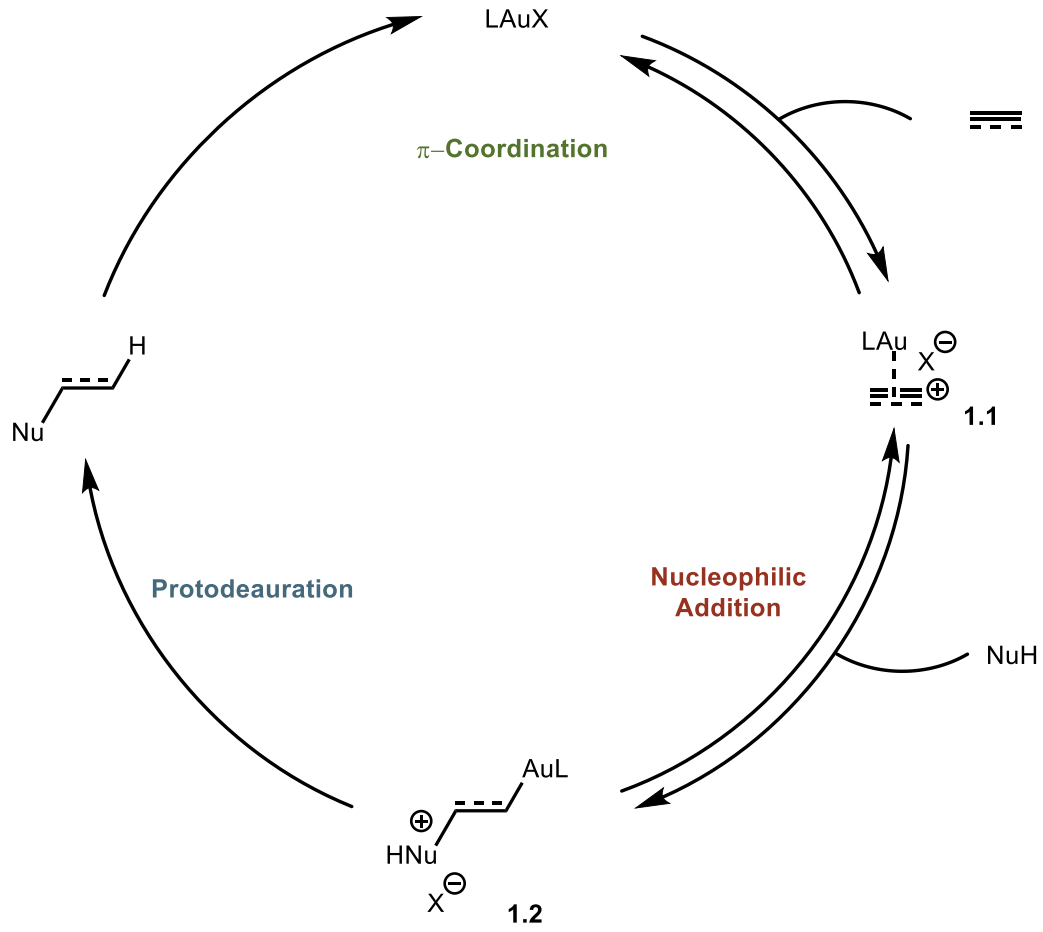

Figure 1 General Cycle for Au(I) Catalysis

First, π-coordination by gold to the alkyne or alkene leads to π-complex **1.1**. Lewis acidity of the gold catalyst opens the alkyne to nucleophilic attack, leading to vinyl or alkylgold intermediate **1.2**. Protodeauration of **1.2** furnishes product **1.3** and regenerates Au(I) to restart the cycle. This general scheme is believed to hold for both alkene and alkyne substrates, with some differences in reactivity. Vinylgold intermediates of type **1.2** are notably more basic than their alkylgold counterparts, thereby undergoing protodeauration much more rapidly.[8]

While the scope of its applications have increased over time, the most frequent use case for Au(I) catalysis remains the activation of alkynes for nucleophilic addition.[4–6,9] Many of the earliest reports involve the Au(I) and Au(III) activation of alkynes for hydroalkoxylation, with alcohol solvents acting as nucleophiles to form alkyl and vinyl ethers.[2,10,11]

Following these initial reports of intermolecular additions, chemists quickly realized the possibility for intramolecular additions as well, particularly those affording synthetically desirable heterocycles.

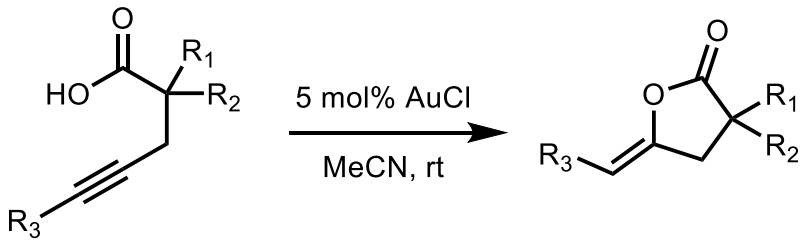

Figure 2 Alkyne Activation to form Lactones

A 2006 report generated lactones from carboxylic acids (**Figure 2**).[12] Coordination of gold to the pendant alkyne opens it to nucleophilic addition by the carboxyl OH. The reaction is specifically selective for the 5-*exo*-dig cyclization, with little to none of the 6-membered cycle being formed. Additionally, the Z/E isomerism favors Z in a 100:0 ratio. This is in accordance with convention and indicates a trans relationship between gold and the nucleophilic oxygen prior to protodeauration. The mild, room temperature conditions also tolerated a wide range of R groups.

Vinylgold Intermediates: Isolation and Reactivity

As illustrated in **Figure 1**, when the coordination site is an alkyne or allene, the resulting species after nucleophilic attack is a vinylgold. Gerald Hammond's group was the first to isolate and report the structure of a vinylgold complex in 2008 (**1.5**, **Figure 3**).[13]

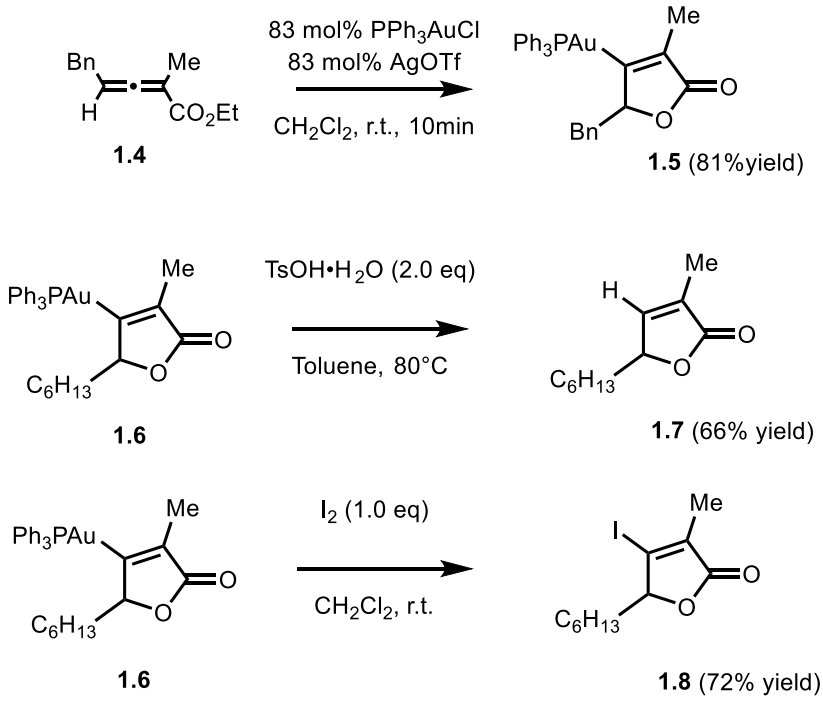

Figure 3 Vinylgold Isolation and Experiments by Hammond

When allenoate **1.4** was treated with near-stoichiometric amounts of a gold catalyst and silver salt, vinylgold species **1.5** was obtained in 81% yield. The structure of **1.5** was confirmed by XRD. To confirm the role of vinylgold as a mechanistic intermediate, analogue **1.6** was reacted at 80 degrees in toluene with TsOH to afford protodeaurated lactone **1.7** in 66% yield. The ability of vinylgold to act as a nucleophile was also demonstrated in this same study when **1.6** was reacted with iodine to afford vinyl halide **1.8** in 72% overall yield.

One year later, in 2009, Hashmi's group was the first to report the isolation of vinylgolds derived from alkynes.[14] Using IPrAuNTf$_2$ and a large excess of base, **1.9** could be converted to vinylgolds **1.10** or **1.11** depending on alkyne substitution. Structure **1.11** was isolated and characterized by x-ray crystallography, whereas the structure of **1.10** was inferred by treating it to a water/acetonitrile mixture, affording the protodeaurated oxazoline.

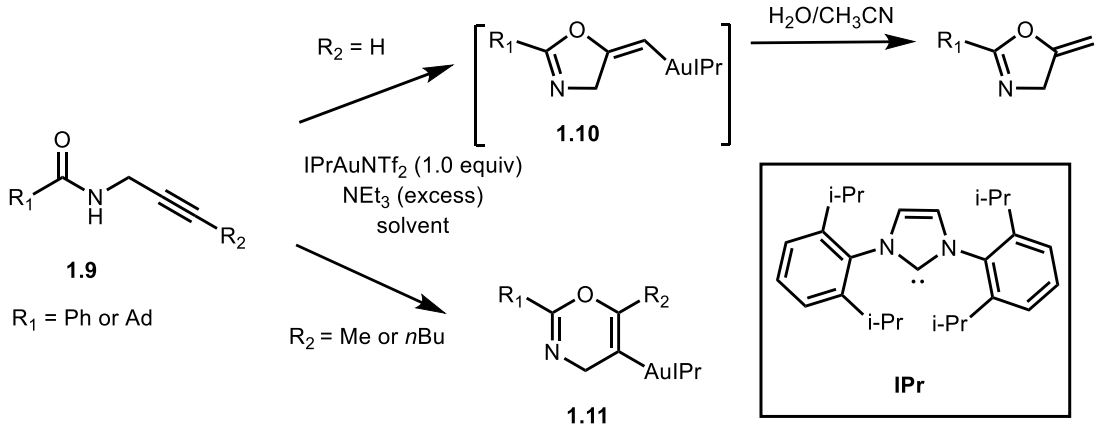

Figure 4 Vinylgold Isolation by Hashmi

The following year in 2010, vinylgolds of benzofuran and indoles were isolated in a follow up paper by Hashmi.[15] Their structures are shown below in **Figure 5**.

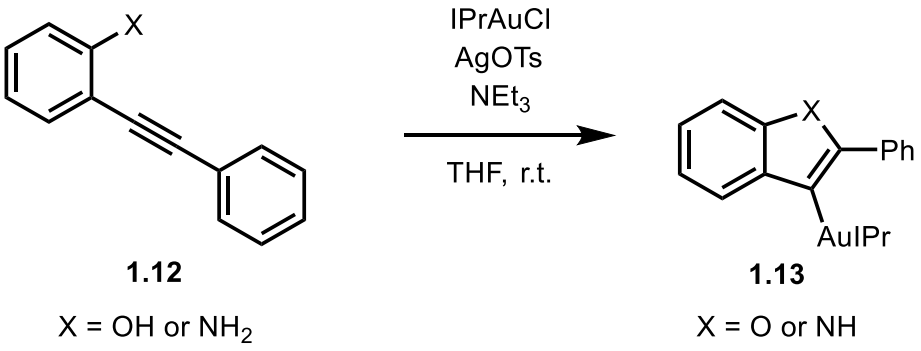

Figure 5 Benzofuran and Indole Vinylgolds

While most final products are typically formed from protodeauration, a number of groups have realized the potential for vinylgolds to act as transient, nucleophilic intermediates for the construction of more complex frameworks.

An early example using a vinylgold as a nucleophile was reported by Toste in 2006.[16] Recognizing the affinity for vinylgold species to undergo rapid protodemetalation, the authors surmised that *in situ* generation of a potent electrophile would induce nucleophilic attack from the vinylgold prior to the regeneration of Au(I) by protodeauration. This strategy was employed on the benzyl ethers seen below in **Figure 6**.

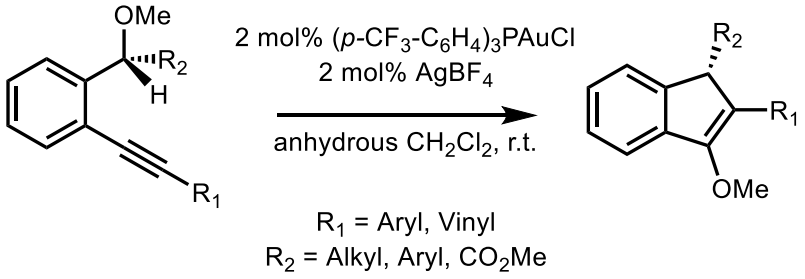

Figure 6 Intramolecular Carboalkoxylation by Toste

Migration of the methoxy group was proved with a perdeuterated OCD_3 group. Additionally, the high %ee and stereoretention of the product allowed them

to propose the mechanism in **Figure 7**. Nucleophilic addition and subsequent alkoxy transfer yields the specific benzyl cation shown, which maximizes orbital overlap with the aryl ring, as well as minimizing steric strain between the alkene and the benzylic R_2 group. This conformation leads to the high retention of stereochemistry. The vinylgold bond acts as a nucleophile to close the ring, regenerating Au(I) and yielding the final product.

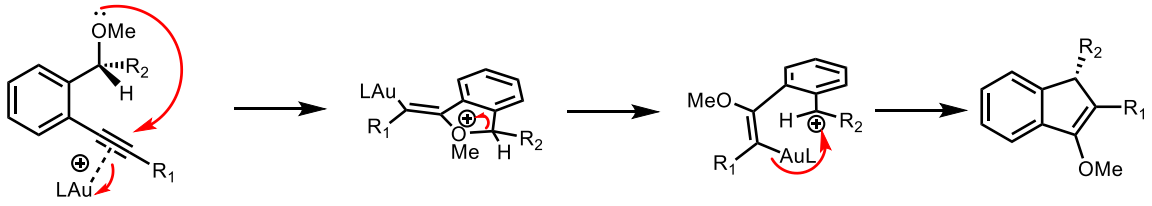

Figure 7 Intramolecular Carboalkoxylation Mechanism

The following year, Toste's group reported an intramolecular [2+2] cyclization of a vinylgold intermediate (**Figure 8**).[17] Coordination to the allene π system opens it to nucleophilic addition by the pendant alkene. Similar to the example above with benzyl esters, a benzylic cation is generated *in situ*, which is then attacked by the vinylgold bond. This step eliminates Au(I) while generating the final bicyclic product in high yield and %ee. This and the other example from Toste's group above point to the capability of vinylgolds to act as nucleophiles when potent electrophiles are generated throughout the reaction profile. The authors did note that the potential for divergent reactivity in the reaction shown in **Figure 8**, as when the reaction was carried out in the presence of three equivalents of methanol, nucleophilic addition to form the methyl ether instead became the sole reaction pathway, with no [2+2] product observed.

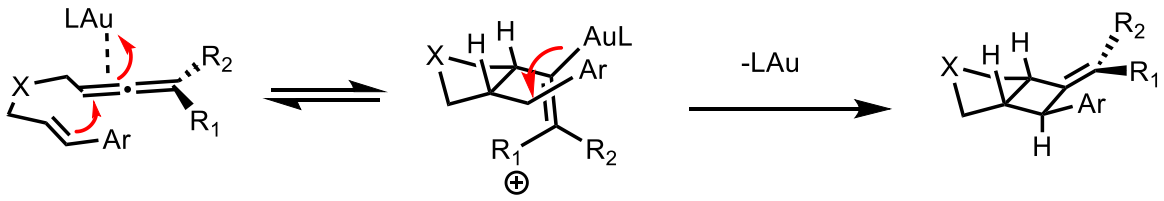

Figure 8 Vinylgold [2+2] Cycloaddition

Vinylgolds have also been used as nucleophiles in tandem metal catalysis, with one example coming from the Blum group in 2011.[18]

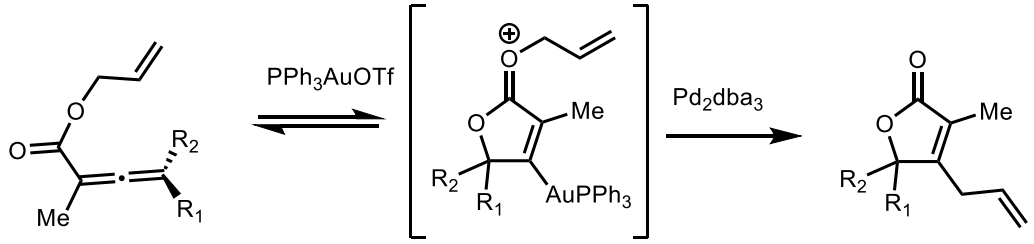

Figure 9 Vinylgold Nucleophile in Tandem Catalysis

Some years later, chemists began to realize the potential for tandem gold and photocatalysis. A particular example of this work comes from Hashmi's group in 2016.[19] Inspired by previous work in transition metal catalysis to form α-aryl ketones, and building off of their own previous work with gold photochemistry,[20] they reported the reaction described below in **Figure 10**.

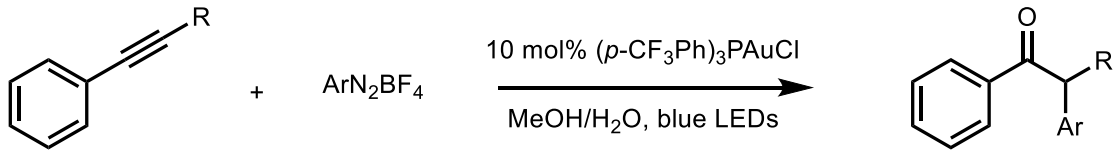

Figure 10 Photochemical and Au-Catalyzed Alkyne Difunctionalization

In the proposed mechanism, single electron transfer and nucleophilic attack of the diazonium salt oxidizes the catalyst from Au(I) to Au(III). The resulting Au(III) species coordinates to the alkyne and opens it to nucleophilic addition of methanol

and subsequent reductive elimination yields a vinyl ether, which undergoes hydrolysis to form the α-aryl ketone.

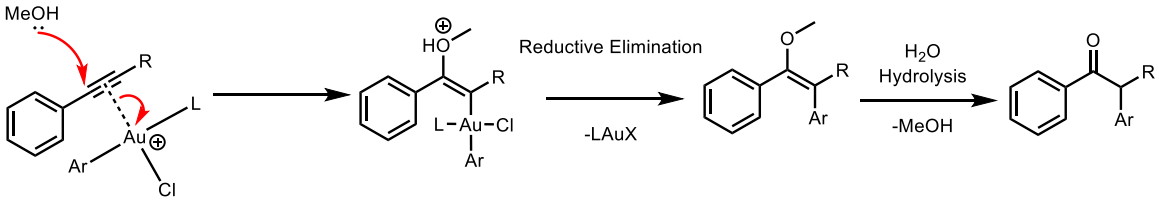

Figure 11 Mechanism of Hashmi Alkyne Difunctionalization

While this reaction itself does not demonstrate a nucleophilic vinyl gold, it served as a precursor to a follow-up report, which revealed a potential for divergent Au-catalyzed reactivity with diazonium salts in the case of *o*-alkynylphenols.[21] In the presence of 450nm light, arylated benzofurans were formed. When the reaction was done in the absence of blue LEDs, an azo-substituted benzofuran would instead slowly form over the course of hours or days. The scheme for these transformations is in **Figure 12**.

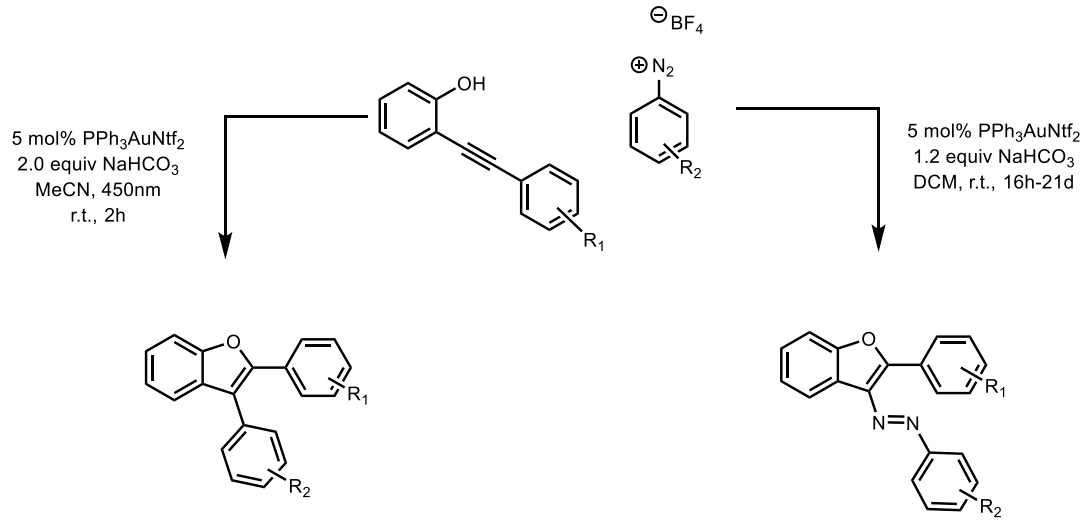

Figure 12 Divergent Reactivity of *o*-Alkynylphenols

Either pathway begins the same, with alkyne coordination by gold opening ito to 5-*endo*-dig cyclization by the phenol oxygen to form a vinylgold. When the reaction is performed under 450nm light, photocatalyzed extrusion of N_2 happens prior to or concurrently with vinylgold addition to the N-bonded carbon. In the absence of LEDs, N_2 is instead retained, and addition instead happens directly to the azo group. Unsurprisingly, the lack of a formal carbocation intermediate in the latter case leads to much slower conversion, but still demonstrates the capability of vinylgold to act as a nucleophile even upon weaker electrophiles.

Gold Acetylides: Mono and Dual Gold Catalysis

While a majority of gold-catalyzed transformations proceed only through π complexes and their subsequent vinyl/alkylgolds, activation of terminal alkynes can uniquely form an intermediate gold acetylide.[22] A typical method of generation is shown in **Figure 13** below. Coordination by gold to alkyne **1.14** forms complex **1.15**. Lewis acidity of gold increases the Bronsted acidity of the alkyne proton by

induction, allowing for facile deprotonation by base, yielding acetylide σ complex **1.16**.

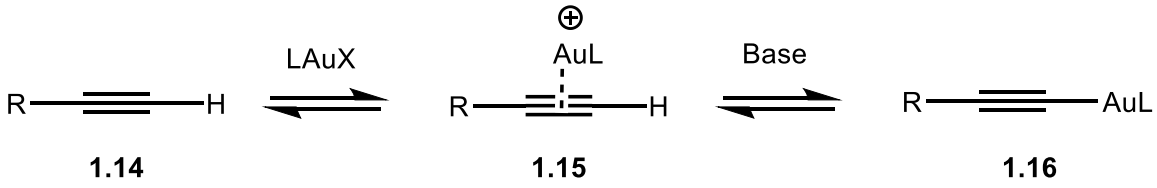

Figure 13 Formation of Gold Acetylides

While generally less reactive, gold acetylides still have a well-demonstrated utility as an intermediate in gold-catalyzed reactions. Many examples of them as intermediates come from reports of dual-gold catalysis of terminal alkynes.[23–30] In such case, a σ,π-complex typically serves as an early intermediate prior to the addition of nucleophiles. One of the earliest examples of a dual-gold σ π system comes from a 2008 experimental and computational report jointly authored by the Toste and Houk groups (**Figure 14**).[31]

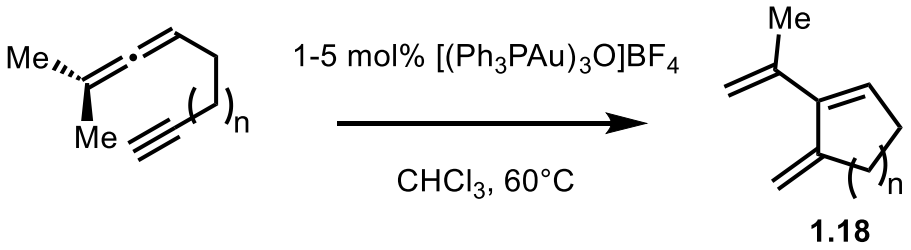

Figure 14 Dual-Gold Catalysis of Allenynes

The mechanism of the reaction was first examined by deuterium labeling experiments (**Figure 15**). When bis-CD_3 labeled **1.19** was cyclized, migration of deuterium from one of the allene methyl groups showed syn-selective incorporation relative to the new C-C bond. By D-labeling the alkyne, the authors

detected proton exchange at the alkyne terminus in a crossover experiment converting **1.21** to **1.22**. Lastly, anti-incorporation of deuterium was observed in the conversion from **1.23** to **1.24** when the reaction was performed in deuterated methanol.

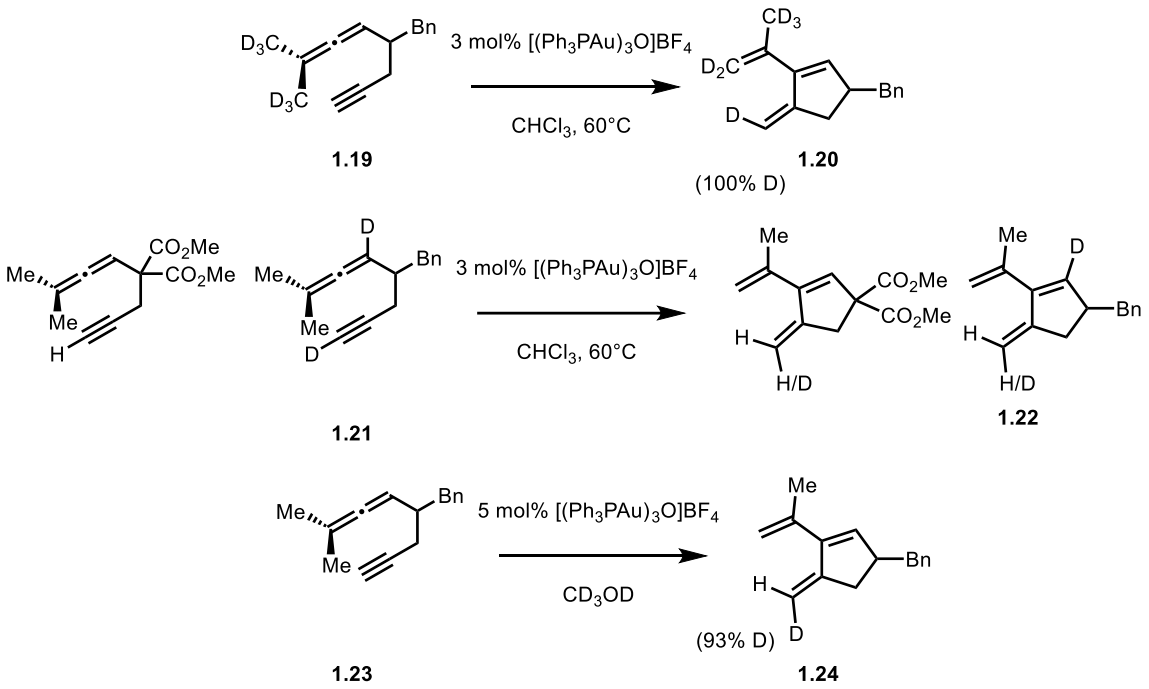

Figure 15 Allenyne Deuterium Labeling Experiments

While this series of experiments did narrow the range of possible mechanisms, the authors could still envision nine different routes through the transformation. To settle on a singular mechanism, computational analysis of the various free energy profiles was performed. Ultimately, it was proposed that the reaction proceeds through a σ,π-complex of the type **1.26** seen in **Figure 16** below. Once **1.26** is formed, C-C bond addition from the allene gives resonance stabilized cation **1.27**. A 1,5-H shift forms geminal digold cation **1.28**, proposed to then quickly protodeaurate to yield final product **1.29**.

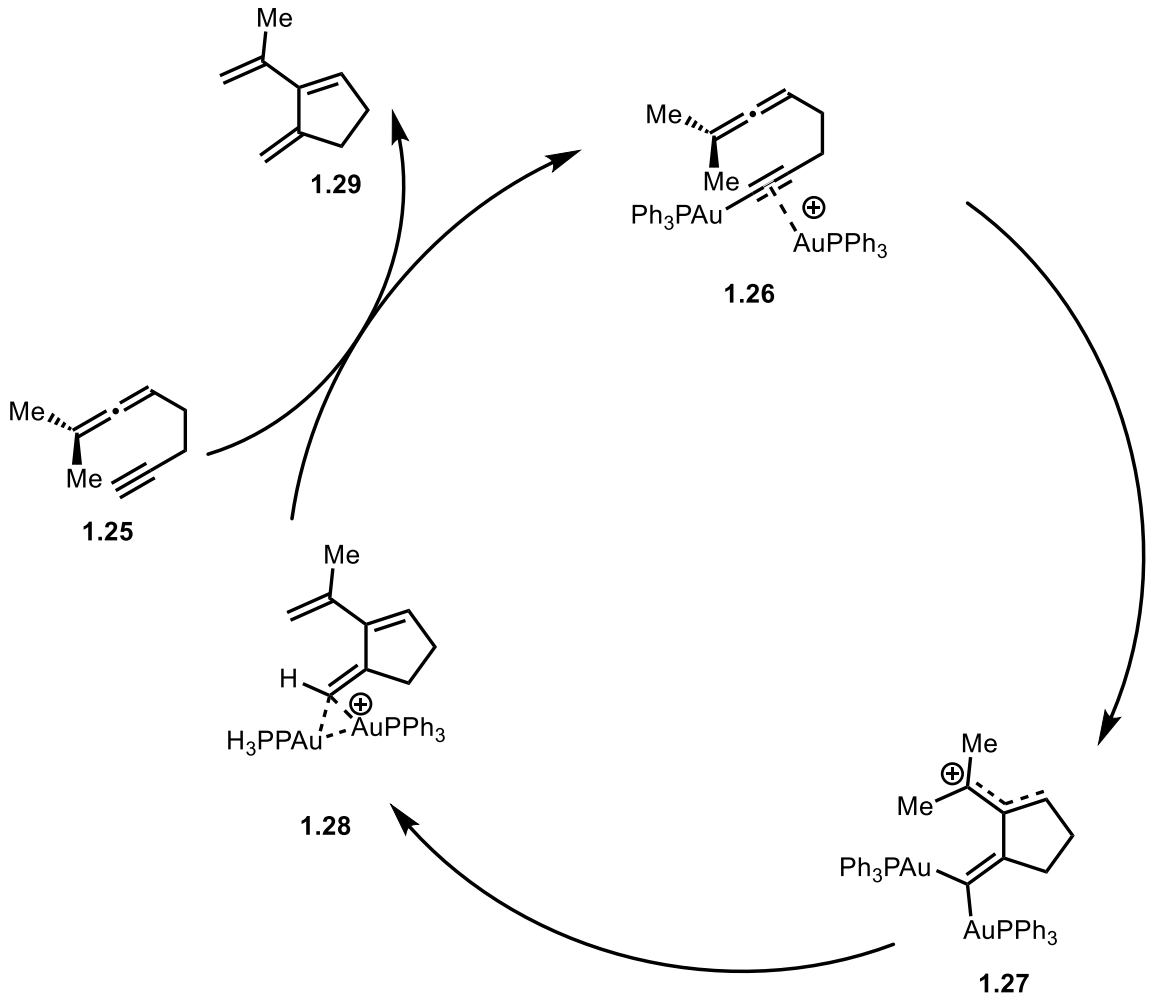

Figure 16 Allenyne Cyclization Mechanism

As the first example of dual-gold catalysis, this publication sparked a great deal of interest and follow-up reports investigating similar transformations.[32] In 2009, Gagosz et al. proposed an alternative mechanism which eschews the catalyst transfer step proposed by Toste and Houk (**1.28** back to **1.26**), instead suggesting stepwise protodeauration of a vinyl digold species by way of the counterion (**Figure 17** below).[33]

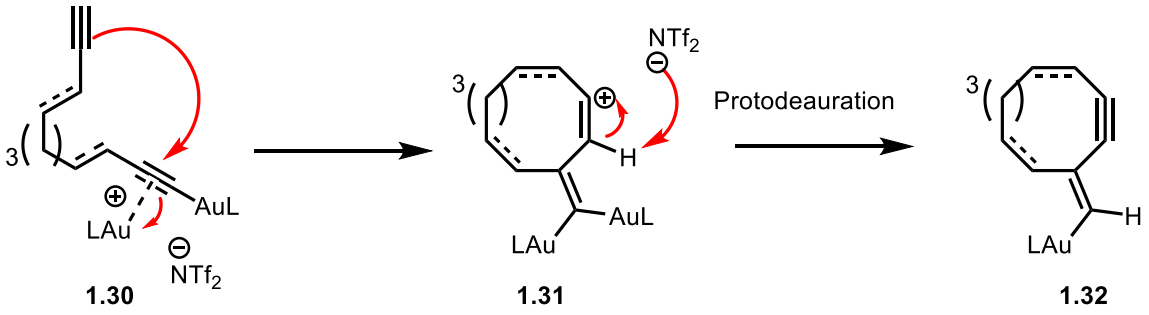

Figure 17 Alternative Mechanism by Gagosz

This mechanism is consistent with the deuterium labeling experiments proposed earlier by Toste and Houk, while also considering the role of the counterion as a proton shuttle and strong Brönsted acid. The ability of gold acetylides to generate acid was well-confirmed a couple of years later, when Hashmi reported divergent reactivity of arene-diynes with benzene in the presence or absence of basic additives.[34]

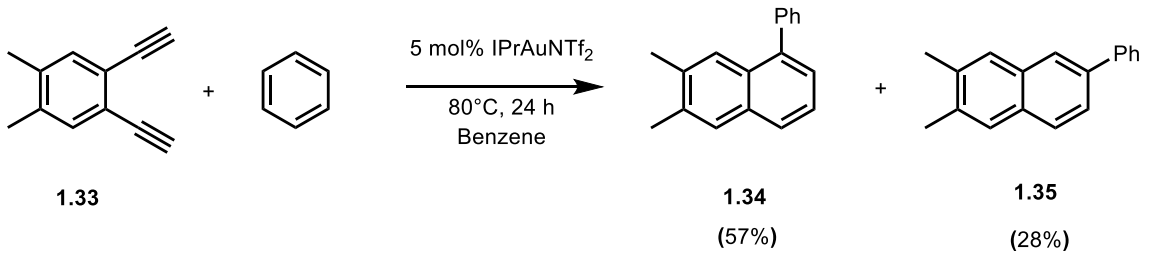

Figure 18 Divergent Reactivity of Arene Diynes

The reaction was discovered serendipitously during solvent screening of the Au-catalyzed addition of methanol to diyne **1.33** in benzene as a solvent. After identifying the arylated side-products, **1.33** was subjected to catalyst conditions in the absence of methanol with benzene as the solvent. Following 24 hours of reaction time, alpha and beta isomers **1.34** and **1.35** were obtained in 57% and 28% overall yield, respectively, with their structures confirmed by XRD. Kinetic

analysis by GC sampling **1.34** is formed quickly during the early phase of the reaction, with its formation slowing over time. However, concurrent with the reduction in formation of **1.34** is the formation of **1.35**, indicating a slow switch in mechanism.

Spurred by the divergent reactivity pathway, the authors performed a survey of various gold catalysts. The first selectivity switch was observed in this survey when the authors noted a significant reactivity switch when IPrAuCl was used with various silver salt activators. When $AgSbF_6$ was used, the product ratio was 74:26 in favor of alpha product **1.34**. Conversely, when $AgNTf_2$ was used instead, the ratio flipped almost entirely, becoming 39:61 in favor of beta product **1.35**. The importance of acid was confirmed in the reaction in the testing of various additives. Silica gel as an acidic support did not play a significant role in changing the reaction outcome, but the use of both basic and neutral aluminum oxide massively alters the ratio in favor of **1.35** to over 90%. Likewise, triethylamine also tips the ratio to 2:98, almost entirely erasing any selectivity for alpha product **1.34**.

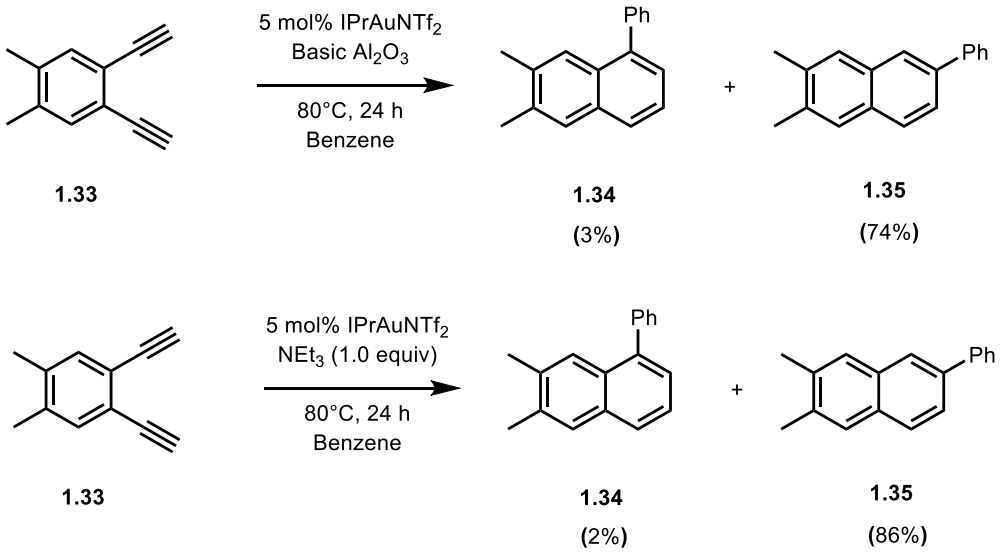

Figure 19 Impact of Base on Selectivity

Suspecting an intermediate gold acetylide, the authors synthesized monogold acetylide **1.36**. When this substrate was treated with a catalytic amount of $IPrAuNTf_2$, **1.35** was obtained as the sole product, affirming the likely role of **1.36** as an intermediate in the formation of **1.35**. The authors concluded that **1.36** is critical for the selectivity between alpha and beta products. In the absence of base, and especially in the case of high catalyst loading, alpha product **1.34** is formed with little to none of beta product **1.35**. Over long reaction times, or in the presence of basic, acetylide **1.36** is formed and acts as the trigger for divergence into the beta pathway which shuttles the reaction towards the formation of **1.35**.

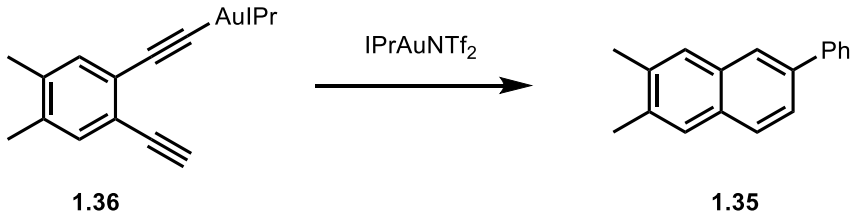

Figure 20 Beta-Selective Acetylide Cyclization

On the basis of the experiments described above and others, Hashmi and coworkers proposed the mechanism in **Figure 1.20**. σ,π-Complex **1.37** is formed slowly over time or quickly in the presence of base. Intramolecular cyclization to the π-activated alkyne gives the digold vinylidene species **1.38**. Addition of benzene gives vinyl digold cation **1.39**, which then undergoes H transfer to regenerate the gold vinylidene in **1.40**. Ring opening of the five-membered ring gives cationic **1.41**, which ejects Au(I) to afford aromatic vinylgold **1.42**. Protodemetalation (presumably by the acid generated during acetylide formation), gives the beta product **1.36**.

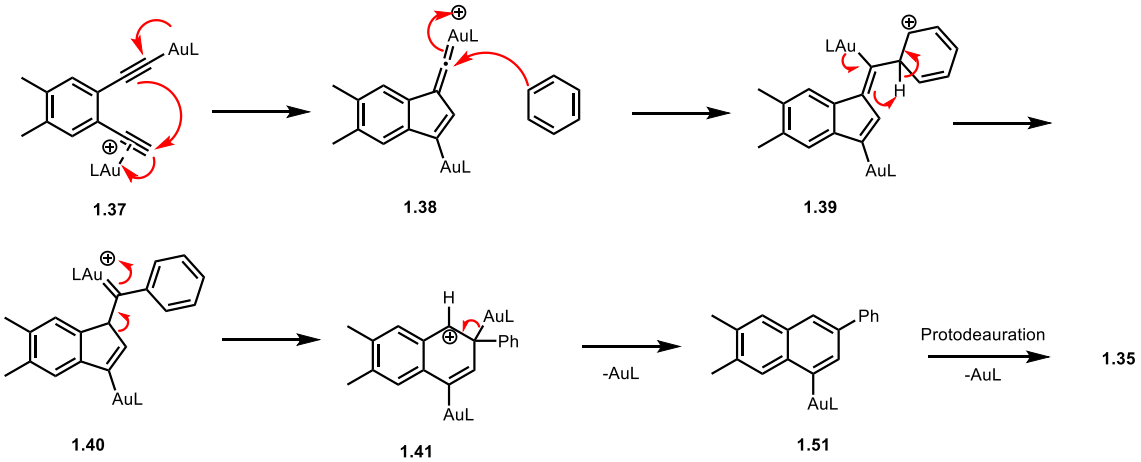

Figure 21 Beta-Selective Reaction Mechanism

Not only does this study demonstrate the potential for digold catalysis, but it also gives an example of acetylides as important reactive species with the

potential to determine reaction outcomes. The role of anions and the acid they generate is also highlighted in the higher formation of **1.35** when NTf_2 is used instead of SbF_6. Unsurprisingly, triflimide, the more basic of the two anions, leads to higher formation of the base-generated beta product. The Hashmi group continued to have success studying similar digold-catalyzed reactions for years thereafter in the formation of fused aromatic and antiaromatic rings.[24,26,35,36]

Geminal Digolds: Degradation Products of Au(I) Catalysis

As described above, in Au(I) activation of an alkyne, a typical resulting species is a vinylgold. In such cases where the following demetallation step is relatively slow, the vinylgold species can be captured by another mole of catalyst, resulting in a three-coordinate, bridged geminal digold structure.[37] Aurophilicity of gold, resulting from constructive orbital overlap between gold atoms near each other in space, results in many of these complexes being highly stable and kinetically inert.[38–41] Their presence as intermediates in gold-catalyzed transformations is typically considered to slow reaction rates, as their high stability often results in irreversible consumption of catalyst. An early report of digold observation comes from Gagne in 2009.[42] During the kinetic study of an intramolecular cyclization of allenes with PPh_3AuNTf_2, ^{31}P NMR showed a pair of peaks in a 1:1 ratio as the catalyst resting state, proposed to be the gem-digold species **1.53**. Vinylgold **1.52** could be obtained when cyclization was carried in out in the presence of 2,6-di-*tert*-butylpyridine. When reacted stoichiometrically with another mole of PPh_3AuNTf_2, **1.52** gives the gem-digold **1.53**. Both **1.52** and **1.53** can be treated with an equivalent of triflimidic acid to afford the demetalated

alkene. If instead only half an equivalent of $HNTf_2$ is used, **1.52** is converted to **1.53** by the release and recapture of free catalyst.

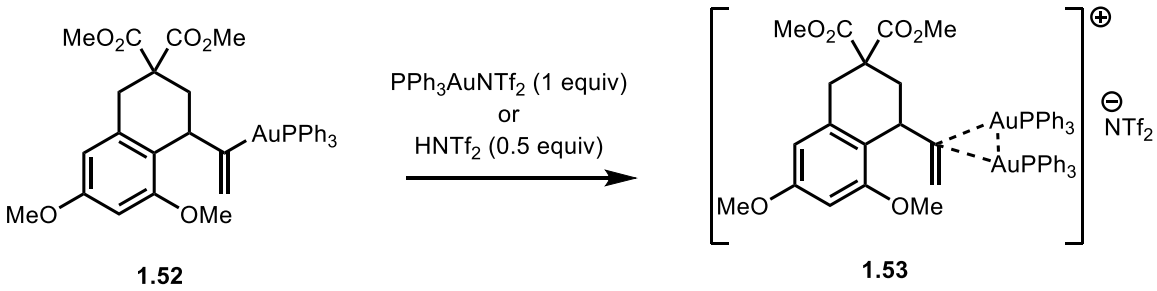

1.52 **1.53**

Figure 22 Geminal Digold Observed by Gagne

Gagne and coworkers followed this report with a study on arylgolds to further probe impacts on vinylgold stability.[43] Arylgold species **1.54** was synthesized and studied. Addition of one equivalent of PPh_3AuNTf_2 resulted in quantitative formation of digold **1.55**, which was characterized by NMR. Slow titration of PPh_3AuNTf_2 into a solution of **1.54** showed gradual formation of **1.55** as more catalyst was loaded. Any additions past one equivalent had no outcome on which species was favored, showing the equilibrium to be highly in favor of products.

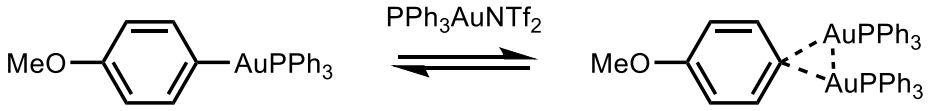

1.54 **1.55**

Figure 23 Aryl Geminal Digold Formation

The same experiment was performed with other triphenylphosphine gold catalysts with varying anions. The authors found that the equilibrium tips in favor of digol as the anion becomes more weakly coordinating. Addition of PPh_3AuOAc

to **1.54** gave no conversion to the digold, whereas PPh_3AuNTf_2 gives total conversion. The trend observed across anions generally followed that more basic anions resulted in less or no digold formation. Digold formation also became more favorable the more electron rich the aryl ring became. **1.54** was converted to **1.55** by both strongly and weakly coordinating anions. However, an electron-deficient aryl ring where OMe was replaced by CF_3 was largely unreactive in the scheme in **Figure 23**, only forming digolds with the least basic anions. This study served as a demonstration that electron rich vinylgolds would form geminal digolds much more readily than electron poor ones.

Another key study came in 2013 from Zhdanko and Maier.[44] They studied the equilibrium constants of geminal digold formation and disproportionation using a survey of ligands and nucleophiles.

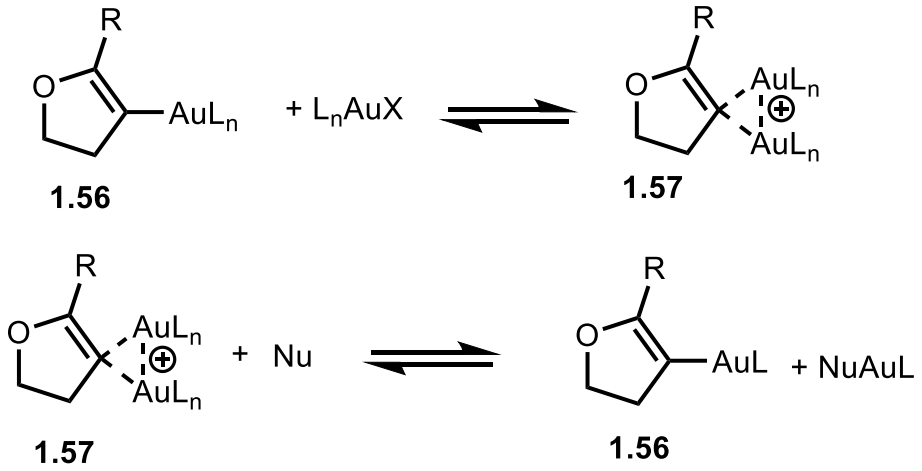

Figure 24 Vinyl Gem-Digold Equilibrium Experiments

A wide survey of vinylgolds derived from enol ethers of type **1.56** was conducted. In the top equation in **Figure 1.24**, both R groups and the ligands on gold were varied. A trend noticed as R was varied was the tendency of more

electron rich alkenes to form more stable (lower k_{eq}) gem-digolds as opposed to electron poor alkenes, driving equilibrium towards species of type **1.57**. Additionally, when R is a conjugated π system (e.g. R = *p*-NMe_2-C_6H_4) and can participate in resonance conjugation with the formed alkene, the equilibrium is driven towards **1.56**, away from gem-digolds.

The impact of ligand was also assessed (**Figure 24**, top scheme), with a similar trend being observed. When the ligand on gold is more strongly electron donating (e.g. Johnphos), gem-digolds became more stable, favoring formation of **1.57**. However, in the case of ligands with large amounts of steric bulk, the equilibrium would instead favor vinylgold **1.56** as steric factors begin to dominate.

Last, the authors also assessed the rate of exchange when the vinylgold was reacted with a nucleophile, such as tetramethylthiourea. (**Figure 24**, bottom scheme). Here, the impact of sterics were observed again, as digolds with extremely bulky ligands reacted very slowly even with potent nucleophiles.

The studies on gem-digolds discussed above illustrate the number of complex factors at play when trying to study a Au-catalyzed reaction. Geminal digolds can be formed when protodeauration is slow, but the extent to which they are a hindrance to reaction rates is highly depended on the electronics and sterics of both the substrate and the catalyst itself.

The Cyclization of N-Propargyl Benzamide: Gold's Most Popular Benchmark

In 2004, Hashmi reported the Au(III)-catalyzed intramolecular cyclization of N-propargyl benzamide, **1.58**, to the corresponding oxazole, **1.60**.[45] The reaction

proceeded smoothly under very mild conditions, with only 5 mol% loading of gold and at room temperature. Reaction times were in the range of twelve to fifteen hours. Of note is the observation of the intermediate non-aromatic oxazoline **1.59** throughout the course of the reaction, forming very quickly relative to the aromatic final product.

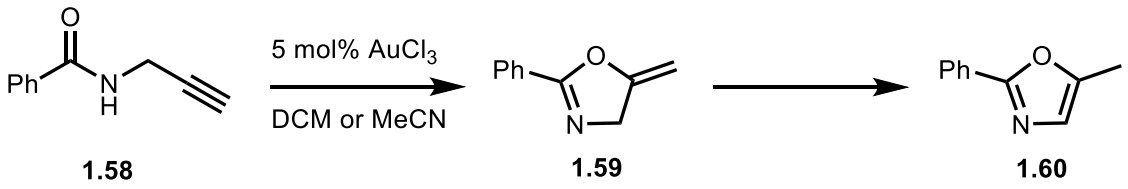

1.58 **1.59** **1.60**

Figure 25 N-Propargyl Benzamide Cyclization

The observation of **1.59** as an intermediate gave an opportunity to study the mechanism in depth. ^{1}H-coupled ^{13}C NMR in conjunction with a deuterium labeling experiment at the alkyne terminus of **1.58** showed preservation of the deuterium label at reaction's end. This was established by disappearance of the 7.9Hz ^{3}J trans ^{1}H-^{13}C coupling from one of the exocyclic alkene protons to the endocylic methylene carbon.

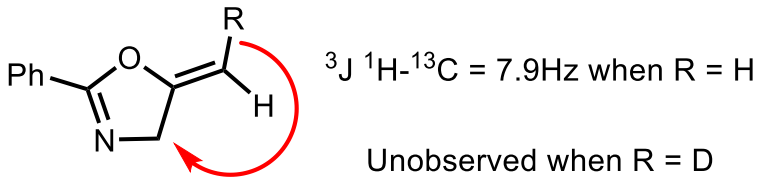

Figure 26 Loss of H-C Coupling in D-Labeling Experiment

This experiment proved that the nucleophilic oxygen is added trans to the catalyst during cyclization. The proton trans to the oxygen in oxazaline **1.59** must

be installed during protodemetalation of the catalyst. Based on this experiment, the authors proposed the mechanism below.

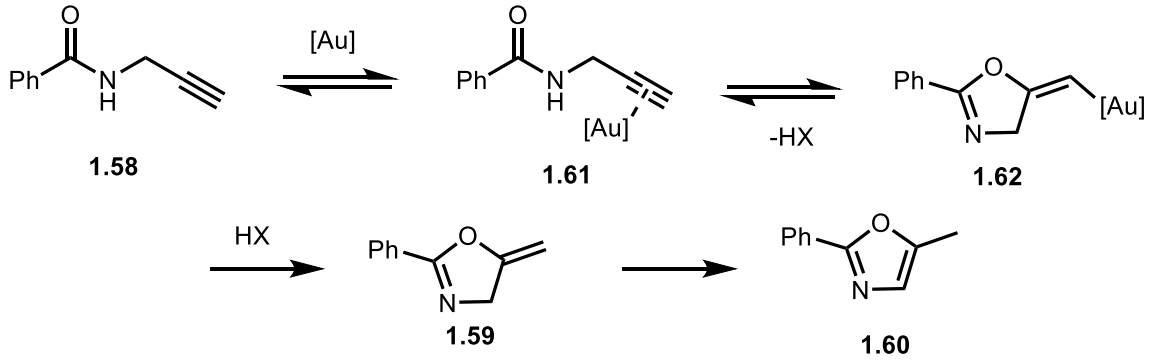

Figure 27 Mechanism of Benzamide to Oxazole Cyclization

Complexation by gold to **1.58** gives π-complex **1.61**. Addition of oxygen trans to the catalyst gives vinylgold intermediate **1.62**. Stereoretentive protodeauration could potentially occur intramolecularly from an N-protonated oxazoline directly preceding **1.62** but is more likely to be facilitated by proton transfer from the catalyst anion. Regardless of mechanism, the protodeauration step yields oxazoline **1.59**, which, over time, gradually isomerizes to aromatic oxazole **1.60**.

Since its publication, this cyclization has become an enormously popular benchmarking reaction for the analysis of new catalytic systems. In the two decades since, it has served as a backdrop with which to survey the effects of ligands, solvents, anions, and reaction additives. The Hashmi group has made use of the reaction many times in the years since, including in their 2009 work characterizing the isolation of vinylgold complexes discussed earlier in this chapter (see **Figure 4**).[14]

Aside from Hashmi's capturing of vinylgolds, the reaction went largely unexplored until another follow-up from the Hashmi group in 2010 surveyed the possible scope of the cyclization.[46] A broad range of amide substituents were assessed, finding the cyclization still performs well when the amide R group is not a simple phenyl ring. Phenyl rings substituted with donating (-OMe) and withdrawing (-F) substituents were tolerated, as well as aromatic heterocycles such as pyridine, furan, and thiophene. Long chain aliphatics, *tert*-butyl groups, and an adamantly substituent also performed well. Replacement of the aryl ring with esters as another carbonyl-containing moiety also gave high yields. Of note was their observation that Au(III) catalysts give aromatic oxazoles similar to **1.60**, whereas Au(I) catalysts allow for slower formation of **1.60** and instead afford the isolation of oxazoline **1.59**.

It was after this 2010 publication that the substrate's use as a catalytic benchmark began to blossom and its appearances in the literature became increasingly frequent.

Ligand Effects in the Cyclization of N-Propargyl Benzamide

In 2012, Hammond and Xu published a seminal report on ligand effects in Au(I) catalysis.[47] A series of intramolecular reactions were studied. The reactions were chosen on the basis of their rate-limiting step, either initial π complexation (and subsequent intramolecular cyclization) or protodeauration. The cyclization of benzamide **1.58** in the presence of Au(I) was chosen as the benchmark reaction

with which to study the kinetics of the protodeauration step, as the broad consensus in the field by this time, based largely on the *in situ* observation and isolation of vinylgolds, was that protodeauration from **1.62** to **1.59** was the turnover-limiting step for the transformation. The ligands surveyed for the reaction are shown below.

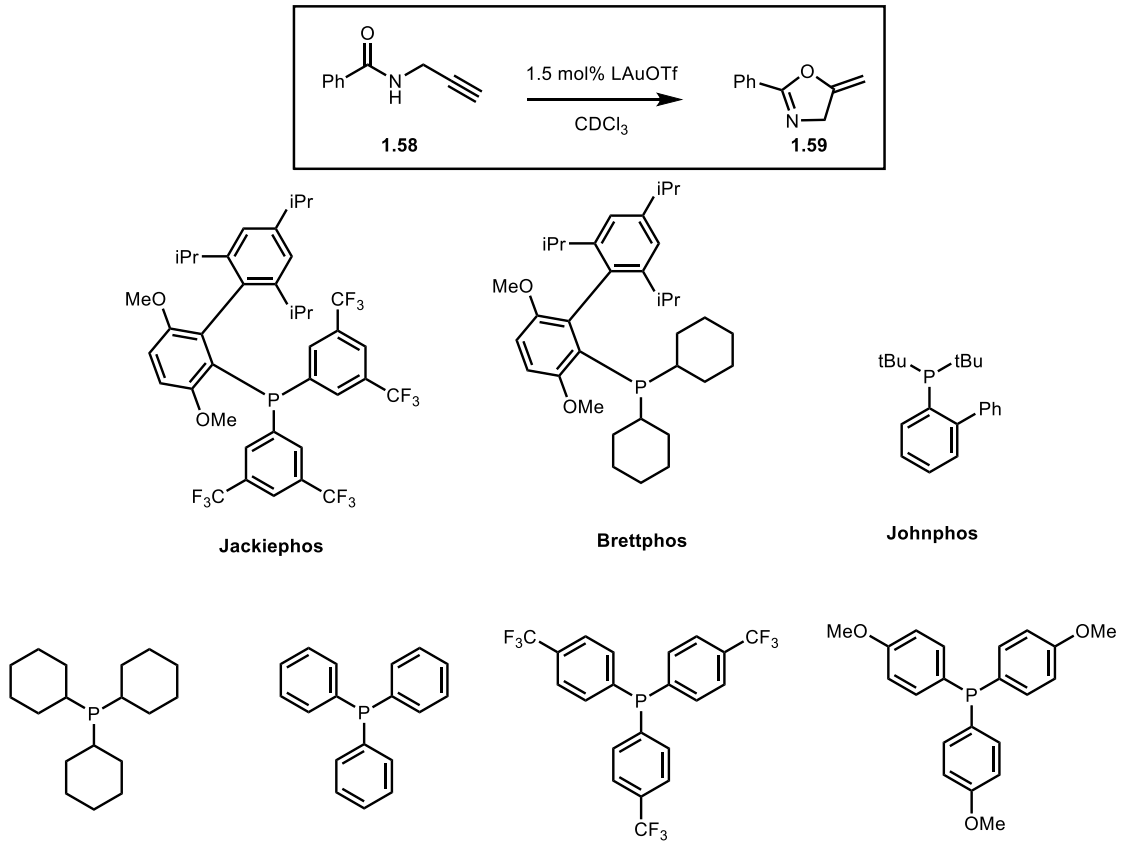

Figure 28 Ligands Assessed by Hammond

In such cases where protodeauration is rate-limiting (conversion from vinylgold **1.62** to oxazoline **1.59**, **Figure 27** for this transformation), a more electron-rich phosphine should hasten the rate of reaction. The resulting Au(I) species will be lower in energy due to more significant sigma donation from the ligand, thereby lowering the barrier for demetallation. When the ligands above

were used in the reaction, observed rates supported the conclusion of rate-determining protodeauration. Cy_3P, the most electron-rich ligand, was the fastest ligand by far, followed by next by Johnphos. Brettphos marginally outpaced 4-methoxytriphenylphosphine. PPh_3 was the next slowest, followed by its tris-CF_3 variant. Jackiephos, the most electron-starved of the collection, performed the slowest by far, giving single-digit conversion to **1.59** after more than four hours (as opposed to Cy_3P, which gave 100% conversion in fewer than two).

This 2012 publication has since become one of the most oft-cited pieces of literature in the field used to describe ligand effects and to denote the cyclization of **1.58** to **1.59** as being rate-limited by protodeauration.

Ligand effects are not uniform with this consensus, as two years earlier another study from the Hashmi group tested the effects of KITPHOS ligands on Au(I) centers.[48] The authors found higher conversion rates in the same cyclization with less electron rich phosphines.

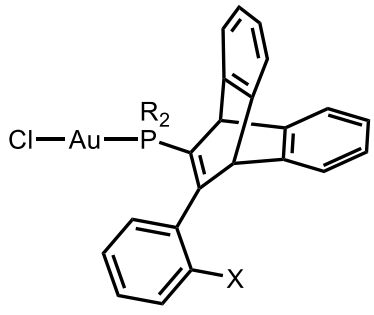

R = Ph or Cy
X = H or OMe

Figure 29 KITPHOS Ligands Studied by Hashmi

When R = Ph, the catalyst provides oxazoline **1.59** in 74% conversion after 30 minutes in room-temperature DCM regardless of the identity of X. When R = Cy, conversions were lowered to 61% and 45% for X = H and OMe, respectively. Notably, this study demonstrates the slowest conversion rate for the most electron-rich phosphine tested, directly contrasting the notion of rate-determining protodeauration asserted by Hammond two years later. The electron-poor KITPHOS ligands universally outpaced the electron-rich for all transformations.

A similar reversal of expected trends was seen in 2019 when Barta and coworkers synthesized and tested the reaction rate of ferrocene-substituted phosphine ligands.[49]

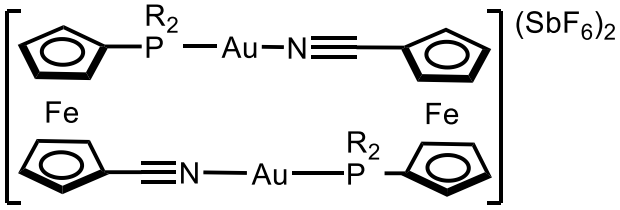

R = iPr, Ph, 2-furyl, Ts

Figure 30 Ferrocene Ligands Studied by Barta

As seen with Hashmi's KITPHOS ligands, the more electron rich phosphines outperformed the electron poor, as the alkyl substituent gave slower rates than those with aryl ones in the cyclization of **1.58** to **1.59**.

Anion Effects in the Cyclization of N-Propargyl Benzamide

Hammond and Xu also contributed one of the more important reports on the impact of counterions.[50] The authors established a pair of index identities for gold counterions according to gold affinity and hydrogen bonding affinity (GAI

and HBI, respectively). A weakly coordinating anion with low gold affinity (e.g. SbF_6) creates a more Lewis acidic gold, which was demonstrated to give fast kinetics in the intramolecular cyclization of **1.63** to **1.64**, where no proton shuttling step occurs. SbF_6 and CTf_3, anions considered to have zero or near-zero affinity for gold, carried out the transformation 21 and 32 times faster, respectively, than the much more strongly coordinating OTf. Essentially, due to the lack of any proton shuttling in the conversion of **1.63** to **1.64**, there is no need for any hydrogen bonding from the anion to facilitate H transfer. The reaction profile is dominated entirely by the Lewis acidity of gold, which is heightened by using the anions with poor gold affinity.

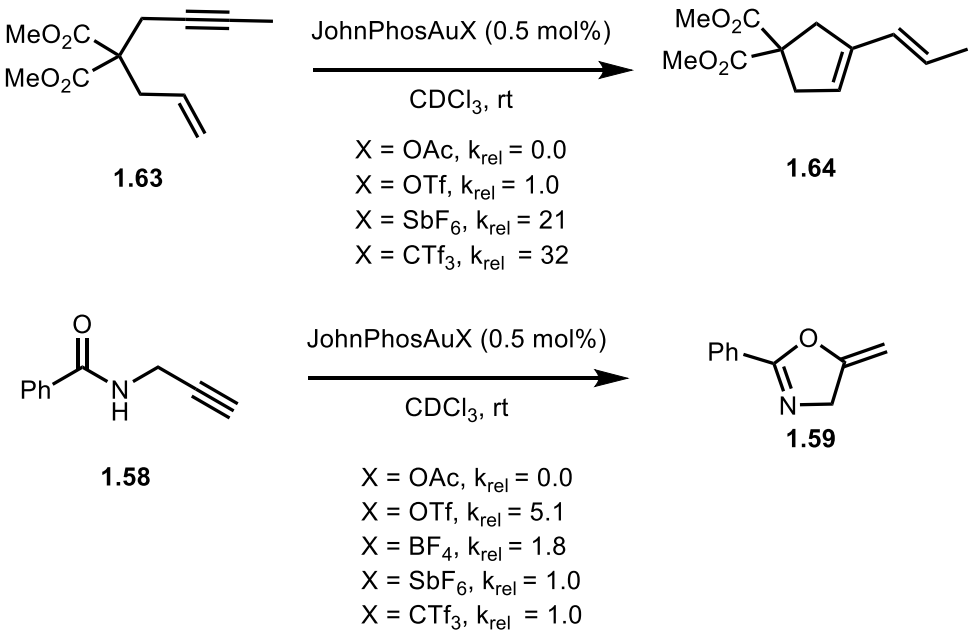

Figure 31 Anion Survey by Hammond and Xu

For the benzamide cyclization, however, the trend reverses, where the more basic OTf catalyzes a faster transformation than the weakly basic SbF_6 and CTf_3. Notably, BF_4, an anion the authors purport to have a higher H-bonding index than

OTf, performs the reaction more slowly than OTf, with a k_{rel} of only 1.8. The only potential reason for this inconsistency given by the authors is a statement that starting materials and/or water clusters may impact reaction rates. Finally, the authors denote that OAc, the anion with the largest H-bonding index, acts as an inhibitor for both reactions due to its similarly high affinity for gold, thereby diminishing Lewis acidity. For a reaction where protodeauration is rate-limited, it should instead be expected that more weakly basic anions would hasten the rate, as they form stronger conjugate acids. SbF_6 should therefore be expected to give rapid catalysis, but the less basic OTf instead wins out.

A 2015 report by the Zuccaccia group continued to explore anion effects in conjunction with select ligands.[51] A pair of weakly coordinating, non-basic anions, BF_4 and OTf, were contrasted with OTs and TFA. The ligands with which they were paired are shown in the figure below.

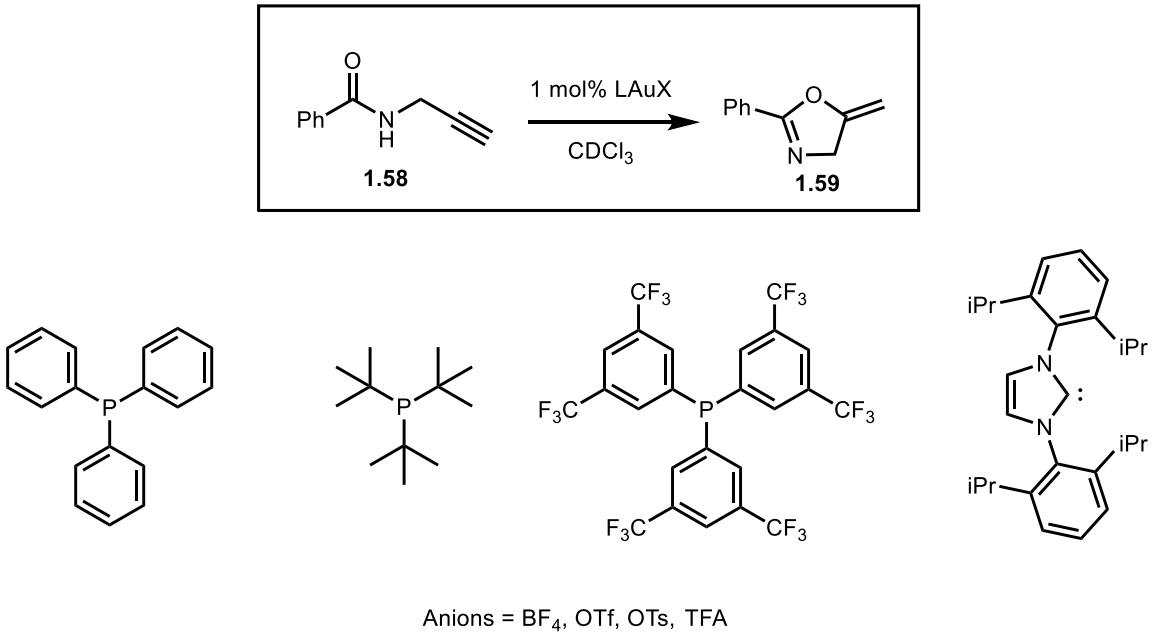

Figure 32 Anion and Ligand Matching Tested by Zuccacia

All four catalysts above were paired with each of the four anions and used to catalyze the cyclization. The PArF ligand was the least active of all ligands regardless of anion, consistent with rate-limiting protodeauration. When BF_4 is used as the anion, all ligands except the fluorinated phosphine give over 98% conversion inside of two hours, with PArF providing only 55%. When the anion is switched to OTf, the activity of all ligands notably decreases. The most intriguing results come from when tosylate is chosen as the anion. The catalytic activity of PPh_3 and $PtBu_3$ substantially increases, giving quantitative conversion of **1.59** in 63 and 40 minutes, respectively. However, the conversion rate of the NHC ligand becomes markedly sluggish, with even the PArF ligand giving faster cyclization. Trifluoroacetate, the most basic anion surveyed, slows catalysis and decreases yield of **1.59** for all ligands except $PtBu_3$, which gave quantitative yield in 73 minutes.

The conclusion reached by the authors is that a delicate balance of basicity and coordination must be achieved, and which anion gives the best results will be dependent on the electronic character of the ligand.

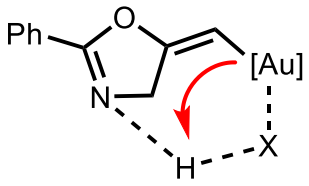

Figure 33 Protodeauration Mediated by Anion

In **Figure 33** above, when the anion is poorly-coordinated to the gold fragment (as mediated by ligand characteristics), the basicity of the anion becomes the dominant characteristic. The authors note this is the case for ligands PArF and IPr in **Figure 32**. However, when the anion is more capable of coordinating to gold, relative basicity and H-bonding affinity become larger factors. This is posited to be the case for PPh_3 and $PtBu_3$.

Another key observation stems from an NMR study performed by the authors in this same report. Given the broad consensus by the time of publication that protodeauration is rate-limiting for this cyclization, the authors monitored the reaction by ^{31}P NMR and suggest the reaction proceeds with vinylgold as a resting state, affirming rate-limiting protodeauration in the case of all ligand and anion combinations. The basis for this claim is a prominent resonance at approximately 43ppm in the ^{31}P spectrum (L = PPh_3), closely matching the chemical shift observed for vinylgolds of viny ethers isolated and characterized in a 2010 report by Furstner (L = PPh_3).[52]

The Zuccaccia group continued exploration of these same anions in 2021.[53] IPrAuX was the sole ligand used in conjunction with the same four anions (BF_4, OTf, OTs, and TFA) for cyclizing **1.58** to **1.59** in non-volatile green solvents (e.g. cyclohexanone, isopropyl acetate, and furfuryl alcohol, among others). When catalysis was performed in propionic acid, an inverse correlation between basicity and turnover frequency was observed, linearly following the trend of BF_4, OTf, OTs, and TFA. TFA, again the most basic of the set, gave the poorest conversion.

Solvent and Additive Effects in the Cyclization of Propargyl Benzamide: The Role of Hydrogen Bonding

In addition to serving as a backdrop for the assay of ligand and anion effects, the cyclization of propargyl benzamide has additionally served as a benchmark for the impact of additives on reaction rate. Just as is the case for ligands and anions, Hammond and Xu again claim one of the most important studies on this topic.[54] In their 2014 publication, they performed this transformation in the presence of various reaction additives with strong H-bonding ability. Given the rate-limiting nature of protodeauration, the authors surmised that the addition of a potent H-bonding species would hasten reaction rates by way of more facile proton shuttling to the vinylgold intermediate.

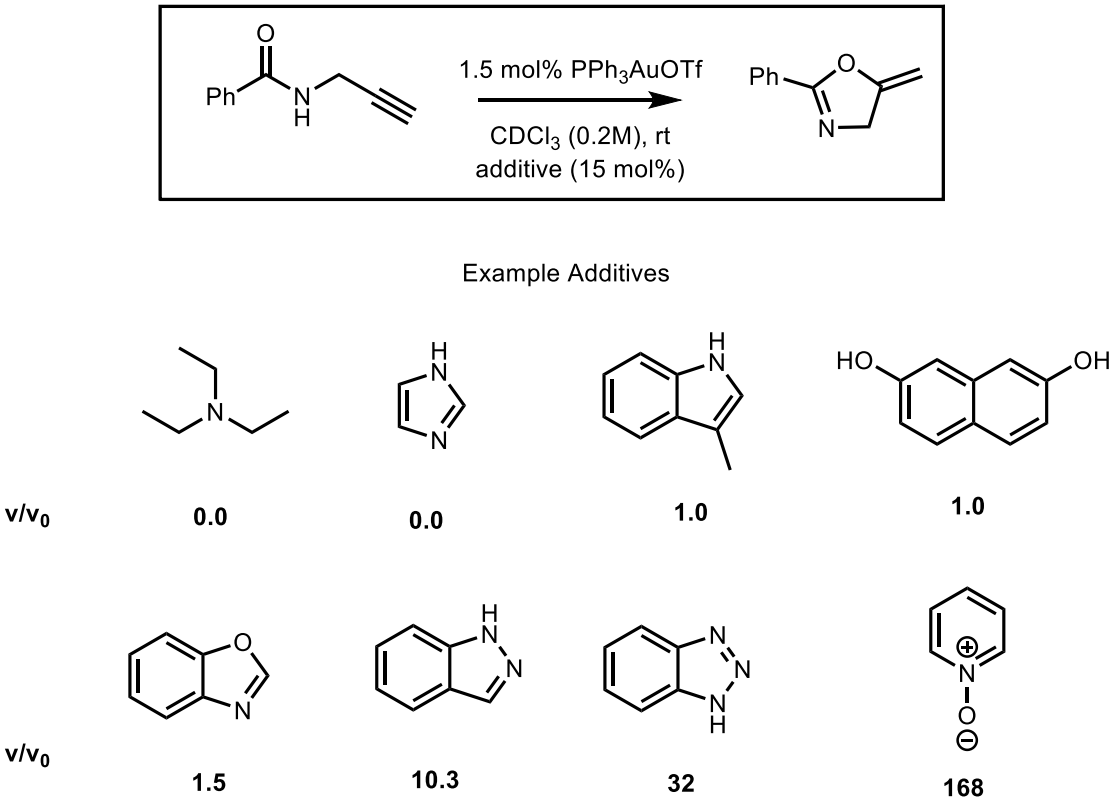

Figure 34 Influence of H-Bonding Additives on Reaction Rates

The reaction conditions and structures of various additives are shown in the figure above. The ratio of $v:v_0$ is constructed from the initial rate of the reaction in the presence of additive (v) divided by the initial rate of the reaction in the absence of any additives (v_0). Those numbers are shown in bold underneath the additives shown.

As seen in **Figure 33**, addition of fairly strong bases such as triethylamine and imidazole hinder the reaction entirely. The authors propose this is due to the quenching of acid generated and needed to facilitate protodeauration. Other additives had no effect, such as 3-methyl indole and naphthalene-2,7-diol. Benzoxazole gives a 50% rate increase and stands as an interesting entry given its structural similarity to the fully aromatic oxazole product sometimes seen in the

course of this reaction. Indazole affords a ten-fold rate increase, while addition of a third nitrogen to the ring in benzotriazole multiplies the reaction rate by a factor of 32. Most remarkable by far is the addition of pyridine N-oxide, which affords a colossal increase of rate by a factor of 168. To contextualize these results with H-bonding capabilities, Hammond and Xu turned to a database reported in 2009 by Laurence and coworkers which measured hydrogen bond basicity (denoted as pK_{HBX}). They found the performance of additives correlated linearly with pK_{HBX}, demonstrating the importance of hydrogen bonding in helping to deliver a proton to the vinylgold to complete the reaction.

Two years later, Hammond and Xu continued their study of co-catalysts for Au(I) catalysis in a study on acidic additives to gold reaction mixtures.[55] The authors observed rate increases to a variety of gold-catalyzed reactions, likely for one or both of two reasons. One, the deactivation of gold by formation of gold acetylides in the catalysis of terminal alkynes, and two, the hastening of protodeauration by the abundance of acidic protons with which to demetalate a long-lived vinylgold intermediate.

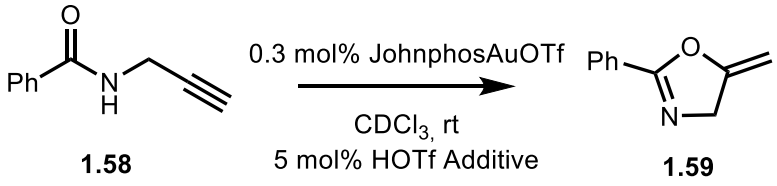

1.58 **1.59**

Little to no rate increase observed

Figure 35 No Impact on Cyclization Rate by Acidic Co-Catalyst

Intriguingly, the authors observed virtually no influence on rate by the addition of acid to a cyclization of propargyl benzamide. It is hard to rationalize this result in the context of results obtained by others. Namely, if H-bonding is important for proton-shuttling to form **1.59**, it would certainly be expected for an acidic co-catalyst to likewise increase the rate of reaction. A direct quote from the report is as follows: “Our preliminary explanation for this lack of co-catalyst effect was that that the protodeauration step and/or gold-catalyst deactivation were not limiting factors in the catalytic cycle. Further investigation is required to understand why acidic co-catalysis may be beneficial for some transformations but not for others.” Catalyst degradation by formation of acetylides is not precedented for this reaction, but rate-limiting protodeauration absolutely is. This observation stands noticeably in contrast to these claims of rate-limiting protodeauration, a conclusion frequently espoused by the very same authors.

However, the Hashmi group reported a modest increase of rate for the transformation in the presence of small amounts of water.[56] The formation of oxazoline **1.59** from **1.58** with PPh_3AuNTf_2 in CD_2Cl_2 with varying water content was analyzed by ^1H NMR.

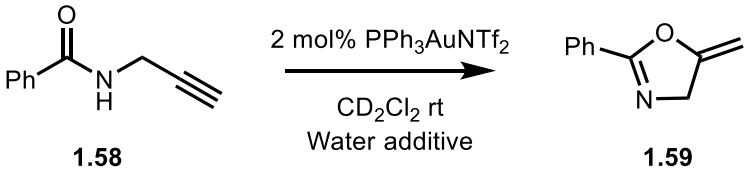

1.58 **1.59**

No water k_{rel} = 1.0
0.2μl/1mL k_{rel} = 1.07
2.54μl/1mL k_{rel} = 1.14

Figure 36 Impact of Water Addition on Rate

Given the poor miscibility of dichloromethane and water, additions of water greater than the amounts above in **Figure 36** gave biphasic mixtures, which were impossible to analyze by NMR. It is worth noting that the rate increase seen is fairly small. Additionally, several other reactions were analyzed in this study, not all of which include rate-limiting protodeauration, but which did still give similar results in the presence of small titrations of water. The authors themselves note that, due to this observation, it is beyond the study's scope to propose what role water may be playing in the various mechanisms.

A likely explanation still involves hydrogen bonding, which became an increasingly popular topic of discussion as the amount of studies on its influence for the transformation grew. A 2020 report demonstrated the possibility for self-activation of NHC gold chlorides by a sidearm of the ligand capable of H-bonding abstraction of the chloride ligand *in situ*.[57]

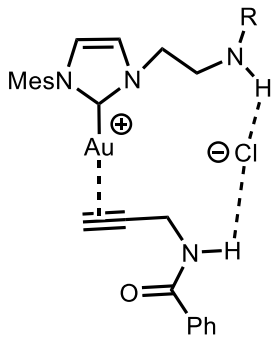

Figure 37 Gold Chloride Activation by H-Bonding Sidearm

Similar to Hashmi's report, various amounts of water were added as a titrant to a reaction mixture of 1 mol% of the catalyst in dichloromethane. 100 and 200ppm additions of water linearly increased the rate of cyclization, whereas 250ppm gave slower conversion than 200ppm, but faster than 100ppm. 450ppm

rendered the reaction extremely sluggish, to the point of halting it almost entirely. The authors did demonstrate the value of water as an H-bonding additive for their specific ligand by performing a 200ppm titration of water into a reaction mixture with 1 mol% of $IPrAuNTf_2$, the NHC ligand most commonly used in Au(I) transformations but which does not include any H-bonding moieties. The rate of reaction was slower than with that of the catalyst shown in **Figure 37** even in the absence of water, demonstrating that H-bonding with water plays no role in cyclization with $IPrAuNTf_2$, or even slows the reaction instead.

Other reports also commented on the potential of other additives. Another paper from Hammond and Xu showed a significant rate increase with $KCTf_3$ as a promoter.[58] When benzamide cyclization was performed with 1.5 mol% of PPh_3AuOTf and 3 mol% of $KCTf_3$, an eleven-fold rate increase was observed.

Hydrogen bonding likewise remained a topic of focus. “Silver effects” are a known issue for Au(I) catalysis, where the abundance of silver in reaction mixtures where Au(I) catalysts are formed *in situ* can be problematic for rates and yields.[59–64] Similar to the self-activating NHC ligand described above, much attention has been paid to H-bonding activators which will provide silver-free conditions for the activation of Au(I) catalysts. Alternatives to silver salts include activation by N-heterocyclic Iodazolium salts[65] and H-bonding squaramides.[66] Both of these example promoters are capable of activating gold-chlorides for catalysis in place of a silver salt and their performance was tested in this common benchmark reaction.

Where ligand and anion effects for the transformation have been studied extensively, literature on the impact of solvent choice is much more sparse. In the vast majority of cases, this cyclization is performed in halogenated solvents, typically chloroform or dichloromethane. The aforementioned study by Zuccaccia analyzed the performance of NHC-based catalysts in green solvents,[53] but this example is one of few.

One solvent which has garnered significant attention in recent years is hexafluoroisopropanol (HFIP), which has become an increasingly common solvent of choice in synthetic transformations owing to its high affinity for hydrogen bonding.[67] In 2022, Tzouras and coworkers were the first to report the solvent as an activator for gold chlorides in the cyclization of **1.58** to **1.59**.[68]

What makes this study especially significant is the demonstration of HFIP's ability to activate precatalytic gold chloride species by hydrogen bonding, forming potent catalysts *in situ*. For most transformations, gold(I) chlorides of the type LAuCl are largely or completely inert, requiring conversion to an active catalyst by anion exchange with a silver salt or one of the silver-free activators described above. What the authors uncovered with this study is the H-bonding ability of HFIP is so significant, it will activate the gold-chlorine bond *in situ* to form an active species with which to activate π bonds. The transformation was viable for a wide range of gold chlorides bearing both phosphine and NHC ligands, and at only 1 mol% catalytic loading. The reaction performed best with NHC ligands of relatively minimal steric bulk. Furthermore, no reaction occurred when the chloride ligand was replaced with iodide, demonstrating the importance in choice of halogen.

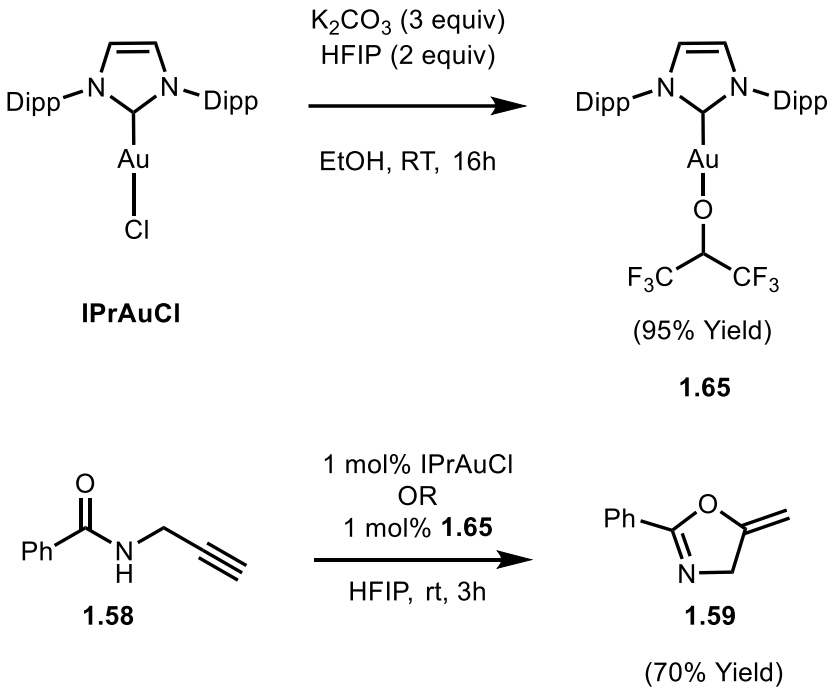

Figure 38 Catalysis in HFIP

A notable result from the paper is shown in the figure above. The gold alkoxide species **1.65** was synthesized from IPrAuCl and HFIP under mild conditions. The complex proved extremely stable, enough so to obtain a crystal structure. When **1.65** was used as catalyst, it gave identical results to IPrAuCl, pointing to **1.65** as likely being the catalytic species *in situ*.

A follow-up from the same group was reported in 2023.[69] While the benzamide cyclization was not extensively explored outside of a few structural variations, the authors did demonstrate the multifunctionality of HFIP as a solvent, activator, and as a reagent which can actually be incorporated into the product of various other reactions. The substantial induction of the trifluoromethyl groups enhances the leaving group ability of the alkoxide, which was utilized in a string of downstream functionalizations following catalysis by gold.

Functionalization

As has been demonstrated above, the cyclization of N-propargyl benzamide has served as a rich proving ground for new catalytic systems involving ligands, anions, additives, activators, and solvents. It has also seen use as a scaffold for testing functionalization of the oxazole or oxazoline product by the addition of secondary reagents or co-catalysts.

In 2012, Hashmi reported the formation of oxazole peroxides by exposing reaction mixtures to air.[70] Despite gold's typical tolerance of air and water, the initial oxazoline product spontaneously oxidized in the presence of atmospheric oxygen to the corresponding hydroperoxide. It was confirmed gold was not necessary for the conversion, as a control experiment in which oxazoline product **1.67** was exposed to air both in the presence and absence of catalytic Au(I) yielded identical products in identical rates.

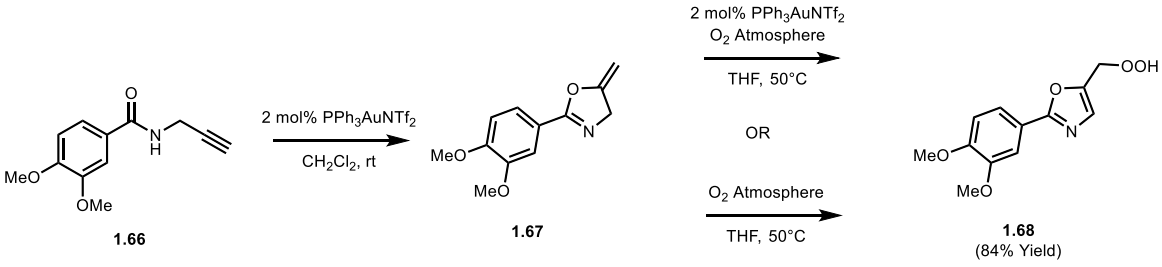

Figure 39 Autoxidation of Oxazoline Product

Peroxide formation was broadly tolerant of functional groups on the aromatic ring. Additionally, peroxides of type **1.68** could undergo facile reduction with $NaBH_4$ to afford the corresponding alcohol, thereby accessing a functionalized oxazole under a series of mild reaction conditions.

Oxidative chemistry was further explored for this cyclization in a 2015 report from the Shi group.[71] Synergistic co-catalysis of gold and iron in the presence of oxygen gave an oxazole-aldehyde **1.69** as a product. The use of tBuOOH as a radical promoter was found to give higher conversion and yields than the use of molecular oxygen alone, and an ^{18}O labeling experiment with $^{18}O_2$ confirmed the oxygen of the aldehyde originates from O_2.

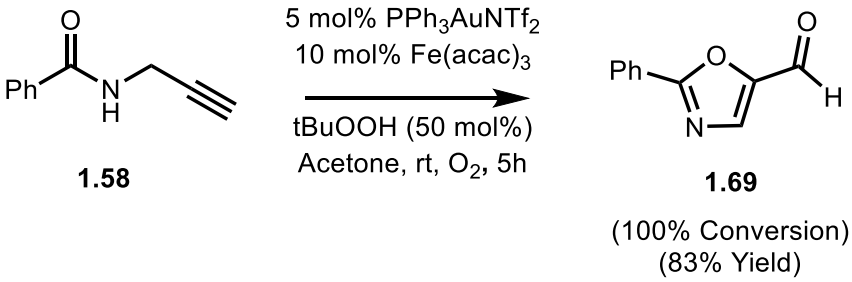

Figure 40 Dual Gold-Iron Catalysis

Mechanistic experiments were conducted to determine what intermediates may be involved. Importantly, the authors sought to confirm if the catalysis was stepwise (a full gold cycle which then transferred into an iron cycle), or tandem. A stepwise mechanism was ruled out when the conversion of **1.70** to **1.72** under dual-catalyis conditions gave a faster rate than the conversion of oxazoline intermediate **1.71** to **1.72** under iron conditions only. This strongly hinted that the iron portion of the catalytic cycle must begin with an intermediate involved in the gold cycle.

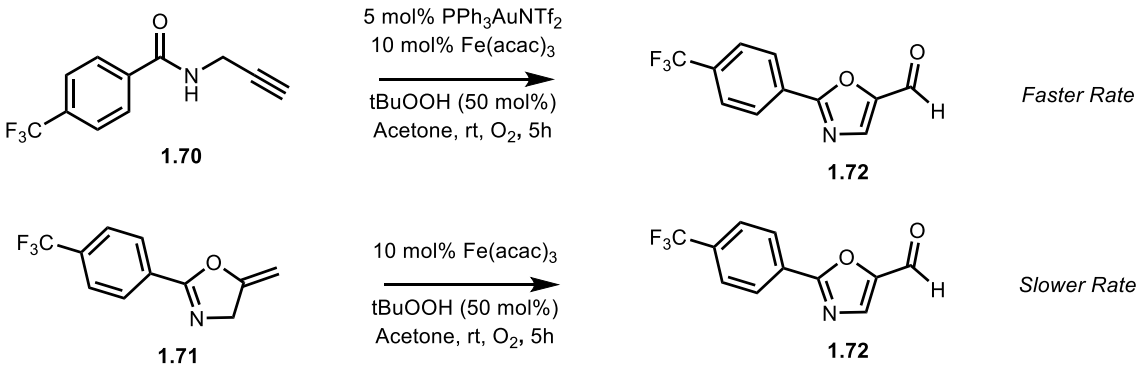

Figure 41 Gold and Iron Control Experiments

The intermediacy of a vinylgold species was confirmed when one was isolated and treated to the Fe\O_2 conditions, giving 30% conversion to the aldehyde product. A radical mechanism was likewise confirmed when addition of 1 equivalent of TEMPO as a radical trap halted the reaction.

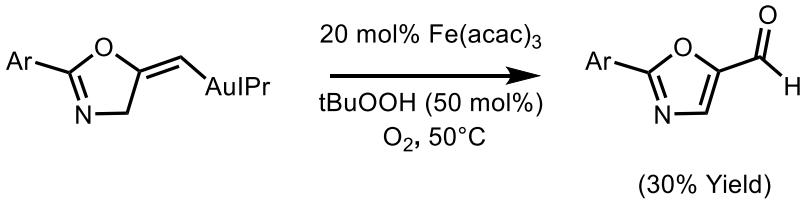

Figure 42 Vinylgold Oxidation Control Experiment

A pair of analogous transformations were reported in 2017 by Mai and coworkers.[72] Inspired by the oxidative chemistry from Shi described above, the authors sought to perform similar chemistry by installing nitrogen-bearing functional groups outside the formed oxazole ring. 5-oxazolecarboxamides were synthesized by tandem catalysis with gold, copper, and N-hydroxyphtalamide (NHPI). Tert-butyl nitrite (tBuONO) was used as an oxidant and nitrogen source. Alternatively, nitriles could be isolated as products instead via a change to a nickel co-catalyst.

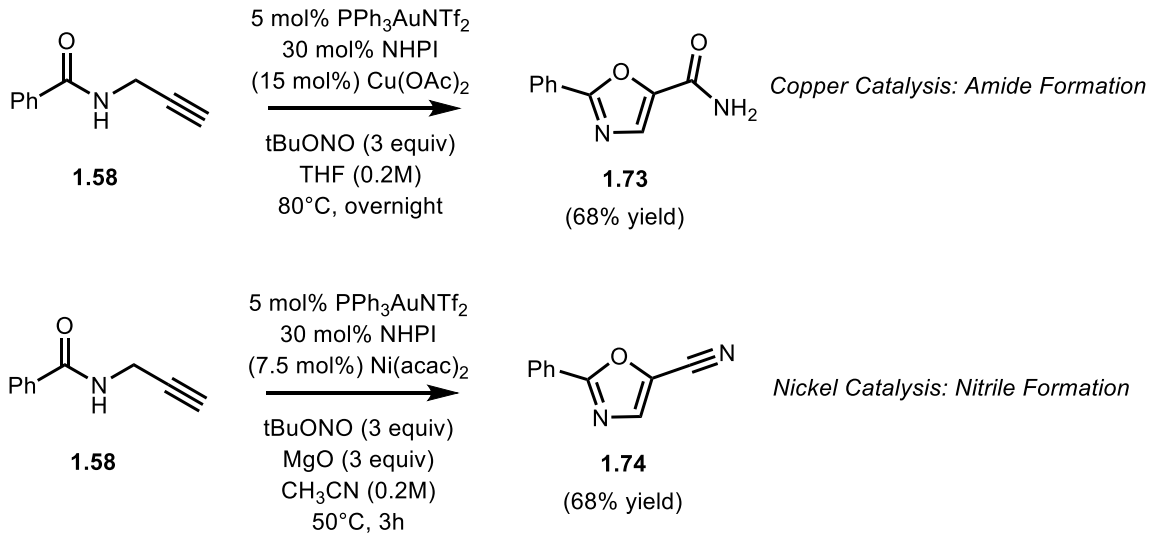

Figure 43 Chemodivergent Oxazole Synthesis

Like the study by Shi, the intermediacy of oxazoline was ruled out when it gave 0% conversion to either both amide **1.73** and nitrile **1.74** in the presence of non-gold reagents. The oxazole tautomer was also disproven as an intermediate when it also failed to give any products under the same conditions. Unlike Shi's Au/Fe chemistry, the vinylgold was eliminated as a key intermediate when it gave partial conversion to **1.74** in the presence of gold catalyst, but none in its absence. What they eventually discovered was the role of aldoxime **1.75** as an intermediate, which could be converted to both the amide and nitrile products depending on choice of conditions. Both **1.73** and **1.74** could be formed from **1.75** in the presence or absence of gold, but its absence lowered yield of **1.73** by 11%. The yield for **1.74** was less impacted by gold's absence, dropping only by 3%.

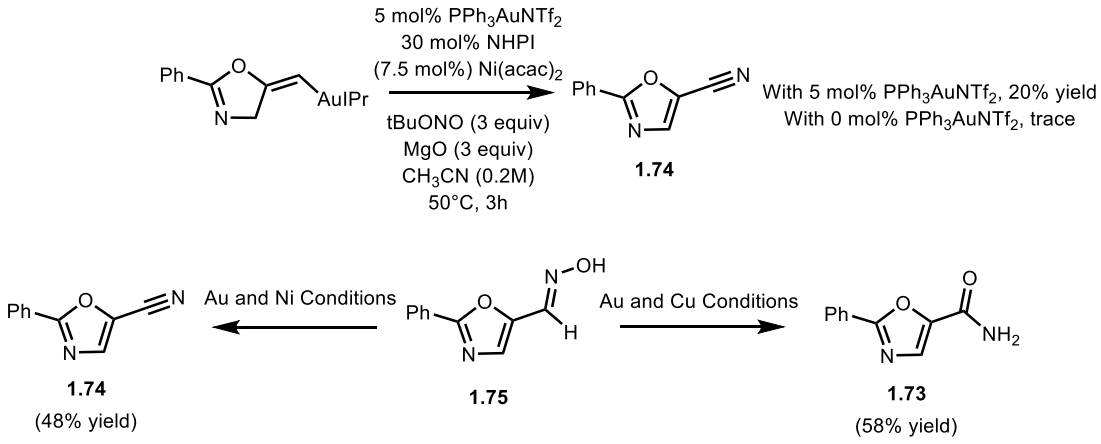

Figure 44 Aldoxime as an Intermediate

As mentioned above, when the vinylgold was treated to typical reaction conditions in the absence of more gold catalyst, no conversion to products was observed. With the addition of catalytic gold, however, conversion to the amide product was observed. What the authors thereby proposed is that the vinylgold must, itself, react with another mole of catalyst to form a different gold complex, which then reacts with tBuONO as an oxidant to form a radical species which then demetalates to form the aldoxime intermediate **1.75**. **1.75** then goes on to react in the rest of the cycle, either with nickel or copper, to furnish the two possible products.

The transformations above and in tandem with those shown earlier in this chapter (**Figure 11**) demonstrate the burgeoning interest in photoredox chemistry with gold catalysts.[73] Exploration of photoredox gold chemistry and functionalization of the benzamide scaffold continued in a report from Liu and coworkers on the synthesis of polyfluorinated oxazoles from the substrate.[74] The benzamide was reacted with PPh_3AuNTf_2 and K_2CO_3 in the presence of a

polyfluoroalkyl iodide under blue light irradiation, giving the functionalized oxazole products shown in **Figure 45**.

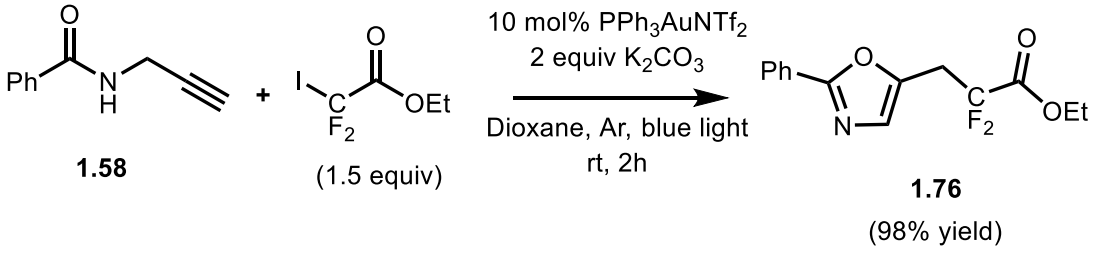

Figure 45 Polyfluorinated Oxazole Synthesis

Through a series of mechanistic and kinetics experiments, it was discovered the protodeauration of the oxazoline vinylgold to form oxazoline **1.59** is still the rate-limiting step, just as it is for the regular cyclization. **1.59** then undergoes radical addition by the perfluoro ester fragment, forming radical heterocycle **1.77**. Single electron oxidation by Au(II) formed earlier during the generation of the radical ester fragment regenerates Au(I) and gives carbocation **1.78**. Deprotonation by base forms oxazole product **1.76**.

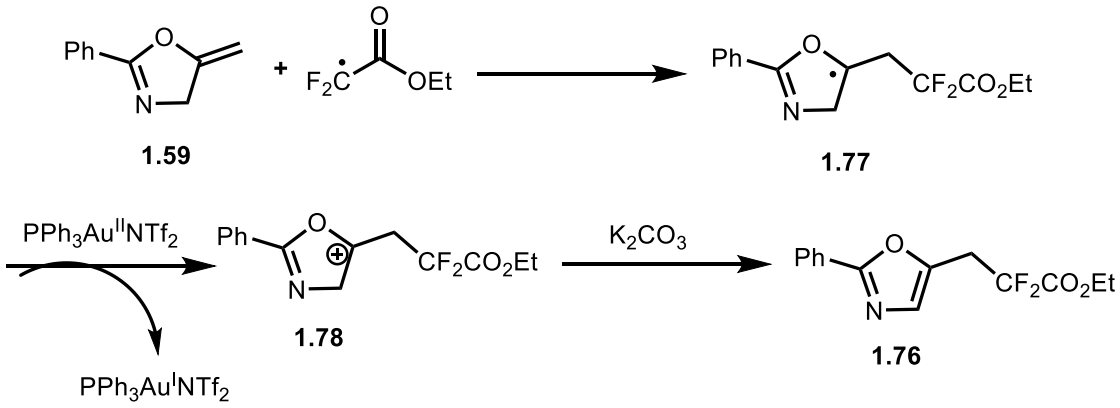

Figure 46 Fluorinated Oxazole Mechanism

While fewer in number, there have been instances of pericyclic reactions being performed in tandem with the Au-catalyzed cyclization as well. In 2018,

Hashmi reported the use of the initial alkylideneoxazoline product in a one-pot two-metal catalyzed Alder-ene reaction.[75] Inspiration came from natural products bearing chiral centers at the beta carbon of oxazoles. A procedure to install this chiral center was developed and is shown in **Figure 47**.

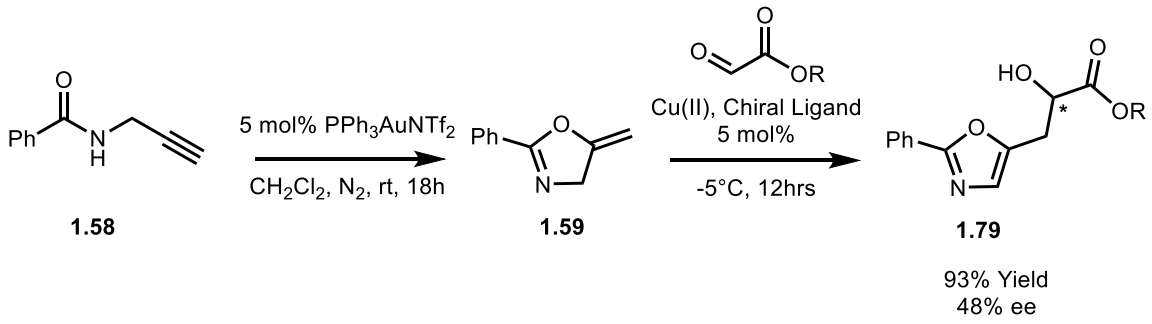

Figure 47 Alder-Ene Reaction of Oxazoline

Enantioselectivity was achieved by use of chiral bisoxazoline ligands for the Cu(II) catalyst. Proof-of-concept for the second part of the reaction was performed by first forming and isolating **1.59** and its variants, after which the copper conditions were tested and verified. The reaction was largely insensitive to substituents on the phenyl ring of **1.59**, with electron withdrawing and donating groups both performing well in the reaction. The reaction could also be performed in all solvents surveyed, though yield and enantioselectivity was highest in dichloromethane at 87% and 81%, respectively. Acetonitrile was the worst solvent tested, giving a decent yield of 66%, but lowering %ee to 21%. Ideal copper conditions were tested directly from the oxazoline variants of type **1.59** in the absence of any gold. Gratifyingly, the reaction also worked well in a tandem catalysis one-pot procedure. A concern was the potential for ligand exchange between the gold and copper metal centers. This problem seemingly did not occur, which the authors attributed

to gold's high affinity for phosphane ligands over nitrogen-coordinating ones such as the BOX ligands used. The yield for the common substrate is shown in **Figure 47** above. Enantioselection was better than 48% for most aryl substituents.

In 2021, Dong and coworkers reported the asymmetric allylation of oxazolines formed in the cyclization of N-propargyl benzamide.[76] Use of a chiral squaramide co-catalyst provided enantioinduction in the allylation step following a Au(I) cycle.

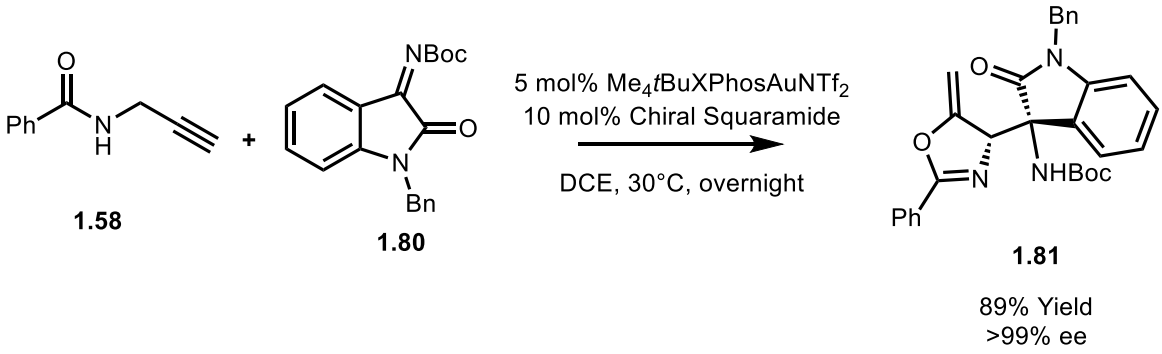

Figure 48 Enantioselective Allylation

Mechanistic control experiments confirmed the necessity of both the gold and organocatalysts for the formation of products such as **1.81**. Stepwise catalytic cycles were ruled out when treatment of alkylidenoxazoline **1.59** to regular conditions both with and without gold failed to provide product. When **1.59** was instead reacted with ketimine **1.80** under high temperature without either catalyst, oxazole products **1.60** and **1.82** were formed. This pair of experiments ruled out the intermediacy of oxazoline **1.59**.

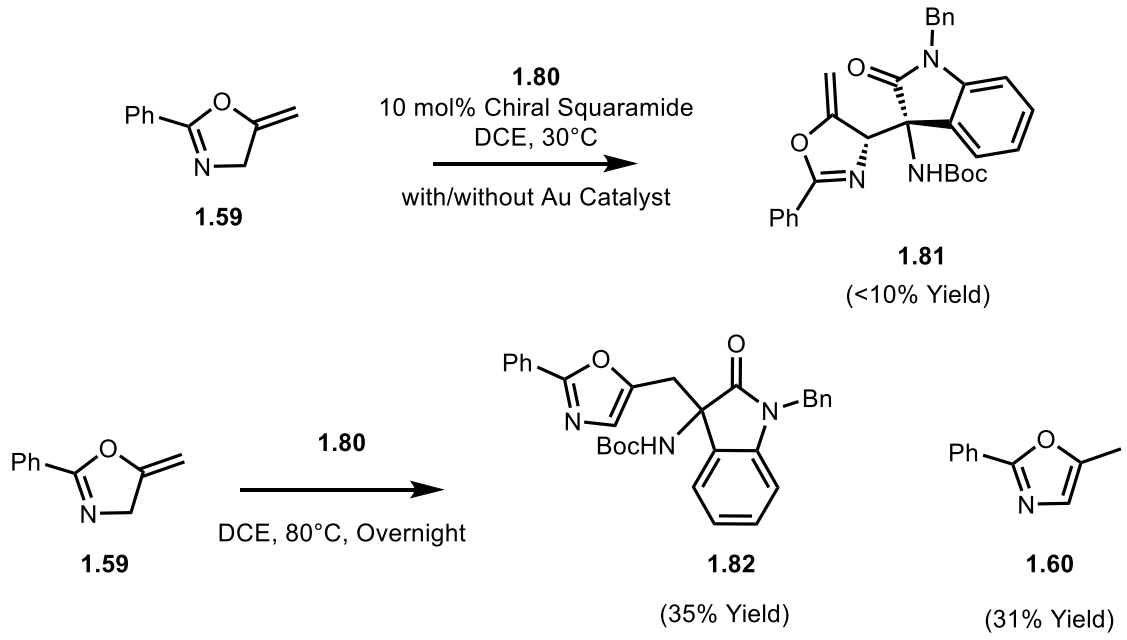

Figure 49 Oxazoline Disproved as Intermediate

Based on the results above, the authors deduced the key intermediate for reaction with **1.80** must be an intermediate involving gold. Given the relative abundance of literature positing vinylgolds as key intermediates, and given their successful isolation and characterization in the past, the authors attempted to isolate a vinylgold by stoichiometric reaction of **1.59** with Me_4*t*BuXPhosAuNTf_2 in a DCM/hexane mixture with five equivalents of triethylamine. Stunningly, the species isolated in 95% yield after evaporation of the solvent under Ar atmosphere is the *alkylgold* oxazole **1.83**, *not* the vinylgold oxazoline. This result stands in stark contrast to previous vinylgold isolations for this transformation, where superstoichiometric equivalents of base halted transformation at the vinyl, not alkylgold.

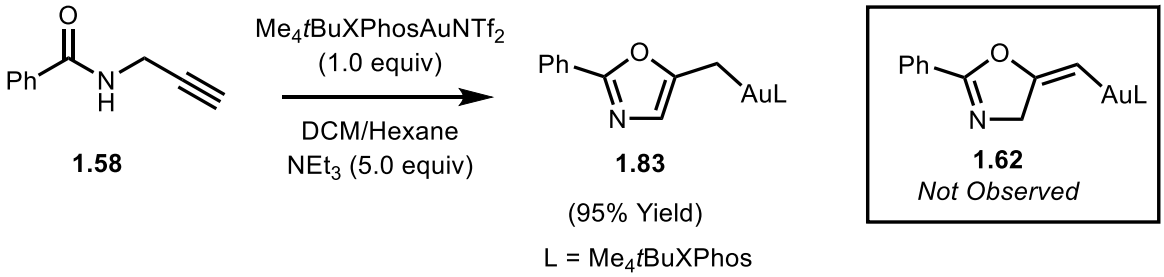

Figure 50 Formation of Alkylgold Oxazole

Even more intriguingly, the identity of **1.83** as the key gold intermediate for the formation of **1.81** was confirmed when it reacted with **1.80** and the organocatalyst to form **1.81** in high yield.

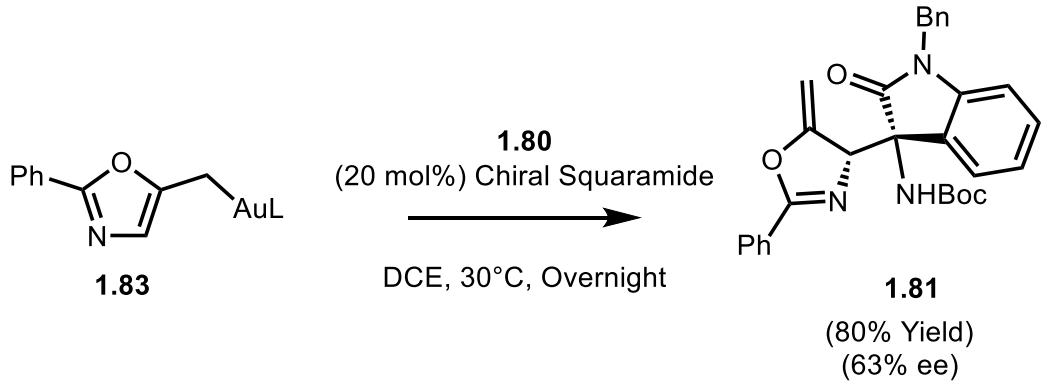

Figure 51 Alkylgold is the Key Intermediate

This was the first report to demonstrate downstream functionalization of an alkylgold intermediate for the N-propargyl benzamide cyclization. Prior literature confirmed (or assumed) intermediacy of a vinylgold species.

The same group followed this result with another paper in 2024 in which the same alkylgold intermediate was used in a [4+2] cycloaddition.[77]

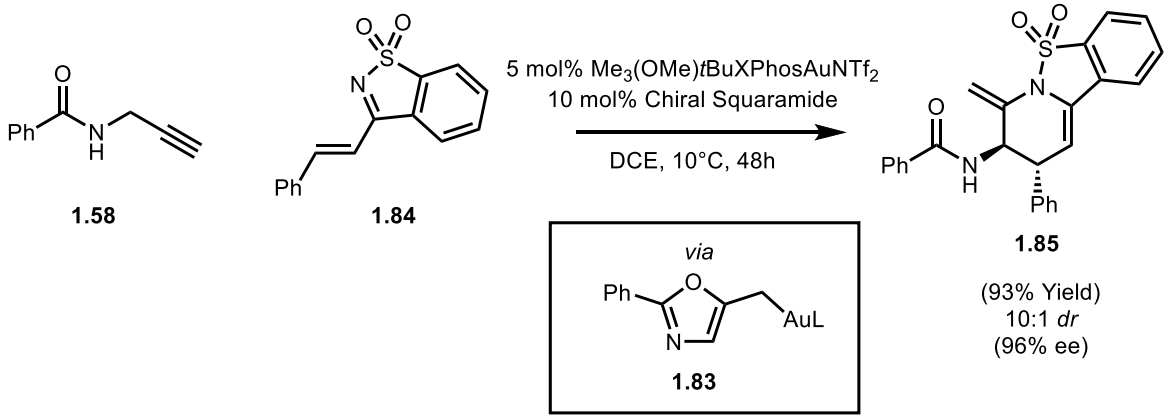

Figure 52 [4+2] Cycloaddition with Alkylgold

Similar to their previous report, mechanistic experiments were performed to affirm the presence of alkylgold intermediates of type **1.83**. The reaction of **1.58** and **1.84** absent any organocatalyst yielded only alkylideneoxazoline **1.59**, whereas their treatment with squaramide organocatalyst in the absence of gold returned only starting material. Just as in the previous study, treatment of alkylideneoxazoline **1.59** with cycloaddition partner **1.84** in the presence of the organocatalyst also returned starting material. When the reaction in **Figure 51** was performed with **1.83** in place of the typical Au catalyst, **1.85** was formed in high yield, %ee, and *dr*. Lastly, carrying out the reaction under acidic conditions yield only **1.59** as a product, indicating the formation of alkylgold **1.83** must proceed under neutral or basic conditions. All of these experiments pointed, again, to the role of **1.83** as a key intermediate. DFT calculations were performed propose a potential mechanistic pathway to cycloadduct **1.85**, which is shown in **Figure 52** as a stepwise [4+2] cycloaddition (squaramide catalyst omitted for clarity).

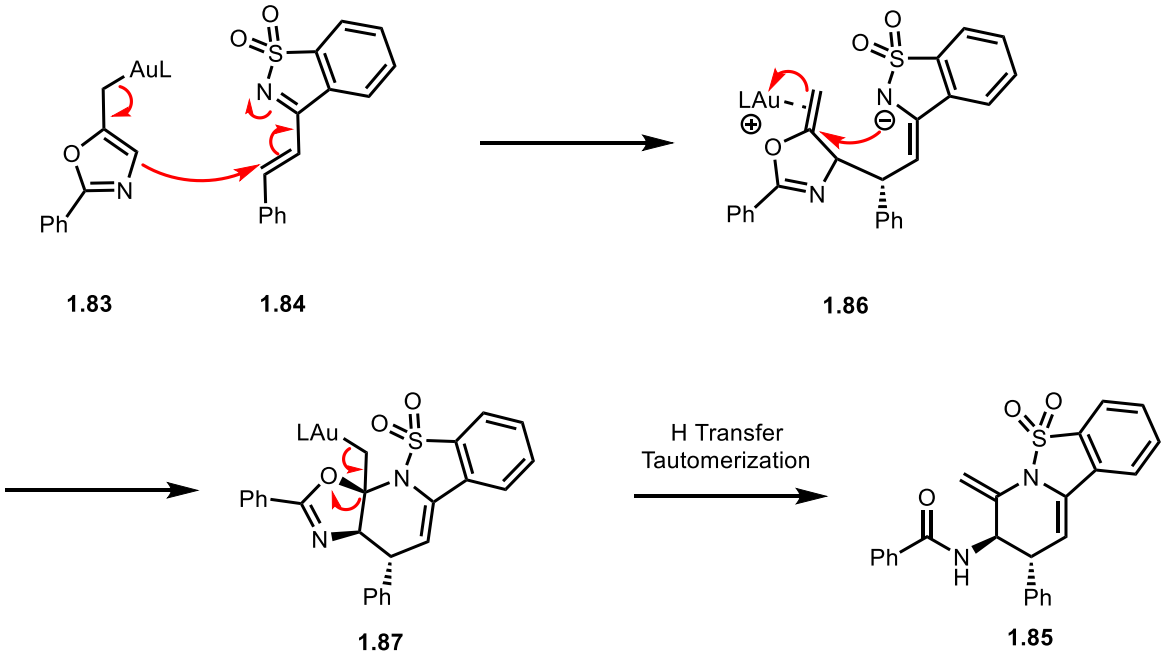

Figure 53 Mechanism of Stepwise [4+2] Cycloaddition

First, elimination of Au(I) pushes electrons into the ring to reform the alkylideneoxazoline and catalyze addition to sulfonamide **1.84**, giving intermediate **1.86**. The resulting anionic nitrogen and π-coordination by gold open the newly formed alkene to ring-closing attack, forming new alkylgold species **1.87**. Another elimination of gold(I) reestablishes aromaticity and, after proton transfer and tautomerization, regenerates the benzamide moiety and yields final product **1.85**.

Conclusion

The many studies detailed above provide a comprehensive background for the Au(I) catalyzed activation of alkynes. Typical and atypical mechanisms are shown. Discussion of common degradation products such as gem-digolds allows a glimpse into how and why catalysis sometimes fails. Finally, the cyclization of N-propargyl benzamide as a tremendously popular benchmarking reaction has been

discussed at length. While there is broad consensus on the characteristics of the reaction, some reports are conflicting. Rate-limiting protodeauration is consistent with more electron-donating ligands and less-coordinating anions with stronger conjugate acids, but the inverse of these trends have been observed and reported. Solvent effects, outside of potent H-bonders such as HFIP, are relatively understudied and poorly understood. Lastly, the cyclization has a demonstrated use as a scaffold for functionalization during or after a Au(I) catalytic cycle. In summary, the reaction has seen bountiful use in the past two decades as a proving ground for myriad new catalytic systems and transformations.

Chapter 2: Mechanistic Analysis of the Au(I)-Catalyzed Cyclization of N-Propargyl Benzamide

Introduction

The work describing examination of reaction kinetics in this chapter has been published in the Journal of Organic Chemistry. (Norman, S. G., Jiao, L., Yi, J. Ding, W., Jones. A. C., Solvent-Dependent Change in the Rate-Determining Step of Au(I) Catalyzed N-Propargyl Benzamide Cyclization, *Accepted Submission to J. Org. Chem.*, **2025**. DOI: 10.1021/acs.joc.5c00787)

As discussed in the previous chapter, the gold-catalyzed cyclization of N-propargyl benzamide to its corresponding alkylidene oxazoline was first published in 2004 by Hashmi.[78] In the decades since, it has become an exceedingly common benchmarking reaction for assessing the role of ligand,[49,79–92] anions,[50,51,61,93–97] additives,[54–58,65,98–101] solvents,[68,69,102] and downstream transformations.[70–72,74–77] Overwhelmingly, the literature consensus is in support of protodeauration as the rate-limiting step.[51,74,103–105] Given its immense popularity as a benchmark and test reaction, many conclusions have been made on the basis of this consensus. These conclusions often grow to carry weight in the field of gold (I) catalysis as a whole, extending the impact of these conclusions outside of the systems in which they were assessed. As has been discussed briefly earlier in this work, the trends are inconsistent.

The Argument For and Against Rate-Limiting Protodeauration

As seen in chapter 1, the Hashmi group was able to isolate both the 6-endo and 5-exo-generated vinylgold species by performing the cyclization with stoichiometric gold and excess triethylamine.[106] While the 6-membered cycle could be isolated by purification on basic alumina, the 5-membered cycle could not be, with its structure only determinable by inference following demetallation in aqueous acetonitrile. The Shi group successfully isolated a variant of the 5-membered vinylgold by performing the reaction under similar conditions as Hashmi.[71]

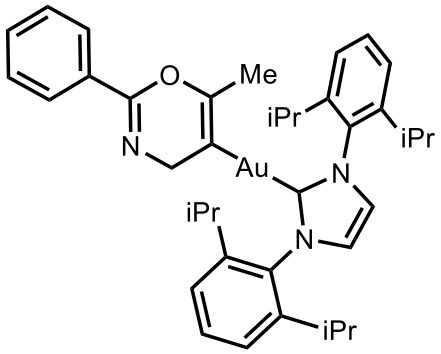

Hashmi, 2009

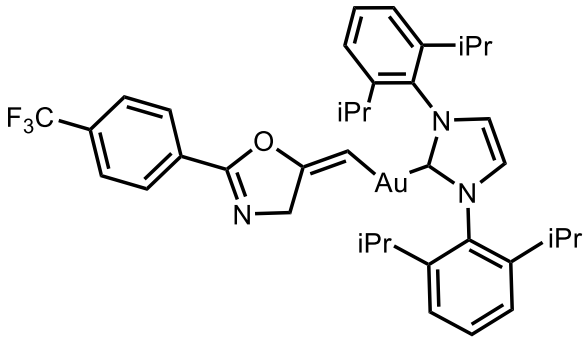

Shi, 2015

Figure 54 Benzamide-Derived Vinylgolds Isolated and Characterized

While the successful isolation of these species does not intrinsically define protodeauration as rate-limiting, it does provide ample support for the intermediacy of a vinylgold which can be captured under strongly basic conditions. Notably, the species above represent the only two vinylgolds ever successfully isolated and characterized for this cyclization, both bearing the same NHC ligands. Contrary to other systems, e.g. Hammond's report of the first successful isolation of vinylgolds in 2008,[107] phosphine-ligated vinylgolds have never been isolated for the propargyl

benzamide cyclization. In their seminal report on ligand effects, Hammond and Xu proposed a vinylgold resting state on the basis of a ^{31}P resonance observed throughout the course of the reaction.

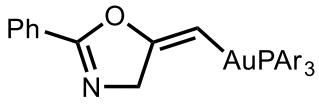

Figure 55 Vinylgold Proposed by Hammond

The chemical shift of the proposed resting state is never mentioned directly in the text, instead only being referred to in a scheme, which shows the structure in **Figure 55** with a proposed shift of -42ppm. Other reports of vinylgolds where L = PPh_3 place this chemical shift in the positive 40s, not negative. (For a representative example, see the triphenylphospine-ligated vinylgold isolated by Gagne where δ = 43.0ppm.[42]) Therefore, it's reasonable to conclude this was a typo on the part of the authors and the number observed was 42. In addition, the authors make no mention in the text of what specific triaryl phosphine ligand is being used in the scheme. Four different catalysts in the ligand survey are a potential match, but a stronger argument would show the ligands and the expected δ range. No clarity is found in the supplemental, as no spectroscopic data was provided. It remains unclear exactly which ligand gives rise to this observed ^{31}P resonance. In their report on gold catalysis with H-bonding additives,[108] they again propose the vinylgold as the resting state where L = PPh_3. ^{31}P NMR spectroscopic data *is* provided in this case, but the shifts observed lie in the 44-45ppm range, not 42. Somewhat conspicuously, those shifts lie closer to proposed bisphos (L-Au-L) decomposition products.[109] These composition products are generally considered

to be catalytically inert, however, and the resonance at 44-45ppm range in Hammond's spectra does vanish over the course of the reaction profile. Unfortunately, no ^{1}H spectra of the reaction mixtures are provided, meaning we cannot assess those spectra to see if they reinforce a resting vinylgold intermediate. Regardless, the proximity of the observed ^{31}P resonances to other reported species, the scarcity of data provided with which we can analyze them, and the inability to isolate them under the same reaction conditions used to afford the AuIPr vinylgolds in **Figure 54** does weaken the argument for rate-limiting protodeauration in the case of phosphine-ligated Au(I) catalysts.

Computational work supporting rate-limiting protodeauration for the N-propargyl benzamide cyclization has also been reported. In their work detailing the use of green solvents, the Zuccaccia group performed DFT calculations which supported demetallation as rate-limiting for the reaction.[102] Computed energy barriers for the protodeauration step exactly corresponded to their observed rates for a survey of anion. The lowest computed barriers corresponded to the fastest reactions. In 2022, Ma and coworkers published a purely computational paper studying the effects of various NHC ligands in which they also found the protodeauration step to be rate-limiting.[104] Intriguingly, they computed the reaction to be autocatalytic, proposing that the nitrogen of the oxazoline product acts as a shuttle for protonation of vinylgolds.

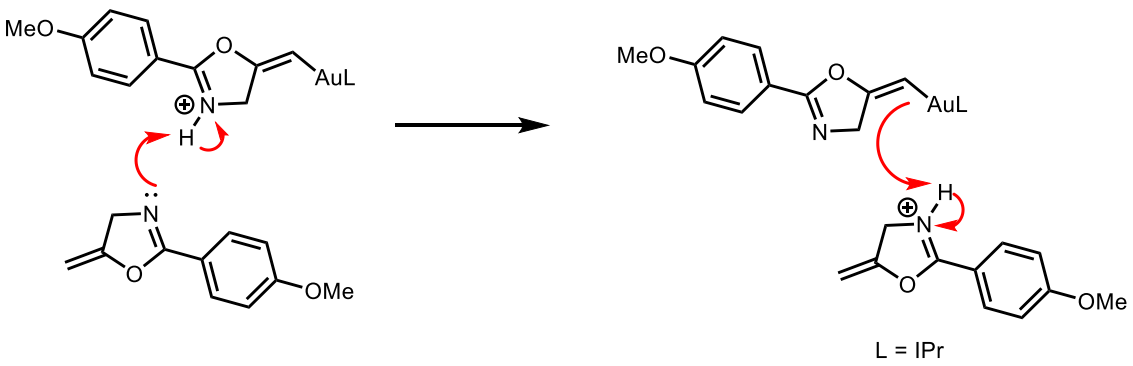

Figure 56 Autocatalytic Protodeauration

While this is the conclusion reached computationally, experimentally, autocatalysis by the product would likely be expected to hasten the reaction over time, leading to a nonlinear reaction rate. One year later, the same group published a computational survey of anions for the transformation, again finding protodeauration to be rate-limiting.[105] In this paper, they specifically argue that tosylate is a poor choice of anion in chloroform as its higher basicity relative to other common anions results in the competitive backwards reaction in which the ring of the oxazoline is reopened, regenerating the gold-alkyne π-complex.

As discussed in chapter 1, ligand effects also conflict. In the case of Barta's ferrocene[49] and Hashmi's KITPHOS[79] ligands, reaction rates quickened with more inductively-withdrawing phosphines, contrasting with rate-limiting protodeauration as the resulting Au(I) species would be expected to be higher in energy. At the same time, Hammond's paper on ligand effects saw the opposite trend, with the more electron-rich phosphines cleanly outpacing the electron-poor.[103]

Survey of Ligand and Anion Effects in N-Propargyl Benzamide Cyclization

To provide clarity on these conflicting trends observed in the literature, N-propargyl benzamide **2.1** was cyclized in the presence of various catalysts to afford oxazoline **2.2**. Rates were determined by monitoring reaction progress by ^{1}H NMR at consistent intervals.

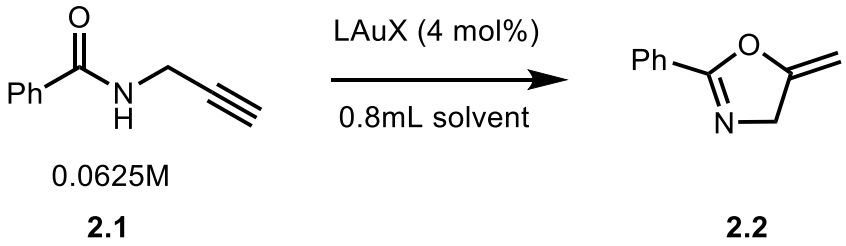

Figure 57 Conditions for Benzamide Cyclization

Reactions were first performed in dichloromethane. Depending on which particular reaction is being discussed, the dichloromethane was either protonated or deuterated. To ensure a lack of a solvent kinetic isotope effect, multiple trials were performed with catalyst **C1** and **C2**. Whether CH_2Cl_2 or CD_2Cl_2 is used was determined to have no impact on rate for the cyclization under these conditions (see **Tables I** and **II**). Ligands assessed are shown in **Figure 58** below. Choice of anion was varied and will be discussed on a case-by-case basis.

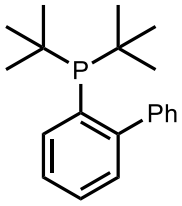

L1 (Johnphos)

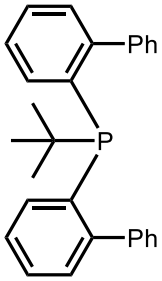

L2

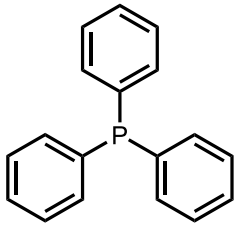

L3

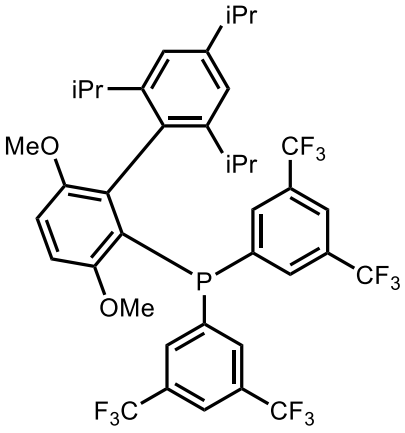

L4 (Jackiephos)

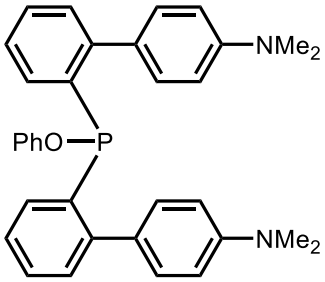

L5

Figure 58 Ligands used in Benzamide Cyclization Studies

Propargyl Benzamide Cyclization in Dichloromethane

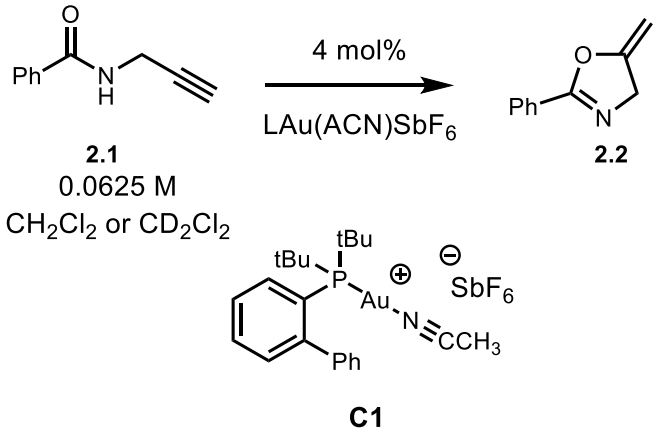

Figure 59 Cyclization of **2.1** in the Presence of **C1**

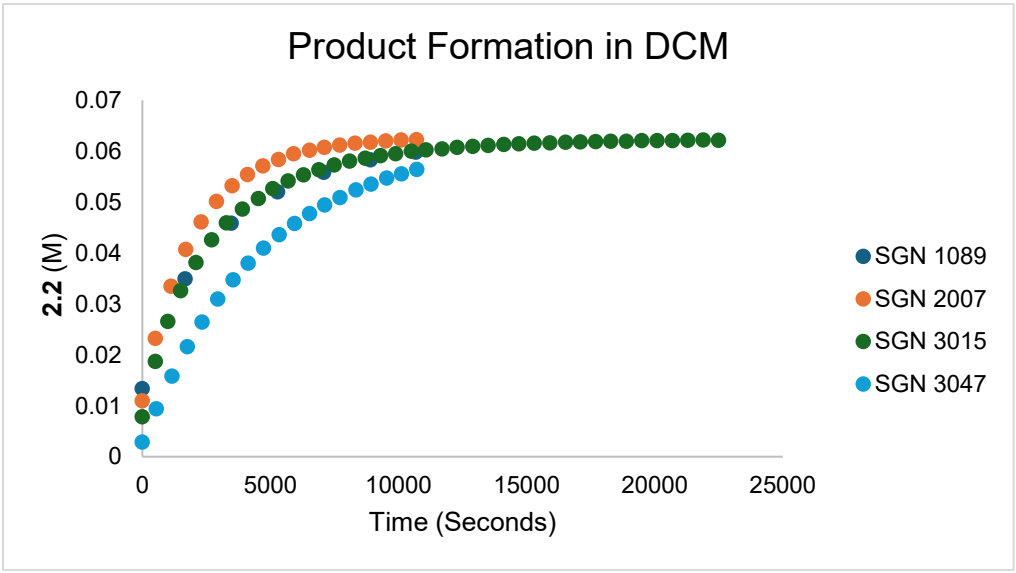

Figure 60 Change in **2.2** Concentration in DCM in the Presence of **C1**

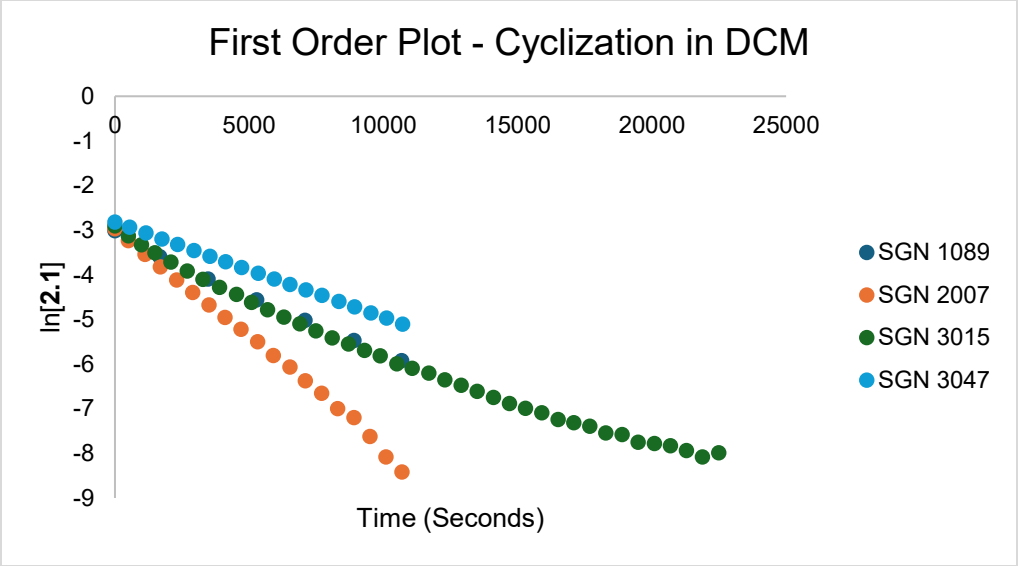

Figure 61 First Order Decay of **2.1** in DCM in the Presence of **C1**

	Solvent	**Catalyst Amount**	**Catalyst Loading**	$k_{obs/S}^{-1}$
SGN 1089	0.8 mL CD_2Cl_2	0.002 mmol	4 mol%	$2.68 \times 10^{-4} \pm 6.25 \times 10^{-6}$
SGN 2007	0.8 mL CD_2Cl_2	0.002 mmol	4 mol%	$4.93 \times 10^{-4} \pm 5.88 \times 10^{-6}$
SGN 3015	0.8mL CH_2Cl2	0.002 mmol	4 mol%	$2.26 \times 10^{-4} \pm 4.88 \times 10^{-6}$
SGN 3047	0.8mL CD_2Cl_2	0.002mmol	4 mol%	$2.13 \times 10^{-4} \pm 3.79 \times 10^{-7}$
Average Rate				$3.0 \times 10^{-4} \pm 4.35 \times 10^{-6}$

Table I Cyclization Rates of **2.1** in dichloromethane in the presence of C1

The reaction proceeds smoothly in dichloromethane in the presence of **C1**. As observed in the figures and **Table I** above, deuteration of the solvent is immaterial to the rate of cyclization, with the same average rate being observed regardless of whether CH_2Cl_2 or CD_2Cl_2 is used. The commercially available acetonitrile precatalyst was used due to the poor coordinating ability of the SbF_6 anion.

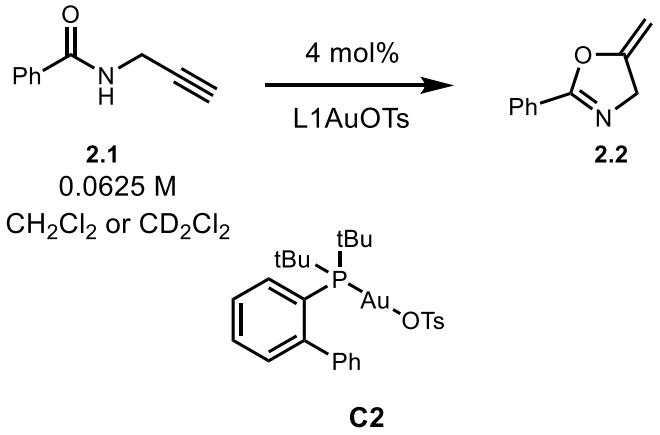

Figure 62 Cyclization of **2.1** in the presence of **C2**

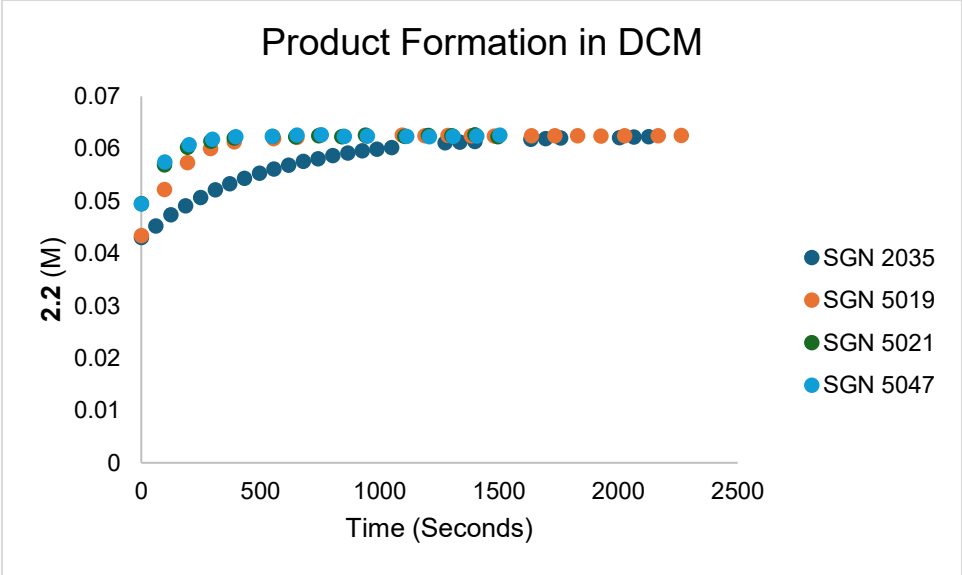

Figure 63 Change in **2.2** Concentration in DCM in the Presence of **C2**

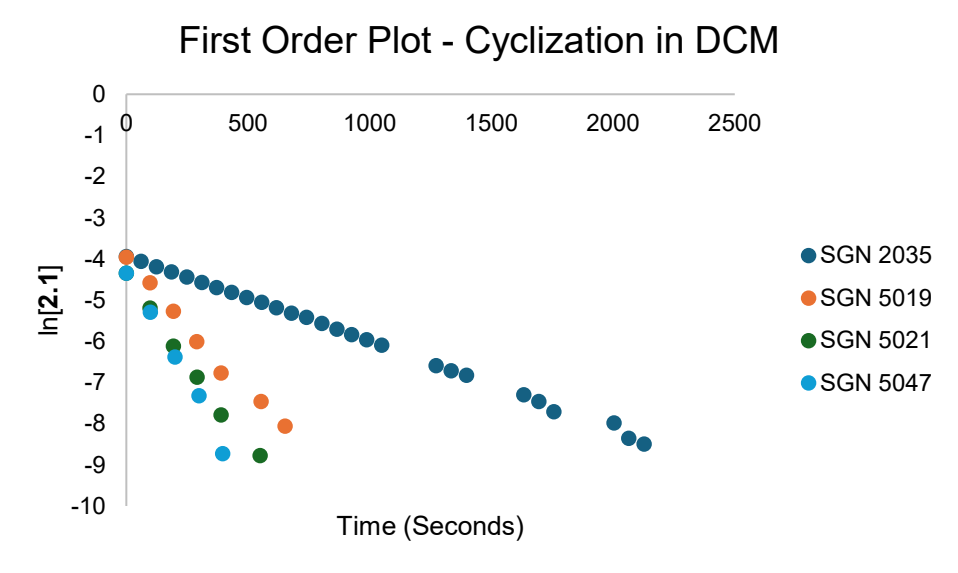

Figure 64 First Order Decay of **2.1** in DCM in the Presence of **C2**

	Solvent	**Catalyst Amount**	**Catalyst Loading**	$k_{obs/S}^{-1}$
SGN 2035	0.8 mL CD_2Cl_2	0.002 mmol	4 mol%	$2.11 \times 10^{-3} \pm 1.55 \times 10^{-5}$
SGN 5019	0.8 mL CH_2Cl_2	0.002 mmol	4 mol%	$6.34 \times 10^{-3} \pm 2.64 \times 10^{-4}$
SGN 5021	0.8mL CH_2Cl2	0.002 mmol	4 mol%	$8.18 \times 10^{-3} \pm 3.10 \times 10^{-4}$
SGN 5047	0.8mL CH_2Cl_2	0.002mmol	4 mol%	$1.09 \times 10^{-2} \pm 4.88 \times 10^{-4}$
Average Rate				$6.89 \times 10^{-3} \pm 2.69 \times 10^{-4}$

Table II Cyclization Rates of **2.1** in Dichloromethane in the Presence of **C2**

Reaction with **C2** is substantially faster than with **C1** (compare rates in tables **I** and **II**), demonstrating a substantial anion effect. First order plots are shown to the furthest point of linearity.

Summary Data of Propargyl Benzamide Cyclization in Dichloromethane

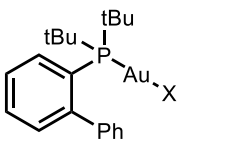

C1, X = $[NCCH_3]SbF_6$
C2, X = OTs
C3 X = OTf
C4 X = NTf_2

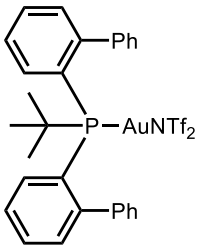

C5

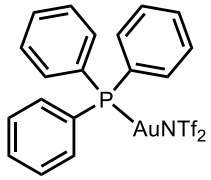

C6

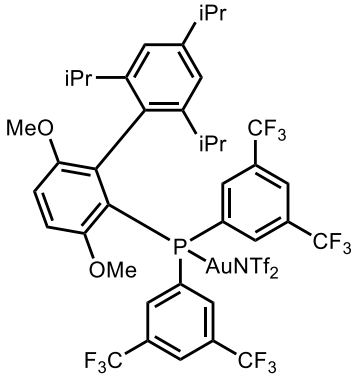

C7

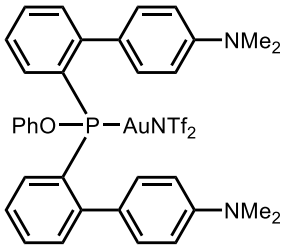

C8

Figure 65 Catalysts Used in Benzamide Cyclization

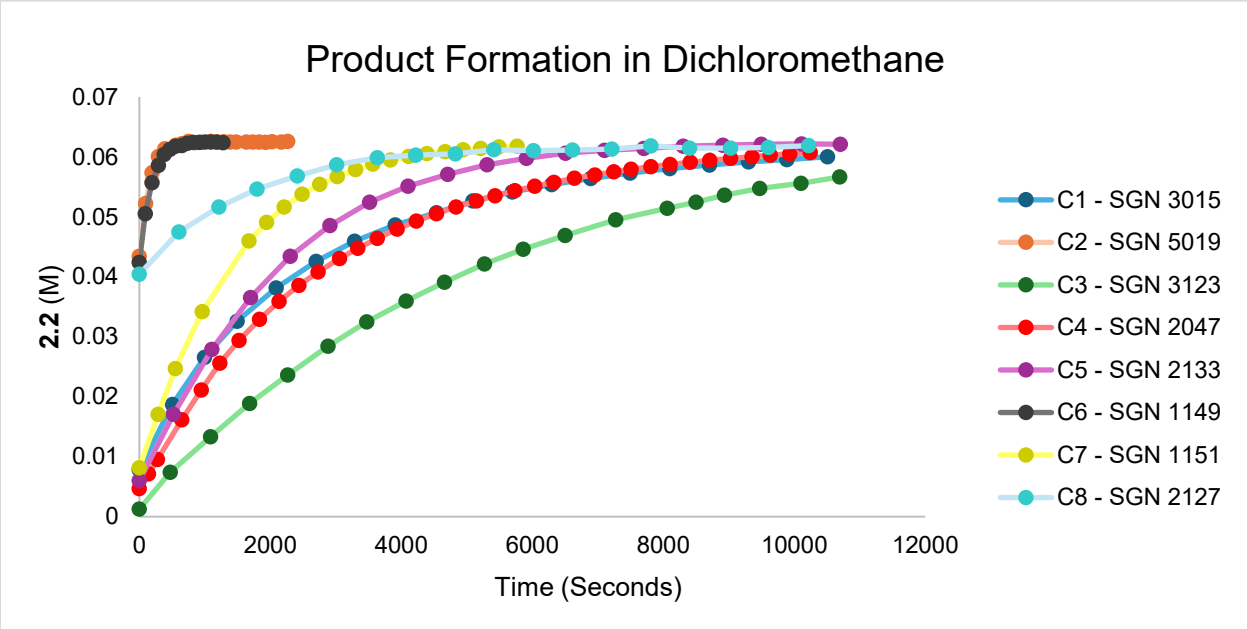

Figure 66 Comparative **2.1** Formation in Dichloromethane

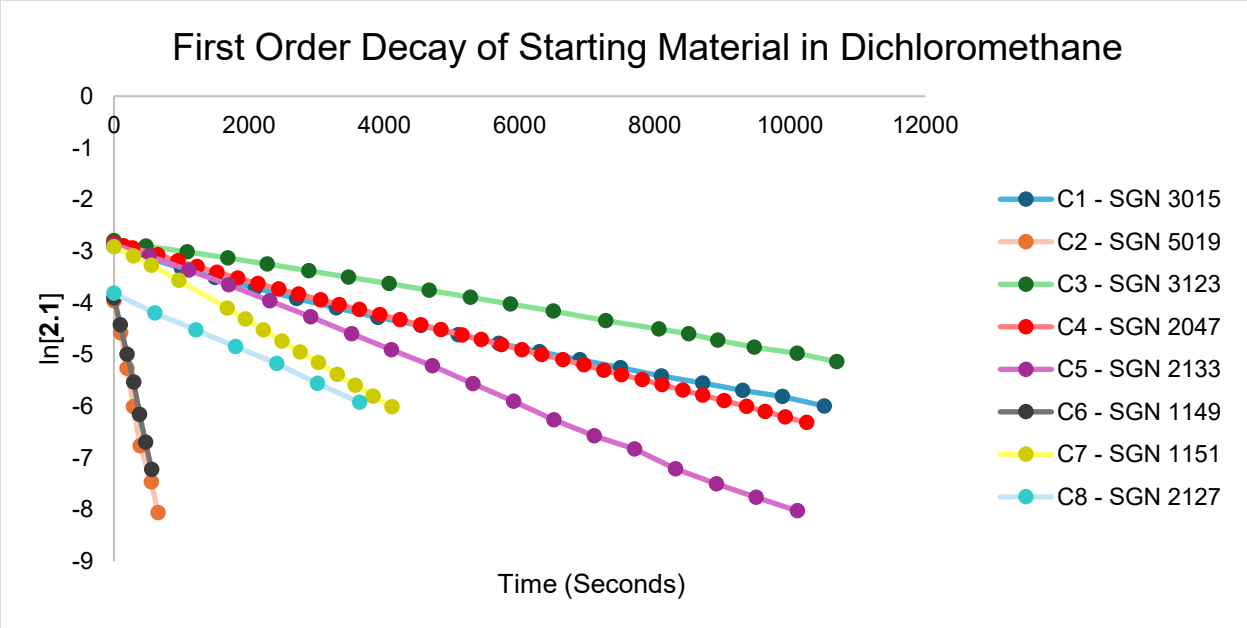

Figure 67 Comparative First Order Decay of **2.1** in Dichloromethane

Discussion of Benzamide Kinetics in Dichloromethane

As discussed earlier, the strong consensus amongst the field is that protodeauration (see **Figure 68** below) is rate-limiting for this cyclization. This comes with two important expectations for the behavior of the reaction depending on the choice of ligand and anion. First, the reaction is expected to proceed most quickly with an electron-donating ligand (e.g. **L1**, “Johnphos”). This stems from a lower relative energy of the Au(I) species, thereby lowering the energy barrier for protodeauration. Second, the reaction is expected to proceed more quickly with less basic, less strongly-coordinating anions. The reason for this is formation of a stronger conjugate acid, which is expected to more easily demetallate the vinylgold intermediate.

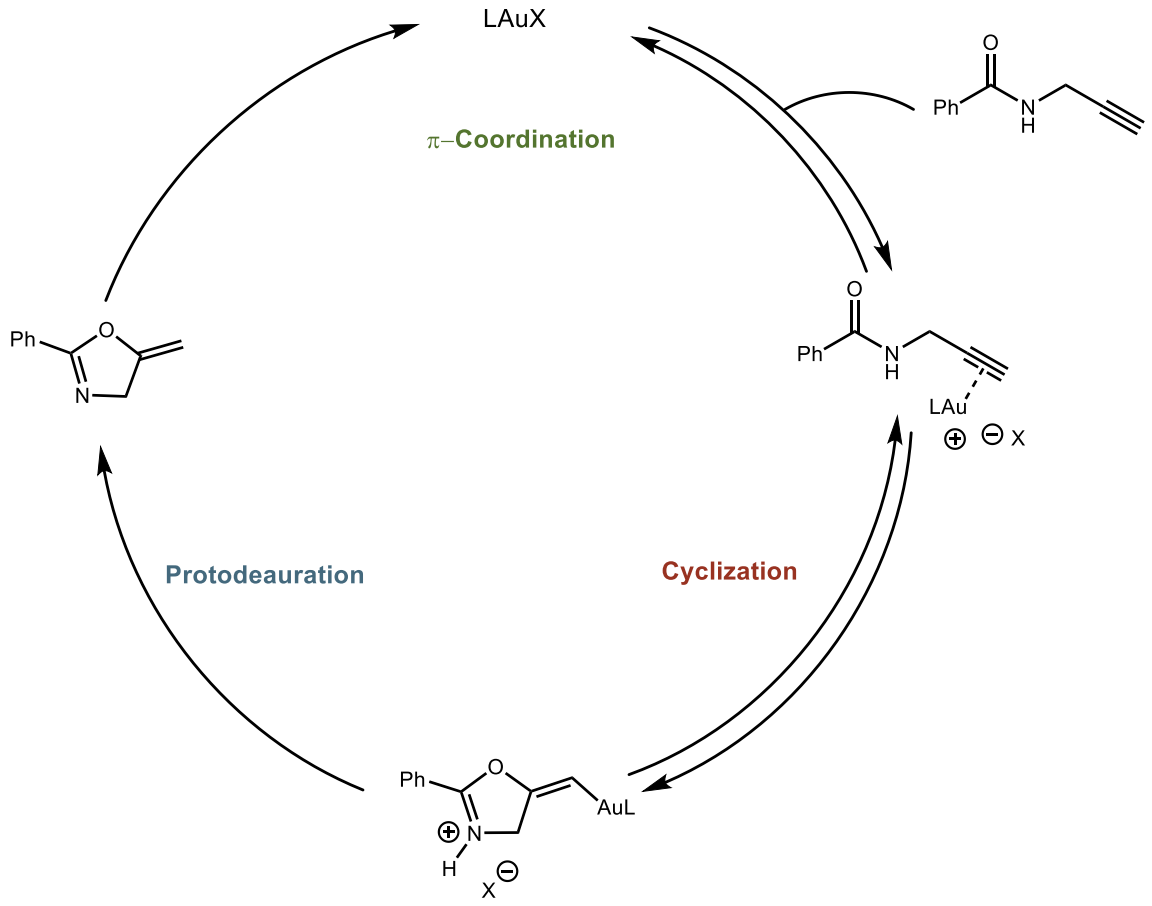

Figure 68 Mechanism of the N-Propargyl Benzamide Cyclization

Strikingly, neither of these expectations are met in this series of reactions, as seen in **Table III**.

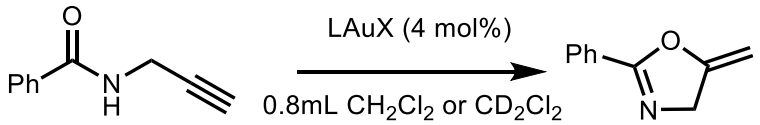

0.0625M

2.1 **2.2**

Entry	Catalyst	k_{obs}	Entry	Catalyst	k_{obs}
(1)	L1AuSbF$_6$[b]	1[a]	(5)	L2AuNTf$_2$	1.75
(2)	L1AuOTs	23.0[c]	(6)	L3AuNTf$_2$[c]	18.6
(3)	L1AuOTf	0.73	(7)	L4AuNTf$_2$	2.56
(4)	L1AuNTf$_2$	1.11	(8)	L5AuNTf$_2$	1.9

Table III Rates of **2.**1 cyclization in dichloromethane with various catalysts

[a]k_{rel} of entry 1 is defined $k_{obs} = (3.0 \times 10^{-4} \pm 4.35 \times 10^{-6})$

[c]k_{obs} of entry 2 is defined as $k_{obs} = (6.89 \times 10^{-3} \pm 2.69 \times 10^{-4})$

[b]precatalyst [L1Au(NCCH$_3$)]SbF$_6$ [d]precatalyst L3AuNTf$_2$·1/2 toluene

First, **L1**, Johnphos, is the most electron rich ligand surveyed, with all other ligands having less donating ability. Looking at entries 4-8, the triflimide anion is held constant. In this series, **L1** is the slowest performer, being universally outpaced by the more electron-starved phosphines. **L4** (Jackiephos) or **L5** would be expected to be the most inductive, and yet both outperform **L1** by a substantial margin. **L3**, triphenylphosphine, is remarkably fast in the transformation, but this could potentially be owed to a diminished steric profile. This observed trend directly contrasts with the consensus of rate-limiting protodeauration. Another notable datapoint is entry 2, reaction with **L1**AuOTs. There is a modest anion effect for Johnphos in entries 1, 2, and 4, but tosylate performs the reaction more than

twenty times faster than the baseline. Conspicuously, tosylate is the most basic of the anions surveyed. Again, a reaction with rate-limiting protodeauration is expected to be hastened by less basic anions due to the formation of a potent conjugate acid. Despite this, OTs is the fastest anion by far, again contrasting with expected behavior.

Impact of Methanol on N-Propargyl Benzamide Cyclization

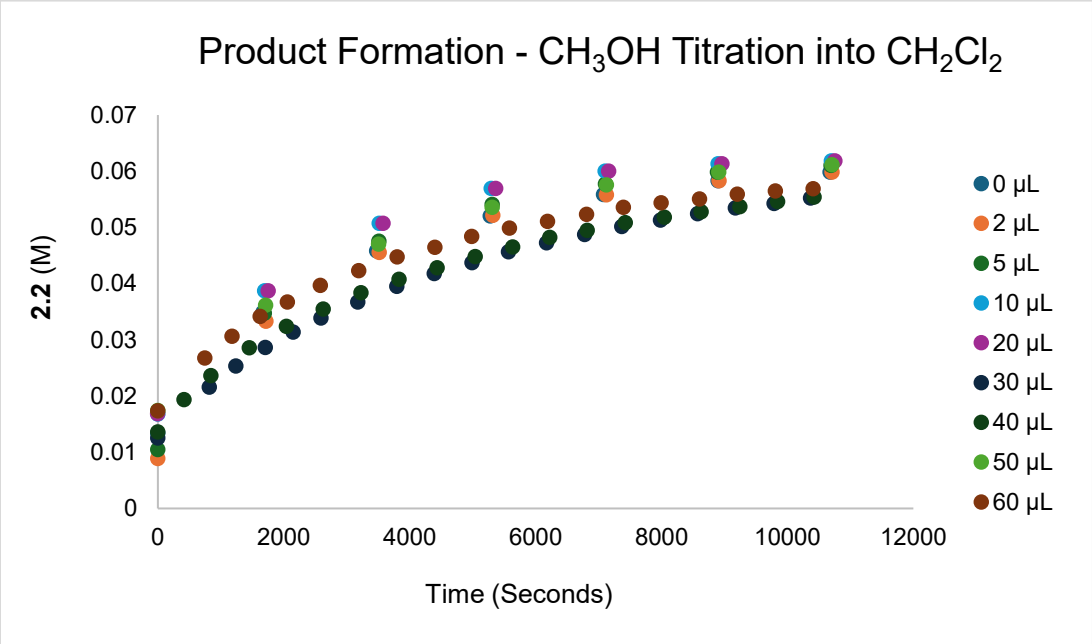

Figure 69 Product formation over time in presence of methanol titration and **C1**

The group had observed a substantial cosolvent effect in the context of Au(I)-catalyzed alkene hydroamination, finding small titrations of water or methanol into the reaction mixture afforded a faster rate.[110] Building on this result, a similar titration study was performed in the context of this reaction, wherein small volumes of methanol were titrated into a reaction mixture in dichloromethane. Methanol was added in increasing volume, from 2µL to 60µL and reacted in the presence of 4mol% **C1**. The results are shown in the figures and table below.

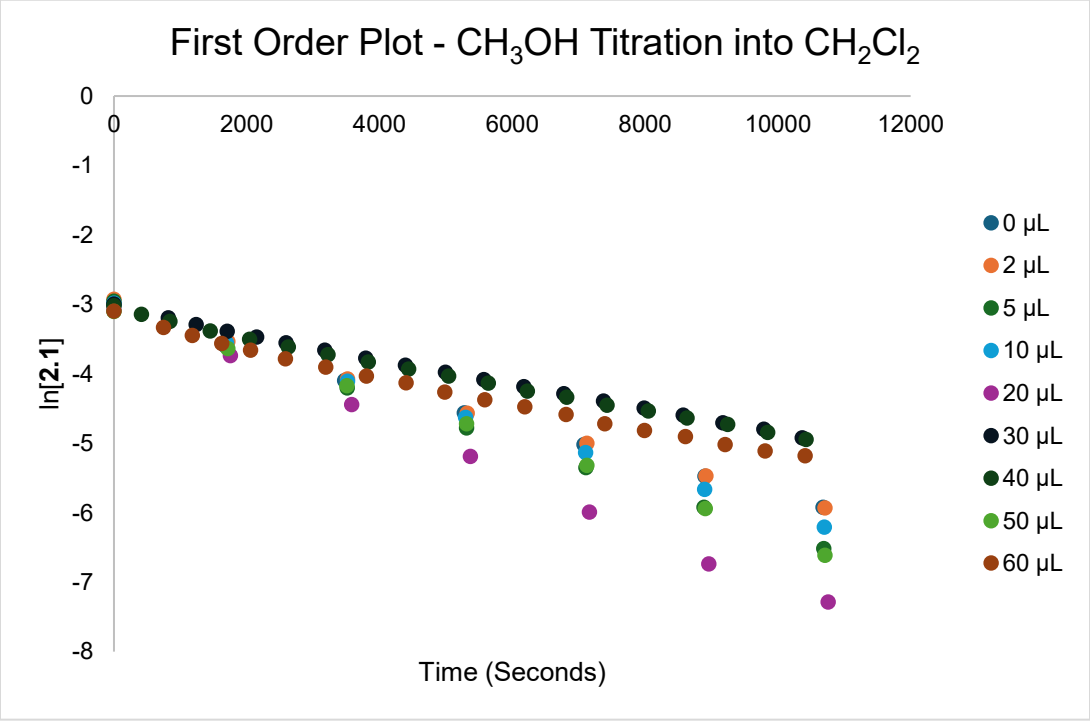

Figure 70 First order decay of **2.1** in the presence of **C1** with titrated methanol

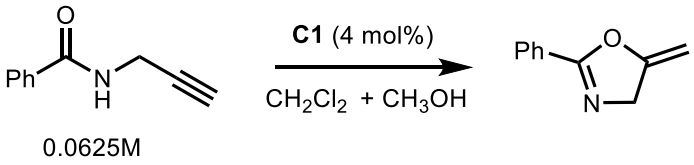

0.0625M

2.1 **2.2**

	CH_3OH Volume (µL)	**Catalyst Amount**	**Catalyst Loading**	**$k_{obs/S}^{-1}$**
SGN 1089	0	0.002 mmol	4 mol%	$2.68 \times 10^{-4} \pm 6.25 \times 10^{-6}$
SGN 1103	2	0.002 mmol	4 mol%	$2.76 \times 10^{-4} \pm 7.55 \times 10^{-6}$

SGN 1107	5	0.002 mmol	4 mol%	$3.23 \times 10^{-4} \pm 3.49 \times 10^{-6}$
SGN 1111	10	0.002 mmol	4 mol%	$2.97 \times 10^{-4} \pm 3.14 \times 10^{-6}$
SGN 1101	20	0.002 mmol	4 mol%	$4.0 \times 10^{-4} \pm 7.03 \times 10^{-6}$
SGN 4139	30	0.002 mmol	4 mol%	$1.8 \times 10^{-4} \pm 1.68 \times 10^{-6}$
SGN 4143	40	0.002mmol	4 mol%	$1.79 \times 10^{-4} \pm 2.44 \times 10^{-6}$
SGN 1113	50	0.002 mmol	4 mol%	$3.25 \times 10^{-4} \pm 6.01 \times 10^{-6}$
SGN 4147	60	0.002 mmol	4 mol%	$1.96 \times 10^{-4} \pm 3.83 \times 10^{-6}$

Table IV Rates of **2.1** cyclization in dichloromethane with **C1** and titrated methanol

As evidenced in the plots and tables above, methanol titrations have no visible impact on the cyclization of **2.1** to **2.2**. Variations in rate are seemingly random, showing no correlation with the amount of titrated methanol. Even at a titration volume of 60μL, at which point the ratio of methanol to starting material is nearly 30:1, no rate impact is observed. Therefore, unlike our observation of methanol titration in the case of alkene hydroamination, there appears to be no direct involvement of methanol in the mechanism.

To further probe solvent effects, the cyclization was performed with pure methanol as the solvent. The results of these experiments are summarized in the figures and tables below.

Summary Data of Propargyl Benzamide Cyclization in Methanol

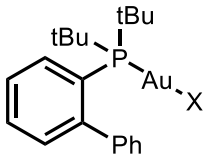

C1, X = $[NCCH_3]SbF_6$
C2, X = OTs
C3 X = OTf
C4 X = NTf_2

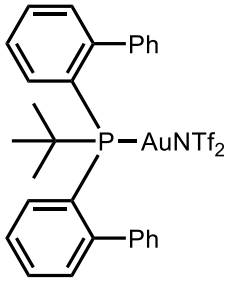

C5

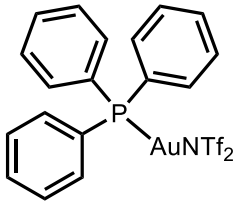

C6

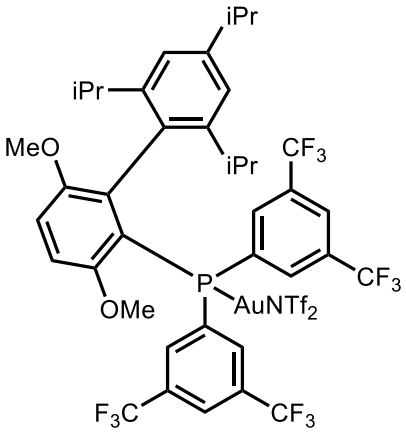

C7

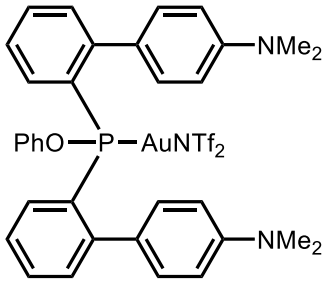

C8

Figure 71 Catalysts Used in Benzamide Cyclization

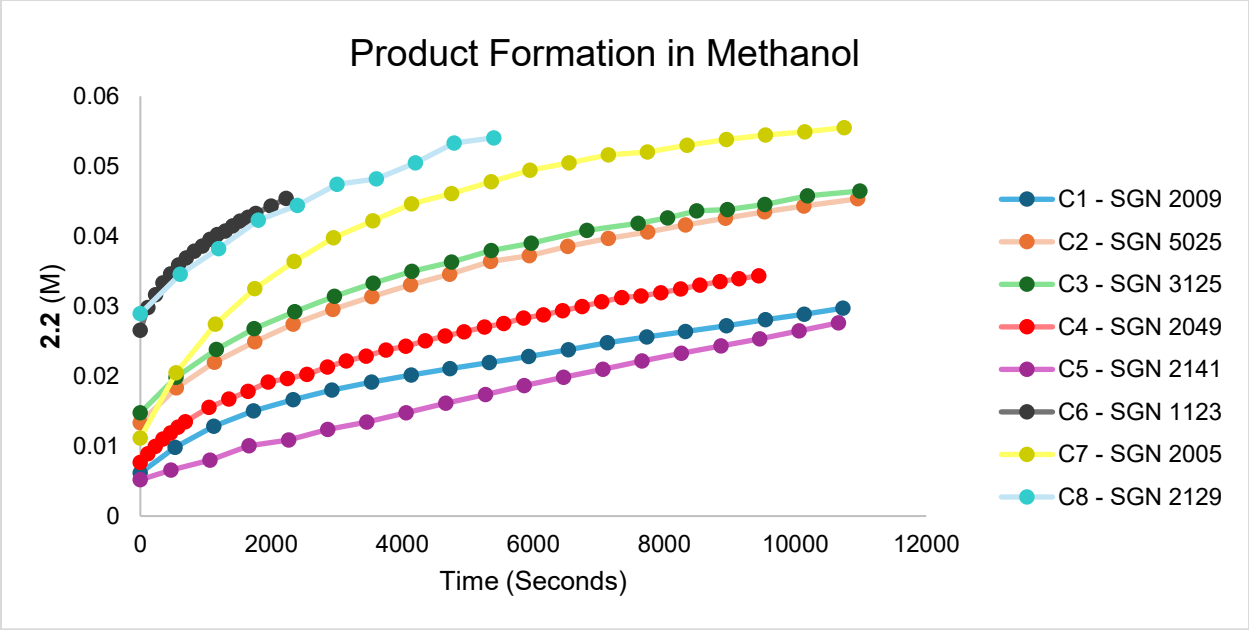

Figure 72 Comparative **2.1** Formation in Methanol

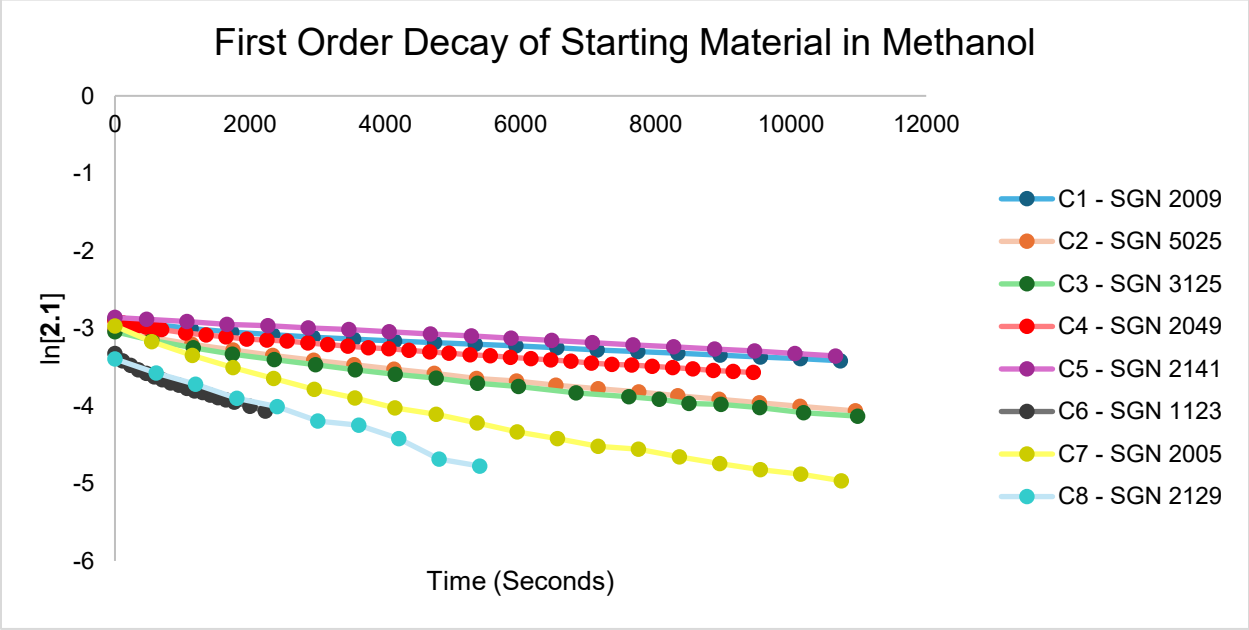

Figure 73 Comparative First Order Decay of **2.1** in Methanol

Discussion of Benzamide Kinetics in Methanol

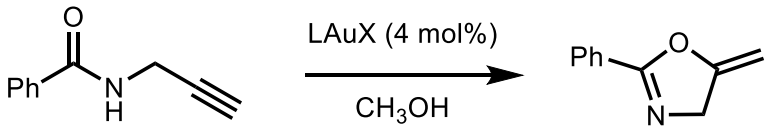

0.0625M

2.1 **2.2**

Entry	Catalyst	k_{obs}	Entry	Catalyst	k_{obs}
(1)	L1AuSbF$_6$[b]	0.12	(5)	L2AuNTf$_2$	0.15
(2)	L1AuOTs	0.21	(6)	L3AuNTf$_2$[c]	1.07
(3)	L1AuOTf	0.31	(7)	L4AuNTf$_2$	0.60
(4)	L1AuNTf$_2$	0.22	(8)	L5AuNTf$_2$	0.84

Table V Rates of **2.1** cyclization in CH3OH with various catalysts

[a]k_{rel} of (entry 1) is defined k_{obs} = (3.0 x 10^{-4}±4.35 x 10^{-6}), the average rate of L1AuSbF$_6$ in dichloromethane

[b]precatalyst [L1Au(NCCH$_3$)]SbF$_6$ [c]precatalyst L3AuNTf$_2$·1/2 toluene

Cyclization in CH$_3$OH is invariably slower than cyclization in dichloromethane. Many reactions do not achieve 50% conversion even in the timespan of three hours, where most reactions in dichloromethane are at or near 100% conversion by the same time. A combination of **Tables III** and **V** are shown in **Table VI**, showing the enormous reduction in rate across the two solvents.

Entry	Catalyst	$k_{rel}(CH_2Cl_2)$	$K_{rel}(CH_3OH)$
(1)	L1AuSbF$_6$[b]	1[a]	0.12
(2)	L1AuOTs	23.0[c]	0.21
(3)	L1AuOTf	0.73	0.31
(4)	L1AuNTf$_2$	1.11	0.22
(5)	L2AuNTf$_2$	1.75	0.15
(6)	L3AuNTf$_2$[d]	18.6	1.07
(7)	L4AuNTf$_2$	2.56	0.60
(8)	L5AuNTf$_2$	1.9	0.84

Table VI Rates of **2.1** cyclization in dichloromethane and methanol

[a]k_{rel} of 1 (entry 1) is defined defined k_{obs} = (3.0 x 10^{-4}±4.35 x 10^{-6}), the average rate of L1AuSbF$_6$ in dichloromethane

[c]k_{obs} for entry 2 in dichlormethane defined as k_{obs} = (6.89 x 10^{-3}±2.69 x 10^{-4})

[b]precatalyst [L1Au(NCCH$_3$)]SbF$_6$ [c]precatalyst L3AuNTf$_2$·1/2 toluene

Visibly, there is a substantial solvent effect when methanol is used. While the titrations had virtually no impact on the rate of product formation, the impact when methanol is the pure solvent is enormous. Most catalysts gives rates one tenth or less their original rate. There is an especially large impact on **C2** and **C6**. **C6** is reduced approximately one seventeenth its original rate. **C2**, the fastest catalyst in dichloromethane, has its rate cut by a factor of more than 100. This is likely owed to the relatively high basicity of OTs relative to other anions surveyed, which becomes more problematic in protic solvent. The anion effect for the **L1**-

based catalysts is minimized, with all of them now giving very similar rates. **C8** is less starkly affected than the rest, giving a rate closer to its rate in DCM than the other catalysts do. This is potentially due to a reduction in degradation products (see discussion in chapter 3). While the reaction is sluggish in methanol relative to DCM, the general trend is still observed, with the less electron poor ligands still giving faster rates than the electron rich. What is most intriguing is that the reaction is slow in methanol in the first place. If the protodeauration step is taken to be rate-limiting, a protic solvent such as methanol might be expected to hasten the reaction, not slow it down.

The Impact of Deuterated Methanol

In addition to the impact of methanol as a cosolvent, the group had also previously observed a substantial solvent kinetic isotope effect in the context of alkene hydroamination.[110] Inspired by this previous discovery, the cyclization of **2.1** was repeated in CD_3OD. For catalyst **C1**, there is an additional order of magnitude decrease relative to the same conditions in CH_3OH, and a 100-fold decrease relative to the same conditions in dichloromethane. The reaction is so slow that a 12-hour kinetic experiment captured only ~12% conversion and the reaction was incomplete even after 11 days.

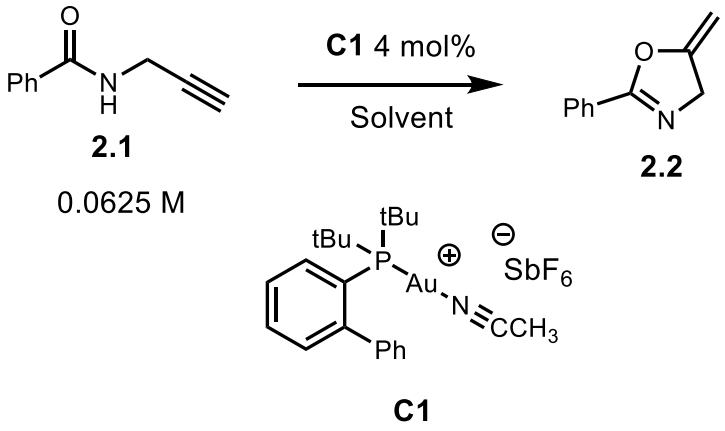

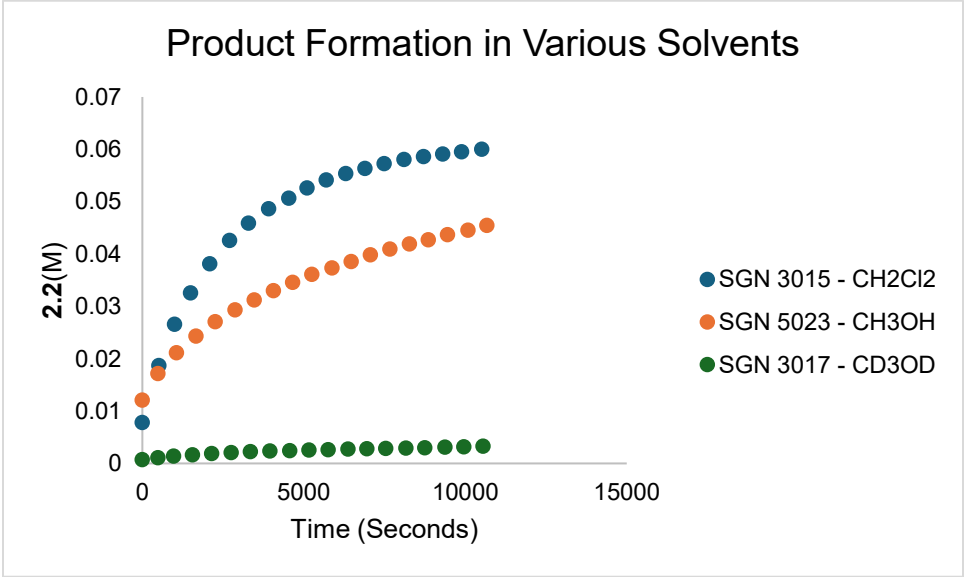

Figure 74 Product **2.2** formation in various solvents in the presence of **C1**

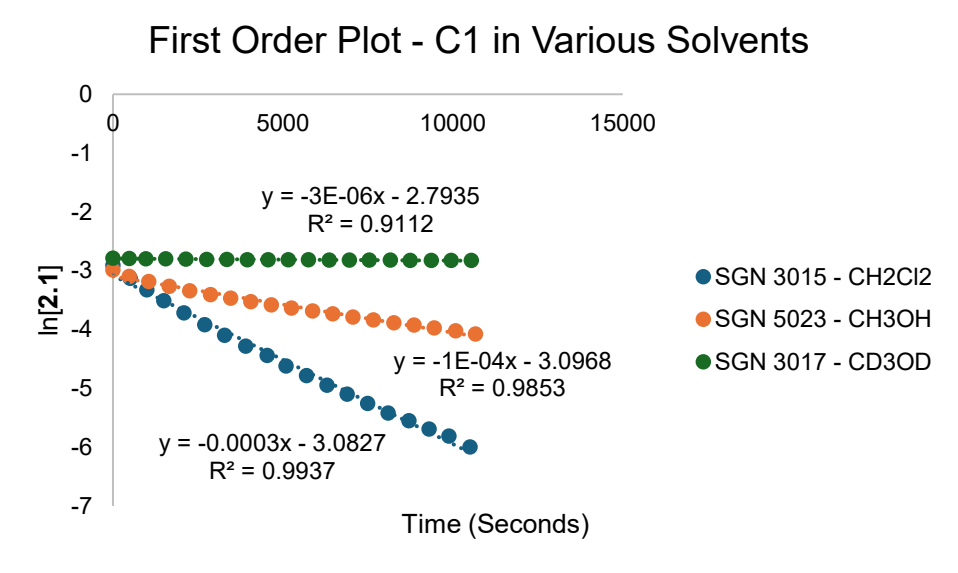

Figure 75 First order decay of **2.1** in various solvents in the presence of **C1**

As the reaction with **C1** in CD_3OD slowly cyclized over the course of several days, changes were noted in the ^1H NMR spectrum of the mixture. Unsurprisingly, the NH resonance disappears due to deuterium exchange with the solvent. The result of this is simplification of the N-bonded methylene signal, which reduces from a doublet of doublets to a doublet. In the product, the same methylene is endocyclic and gives an apparent triplet as its signal due to the J^4 cis and trans couplings to the exocyclic vinyl protons being approximately the same. In deuterated solvent, the triplet simplifies to a doublet due to the loss of one J^4 coupling partner as it is replaced by deuterium. Comparative

spectra are shown in the figures below.

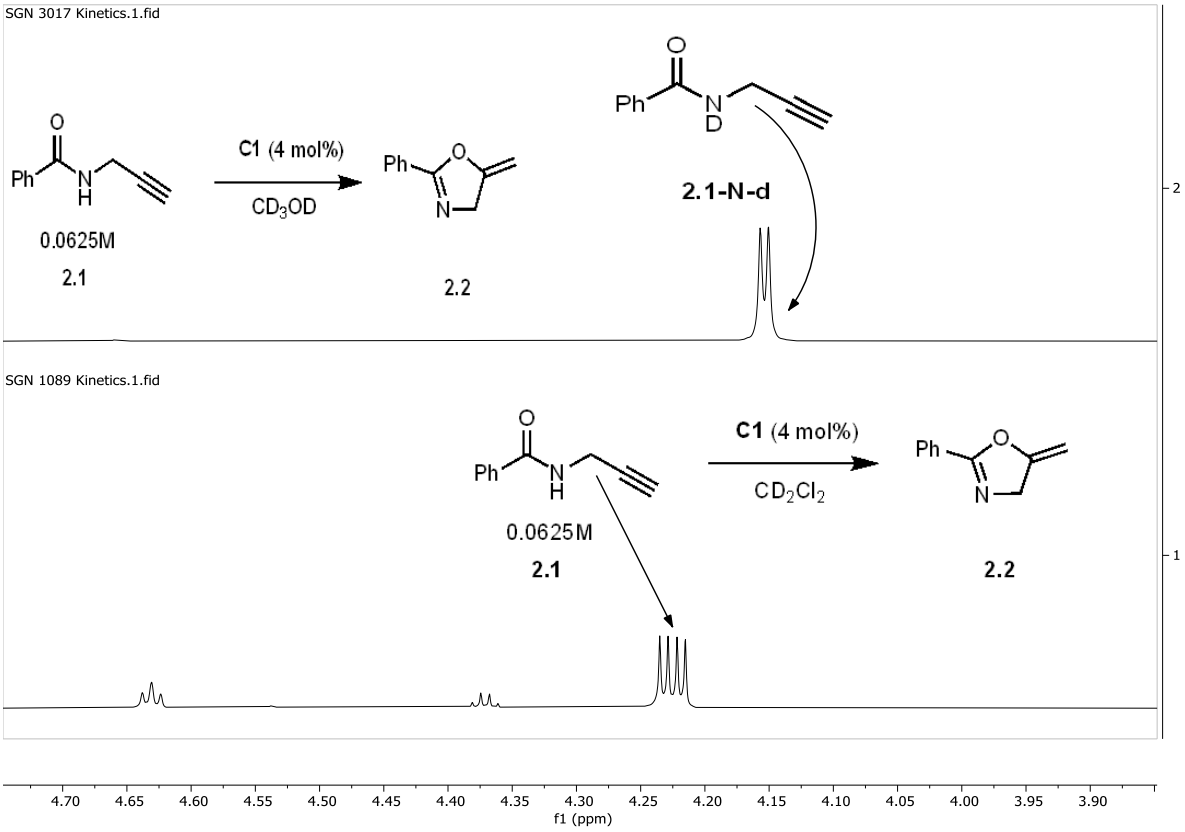

Figure 76 Simplification of Starting Material Peaks in CD3OD at Zero Minutes of Reaction Time

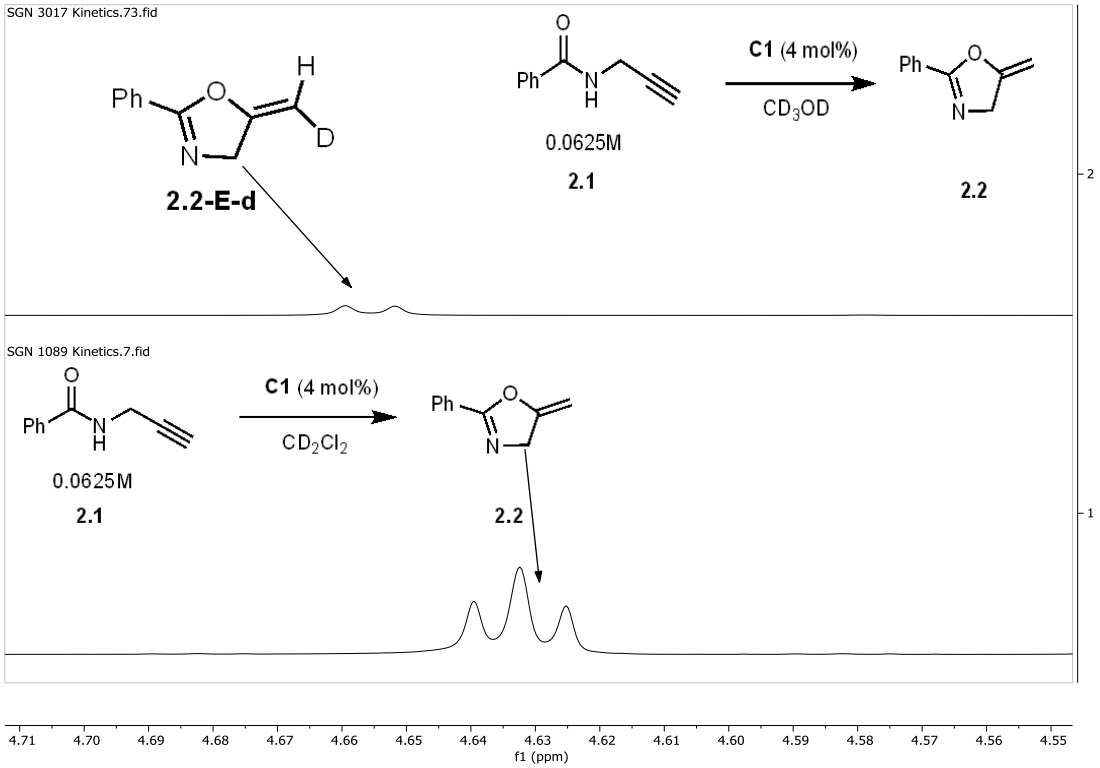

Figure 77 Simplification of Product Peaks in CD3OD

Taken in isolation, this result is not remarkable. The labile NH proton will obviously readily exchange with the deuterium in the solvent, and that same proton is the one which then needs to move throughout the reaction course to regenerate the gold(I) catalyst and afford the final product. Deuteration at the alkene of **2.2** trans to the oxygen would be expected in this case. What was more surprising was the observation that, as the reaction slowly proceeds over multiple days, the integrals of the methylene in **2.1** and the CH terminus no longer integrate 2:1, with the CH integral gradually shrinking over time relative to the CH_2 integral. The effect of this could also be observed at the CH_2, which becomes lopsided as an apparent singlet appears underneath its usual doublet.

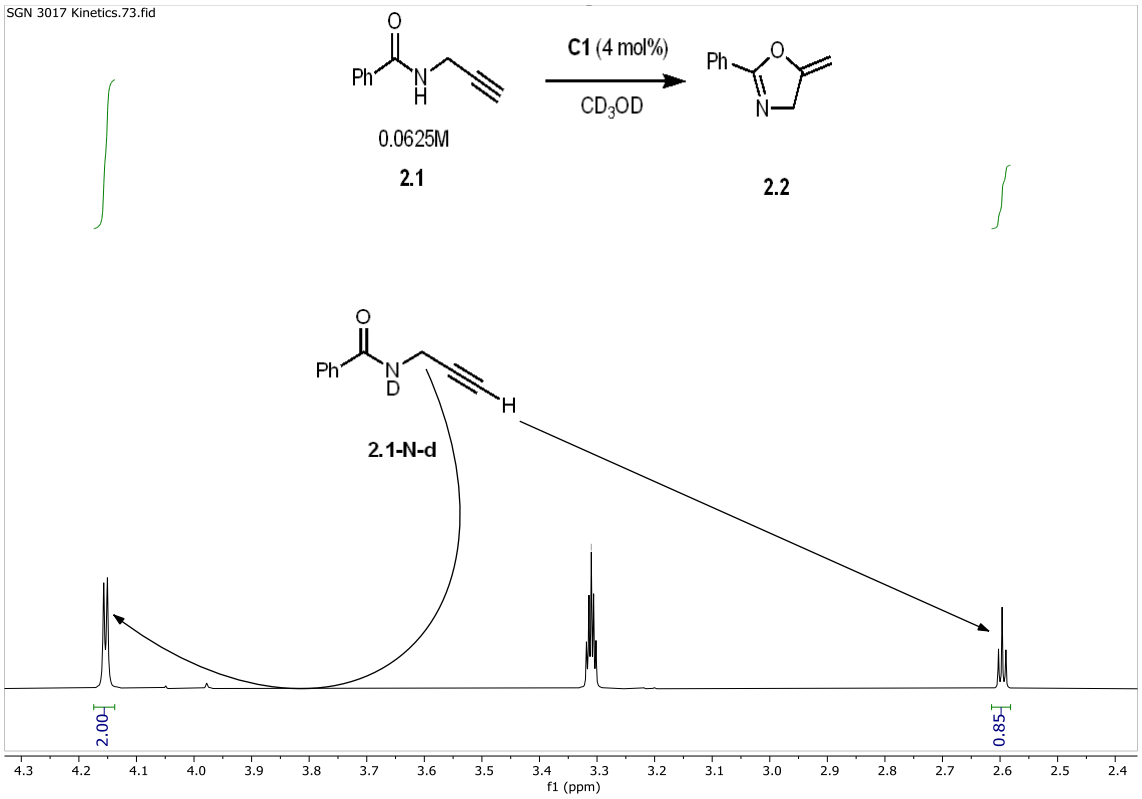

Figure 78 Integration Values for **2.1-N-d** in CD3OD at Reaction Time 12 Hours

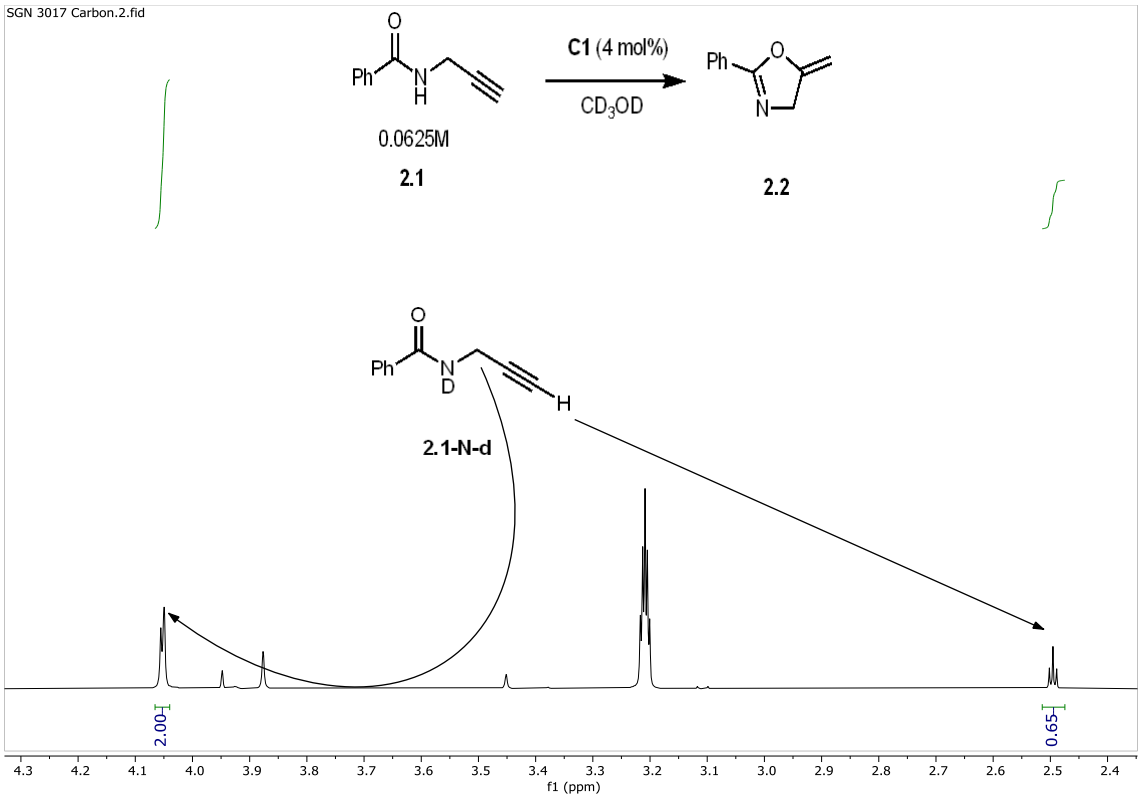

Figure 79 Integration Values for **2.1-N-d** in CD3OD at Reaction Time Five Days

This can be explained by slow incorporation of deuterium at the alkyne, not just the nitrogen. Alkyne protons do not exchange with solvent deuterons under typical conditions. A control experiment (SGN 3019) in which **2.1** was dissolved at the same concentration in CD_3OD in the absence of catalyst showed the expected NH exchange but none of the exchange at carbon. A likely explanation for this alkyne deuteration is as follows: slow cyclization means the equilibrium between free substrate and π-coordinated substrate is given days to persist. π-Coordination by gold increases not only alkyne electrophilicity but also acidity. The combination of these factors mean that methanol, being much more basic than dichloromethane, then abstracts the alkyne proton to form a gold acetylide.

Formation of an acid-base equilibrium with the deuterated solvent results in slow deuteration of the alkyne terminus.

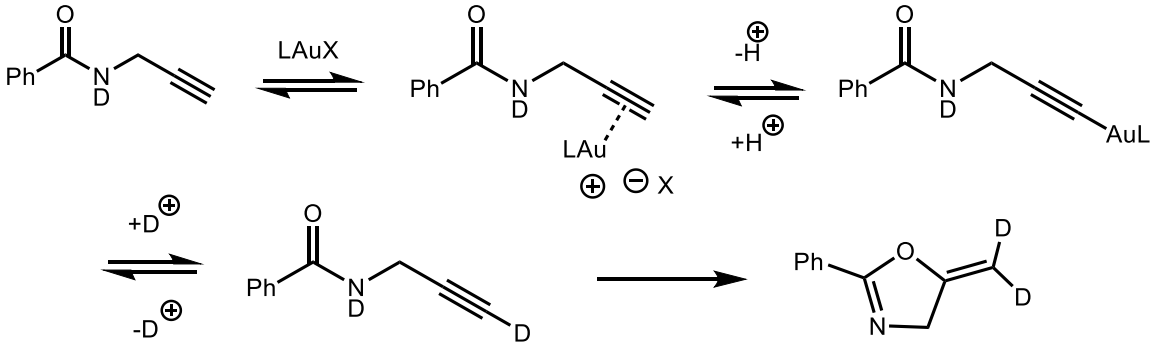

Figure 80 Mechanism of Deuterium Incorporation

Further confirmation of D incorporation was given when a ^{13}C NMR was collected of the reaction mixture, which showed the signal of the exocyclic carbon at ~83ppm to be a 1:1:1 triplet, consistent with deuterium coupling. A second deuterated species could be seen at 80ppm, the identity of which could not be confirmed.

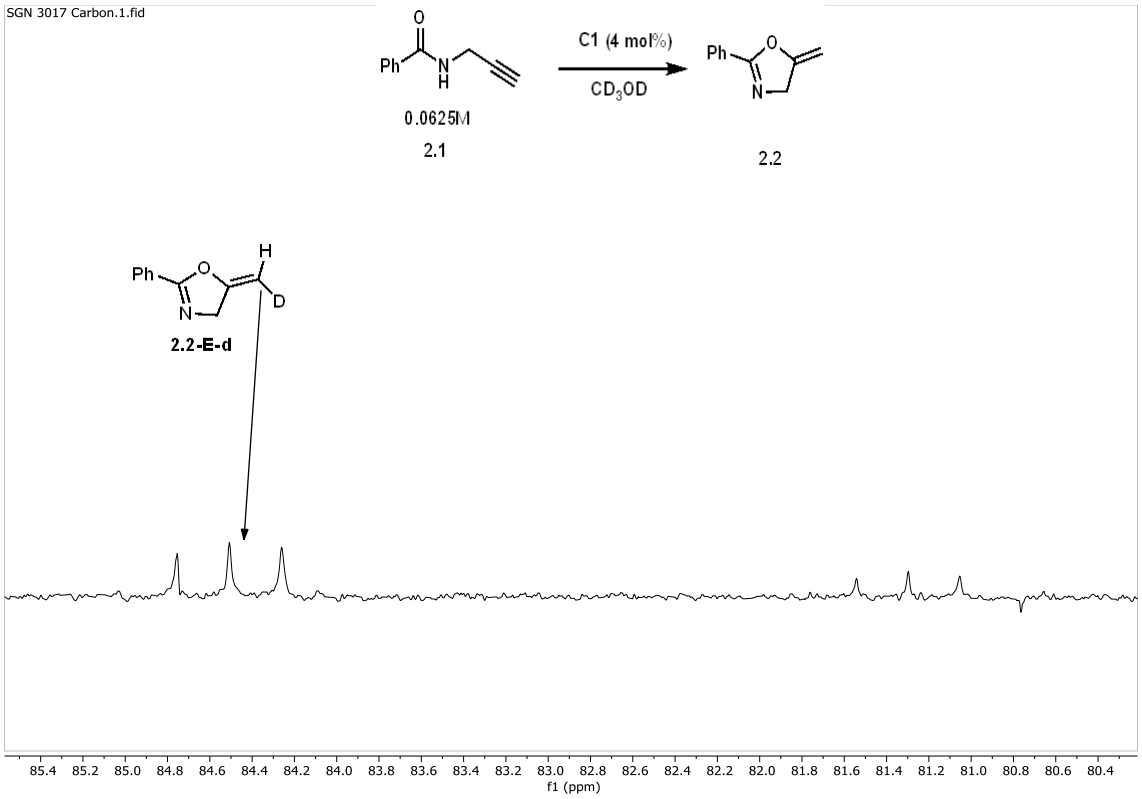

Figure 81 ^{13}C NMR Spectrum Showing Deuterium Incorporation Into Product

Isotopic Labeling Studies to Probe Kinetic Isotope Effect

Observation of deuterium incorporation as well as the drastically reduced rate raised questions of how much of the kinetic isotope was due to a solvent KIE, or a traditional KIE stemming from deuteration of the substrate. To answer this question, D-labeled analogues of **2.1** were synthesized.

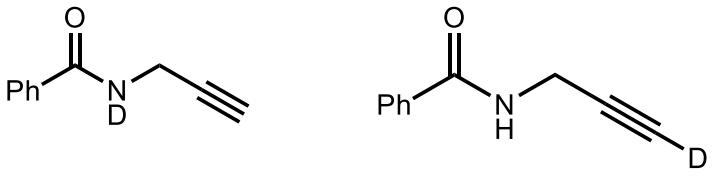

2.1-N-d **2.1-C-d**

Figure 82 Deuterated Analogues of Propargyl Benzamide **2.1**

2.1-N-d cannot be cyclized in CH_3OH as the deuterium label will immediately exchange with the solvent. A similar issue arose when **2.1-N-d** was cyclized in dichloromethane, as the labile deuterium atom was exchanged with residual water in the solvent. This was confirmed by ^2H spectroscopy, which showed a substantial HDO peak at the reaction's end. This was not an issue with **2.1-C-d**, which showed full retention of the label in DCM.

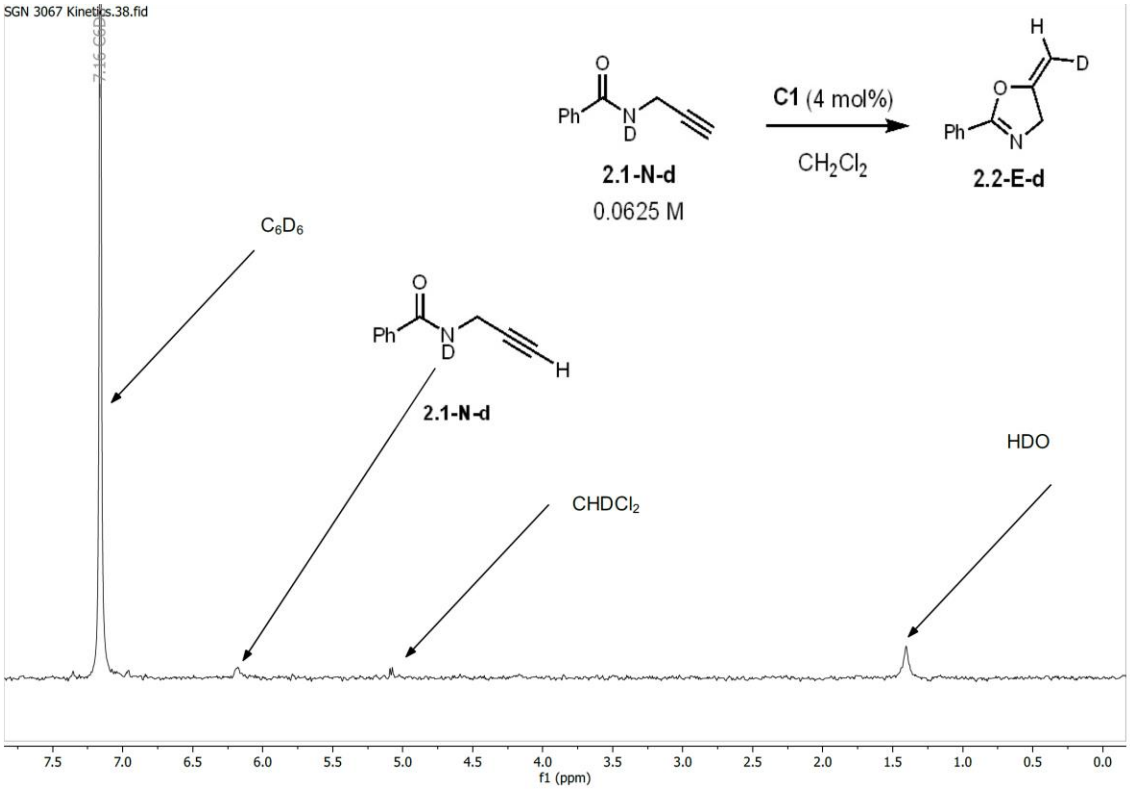

Figure 83 ^2H Spectrum Showing Loss of Deuterium Label for **2.1-N-d**

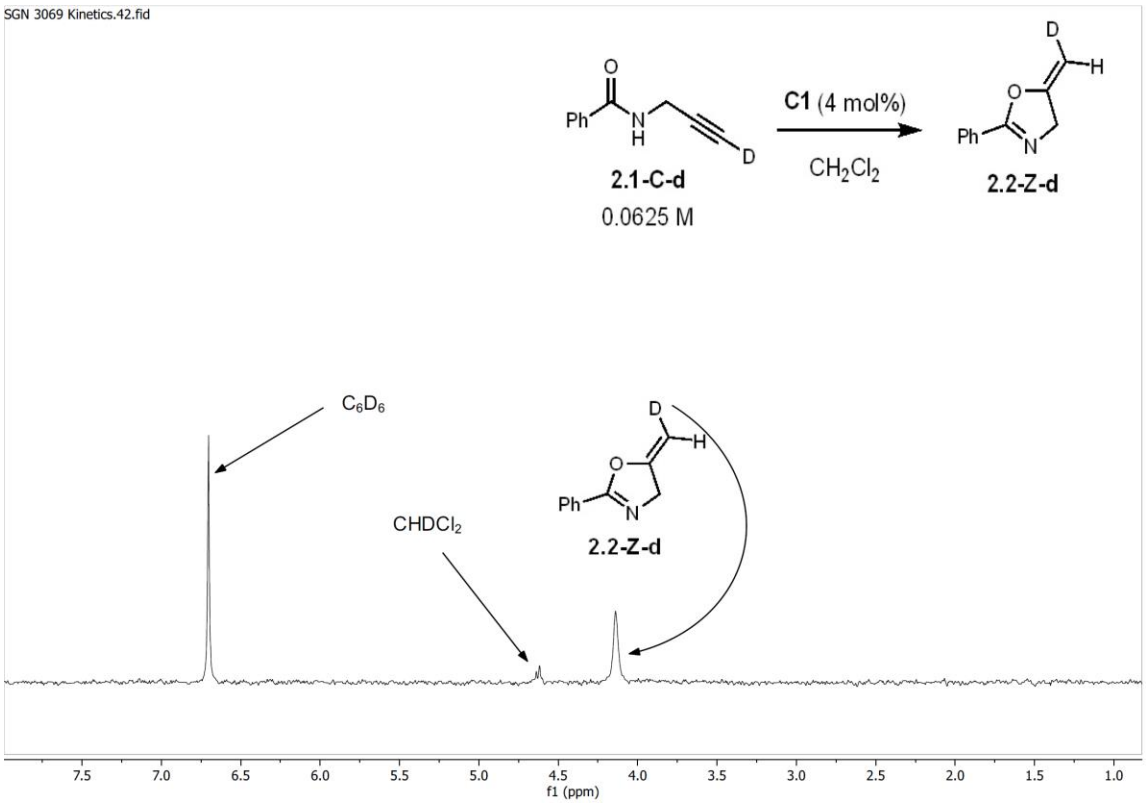

Figure 84 ^{2}H Spectrum Showing Retention of Deuterium Label for **2.1-C-d**

To retain the label of **2.1-N-d**, a CH_3OD titration into CH_2Cl_2 was performed. A titration volume of 20μL of CH_3OD showed no substantial rate impact, but at 30μL the amide proton resonance disappears from the ^{1}H spectrum, indicating full incorporation of deuterium. Since methanol otherwise has no rate impact at these volumes, the difference in rate can be attributed solely to *in situ* generation of **2.1-N-d**. Kinetic plots for the cyclizations of both substrates in the presence of both **C1** and **C2** are shown below.

Kinetics of 2.1-N-d in Dichloromethane with MeOD Titrations with C1

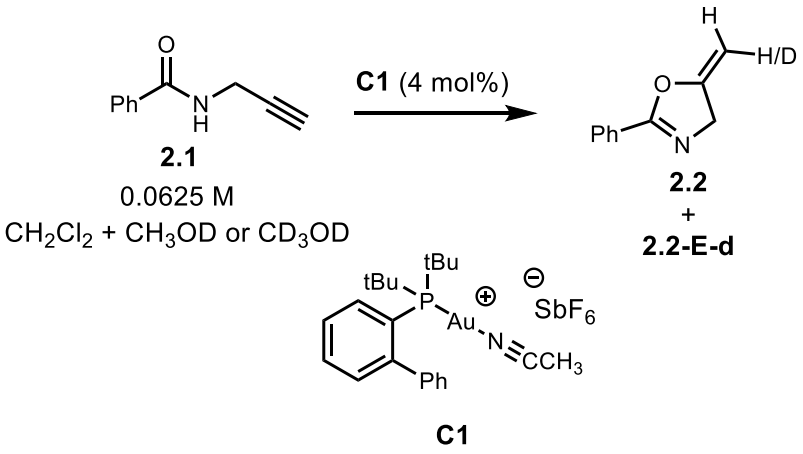

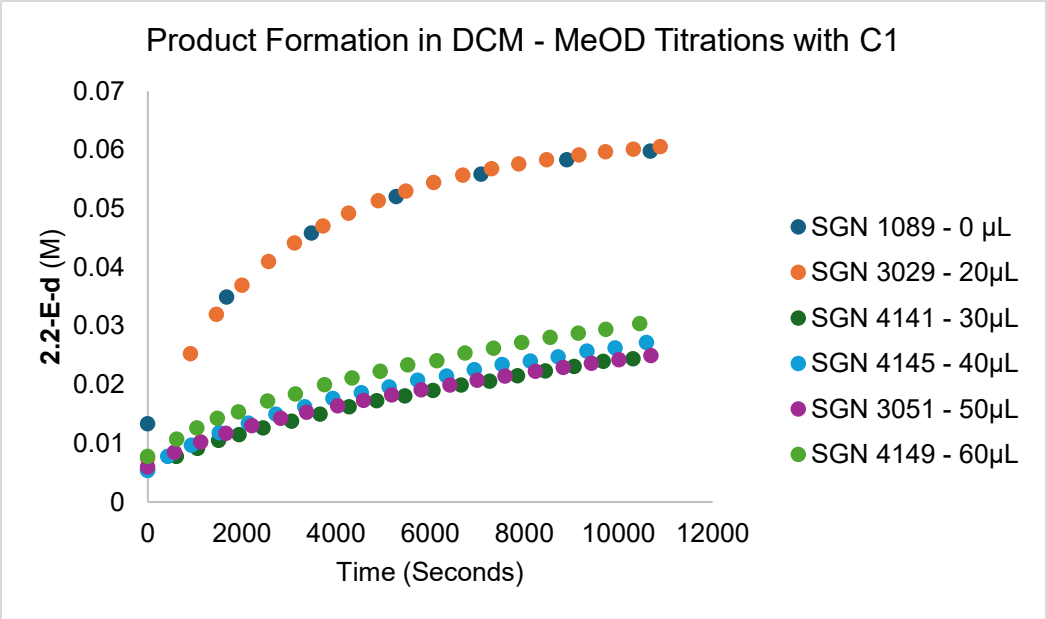

Figure 85 Product Formation in DCM with MeOD Titrations in the Presence of **C1**

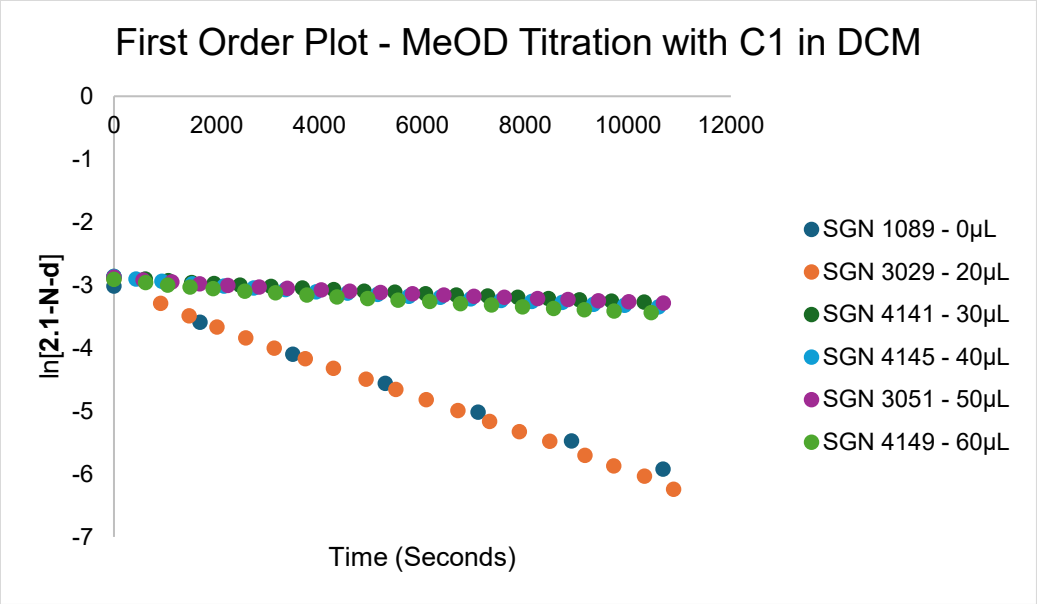

Figure 86 First Order Decay of **2.1-N-d** in DCM with MeOD titrations in the presence of **C1**

	Methanol-d volume (µL)	**Catalyst Amount**	**Catalyst Loading**	$k_{obs/S}^{-1}$
SGN 4141	30	0.002 mmol	4 mol%	$3.80 \times 10^{-5} \pm 9.32 \times 10^{-7}$
SGN 4145	40	0.002 mmol	4mol%	$4.29 \times 10^{-5} \pm 1.43 \times 10^{-6}$
SGN 3031	50	0.002 mmol	4 mol%	$3.62 \times 10^{-5} \pm 1.13 \times 10^{-6}$
SGN 4149	60	0.002 mmol	4 mol%	$4.87 \times 10^{-5} \pm 1.38 \times 10^{-6}$
Average Rate – MeOD Titration				$4.13 \times 10^{-5} \pm 1.22 \times 10^{-6}$
Average Rate – Pure DCM				$3.0 \times 10^{-4} \pm 4.35 \times 10^{-6}$
Primary kH/kD = 7.26				

Table VII Rate of cyclization of **2.1-N-d** with **C1** in DCM with MeOD titration

Kinetics of 2.1-N-d in Dichloromethane with MeOD Titrations with C2

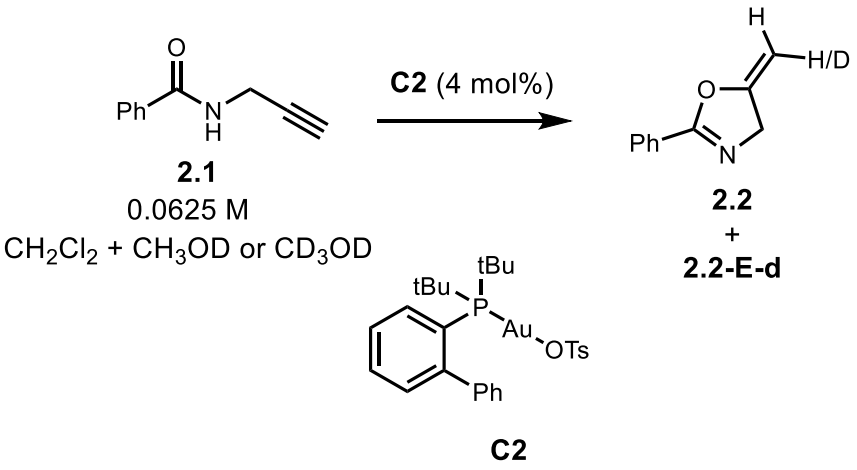

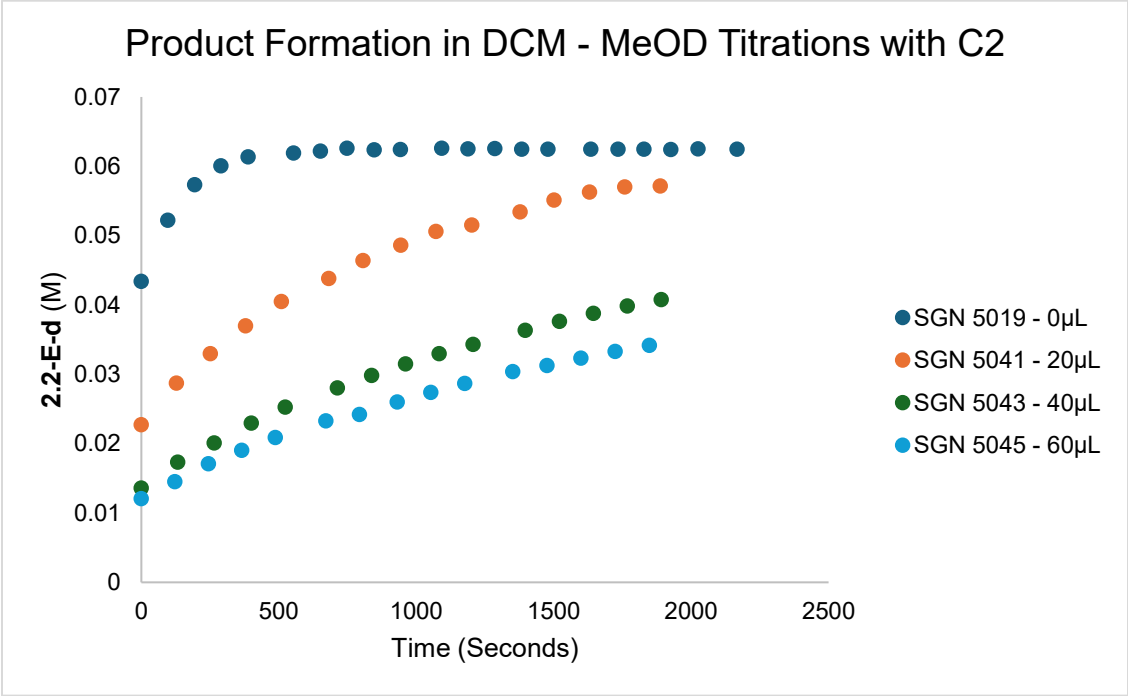

Figure 87 Product Formation in DCM with MeOD Titrations in the Presence of **C2**

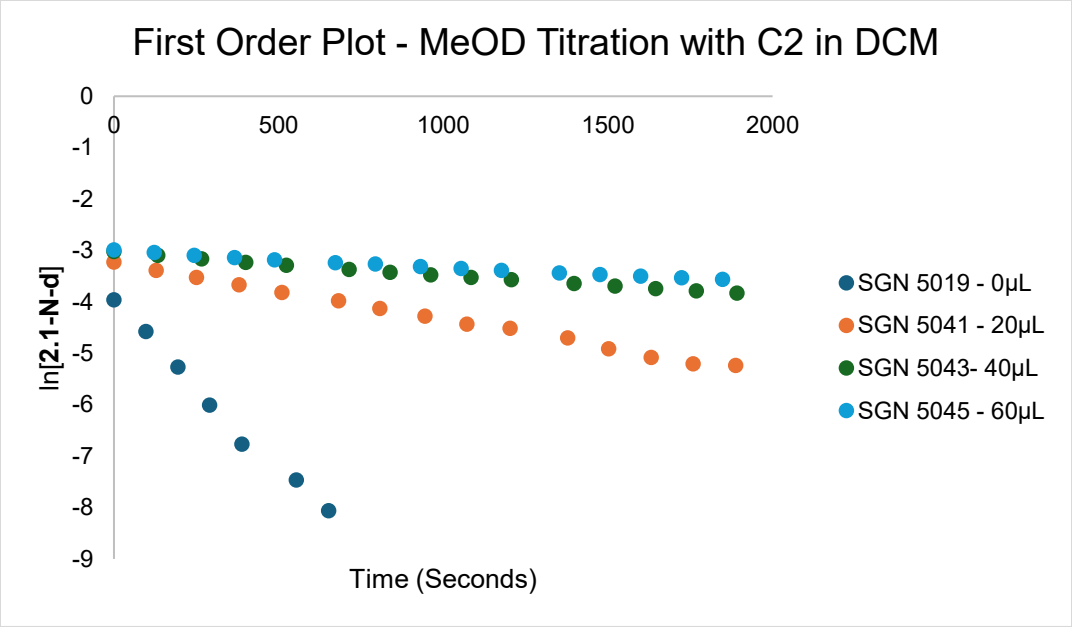

Figure 88 First Order Decay of **2.1-N-d** in DCM with MeOD titrations in the presence of **C1**

	Methanol-d volume (μL)	**Catalyst Amount**	**Catalyst Loading**	$k_{obs/S}^{-1}$
SGN 5041	20	0.002 mmol	4mol%	$1.09 \times 10^{-3} \pm 1.53 \times 10^{-5}$
SGN 5043	40	0.002 mmol	4 mol%	$4.22 \times 10^{-4} \pm 6.81 \times 10^{-6}$
SGN 5045	60	0.002 mmol	4mol%	$3.07 \times 10^{-4} \pm 6.19 \times 10^{-6}$
Average Rate – MeOD Titration				$6.06 \times 10^{-4} \pm 9.43 \times 10^{-6}$
Average Rate – MeOH Titration				$2.54 \times 10^{-3} \pm 3.72 \times 10^{-4}$
Primary kH/kD = 4.19				

Table VIII Rate of cyclization of **2.1-N-d** with **C2** in DCM with MeOD titration

As evidenced by the data tabulated above, in dichloromethane, a primary kinetic isotope effect is observed for **2.1-N-d**. The rates are markedly slower upon deuteration of the nitrogen, showing a primary KIE of ~7 for **C1** and ~4 for **C2**. In either case, the observed rates strongly support rate-limiting protodeauration for

the cyclization, as the N-D bond is broken and reformed throughout the reaction course.

Kinetics of 2.1-C-d in Dichloromethane

To assess any possible secondary kinetic isotope effects, **2.1-C-d** was synthesized and treated to the typical reaction conditions in dichloromethane to examine any possible rate impact of deuteration at the alkyne terminus. Comparative plots and a rate summary table for catalysts **C1** and **C2** are shown below.

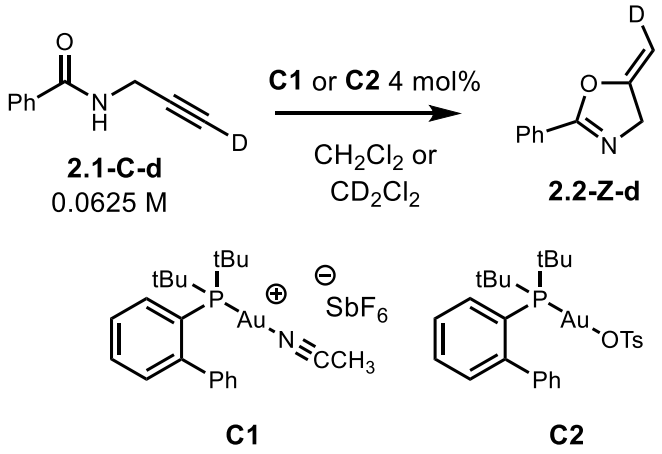

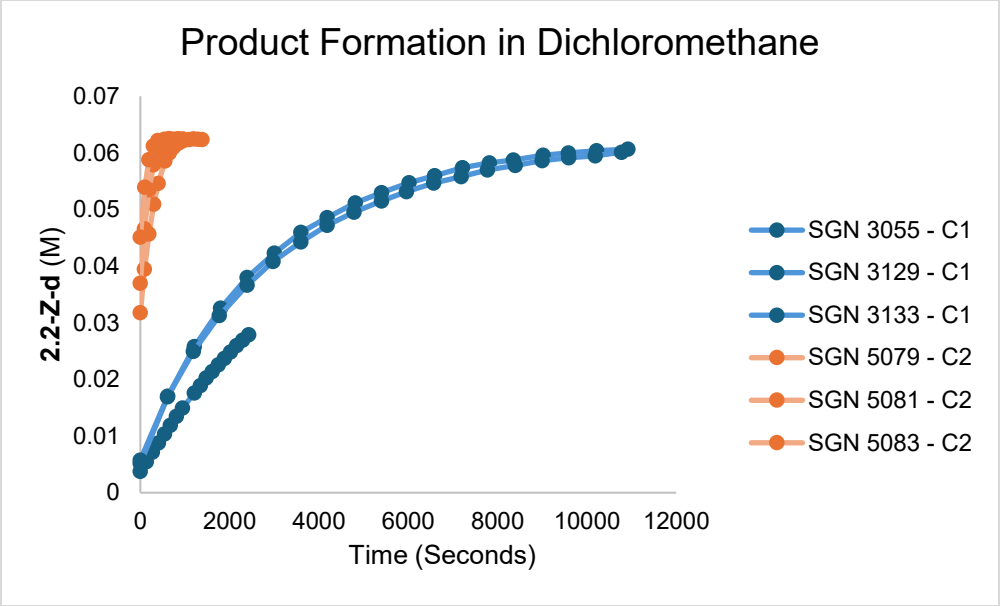

Figure 89 Product Formation with **2.1-C-d** in Dichloromethane

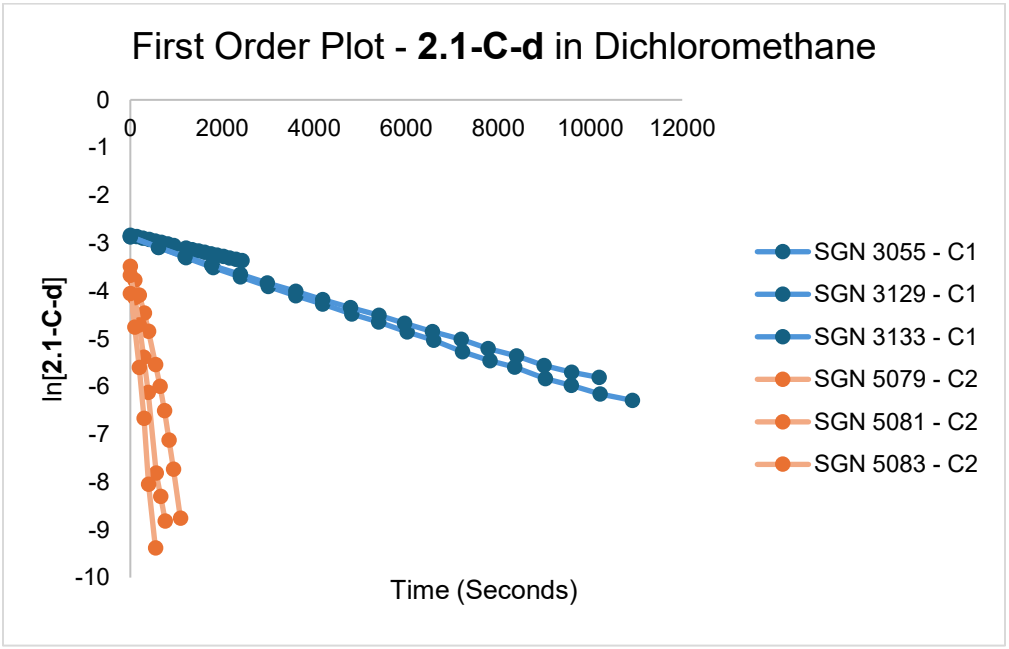

Figure 90 First Order Decay of **2.1-C-d** in Dichloromethane

	Solvent	**Catalyst Amount**	**Catalyst Loading**	$k_{obs/S}^{-1}$
SGN 3055	0.8 mL CD_2Cl_2	0.002 mmol	4 mol%	$2.19 \times 10^{-4} \pm 6.4. \times 10^{-7}$
SGN 3129	0.8mL CH_2Cl2	0.002 mmol	4 mol%	$3.18 \times 10^{-4} \pm 2.80 \times 10^{-6}$
SGN 3133	0.8mL CH_2Cl_2	0.002mmol	4 mol%	$2.88 \times 10^{-4} \pm 2.20 \times 10^{-6}$
Average Rate – D Alkyne				$2.75 \times 10^{-4} \pm 5.64 \times 10^{-6}$
Average Rate – H Alkyne				$3.0 \times 10^{-4} \pm 4.35 \times 10^{-6}$

Table IX Rate of cyclization of **2.1-C-d** with **C1** in DCM

	Solvent	**Catalyst Amount**	**Catalyst Loading**	$k_{obs/S}^{-1}$
SGN 5079	0.8 mL CH_2Cl_2	0.002 mmol	4 mol%	$4.76 \times 10^{-3} \pm 2.15 \times 10^{-4}$
SGN 5081	0.8mL CH_2Cl2	0.002 mmol	4 mol%	$7.20 \times 10^{-3} \pm 2.68 \times 10^{-4}$
SGN 5083	0.8mL CH_2Cl_2	0.002mmol	4 mol%	$1.01 \times 10^{-2} \pm 4.56 \times 10^{-4}$
Average Rate – D Alkyne				$7.35 \times 10^{-3} \pm 3.13 \times 10^{-4}$
Average Rate – H Alkyne				$6.89 \times 10^{-3} \pm 2.69 \times 10^{-4}$

Table X Rate of cyclization of **2.1-C-d** with **C2** in DCM

As seen in **Table IX** and **Table X**, deuteration at the alkyne gives no meaningful change in reaction rate. This is consistent with the observation of a primary KIE in dichloromethane when the nitrogen is deuterated, further supporting the conclusion of rate-limiting protodeauration.

Kinetics of 2.1-C-d in Methanol

Cyclization of **2.1-N-d** in CH_3OH is impossible due to the labile nature of the deuterium label, and was therefore never performed. However, the alkyne label of **2.1-C-d** is not exchangeable with solvent. **2.1-C-d** was therefore cyclized in CH_3OH to determine if deuteration at the alkyne would reveal any kinetic isotope effects in a second solvent.

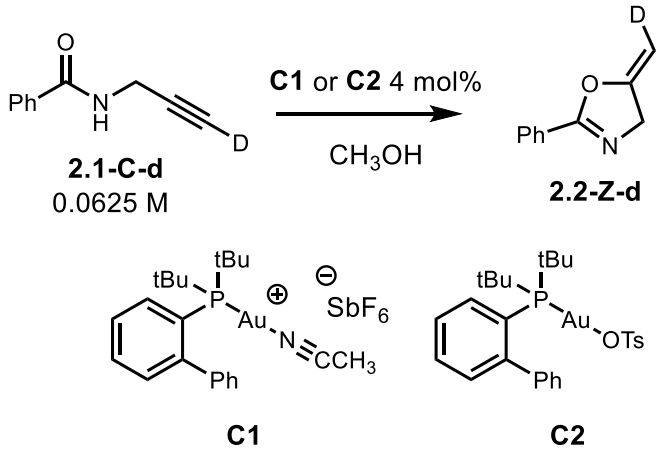

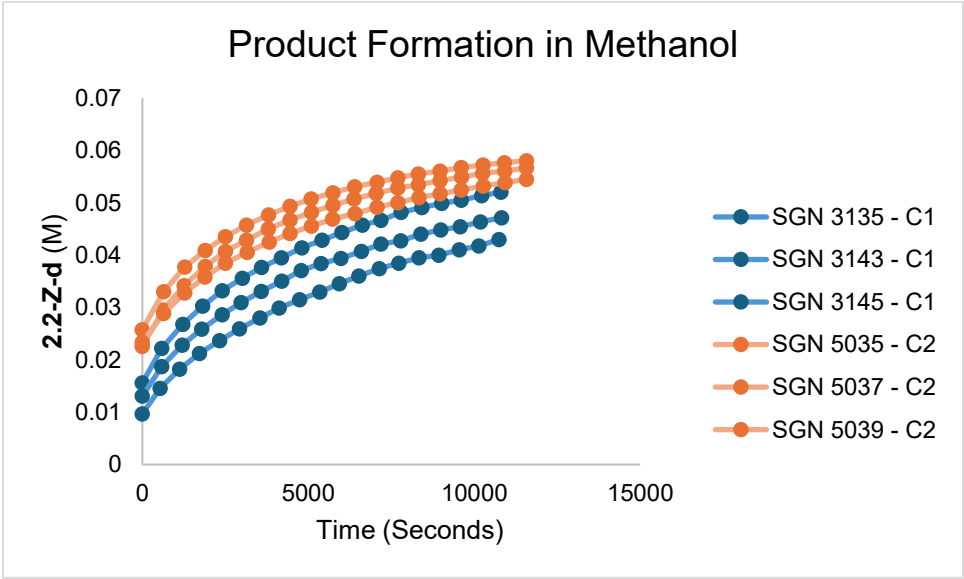

Figure 91 Product formation with **2.1-C-d** in CH3OH

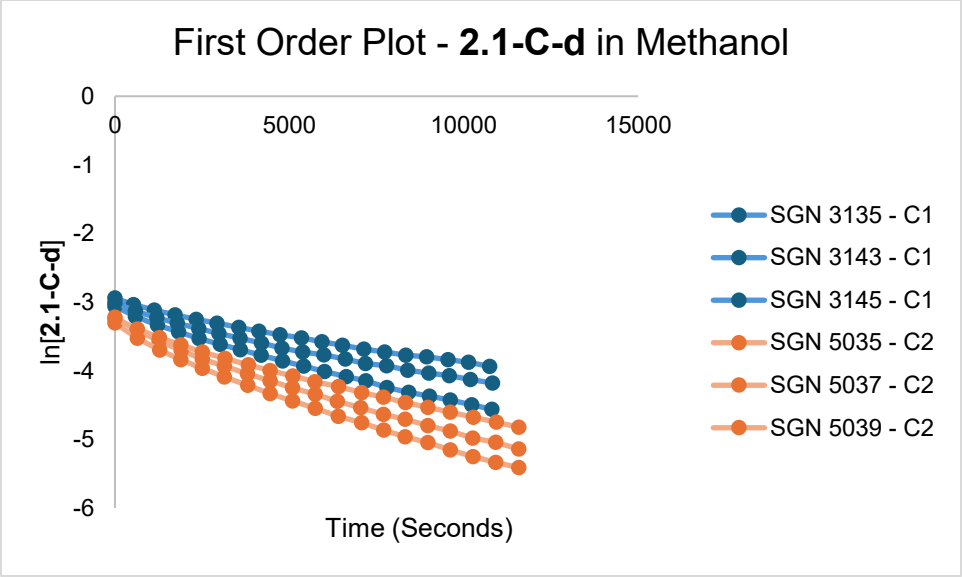

Figure 92 First order decay of **2.1-C-d** in CH3OH in the presence of **C1**

	Solvent	**Catalyst Amount**	**Catalyst Loading**	$k_{obs/S}^{-1}$
SGN 3135	0.8 mL CH_3OH	0.002 mmol	4 mol%	$1.33 \times 10^{-4} \pm 3.06 \times 10^{-7}$
SGN 3143	0.8 mL CH_3OH	0.002 mmol	4 mol%	$8.82 \times 10^{-5} \pm 2.42 \times 10^{-6}$
SGN 3145	0.8 mL CH_3OH	0.002mmol	4 mol%	$1.03 \times 10^{-4} \pm 3.18 \times 10^{-6}$
Average Rate – D Alkyne				$1.08 \times 10^{-4} \pm 3.92 \times 10^{-6}$
Average Rate – H Alkyne				$5.17 \times 10^{-5} \pm 1.65 \times 10^{-6}$
Inverse Secondary kH/kD = 0.479				

Table XI Rate of cyclization of **2.1-C-d** with C1 in CH3OH

	Solvent	**Catalyst Amount**	**Catalyst Loading**	$k_{obs/S}^{-1}$
SGN 5035	0.8 mL CH_3OH	0.002 mmol	4 mol%	$1.58 \times 10^{-4} \pm 4.1 \times 10^{-6}$
SGN 5037	0.8 mL CH_3OH	0.002 mmol	4 mol%	$1.75 \times 10^{-4} \pm 4.48 \times 10^{-6}$
SGN 5039	0.8 mL CH_3OH	0.002mmol	4 mol%	$1.30 \times 10^{-4} \pm 3.14 \times 10^{-6}$
Average Rate – D Alkyne				$1.54 \times 10^{-4} \pm 3.91 \times 10^{-6}$
Average Rate – H Alkyne				$8.31 \times 10^{-5} \pm 2.50 \times 10^{-6}$
Inverse Secondary kH/kD = 0.54				

Table XII Rate of cyclization of **2.1-C-d** with **C1** in CH3OH

Discussion of Deuterium-Labeled Kinetics Experiments and Conclusion

In the MeOD titration experiments, **2.1-N-d** is formed *in situ* in dichloromethane by exchange with the N-bonded hydrogen. As evidenced by tables **VII** and **VIII**, **2.1-N-d** displays a large primary kinetic isotope effect (~7 for **C1** and ~4 for **C2**) for cyclization in dichloromethane with both **C1** and **C2**. This is consistent with rate-limiting protodeauration, as the ND bond breaks and a CD bond is formed at the end of the reaction. In agreement with this result, **2.1-C-d** shows no kinetic isotope effect when cyclized in DCM and returns the original rate (**Tables IX** and **X**). A much more surprising result was obtained when **2.1-C-d** was cyclized in CH_3OH (**Tables XI** and **XII**). In this case, a secondary inverse KIE is observed, with the reaction nearly doubling in rate. Critically, this implies a change of rate-limiting step in methanol as opposed to DCM. For the typical expected mechanism, the CD bond of **2.2-C-d** is never broken as it converts to **2.2-Z-d**. The D-labeled carbon does, however, undergo a hybridization change during the nucleophilic addition of the oxygen, converting from *sp* to *sp2*. This result strongly suggests that the cyclization step is instead rate-limiting in methanol.

Computational investigation of this result was performed by Professor Ding's group. The energetics of the reaction were modeled in both dichloromethane and methanol and are shown in the figure below.

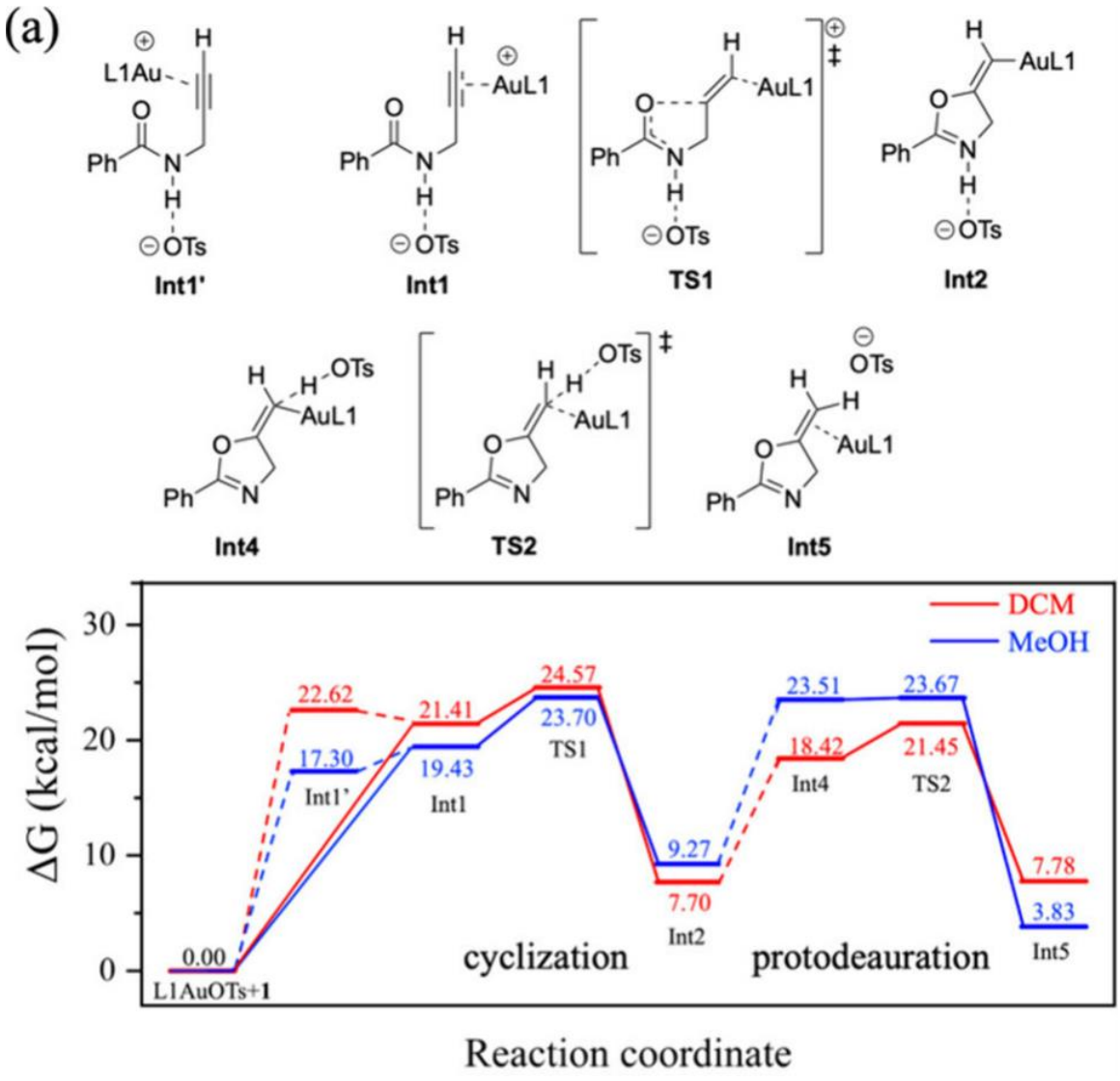

Figure 93 Computational Modeling of the Benzamide Cyclization

The energetics of the reaction in dichloromethane are shown in red, while methanol is shown in blue. Rate-limiting protodeauration is affirmed in dichloromethane, as the 3.33 kcal/mol difference in energy between Int4 and TS2 is the largest barrier seen throughout the reaction coordinate for that solvent. By contrast, protodeauration in methanol is practically barrierless, with almost no change in energy between the two states. For methanol, cyclization is instead

shown to be rate-limiting, as the transition between Int1 and TS1 instead provides the largest barrier. These computed results critically affirm the observations from the deuterium-labeling experiments, showing a solvent-dependent change in rate-limiting step.

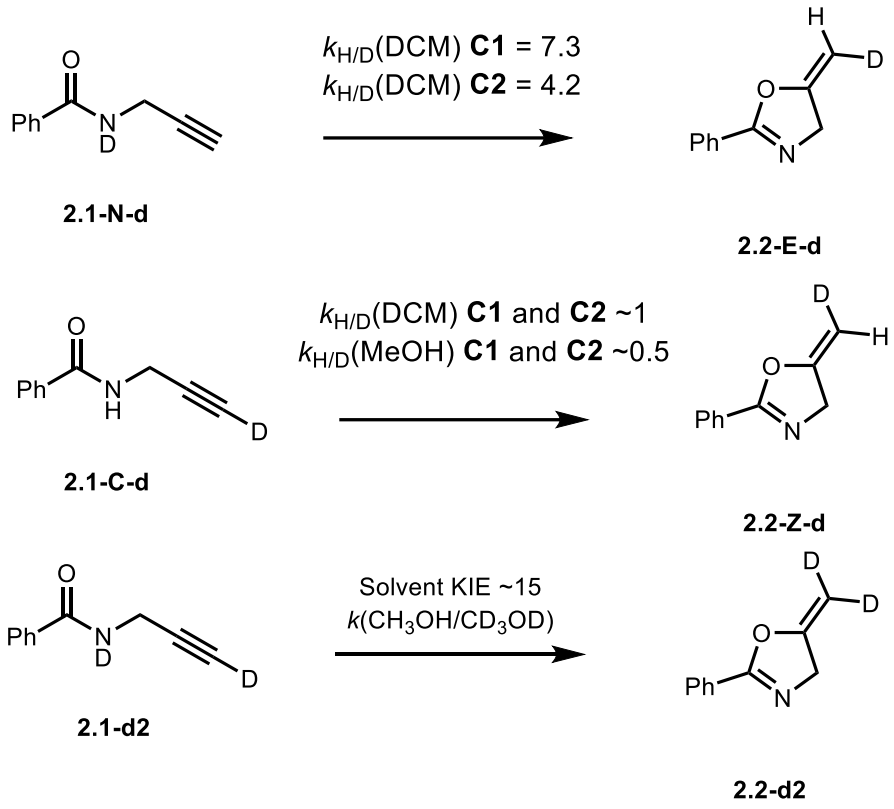

Figure 94 Kinetic Isotope Effects in N-Propargyl Benzamide Cyclization

This is the first observation of a solvent-dependent rate-limiting step in this cyclization. Virtually the entire body of literature on this topic, even those which include solvent studies, arrive at the conclusion that protodeauration is rate-limiting.

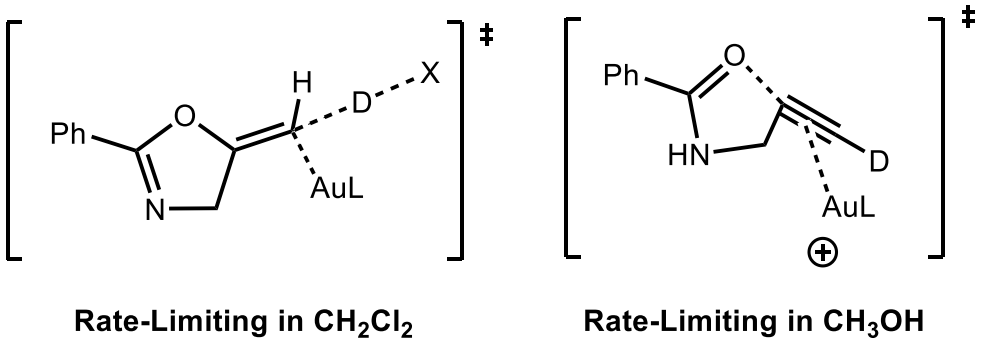

Rate-Limiting in CH_2Cl_2 **Rate-Limiting in CH_3OH**

Figure 95 Rate-Limiting Steps of N-Propargyl Benzamide Cyclization

This result clearly indicates that, despite this reaction's immense popularity as a benchmark, its mechanistic subtleties are still somewhat poorly understood. As a result, many conclusions drawn from using this as a test reaction can be potentially spurious. Furthermore, the observation of deuterium incorporation at the alkyne in CD_3OD implies a reaction which proceeds through a gold acetylide. As discussed in chapter 1, not only do acetylides react differently than π-complexes, they can also be captured by another mole of catalyst to form a digold acetylide. The digold acetylides are typically very stable, leading to catalyst degradation. Furthermore, generation of an acetylide is concurrent with generation of a mole of acid, the strength of which will depend on the choice of anion. The opens the possibility of Bronsted acid catalysis, either in isolation or tandem with gold.

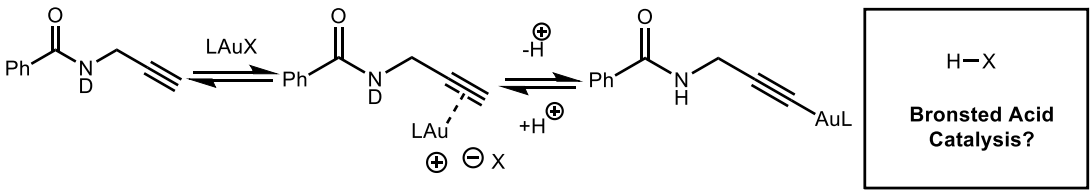

Figure 96 Acetylide and Acid Formation

These alternative pathways of catalyst degradation and acid formation will depend on the choice of ligand, anion, and solvent, and can also explain the contrasting observations in both these experiments and those in the literature. Further discussion of degradation pathways and catalyst identity are found in the following chapter.

Chapter 3: Analysis of Acetylide Intermediates in the Au(I)-Catalyzed N-Propargyl Benzamide Cyclization

Introduction

A substantial portion describing characterization of reaction intermediates in this chapter has been published in the Journal of Organic Chemistry. (Norman, S. G., Jiao, L., Yi, J. Ding, W., Jones. A. C., Solvent-Dependent Change in the Rate-Determining Step of Au(I) Catalyzed N-Propargyl Benzamide Cyclization, *Accepted Submission to J. Org. Chem.*, **2025**. DOI: 10.1021/acs.joc.5c00787)

As revealed by the experiments detailed in chapter two, the Au-catalyzed intramolecular cyclization of N-propargyl benzamide has a solvent-dependent rate-limiting step. In dichloromethane, the rate-limiting step was found to be protodeauration, a result in agreement with the majority of gold literature on the reaction. In methanol, cyclization was instead found to be rate-limiting. This was confirmed by a deuterium labeling study, which showed a primary KIE for the N-deuterated substrate in DCM, and an inverse secondary KIE for the C-deuterated substrate in methanol.

Ambiguities in the observed rates are not limited to the choice of solvent and catalyst. Different rate-limiting steps can lead to different pathways of catalyst decomposition, another potential cause for the discrepancies in observed rates.

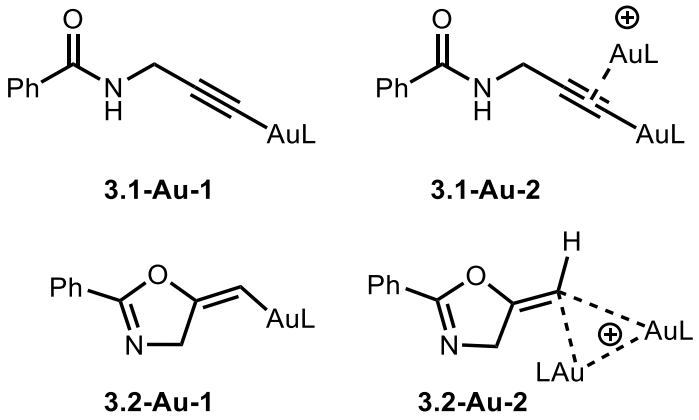

Figure 97 Degradation Products for Benzamide Cyclization

Likely degradation products for the cyclization are shown above in **Figure 96**. Formation of gold acetylide **3.1-Au-1** was demonstrated when the reaction was cyclized in CD_3OD and deuterium incorporation was observed at the terminal alkyne carbon. Slow cyclization leads to a long lifetime for **3.1-Au-1**, which can be captured by another mole of catalyst to form the σ,π-complex digold acetylide **3.1-Au-2**. Alternatively, if cyclization proceeds smoothly and protodeauration is slow, vinylgold **3.2-Au-1** will have a long lifetime instead and can go on to form geminal digold acetylide **3.2-Au-2**. As discussed in earlier chapters, the aurophilicity of gold causes digold complexes of type **3.1-Au-2** and **3.2-Au-2** to be particularly stable, leading to irreversible catalyst degradation and reduced reaction rates. Furthermore, formation of vinylgold **3.1-Au-1** and degradation to **3.1-Au-2** is alleged to be one of the central degradation pathways given the frequent proposal of **3.1-Au-1** as the catalyst resting state. Finally, formation of any one of these products is concurrent with a stoichiometric release of acid, the strength of which will largely depend on the choice of anion. Formation of an especially potent acid

opens the potential for Bronsted acid catalysis, which may occur in isolation or in tandem with the gold cycle.

Survey of Kinetic Reaction Mixtures by ^{31}P NMR

In addition to kinetic analysis by ^{1}H NMR for the experiments described in chapter two, the reaction mixtures were also analyzed by ^{31}P NMR, with spectra typically being collected at the end of three hours of reaction time. This uncovered an additional layer of complexity. Reaction mixtures appear substantially different according to choice of solvent. In dichloromethane, the reactions show little degradation of the catalyst. In methanol, however, catalyst degradation is substantial, typically showing significant diversion into off-cycle species. Recall from chapter two that the reaction is many times faster in dichloromethane than it is in methanol for all catalysts. This degradation would certainly contribute to a slower rate, piling on to the existing solvent effect.

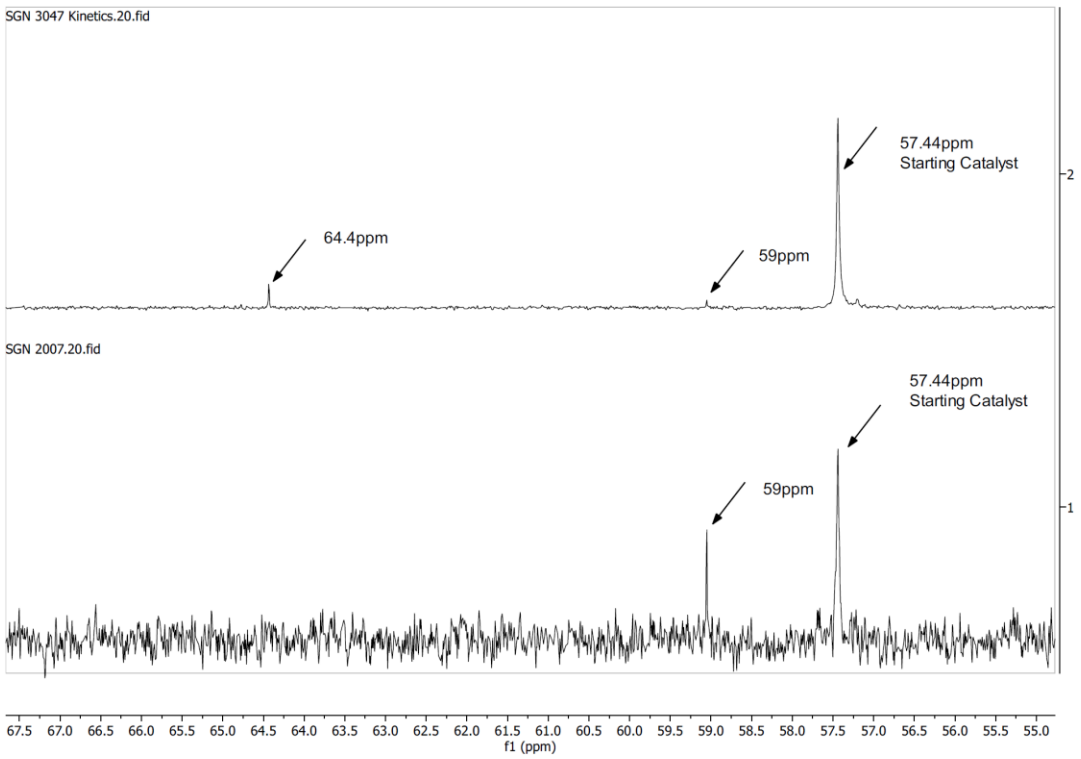

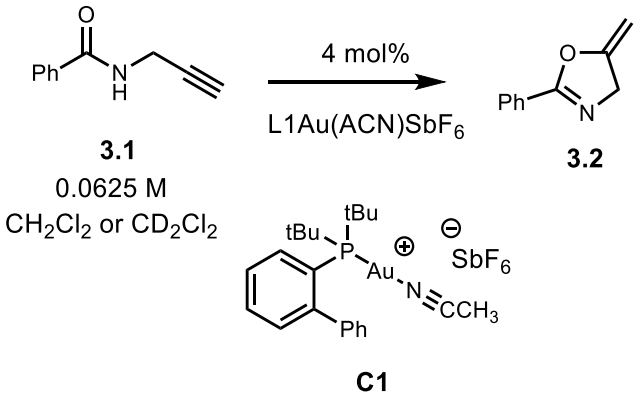

Figure 98 ^{31}P NMR of Cyclization in Dichloromethane with **C1**

In dichloromethane for catalyst **C1**, the predominant peak in the ^{31}P NMR is the starting catalyst, with additional peaks appearing at 59 and 64ppm. These peaks are minor, indicating minimal catalyst degradation during the three hour

experiment. The kinetic behavior in DCM reflects this, with reactions for **C1** and other catalysts performing well in that solvent.

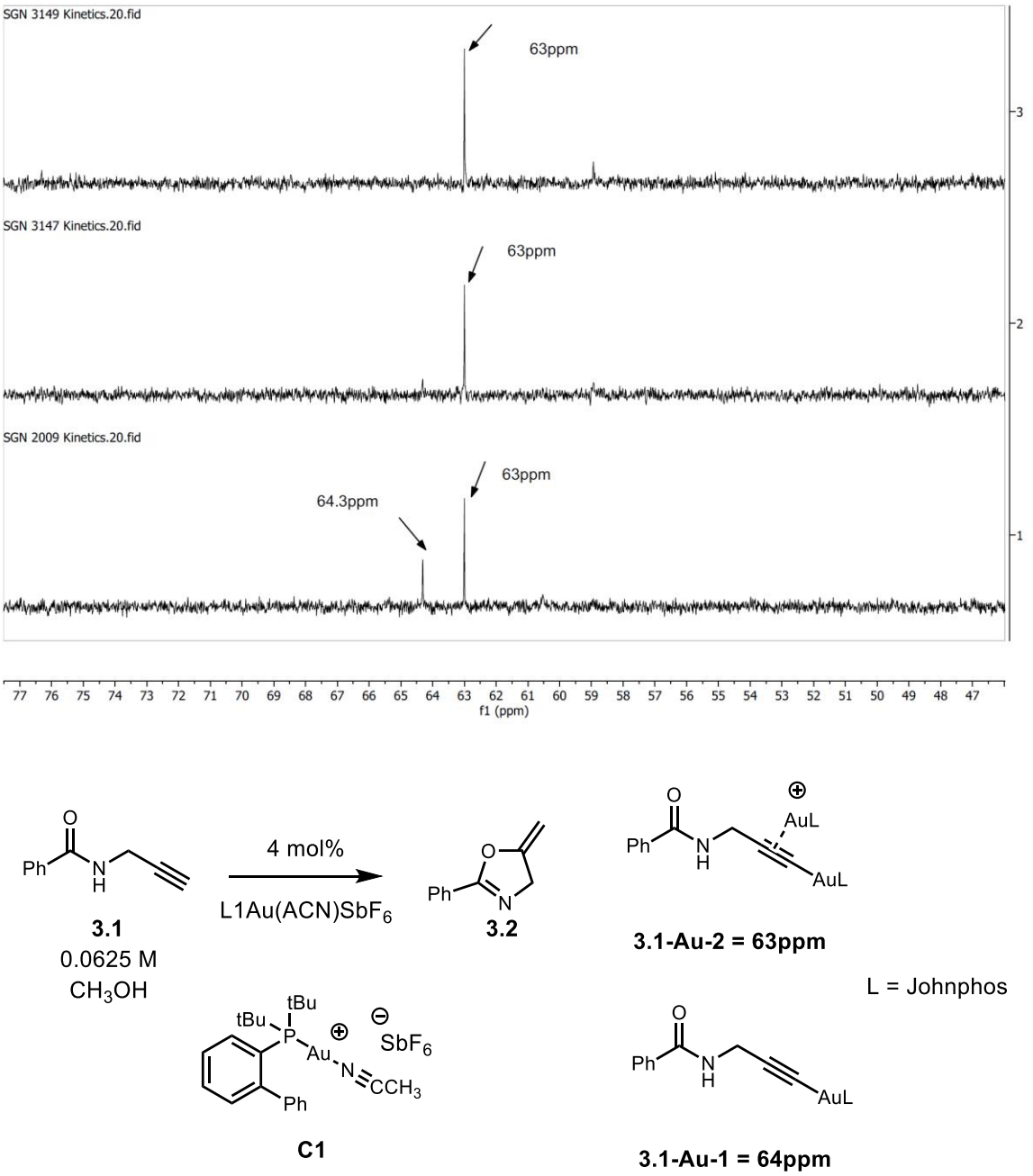

Figure 99 ^{31}P NMR of Cyclization in Methanol with **C1**

In methanol, the major peak is instead the σ,π-complex digold acetylide **3.1-Au-2** at 63ppm. The resonance at 64ppm as the monogold acetylide **3.1-Au-1**.

Later experiments using triethylamine (described below) were what allowed for identification of these species. Little to no free catalyst is observed at the end of three hours, which is the time at which the spectra above in **Figures 97** and **98** were taken. At this same time in the methanol experiments, a substantial amount of unreacted starting material is typically observed in the ^{1}H spectrum, meaning virtually 100% of the catalyst has been captured as the mono or digold acetylide. This is certainly a substantial contributing factor to the slow rate in methanol, as the catalyst is quantitatively pulled off-cycle into acetylide byproducts.

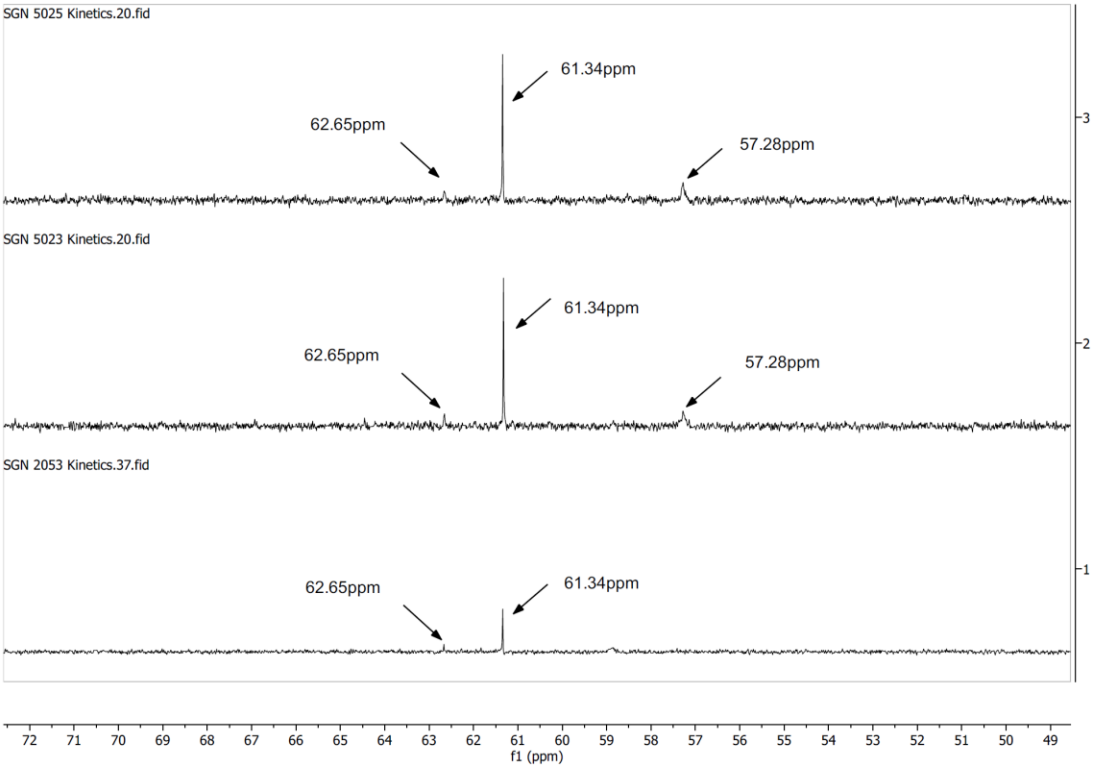

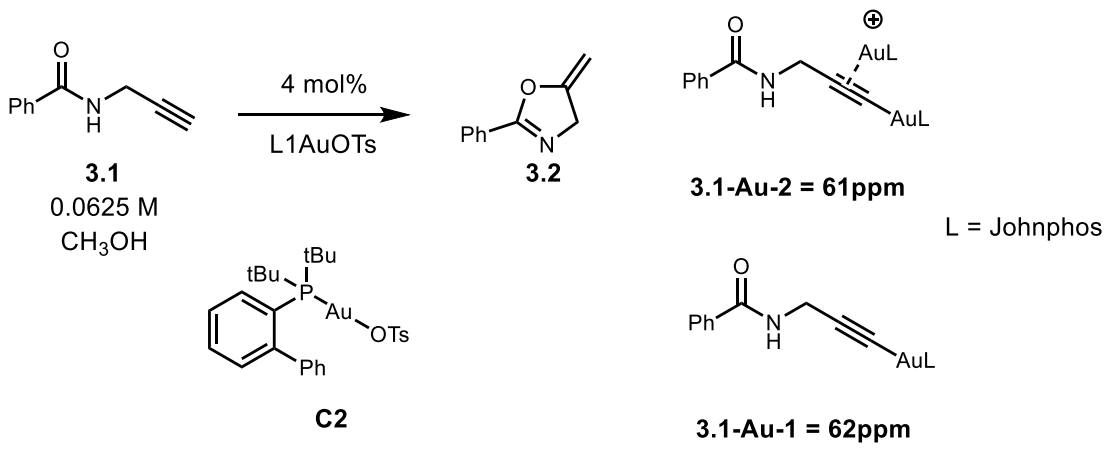

Figure 100 ^{31}P NMR of Cyclization in Methanol with **C2**

The same degradation products can be observed for **C2** in methanol, with a small amount of starting catalyst sometimes being observed around 57ppm. Anion effects in methanol are minimized, but catalyst **C1** is outpaced nearly 2:1 in methanol by **C2**, differing only by choice of anion. The minor portion of surviving catalyst at the end of the three-hour experiment could explain why **C2** is the faster catalyst even in the worse solvent. Much of the effect of methanol is therefore substantial degradation of catalyst rather than purely a solvent effect.

Intriguingly, **C8**, which features a bespoke bisbiphenyl dimethylamino ligand, is the catalyst least impacted by the switch to methanol, having its rate in DCM reduced only by about 44% (**Table VI**, chapter 2). A likely explanation for this is found when examining the ^{31}P spectra of the reaction, which shows no visible degradation at the end of three hours. Spectra of the crude catalyst give muddy ^{1}H and ^{31}P spectra due to likely coordination to gold by the pendant dimethylamino groups (see discussion in chapter 4), but once in the presence of the benzamide substrate, the ^{31}P spectrum sharpens to a signal resonance at ~94-95ppm in both dichloromethane and methanol.

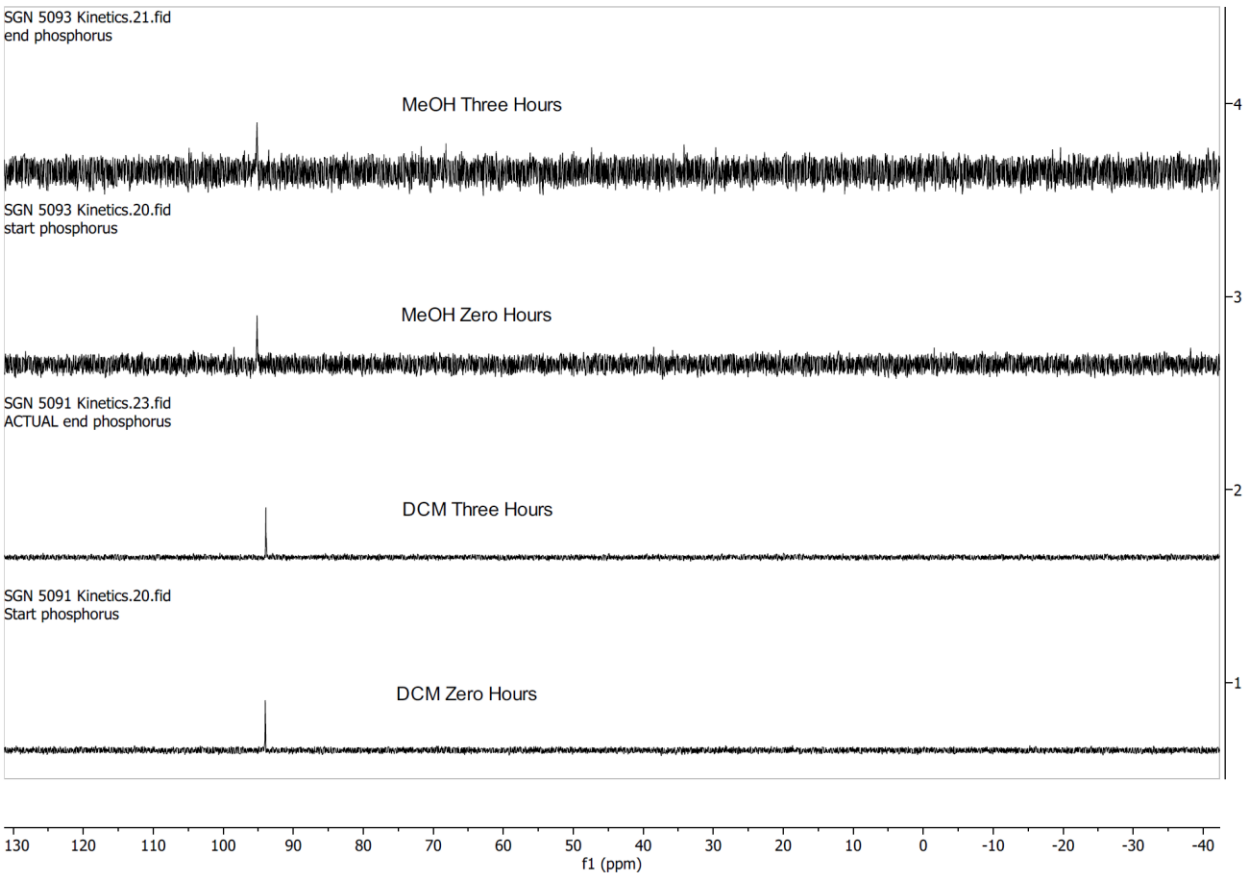

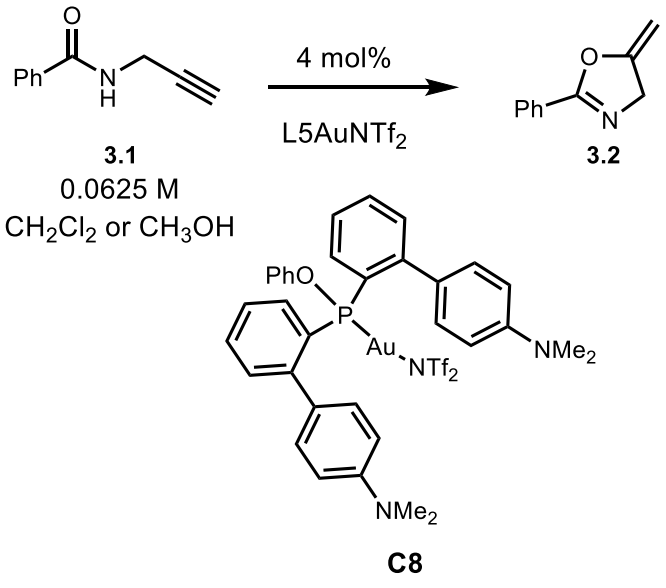

Figure 101 ^{31}P NMR of Cyclization with **C8**

The signal at ~95ppm is the lone peak at both the beginning and end of the experiment. This lack of degradation is the likely cause of **C8**'s relatively high performance in methanol. Additionally, this result indicates that, when catalyst degradation is a non-factor, methanol may only slow the rate by approximately 50%, with any further slowing being attributable to degradation of the catalyst in use.

Initial Triethylamine Studies

To identify the myriad degradation peaks observed in the reaction mixtures, reactions were performed with high loadings of triethylamine. As described in chapter 1, this has proven to be an effective strategy for the isolation of vinyl and alkylgold species in the past[106,112] and was thus utilized here. To better visualize the products by NMR, catalyst loading relative to benzamide was increased to 50 mol%, with 100 mol% of NEt_3.

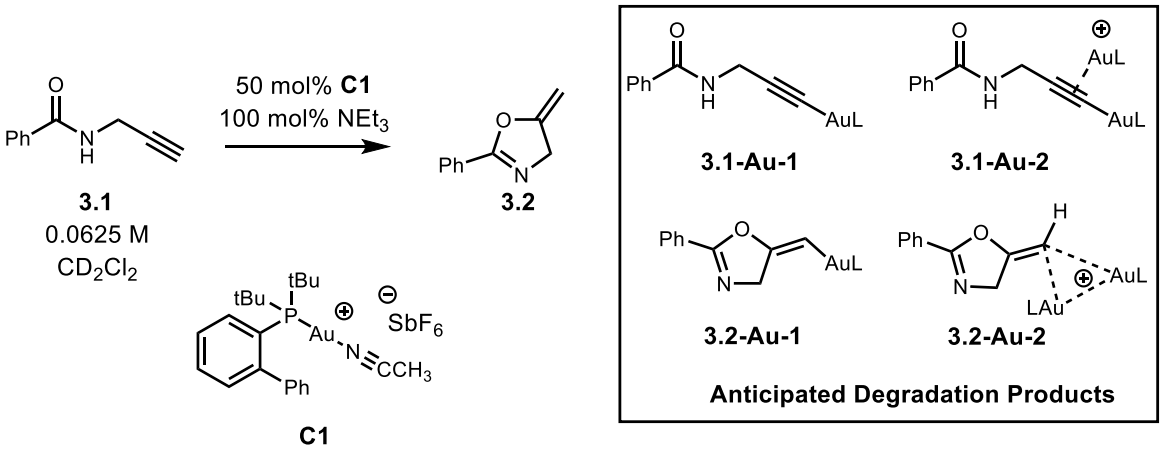

Figure 102 Cyclization with Triethylamine to Identify Intermediates

Further evidence of acetylide formation can first be found in the ^{1}H NMR, wherein the resonance corresponding to the alkyne proton disappears, and ^{31}P

coupling can be observed to the N-bonded methylene. ^{31}P decoupled ^{1}H NMR demonstrated the doublet of doublets at 4.15ppm results from an acetylide product, though whether that product is **3.1-Au-1** or **3.1-Au-2** is not entirely clear.

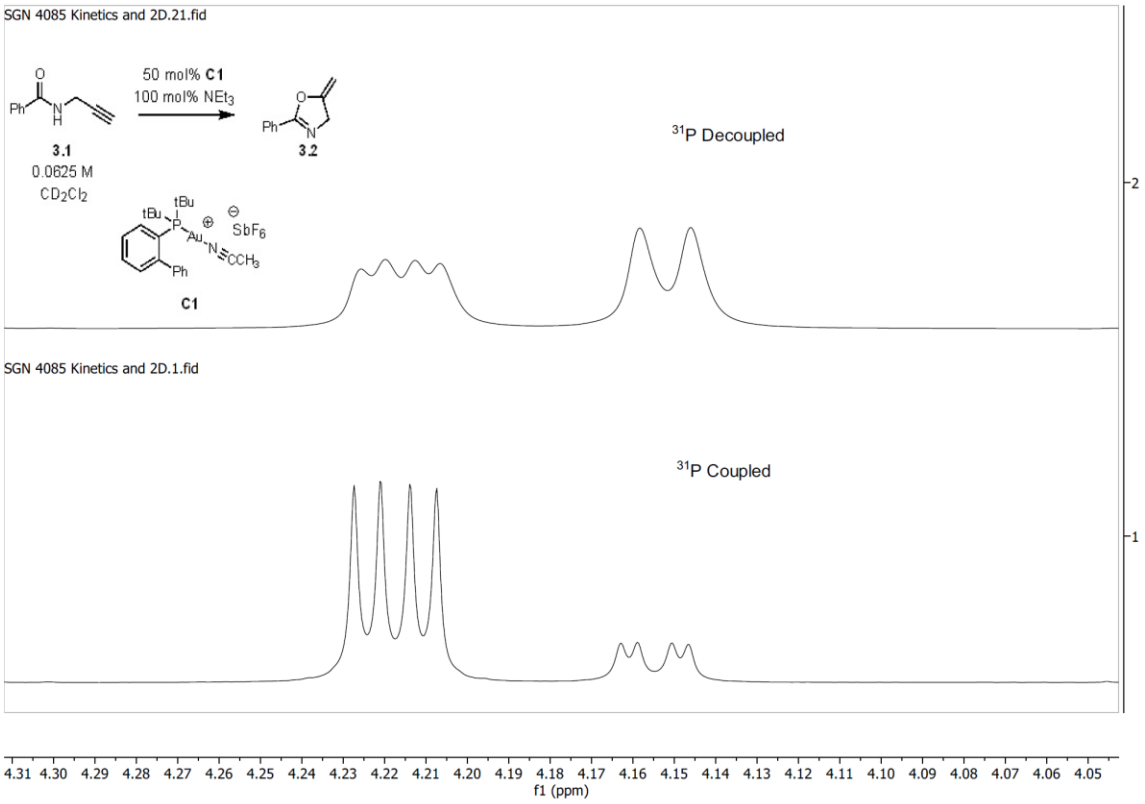

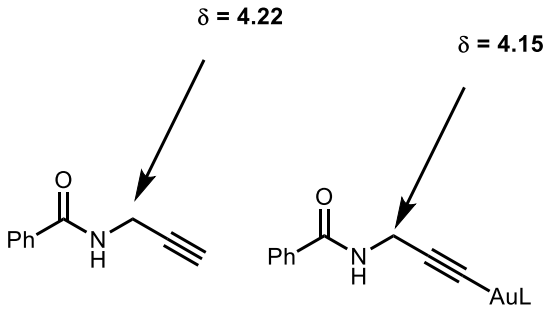

Figure 103 Change in ^{31}P-decoupled 1H NMR due to Acetylide Formation

Under these conditions, the reaction only reaches approximately 55% conversion in three hours, despite the extremely high catalyst loading. The major peaks in the ^{31}P spectrum at the beginning of the reaction are **3.1-Au-1** and **3.1-**

Au-2. These assignments were made on the basis of previously-reported assignments in which the mono and digold **C1** acetylides of phenylacetylene were found at 64.4 and 62.71 in CD_2Cl_2, respectively.[113] A minor peak corresponding to **C1** can be seen at 57ppm, with an unknown peak appearing at approximately 58.5ppm.

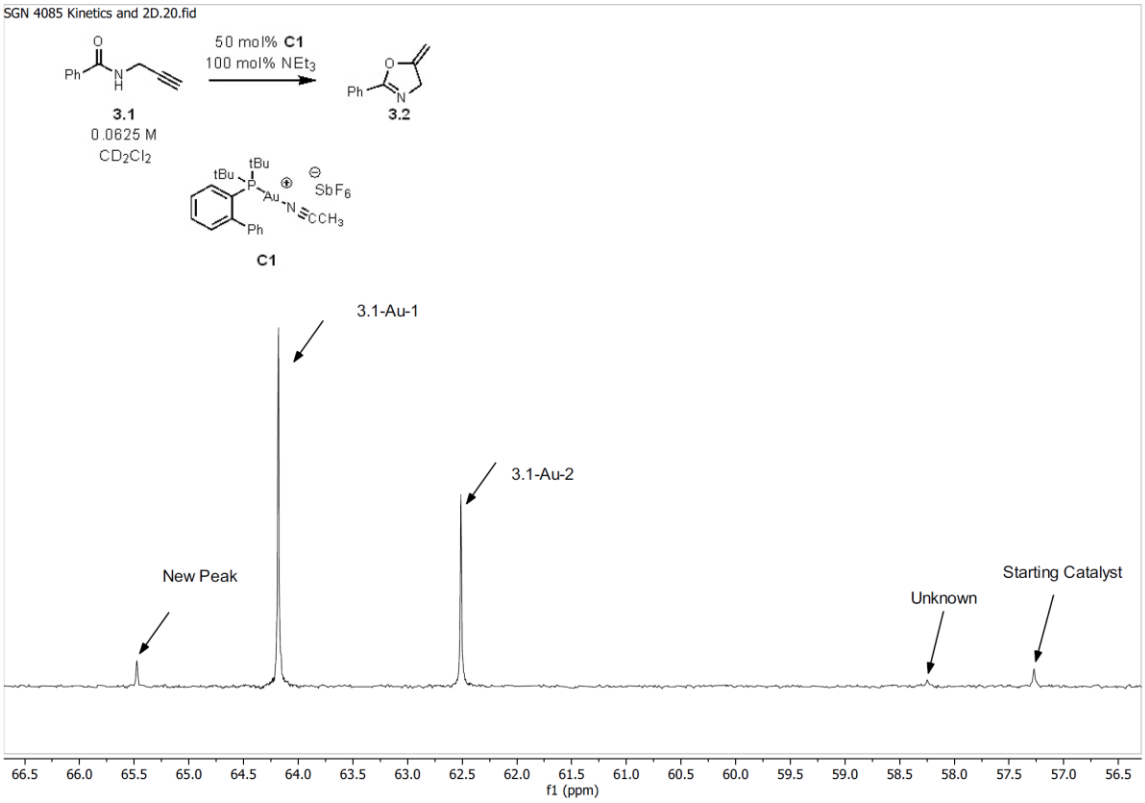

Figure 104 Initial ^{31}P NMR of High Gold and Triethylamine Loading Cyclization

Most intriguing is a new resonance at ~65.5ppm, which doesn't correlate to any species previously observed in the kinetics experiments not doped with triethylamine. This peak, hereby referred to as corresponding to species **3.3-Au-1** (see discussion of its identification below), is the major peak after three hours, and by 12 hours is virtually the only phosphorus species observed in the spectrum.

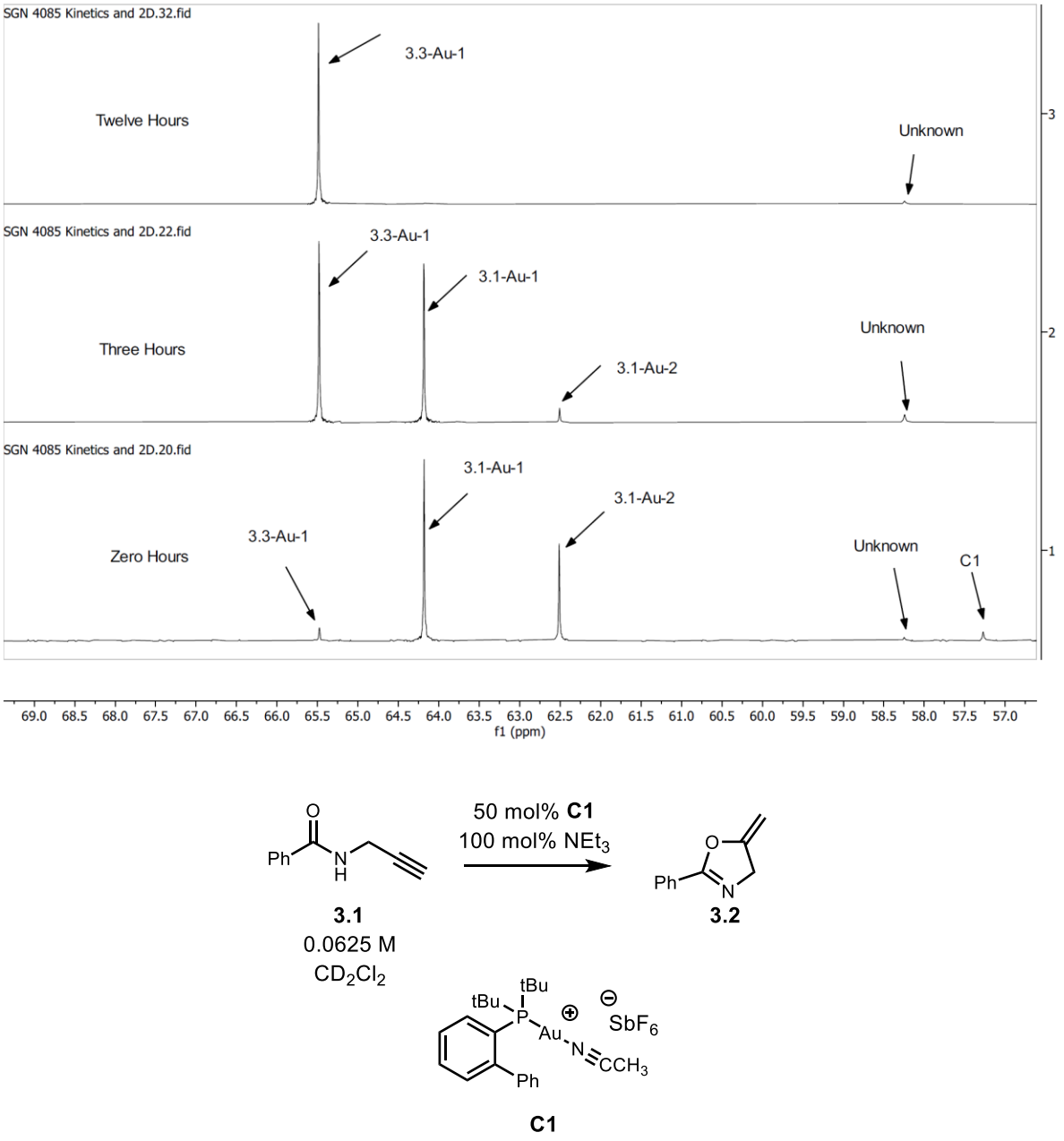

Figure 105 12 Hour Change in ^{31}P NMR of High Gold and Triethylamine Loading Cyclization

Unexpected Outcomes: Impact of Triethylamine on Product Formation

The identity of **3.3** was not immediately gleaned from reaction conditions above. Further attempts to isolate possible vinylgold intermediates were repeated with **C2**, this time using stoichiometric gold and three equivalents of triethylamine to shut down any possible protodeauration pathways. The reaction was also performed at higher concentration (~150% the scale typically used for a kinetics experiment) to better visualize the products formed.

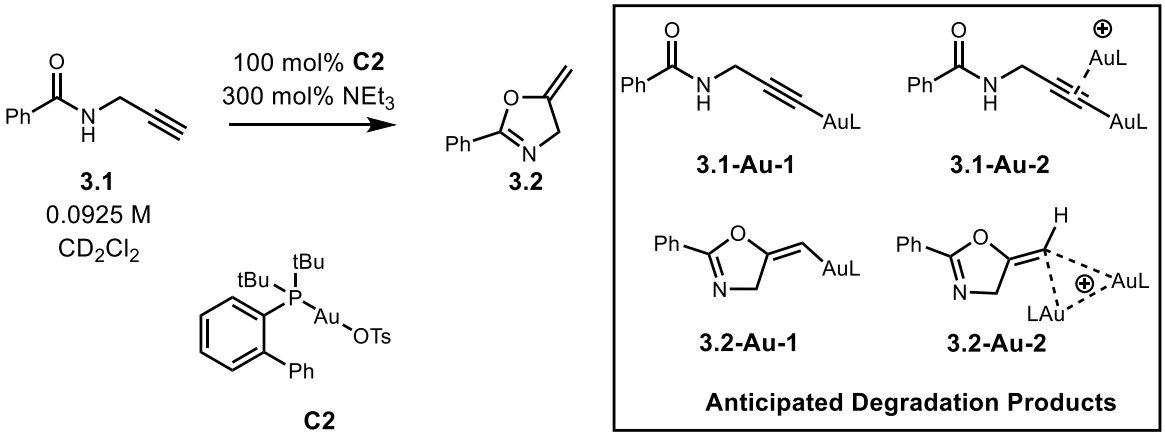

Figure 106 Cyclization with 100 mol% **C2** and 300 mol% Triethylamine

Under these conditions, **3.1-Au-1** is formed near-quantitatively and is the overwhelmingly major product by ^{31}P NMR at a reaction time of forty minutes.

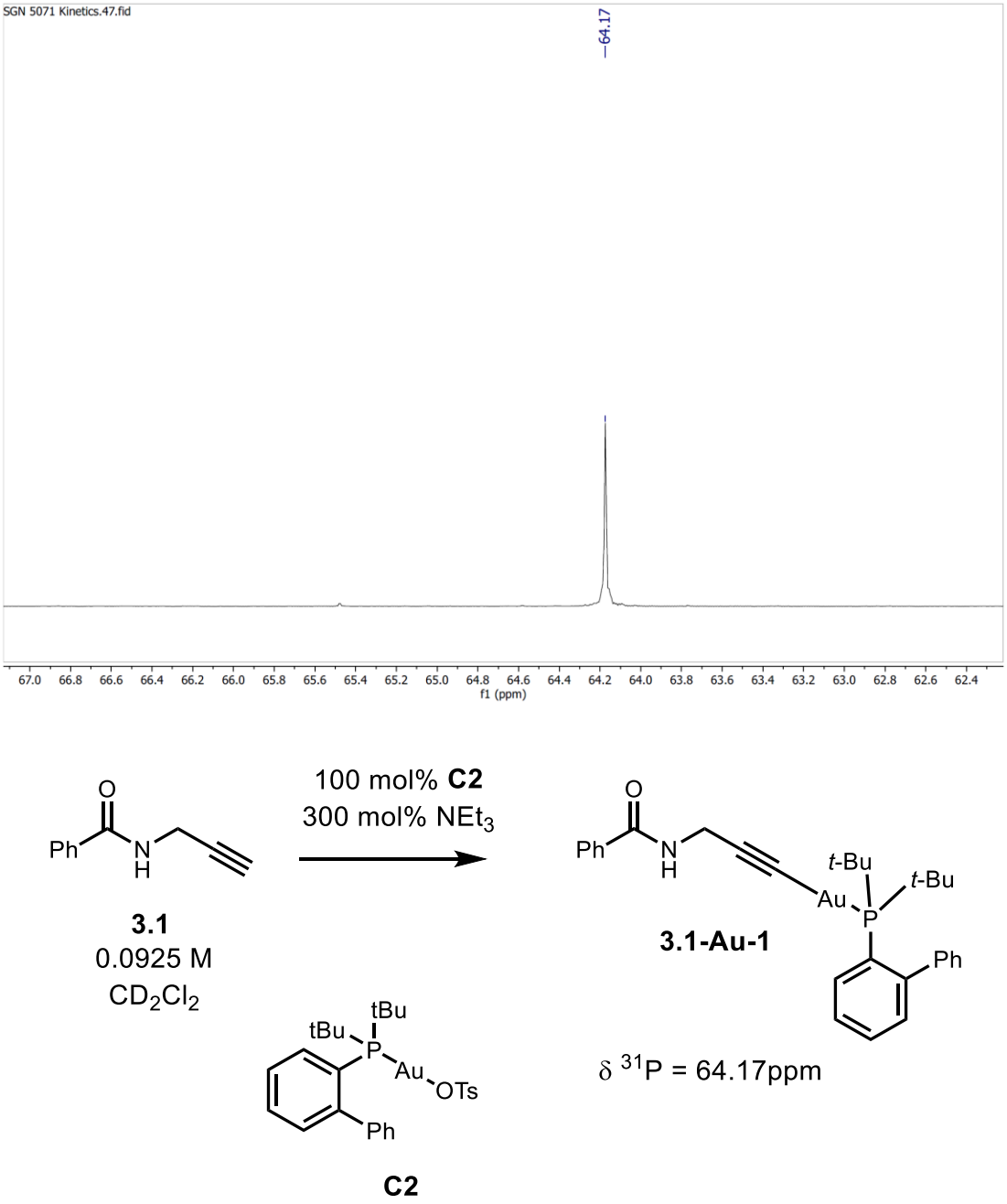

Figure 107 ^{31}P NMR of 3.1-Au-1 at Reaction Time Forty Minutes

The identity of **3.1-Au-1** was further confirmed by comparative ^{1}H NMR spectroscopy with and without phosphorus coupling, which shows a clear simplification of the P-bonded *t*-butyl groups and the N-bonded methylene.

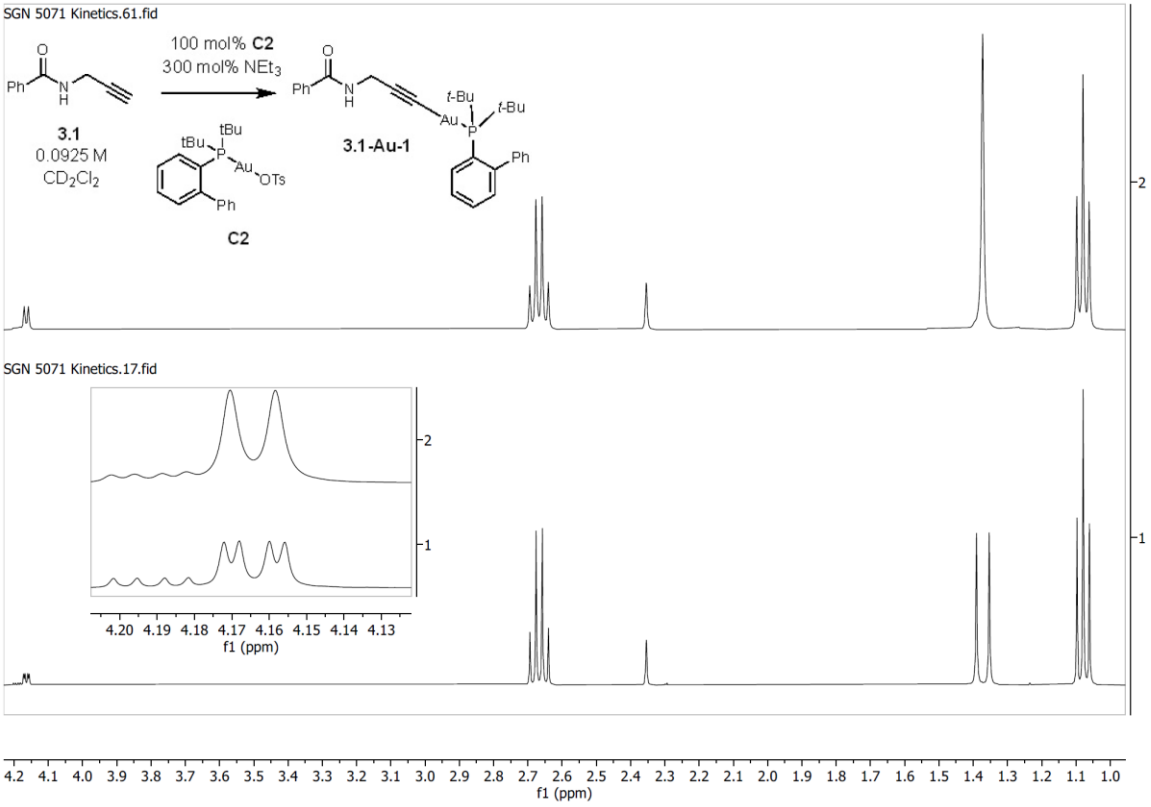

Figure 108 Comparative ^{31}P Coupled and Decoupled ^{1}H spectra of **3.1-Au-1** at Reaction Time Forty Minutes

The identity of the non-aromatic carbons correlating to the original benzamide fragment were identified by HSQC and HMBC spectroscopy. A summary of the most significant nuclei correlations are shown in the figure below.

δ ^{1}H = 4.16ppm, (dd, J^{3}_{HH} = 4.9Hz, J^{5}_{HP} = 1.7Hz, 2H)
δ ^{13}C = 31.26ppm (d, J^{4}_{CP} = 6.88Hz
δ ^{13}C = 96.61ppm (d, J^{3}_{CP} = 23.38Hz)
δ ^{13}C = 127.8ppm large coupling (>100Hz) predicted but not resolved
δ ^{31}P = 64.17ppm

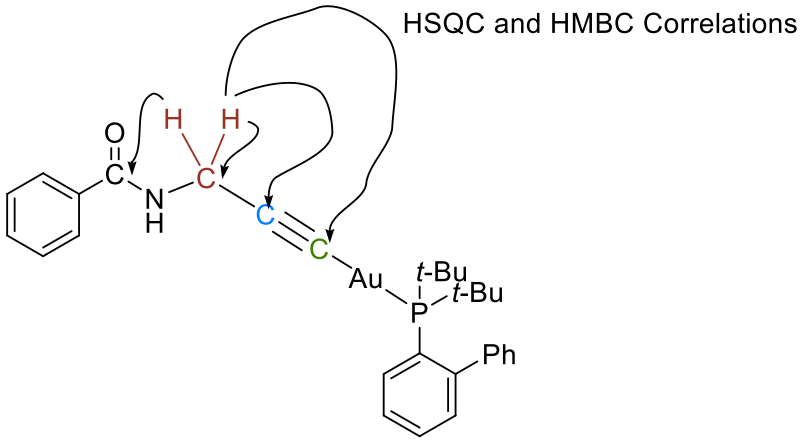

Figure 109 Summary of 2D Correlations for **3.1-Au-1**

The conditions of stoichiometric gold and excess triethylamine allowed for facile identification of **3.1-Au-1**. Having seen conversion to product in the previous experiment with stoichiometric triethylamine and half an equivalent of gold, this reaction mixture was retained for several days and analyzed periodically by NMR. Slow conversion to a different species was observed, but not the expected oxazoline product of **3.2**. The unknown ^{31}P resonance at ~65ppm from the experiment detailed above reemerges and becomes the major product over time. Spectroscopic analysis eventually identified this as the aromatic oxazole alkylgold **3.3-Au-1**.

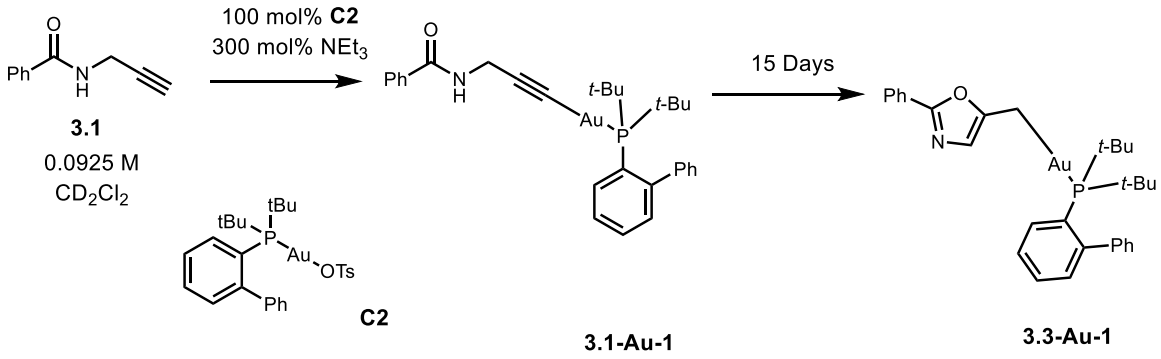

Figure 110 Gradual Formation of Alkylgold Oxazole **3.3-Au-1**

Just as was done with **3.1-Au-1**, a variety of one and two-dimensional NMR spectra were collected. While after 15 days the reaction mixture is impure and features an array of species, similar to the spectra above for the acetylide **3.1-Au-1**, several key resonances and crosspeaks could be used to confirm the identity of **3.3-Au-1**.

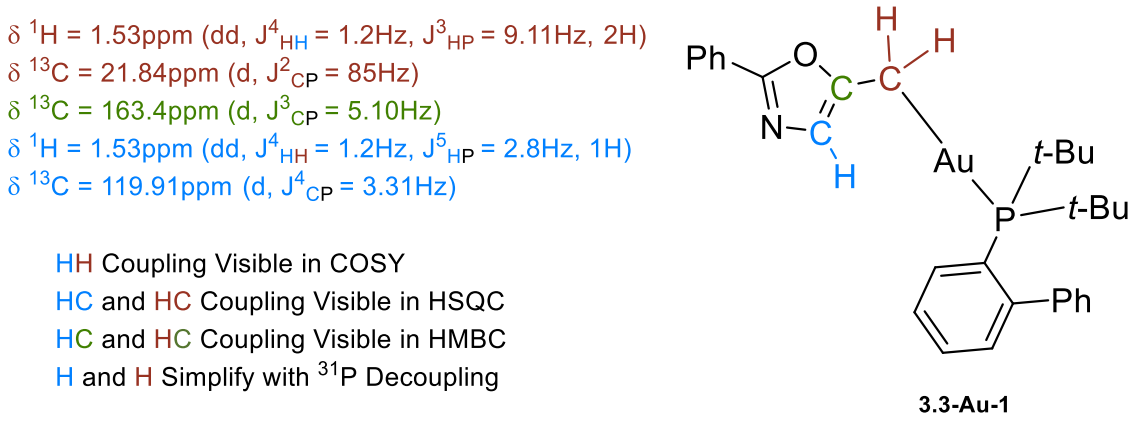

Figure 111 Summary of 2D Correlations for **3.3-Au-1**

Given these same conditions have provided successful isolation of NHC-ligated vinylgold species in the past,[106,112] this result was not anticipated. The vinylgold oxazoline **3.2-Au-1** nor its gem digold counterpart of **3.2-Au-2** are ever observed in this reaction mixture.

To see if vinylgold formation may be possible with a different ligand, the same reaction was performed substituting **C6** in place of **C2**. The reaction was analyzed kinetically for one hour, with 2D spectra immediately afterwards.

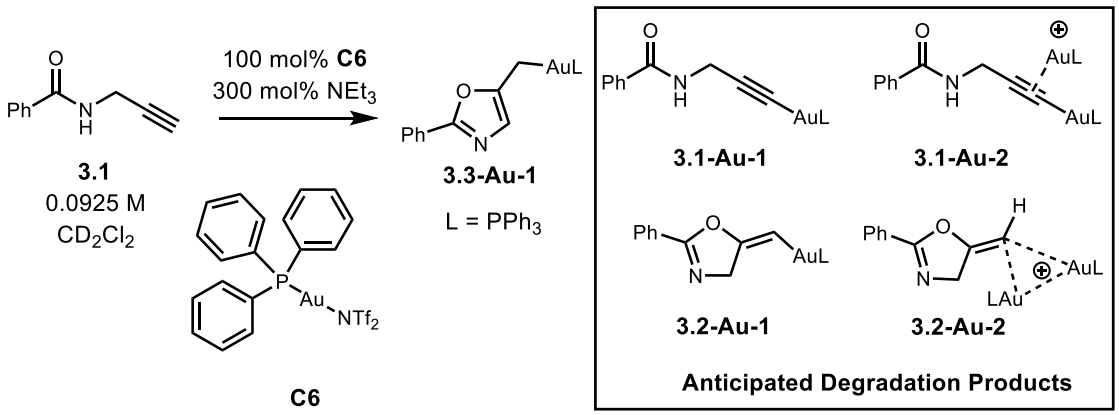

Figure 112 Cyclization with 100 mol% **C6** and 300 mol% Triethylamine

With **C6** used in place of **C2**, a starkly different outcome is observed for the experiment. After analysis of the various one and two-dimensional spectra, a very small amount of the alkylgold product is observed. Instead, a majority of the benzamide is hydrolyzed by residual water in the solvent to form keto-amide **3.4**.

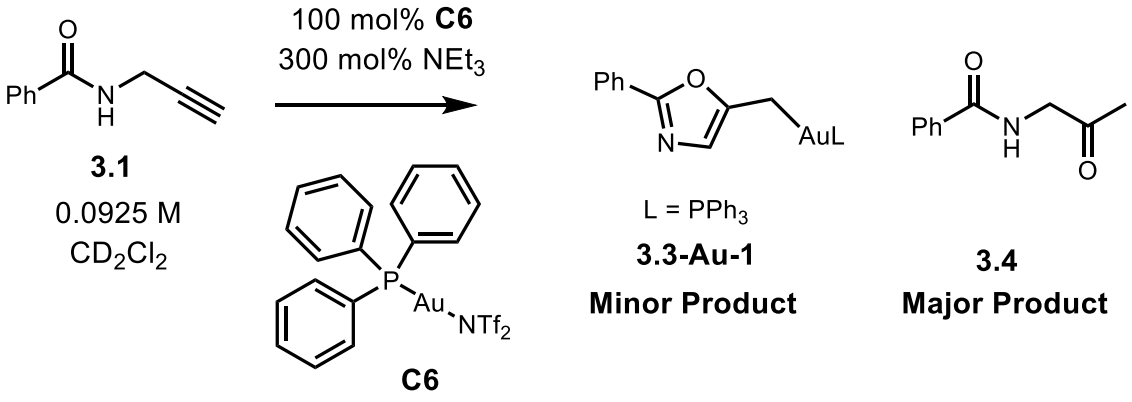

Figure 113 Hydration of Alkyne with 100 mol% **C6** and 300 mol% Triethylamine

Formation of both products is supported by NMR spectra. Starting material is observable at both zero and sixty minutes, accompanied by a new doublet at ~4.31ppm not observed for the cyclization with **C2**. Additionally, a new doublet at ~2.51ppm not associated with the oxazoline **3.2** is formed over time, reaching a much higher concentration in a spectrum collected later at a reaction time of 21 hours. ^{31}P decoupling (see below) demonstrated this peak to belong to the alkylgold product.

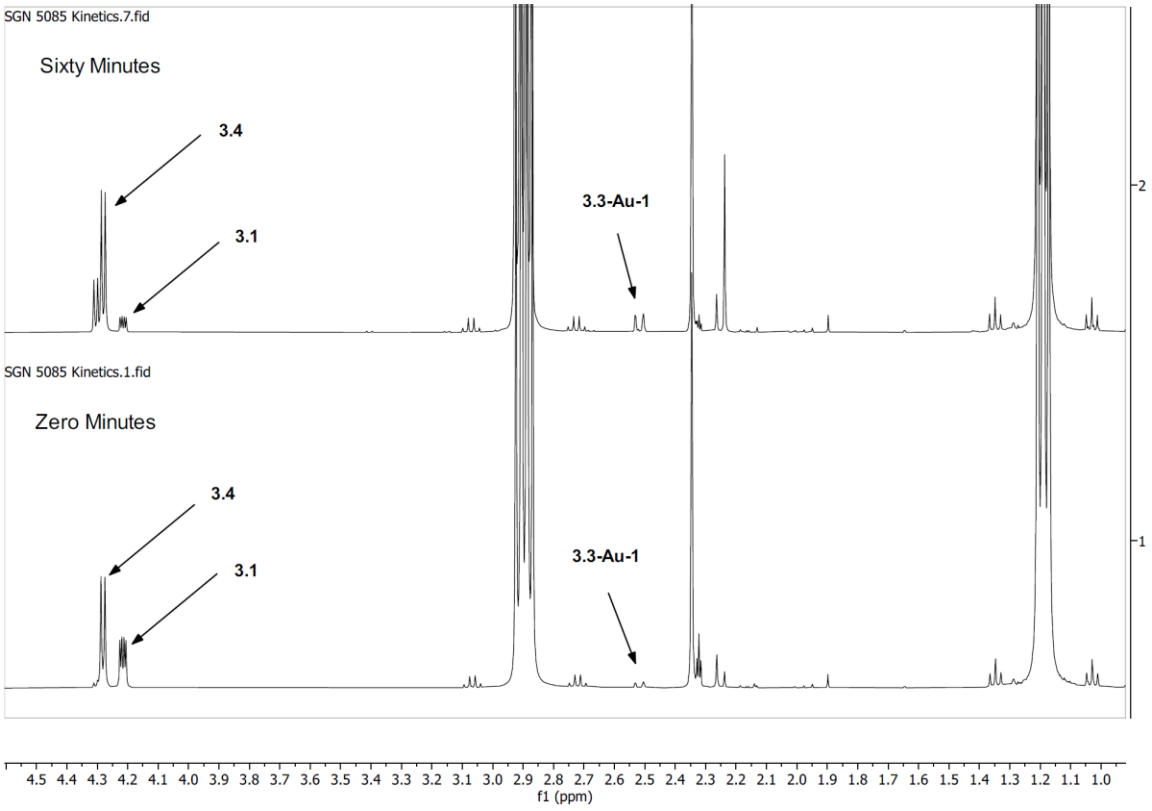

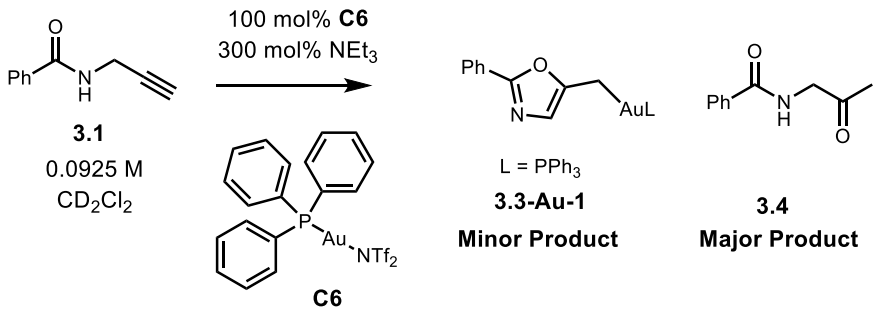

Figure 114 ^{1}H Spectra of Cyclization with **C6** at Zero and Sixty Minutes

^{31}P spectra are largely static throughout the reaction course, except for a minor peak which gradually increases in intensity over the course of 21 hours. Given the slow evolution of the ^{1}H resonance at 2.51ppm later identified as alkylgold, this phosphorus resonance is likely to be that of the alkylgold. Comparative ^{31}P spectra at zero, one, and 21 hours are shown below.

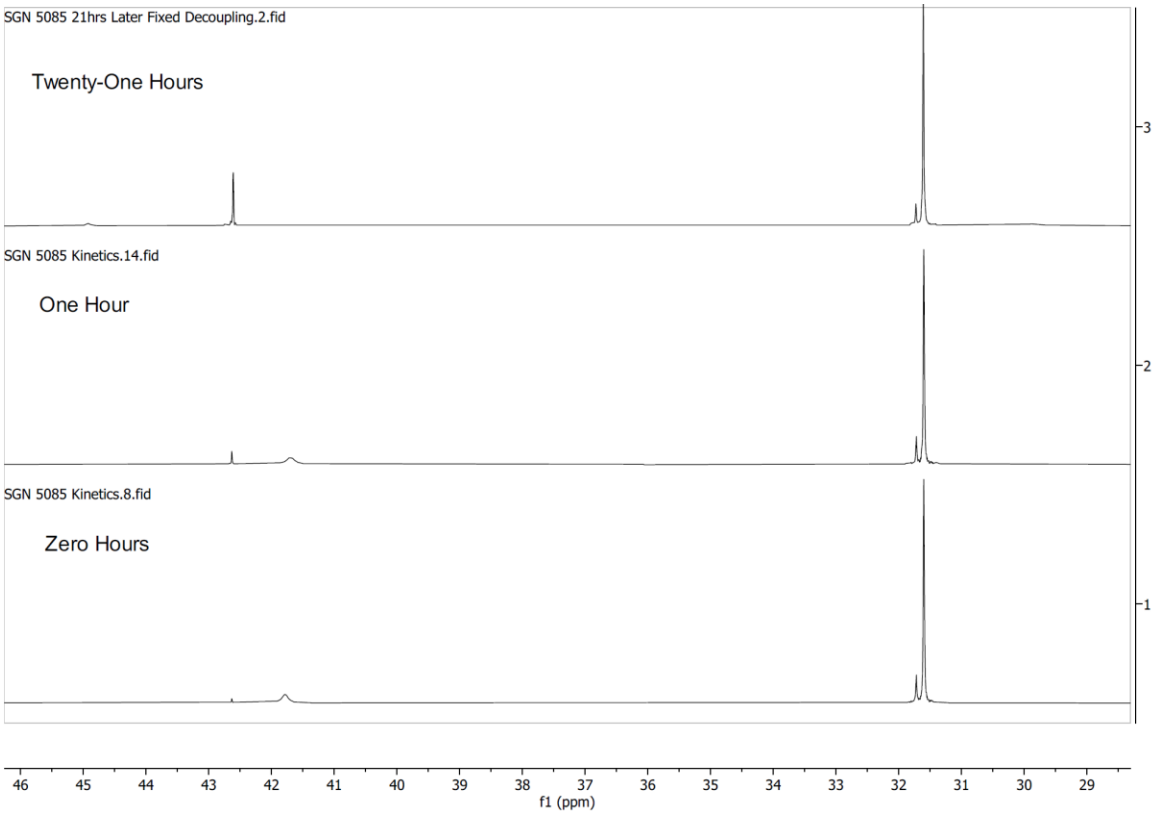

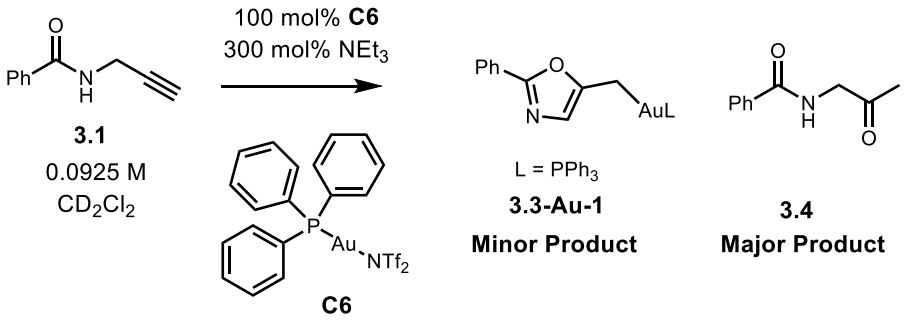

Figure 115 ^{31}P Spectra of Cyclization at Zero, One, and Twenty-One Hours

^{31}P decoupled ^{1}H spectra collected at a reaction time of 21 hours allowed for identification of the doublet at 2.51ppm as the exocyclic methylene of **3.3-Au-1**. The comparative ^{31}P coupled and decoupled spectra are shown below.

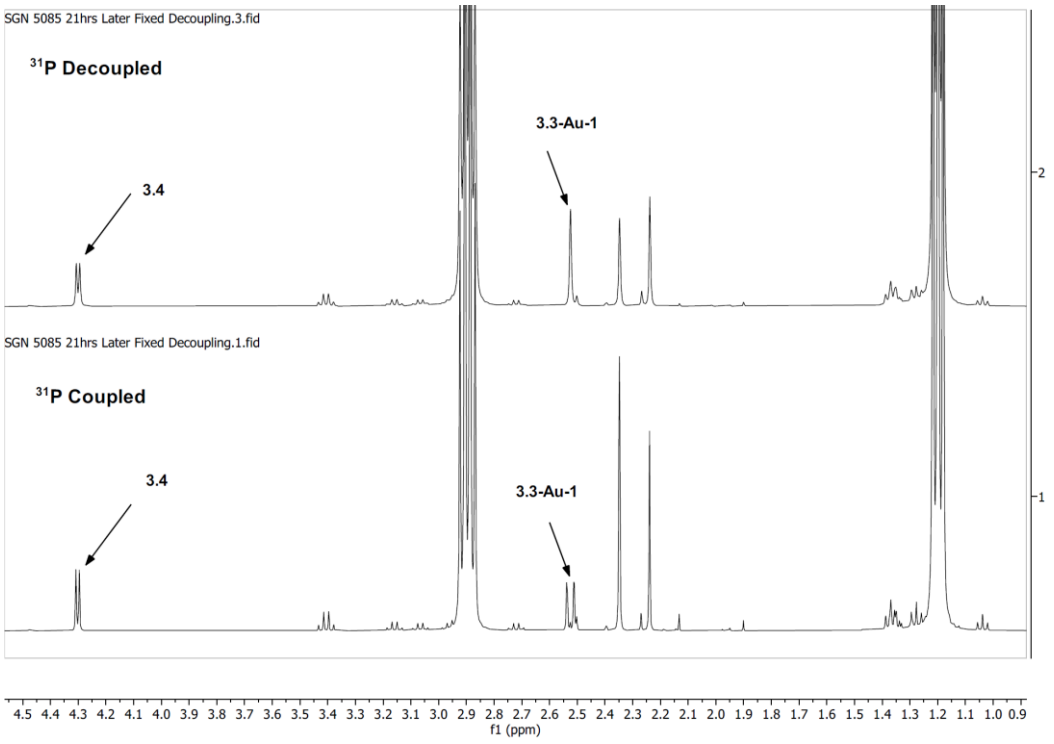

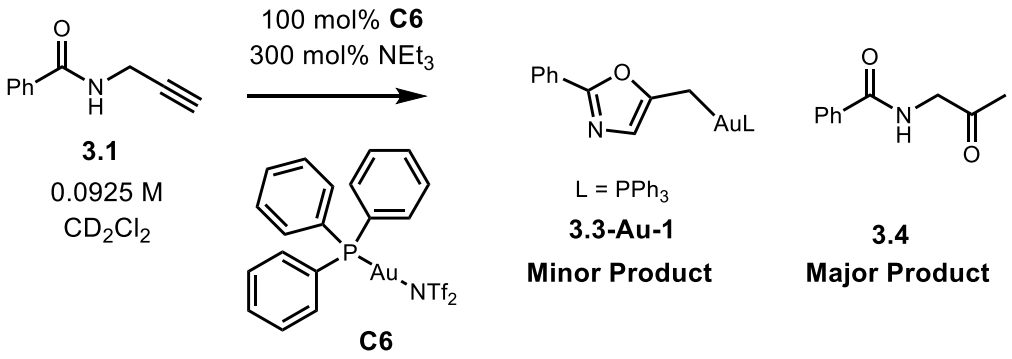

Figure 116 ^{31}P Coupled and Decoupled ^{1}H Spectra of Cyclization at Twenty-One Hours

The identities of both the alkylgold and keto-amide above were further confirmed by 2D analysis.

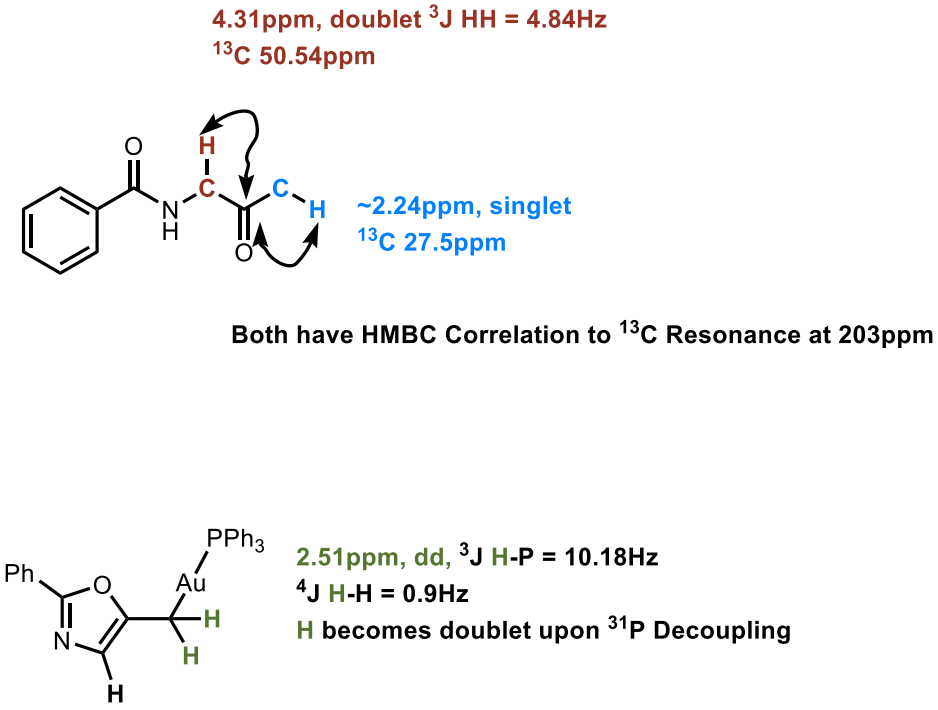

Figure 117 Summary of 2D NMR Correlations for Cyclization with 100 mol% **C6** and 300 mol% Triethylamine

Discussion of Triethylamine Impact on Reaction Outcome

The trends here indicate a significant ligand effect. With Johnphos as the ligand, no hydration product is observed. This can be rationalized by the weaker induction of gold where L = Johnphos. When L = PPh_3, the alkyne π-complex is more electrophilic, resulting in hydration by residual water. For L = PPh_3, this hydration competes closely with cyclization to the alkylgold (integration by ^1H NMR shows the alkylgold:ketone ratio to be ~4:5).

The behavior here also stands in contrast to literature reports where groups have reported successful isolation and characterization of vinylgold species under similar conditions of excess base. Hashmi's group has successfully isolated the oxazoline vinylgold for internal alkynes,[114] but only demonstrated the vinylgold for the terminal alkyne by structural inference following demetallation of the intermediate in aqueous acetonitrile[106]. Shi's group, however, has isolated the terminal alkyne-derived vinylgold (benzamide phenyl replaced by *p*-$CF_3C_6H_4$) under similar conditions of excess triethylamine.[112] Notably, each of the complexes in these examples bore the NHC IPr ligand. Phosphine vinylgolds have never been isolated and characterized for this system, only ever proposed as intermediates observed *in situ*.[103]

The successful isolation of NHC vinylgolds by Hashmi and Shi is also a curiosity given the isolation of phosphine-ligated vinylgolds always fails. NHC ligands are stronger sigma donors than phosphines, thereby forming less electrophilic catalysts. This should concurrently lower the energy barrier for protodeauration of NHC vinylgolds as the resulting Au(I) species is more stable.

The phosphine vinylgolds should therefore be *easier* to isolate than their NHC counterparts due to slower demetallation.

A possible explanation for this discrepancy can be argued along similar lines as the diverging reactivity for hydration vs cyclization when L = Johnphos or PPh_3. π-complexes of Au(I) phosphines will be more electrophilic than those of Au(I) carbenes. Simultaneously, the alkyne proton will also be more acidic for these complexes. Given the observation of acetylides as intermediates, as well as the importance of deuterium-labeling in this mechanism, phosphine vinylgolds may be difficult to isolate for two reasons. One, the release of acid by acetylide formation spurs a different mechanistic pathway in which the vinylgold is never formed. Or two, this release of acid into the reaction mixture results in more facile protodeauration, rendering vinylgolds impossible to isolat

The Search for Vinylgold: Reactions with Lower Triethylamine Loading

In all the triethylamine experiments described above, the mono and digold acetylides for the Johnphos and PPh_3-derived catalysts were identified. Vinylgolds of the type **3.2-Au-1** and **3.2-Au-2** had yet to be isolated or identified in the reaction mixtures. Therefore, triethylamine loadings were reduced to sub-stoichiometric loadings to see if conditions closer to typical, non-basic reaction conditions might afford identification of some of the other ^{31}P signals observed in experiments from chapter two.

Initial conditions were 8 mol% of catalyst **C1** or **C6** with 50 mol% of triethylamine. Higher catalyst loading was used for better visualization of gold-

bonded intermediates by NMR. No reaction occurred under these conditions, demonstrating a need for an abundance of catalyst relative to base for the reaction proceed. When triethylamine loading was halved to 25 mol%, there was still no cyclization, with only acetylides visible as products.

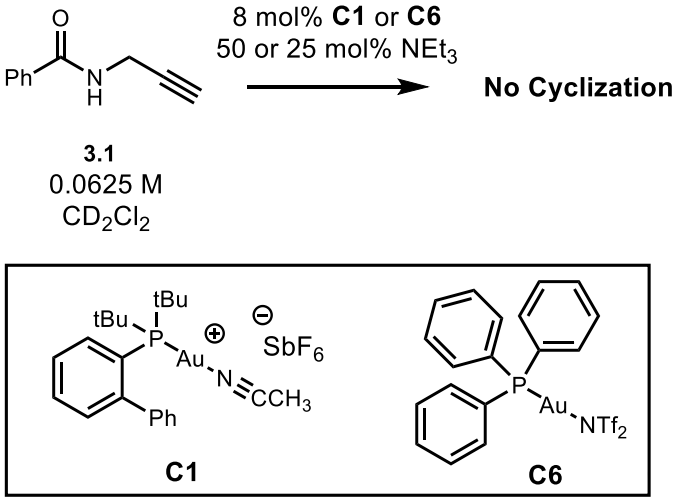

Figure 118 No Reaction at 8 mol% Gold and 25% or 50 mol% Triethylamine

Triethylamine loading was again halved to 13 mol%, at which point the reaction finally began to occur, with **3.2** slowly forming over time when **C1** was used as catalyst. The rate with triethylamine is extremely slow, occurring at ~7% the rate of the typical reaction conditions, despite having double the usual loading of catalyst.

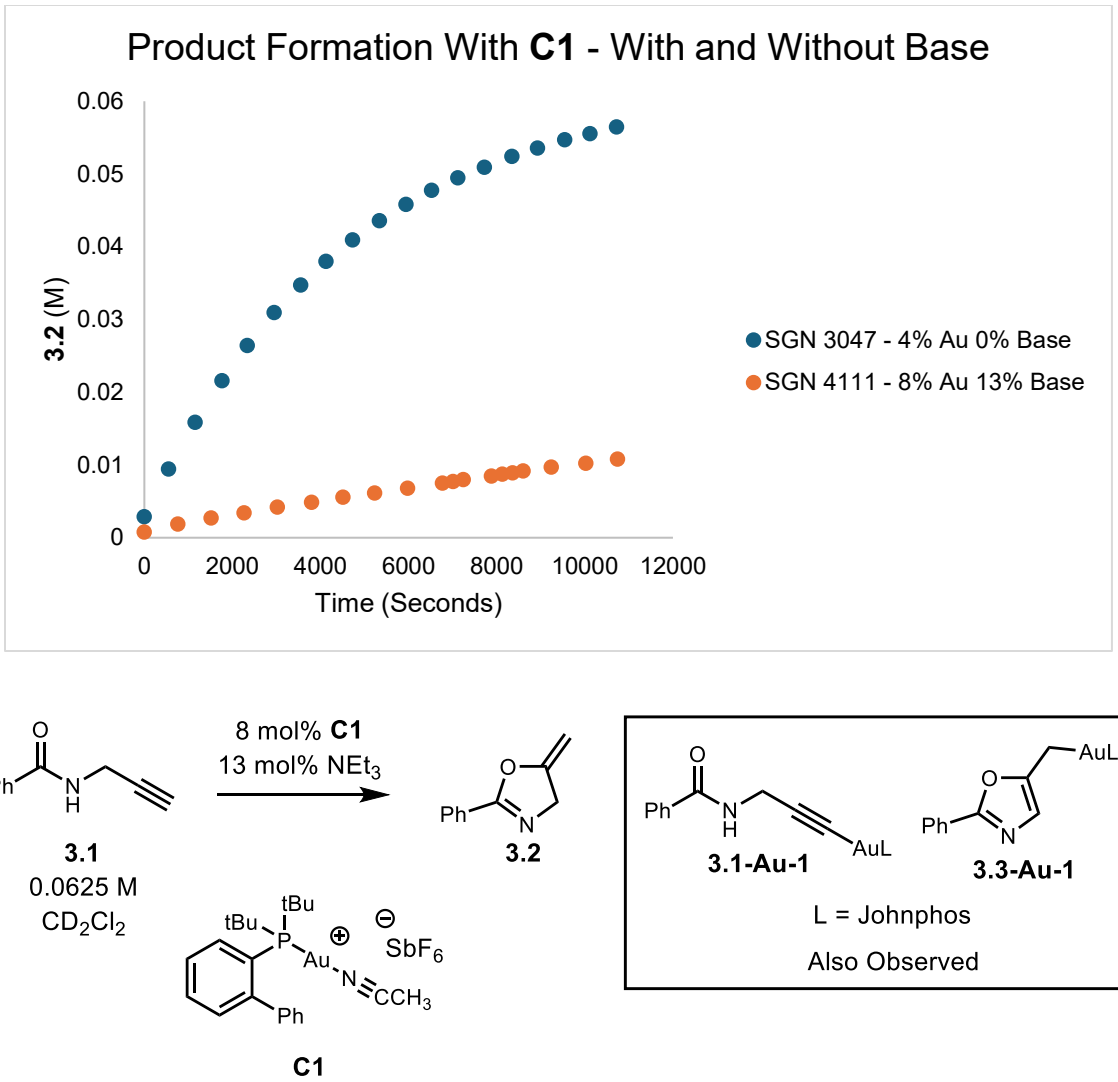

Figure 119 Comparative Product Formation with **C1** with and without Triethylamine

^{31}P spectra tell a familiar story, with alkylgold **3.3-Au-1** featuring as a minor product in the ^{31}P spectrum collected at the beginning of the reaction. After three hours, it is the major product. Intriguingly, the peak proposed to correspond to **3.1-Au-2** vanishes over time, whereas the monogold acetylide **3.1-Au-1** remains present throughout. The presence of alkylgold **3.3-Au-1** is further supported by the presence of a doublet at ~1.5ppm in the ^{1}H spectrum which collapses upon ^{31}P decoupling.

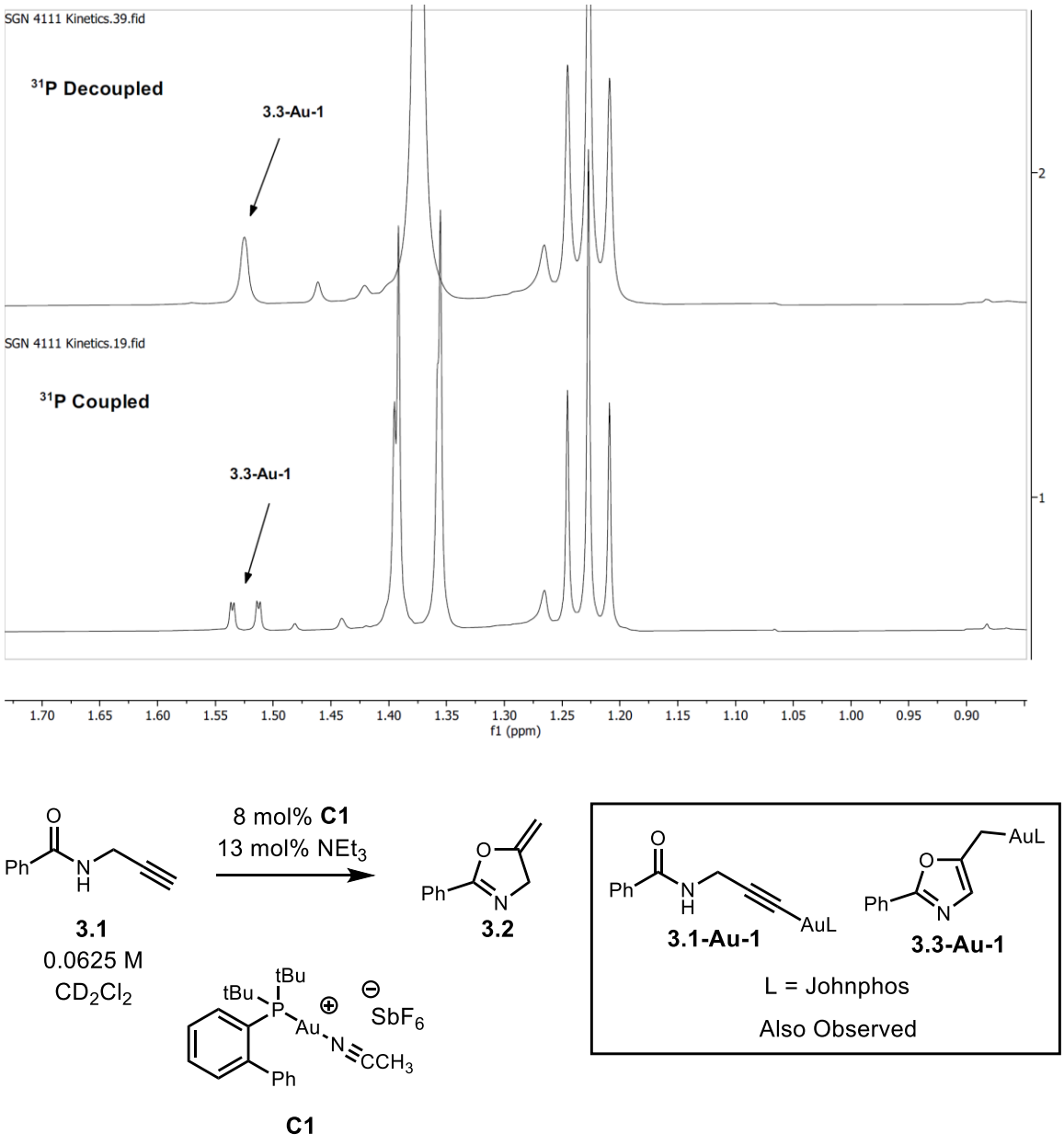

Figure 120 ^{31}P Coupled and Decoupled ^{1}H Spectra Showing Alkylgold with 8 mol% **C1** and 13 mol% Triethylamine

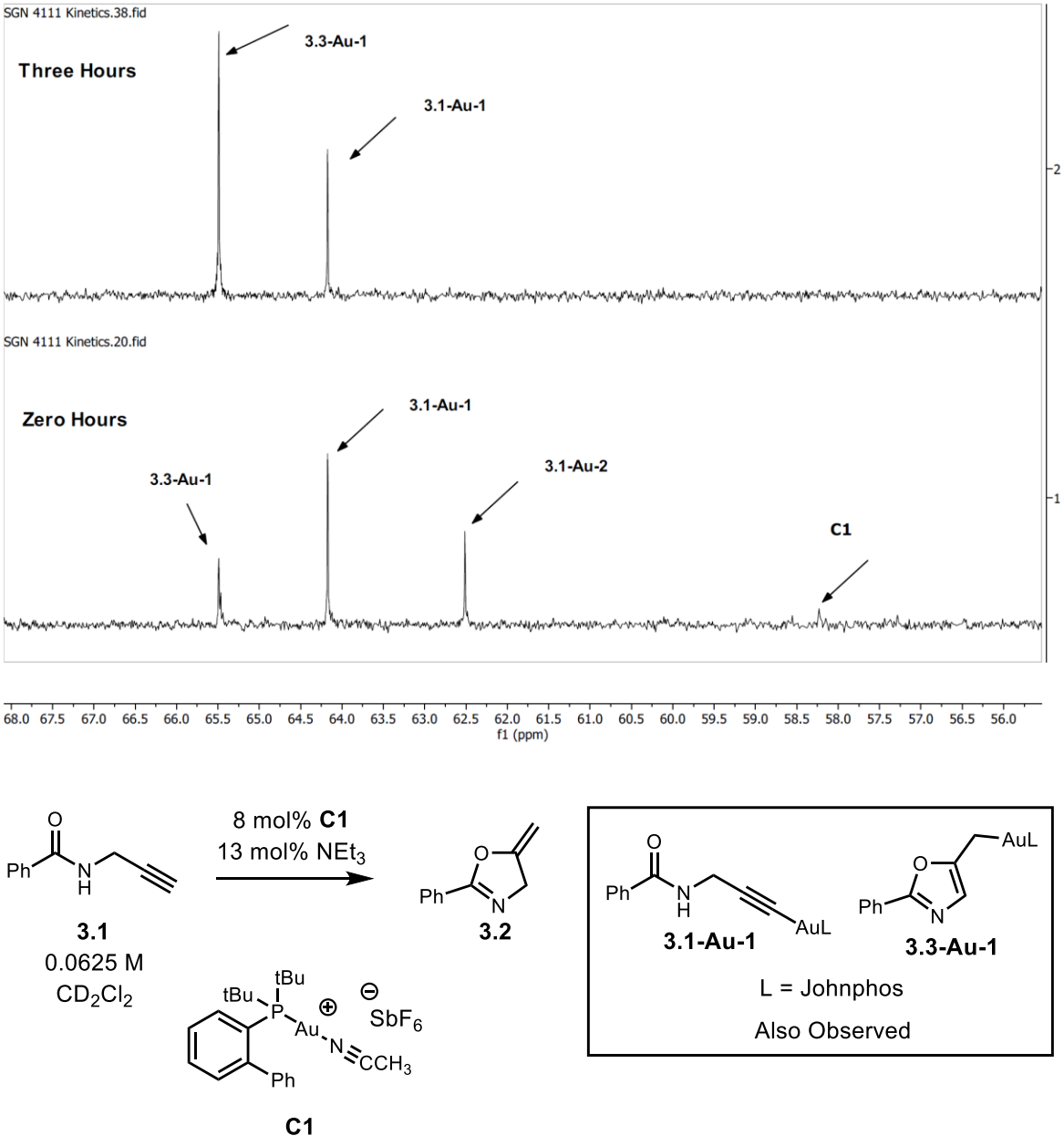

Figure 121 ^{31}P Spectra Cyclization with 8 mol% **C1** and 13 mol% Triethylamine at Zero and Three Hours

13 mol% triethylamine loading also proved to be the tipping point for **C6**, which began to cyclize under these conditions. Due to the extremely fast rate when **C6** is used as catalyst under the typical reaction conditions (see discussion in chapter 2), it was anticipated the rate here may also be fast, albeit slowed by the

presence of base as was observed with **C1**. Therefore, spectra were only collected for one hour of reaction time.

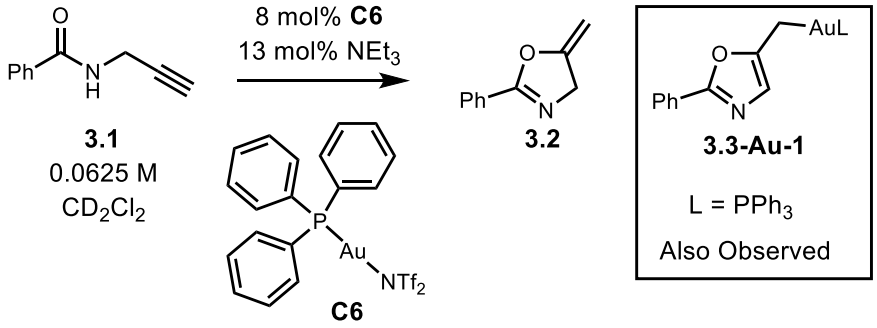

Figure 122 Cyclization with 8 mol% **C6** and 13 mol% Triethylamine

Cyclization is indeed much slower than the rate without base, proceeding at ~27% the original rate. While this slowing is substantial, **C6** is much less impacted by the presence of triethylamine than **C1**, which had its rate reduced to ~7%.

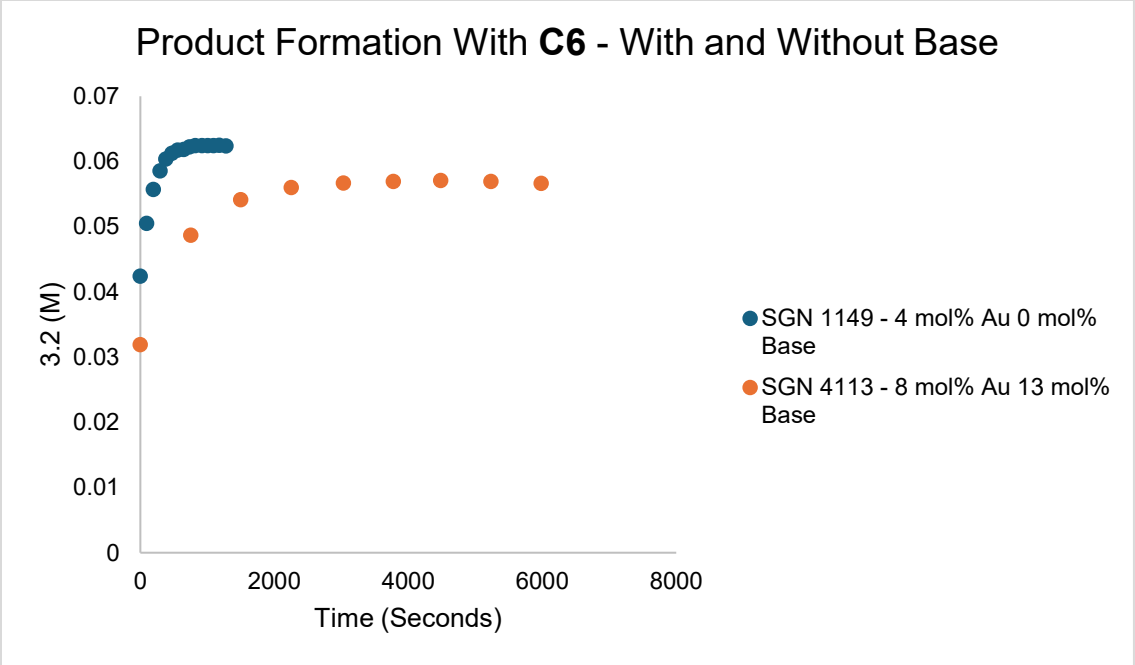

Figure 123 Comparative Product Formation with **C6** with and without Triethylamine

In the ^{1}H spectra, peaks corresponding to **3.2** are visible and major. Intriguingly, the resonance corresponding to alkylgold **3.3-Au-1** are visible from the first spectrum, indicating rapid formation of the alkylgold is possible with these conditions. In the first spectrum collected, the endocyclic methylene of **3.2** and the exocylic methylene of **3.3-Au-1** integrate in a 1:0.17 ratio, showing close to a 5:1 ratio between the two products. At this point in the reaction, approximately half of the starting material **3.1** has been consumed. After one hour, no starting material remains in the ^{1}H spectrum, and the ratio of oxazoline **3.2** to alkylgold **3.3-Au-1** has grown to 1:0.09 (approximately 10:1).

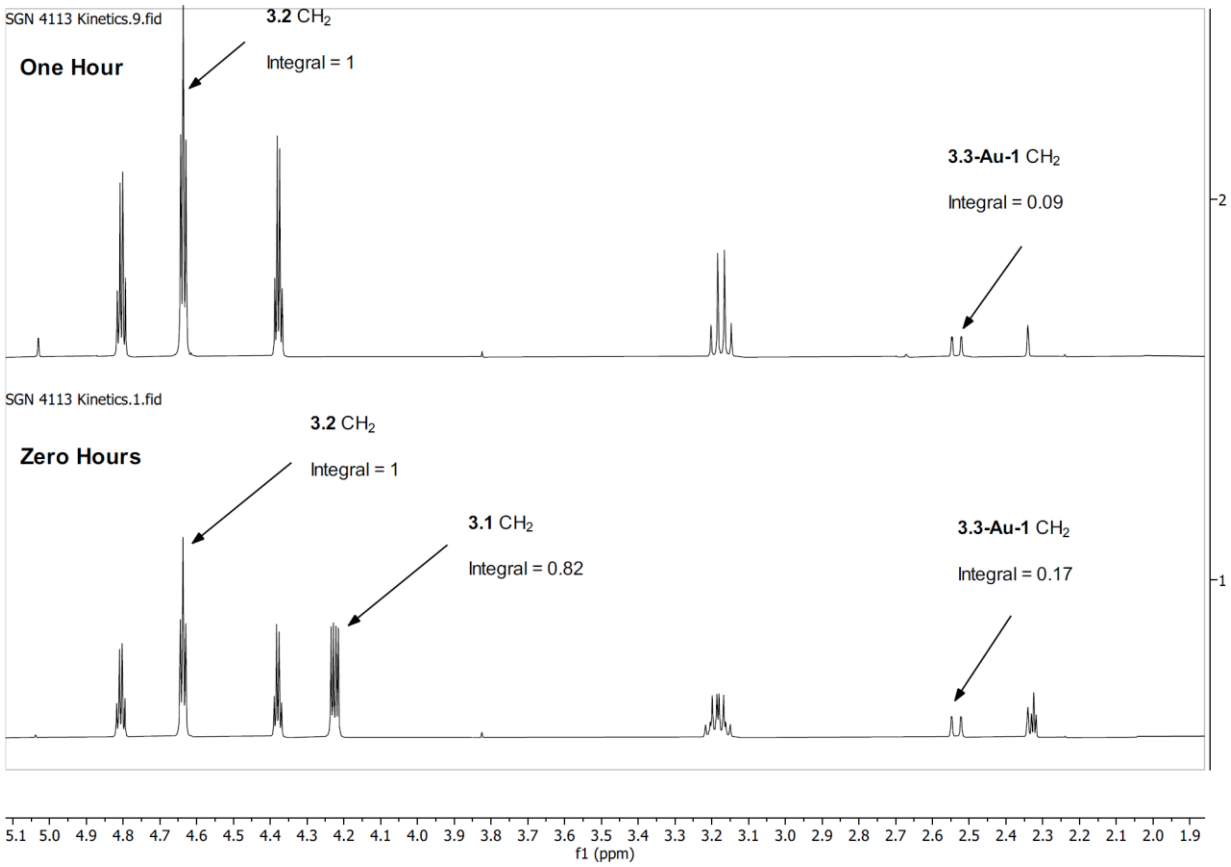

Figure 124 Stacked ^{1}H plot for 3.1 Cyclization with 8 mol% **C6** and 13 mol% Triethylamine

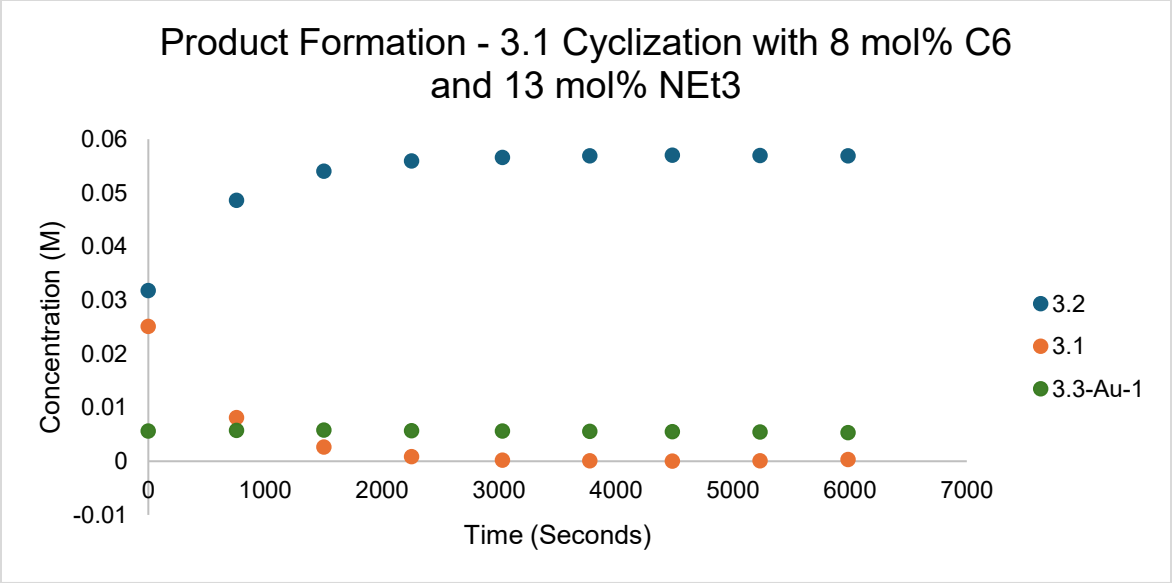

Figure 125 Product Formation over time with 8 mol% **C6** and 13 mol% Triethylamine

Stacked plot analysis shows flat integration values for **3.3-Au-1** over this one-hour period, indicating **3.3-Au-1** is likely formed directly via a pathway involving an acetylide, either **3.1-Au-1** or **3.1-Au-2**. If oxazoline product **3.2** were to undergo gold-catalyzed tautomerization to oxazole **3.3-Au-1**, integrals for **3.3-Au-1** should not remain flat, as the gradual formation of **3.2** would likewise lead to formation of **3.3-Au-1**.

^{31}P NMR spectra over the one-hour reaction do not change, showing two major peaks at 45, 42, and 30ppm. The peak at 30ppm is free catalyst. The identity of the other two peaks is not immediately obvious, but the predominant size of the peak at 42ppm throughout the reaction course and the static integrals for the alkylgold in the ^{1}H spectra mean it likely belongs to **3.3-Au-1**. The identity of the signal at 45ppm is less obvious. It is unlikely to be gold acetylide given the absence

of any of the associated signals in the ^{1}H spectrum. It is likely an off-cycle degradation product.

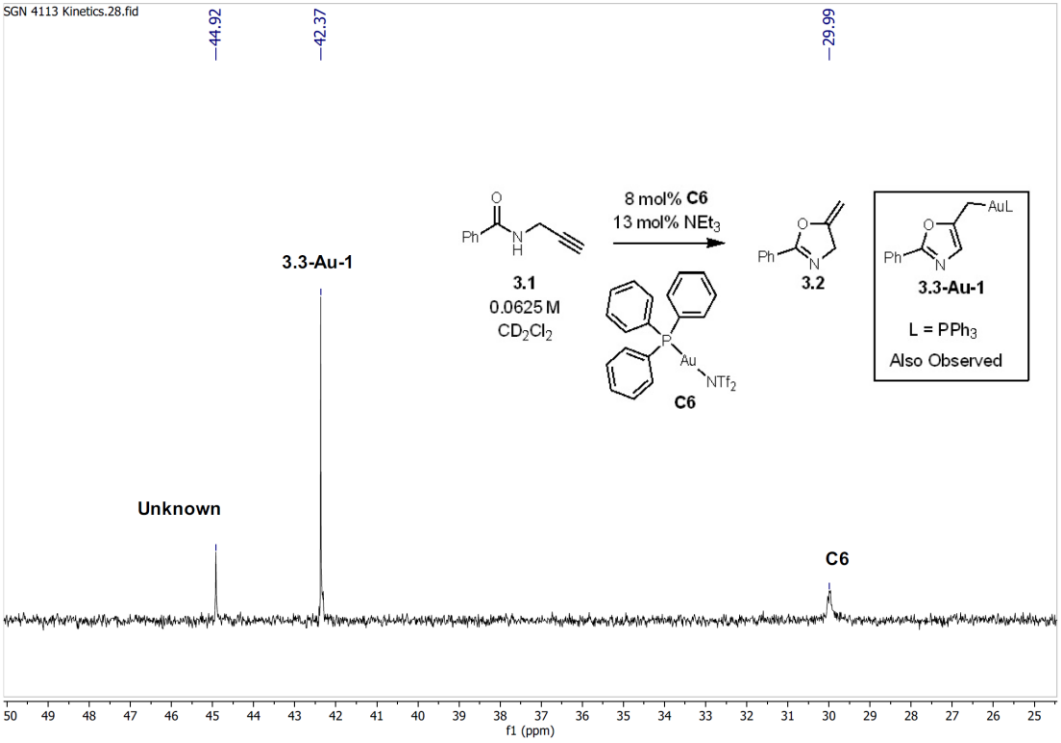

Figure 126 ^{31}P Spectrum of Cyclization with 8 mol% **C6** and 13 mol% Triethylamine at One Hour of Reaction Time

To further explore the impact of triethylamine on the cyclization, its loading was again reduced, this time to 7.2%. At this loading of triethylamine, the catalytic performance of both **C1** and **C6** are still sluggish compared to their rates without base, but both see a modest rate increase as described in **Table XIII** below. The same acetylide and alkylgold intermediates are observed in the ^{1}H and ^{31}P spectra whether triethylamine is at 7.2 mol% or 13 mol%.

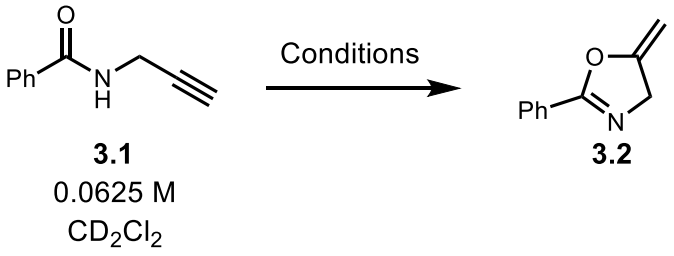

3.1
0.0625 M
CD_2Cl_2

3.2

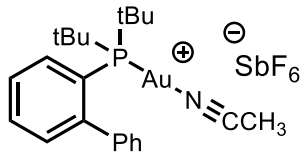

C1

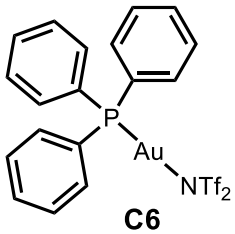

C6

Entry	Catalyst	Au Mol%	NEt_3 Mol%	Rate (s^{-1})
1	C1	8	13	1.62×10^{-5}
2	C1	8	7.2	2.07×10^{-5}
3	C6	8	13	1.59×10^{-3}
4	C6	8	7.2	2.18×10^{-3}

Table XIII Rates of **C1** and **C6** with Varied Triethylamine Loading

Support for the Divergent Pathway of Alkylgold Formation

As discussed above, alkylgold is observed as a side product for benzamide cyclization with **C6** in the presence of triethylamine. It is visible from the first ^1H spectrum collected and its integral value does not change as the reaction proceeds. No acetylide is visible for the base-treated cyclizations with **C6**, so tracking concurrent disappearance of acetylide with alkylgold formation is impossible. For cyclization with **C1** and triethylamine, both monogold acetylide **3.1-Au-1** and alkylgold **3.3-Au-1** are observed, and their integral values do change over time. To confirm the hypothesis that the alkylgold oxazole is formed directly from the acetylide, stacked plot analysis was performed to assess their rate of

formation against one another. As expected, disappearance of acetylide is inverse with appearance of alkylgold.

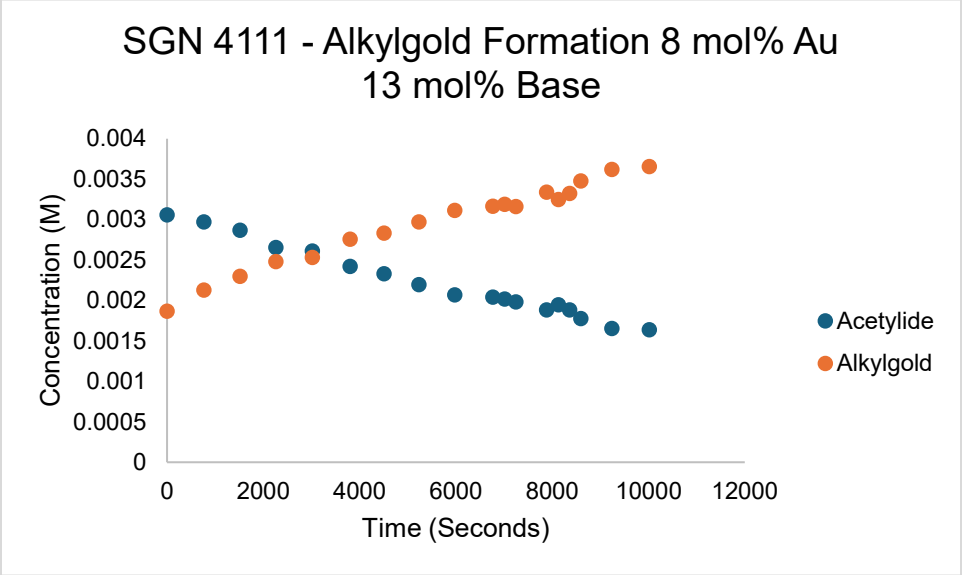

Figure 127 Inverse Relationship between Acetylide and Alkylgold

This relationship is observed at loadings of both 13% and 7.2%. The relative rates of alkylgold formation were also calculated. Very similar rates are seen, indicating triethylamine likely plays no mechanistic role outside of initial formation of acetylide.

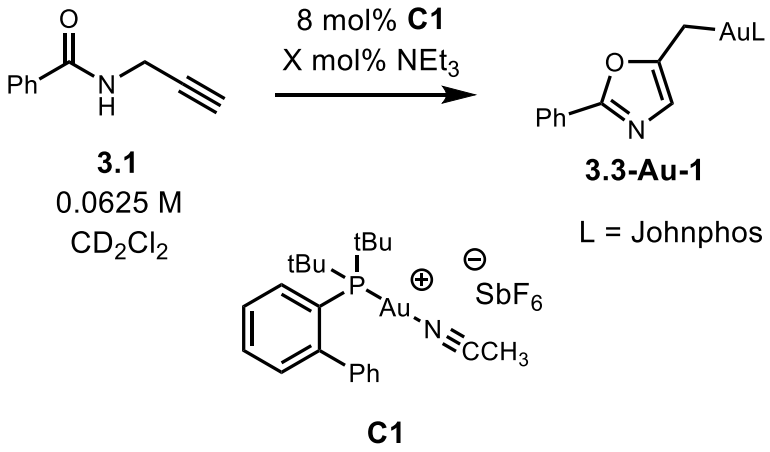

Figure 128 Relative Rates of Alkylgold Formation Depending on Base

As was suspected in the experiments with **C6**, in the presence of added base, two different mechanisms are operative. The typical Lewis acid pathway converts benzamide **3.1** into oxazoline **3.2** via π-complexation, nucleophilic addition, and protodeauration. For the acetylide, the mechanism is less clear, but it is unlikely that its intermediates overlap with those of the typical catalytic cycle. Disappearance of **3.1** is concurrent with appearance of **3.2**. Likewise, disappearance of acetylide **3.1-Au-1** is concurrent with appearance of **3.3-Au-1**. Integrals for the alkylgold are flat throughout the reaction for the cyclization with **C6** even as **3.2** continues to form**,** so **3.3-Au-1** must not be formed from gold-catalyzed isomerization of **3.2**.

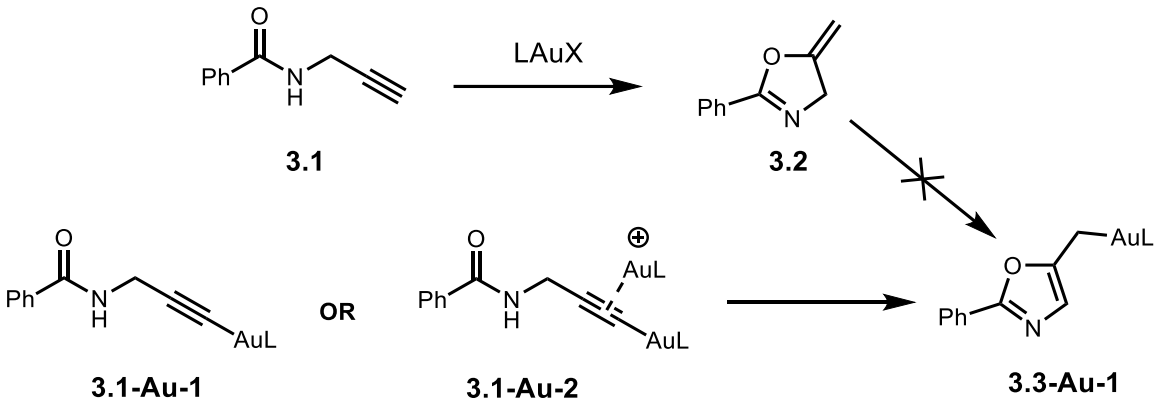

Figure 129 Diverging Mechanisms in Oxazoline and Oxazole Formation

What is notably absent from any of the experiments described above with triethylamine are vinylgold species of the type **3.2-Au-1** or **3.2-Au-2**. Even in CD_2Cl_2 where protodeauration is rate-limiting, no vinylgold species are observed in the reaction mixture by ^{1}H or ^{31}P NMR. Conspicuously, *they are never observed in typical kinetic mixtures, either.* Not even when triethylamine is used at 300 mol% are any of the peaks reported in literature to correspond to a vinylgold species observed. As discussed earlier, Hashmi and Shi's group have successfully isolated NHC-ligated vinylgolds for this cyclization, but no one has successfully isolated a vinylgold of type **3.2-Au-1** where L is a phosphine. When taken in the context of the reaction above, it can be surmised that vinylgold phosphines for this reaction must be far more sensitive than the NHC vinylgolds. However, the isotopic labeling experiments described in chapter 2, as well as computational data obtained by the Ding group support demetallation of a vinylgold phosphine as rate-limiting. It may alternatively be possible that the reason observation of vinylgold phosphines fails is because phosphine-ligated Au(I) catalysts proceed through an entirely different

pathway than those bearing an NHC ligand, but the experiments described here do not give any insight into what that alternative mechanism may be.

Carbamate Substrates: Further Insight on Acetylide Formation

An adjacent set of experiments helps to further the discussion of acetylide formation and the impact of base in this cyclization. Having identified cyclization as rate-limiting in methanol, it was suspected that modifying the substrate to create a more nucleophilic nitrogen would perhaps afford a rate increase in methanol. Therefore, carbamate **3.4** was synthesized by boc protection of propargylamine.

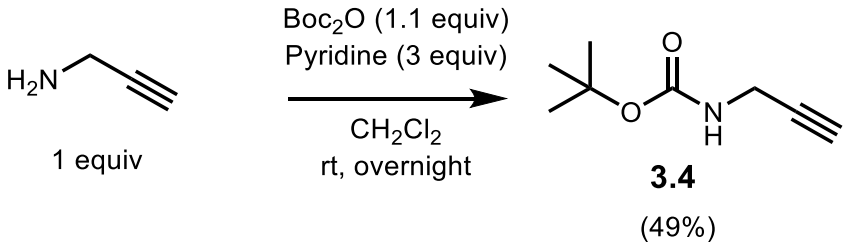

Figure 130 Synthesis of Boc Carbamate **3.4**

The hypothesis behind using this substrate was that increased sigma donation from the alkylated oxygen would afford a faster rate in methanol relative to the benzamide, as the carbonyl oxygen of **3.4** should be more nucleophilic than that of **3.2**. However, the change in relative acidity for the nitrogen proton would also have the potential to change the rate of protodeauration in dichloromethane. The substrate was tested in both solvents.

3.4 was first cyclized under typical kinetic conditions in CH_2Cl_2. Unexpectedly, analysis by ^1H NMR showed no conversion to the heterocycle even

14 hours later. When analyzed by ^{31}P NMR, a single resonance is observed at 62.4ppm, diagnostic of a digold acetylide.

Rather than cyclizing to the expected oxazoline **3.5**, **3.4** is instead captured by two moles of catalyst to form digold acetylide **3.4-Au-2**. While an initial ^{31}P spectrum was not obtained, the lack of any cyclization product or any other ^{31}P signals indicates it is likely formed quickly and quantitatively. Furthermore, unlike the reactions with triethylamine above, the digold acetylide is so stable as to be unreactive in any sort of catalysis. The reaction halts entirely.

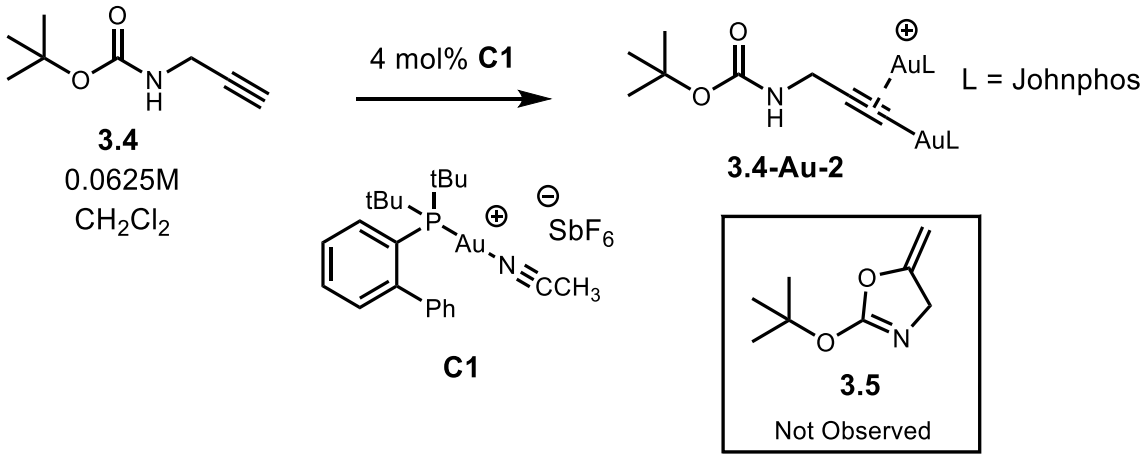

Figure 131 Formation of Digold Acetylide **3.4-Au-2**

In retrospect, this outcome is not entirely surprising when considering the original experimental goals which led to the choice of **3.4** as a reaction substrate. While the carbonyl of **3.4** is certainly more nucleophilic than that of **3.1**, it is also more basic. What likely occurs in this reaction is that which occurs when benzamide **3.1** is cyclized in methanol. Initial π complexation by gold increases the acidity of the alkyne proton, at which point another mole of carbamate **3.4** acts

as a base to form the acetylide, which is then captured by an additional mole of catalyst to form **3.4-Au-2**.

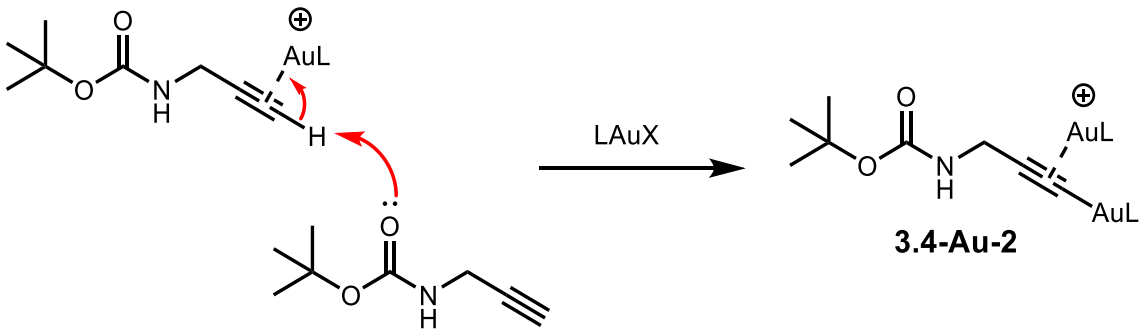

Figure 132 Mechanism of **3.4-Au-2** Formation

Spectra for the same reaction in methanol give a similar result, with no appreciable change in the ^{1}H spectrum, and a single ^{31}P resonance observed at 63ppm.

A much more interesting result is obtained when **C6** is used as the catalyst in CH_2Cl_2. ^{1}H spectra show no peaks corresponding to starting material from the first spectrum, indicating rapid catalysis. When the spectra are analyzed further, several inconsistencies become apparent. The spectrum is not consistent with the expected product oxazoline **3.5**. Too many signals appear in the alkene region, and the integral for the apparent *tert*-butyl group does not correlate in the appropriate ratio. An additional peak also appears in the aliphatic region at 1.22ppm. A ^{13}C NMR revealed a prominent peak at ~152ppm, a resonance consistent with retention of a carbamate carbonyl, which would not be present in the expected product. A ^{31}P spectrum collected at the end of three hours showed myriad peaks, none of them consistent with **3.4-Au-2,** and only a very minor peak observed for free catalyst.

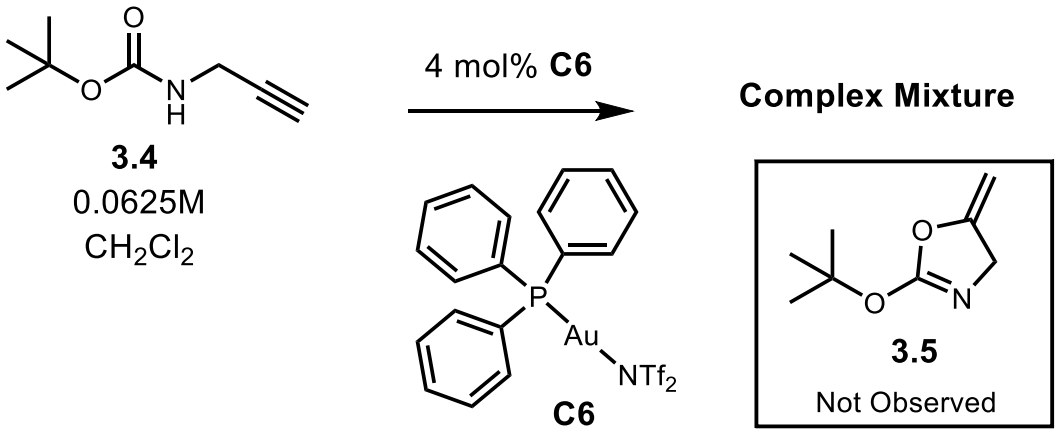

Figure 133 Unexpected Results in **3.4** Cyclization with **C6** in CH_2Cl_2

To identify the various peaks observed, 2D NMR analysis was performed. Three products were identified from the reaction mixture. The ^{13}C resonance at ~152ppm was identified as a new carbamate carbonyl from methylene oxazolidinone **3.6**. The additional alkene and aliphatic resonances were identified as belonging to the *tert*-butyl cleavage products isobutylene and *tert*-butanol.

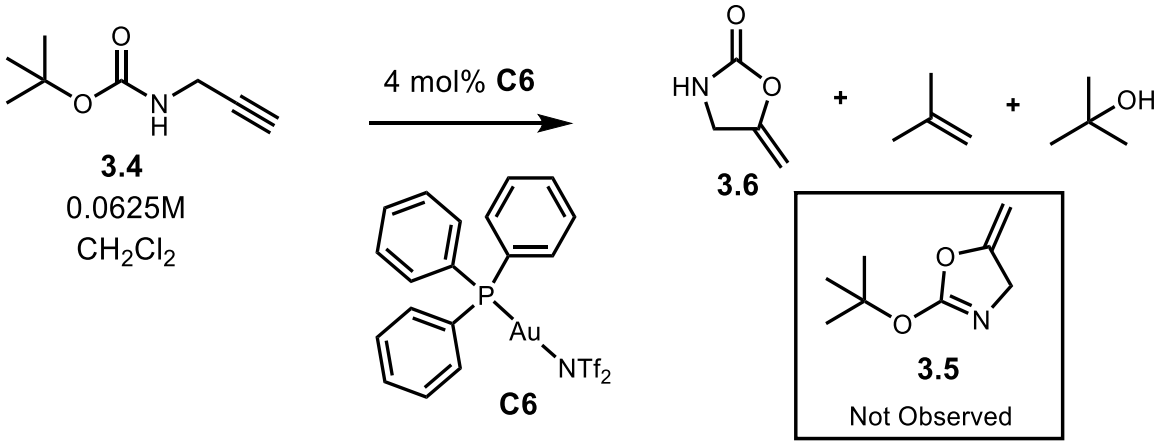

Figure 134 Products formed in Cyclization of **3.4** with **C6** in CH_2Cl_2

While this outcome was unintended, it does point to extremely fast cyclization in dichloromethane when **C6** is used in place of **C1**. **C1** forms an unreactive acetylide which fails to cyclize. No ^{31}P spectrum was collected at the

beginning of reaction with **C6**, but stacked plot analysis shows the reaction mixture in **Figure 3.51** is formed quantitatively by collection of the first spectrum, meaning the reaction either does not form an acetylide, or that the acetylide is still catalytically active. That **C6** is more inductive than **C1** means the π-complexed alkyne with **C6** would be more acidic, but also more electrophilic. It stands to reason that the intramolecular 5-exo-dig cyclization could be more rapid than the intermolecular acid-base reaction between the π-complex and another mole of **3.4**. A likely mechanism for the formation of **3.6** and its side products is shown below.

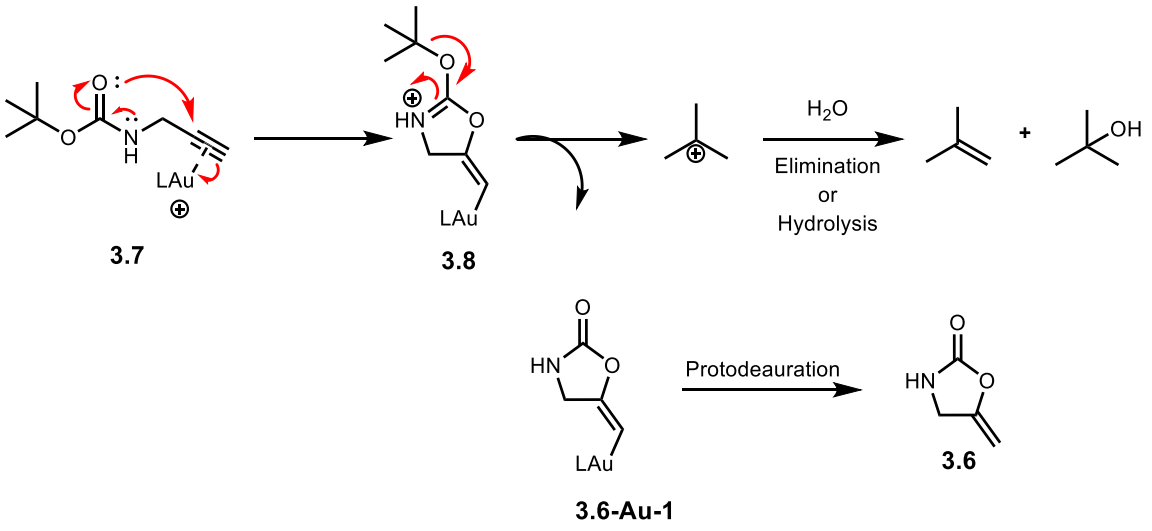

Figure 135 Mechanism of Formation for Oxazolidinone **3.6**

First, cyclization of π-complex **3.7** forms the protonated heterocycle **3.8**. Cleavage of *tert*-butyl cation as a leaving group regenerates the carbamate moiety to form vinylgold oxazolidinone **3.6-Au-1**. Protodeauration yields **3.6**. Simultaneously, the *tert*-butyl cation is captured by residual water in the solvent to form either isobutylene or *tert*-butanol.

A similar result is obtained in methanol, with the substrate degrading by fragmentation. At the end of three hours, the ^{31}P spectrum shows two peaks, one at ~44ppm indicating acetylide, with a minor peak at ~32ppm corresponding to free catalyst.

To combat the issue of *tert*-butyl cleavage, a derivative of the carbamate substrate was synthesized bearing a methyl ester fragment rather than *tert*-butyl.

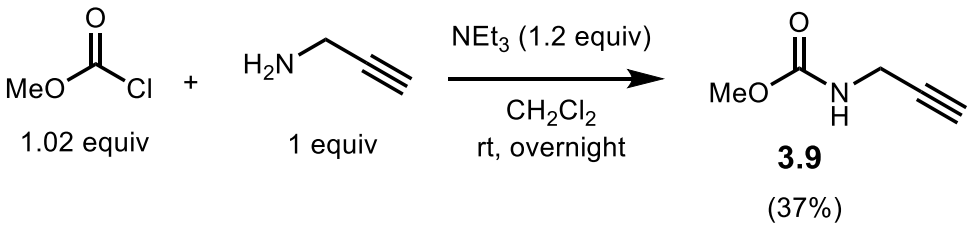

Figure 136 Methyl Carbamate Synthesis

When methyl carbamate **3.9** is treated to kinetic conditions in dichloromethane with 4 mol% **C1**, the same result is obtained as with *tert*-butyl carbamate **3.4**. No cyclization occurs, and the digold acetylide **3.9-Au-2** is observed as the sole peak in the ^{31}P spectrum. Additionally, ^{31}P spectra were collected throughout a three hour period for this substrate. The very first spectrum showed quantitative formation of the digold acetylide, immediately halting catalysis.

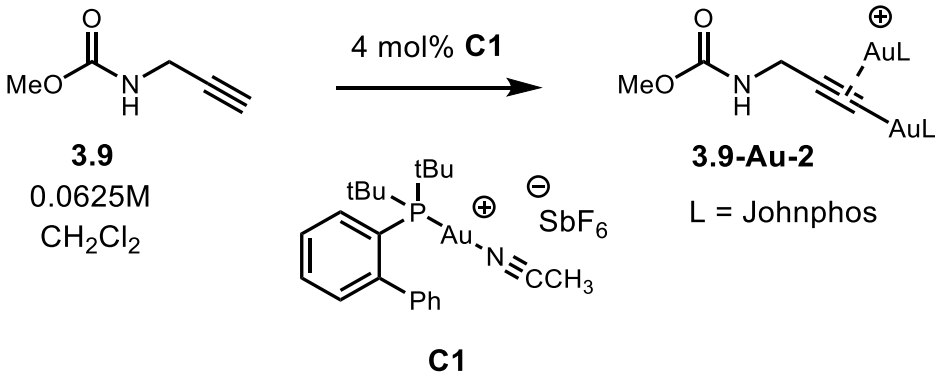

Figure 137 Formation of **3.9-Au-2** in CH_2Cl_2 with **C1**

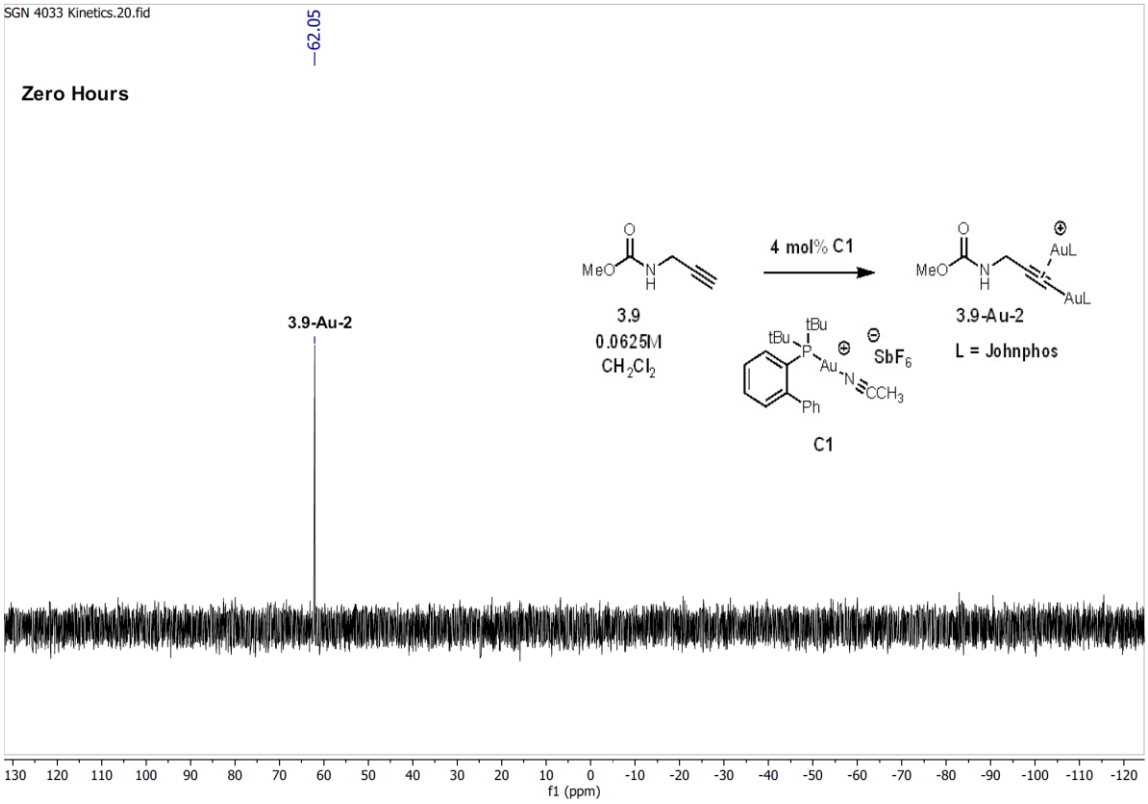

Figure 138 ^{31}P Spectrum of **3.9** and **C1** Reaction Mixture at Reaction Time Zero Minutes

As seen with the original carbamate substrate, the substrate and catalyst also degrade to form the digold when methanol is used as the solvent as well.

For catalyst **C6**, complex mixtures are again obtained. ^{1}H NMR spectra are unclear and do not indicate exactly what product is obtained. The catalyst does not degrade as rapidly for this transformation. A ^{31}P spectrum taken the day after mixing catalyst and substrate shows a pair of peaks, likely an acetylide plus an additional degradation species.

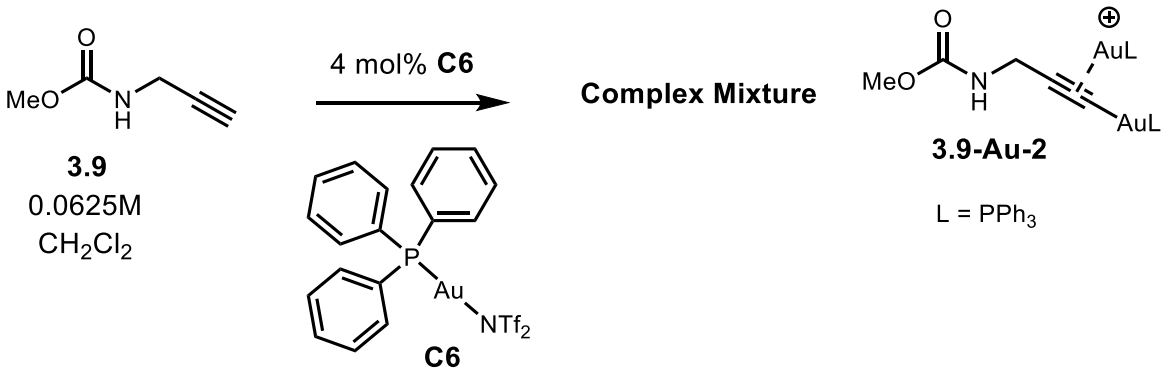

Figure 139 Reaction of **3.9** with **C6** in Dichloromethane

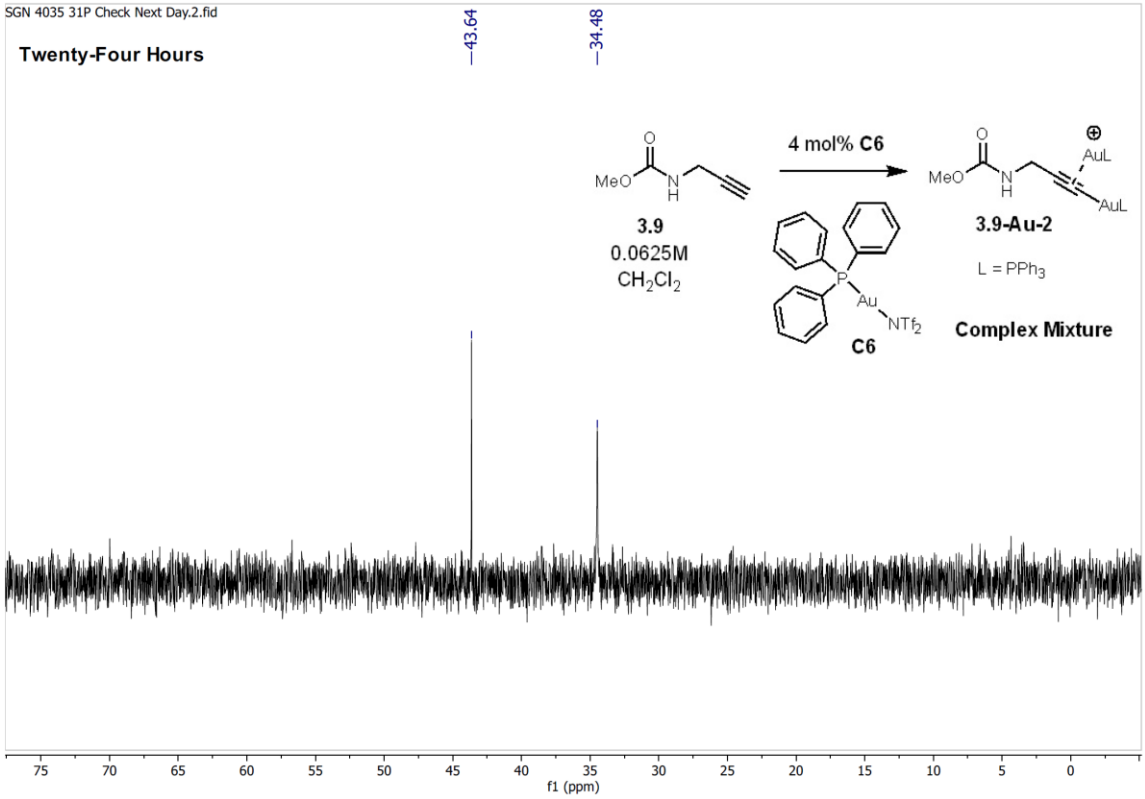

Figure 140 ^{31}P Spectrum of **3.9** and **C6** Mixture at One Day of Reaction Time

In a final effort to see if cyclization could potentially be achieved for **3.9**, a catalyst bearing a bisbiphenyl ligand was used. The increased steric bulk of the ligand should hypothetically limit the formation of digold acetylides due to the energetic strain incurred by placing two equivalents of such a large ligand near each other in space. The triflate variant of **C5** (see chapter 2) was used towards this effort.

When **3.9** was treated with 4 mol% of **L2**AuOTf in both dichloromethane and methanol, complex mixtures and digold acetylide were again observed, with no apparent conversion to the expected heterocycle.

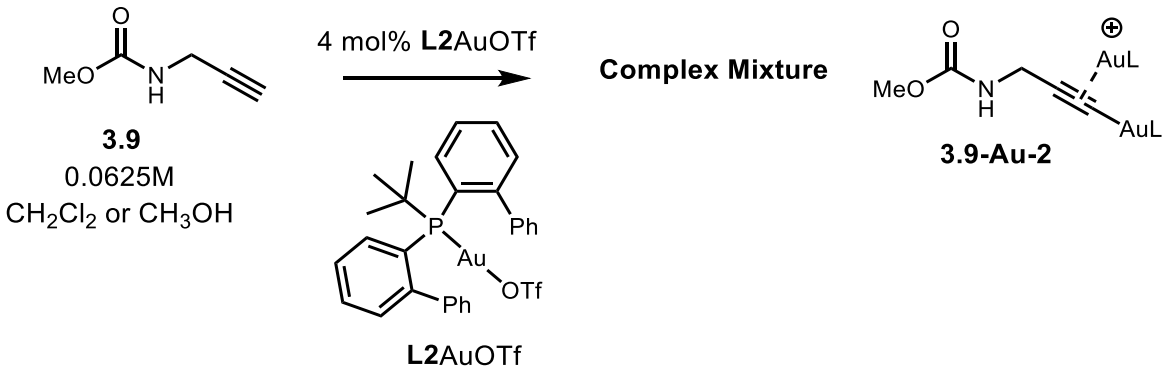

Figure 141 Degradation of Bisbiphenyl Catalyst with Carbamate **3.9**

Cyclization with Electron-Deficient Benzamides

With catalyst degradation being such an issue for the carbamate substrates, the experimental design was reversed. Rather than designing a substrate with a more nucleophilic carbonyl oxygen—which simultaneously results in a more basic carbonyl oxygen—electron-deficient benzamides could be synthesized instead. If the less electron-rich carbonyl gave slower rates in methanol than the baseline benzamide substrate of **3.1**, the same conclusions could be reached.

Benzoic acids **3.10** and **3.11** were therefore purchased as precursors to electron-deficient benzamides **3.12** and **3.13**. It was envisioned that both substrates could be prepared in a one-pot, two-step synthesis by first reacting the acids with thionyl chloride, generating the corresponding acid chlorides as intermediates. Subsequent reaction with base and propargylamine would afford **3.12** and **3.13**.

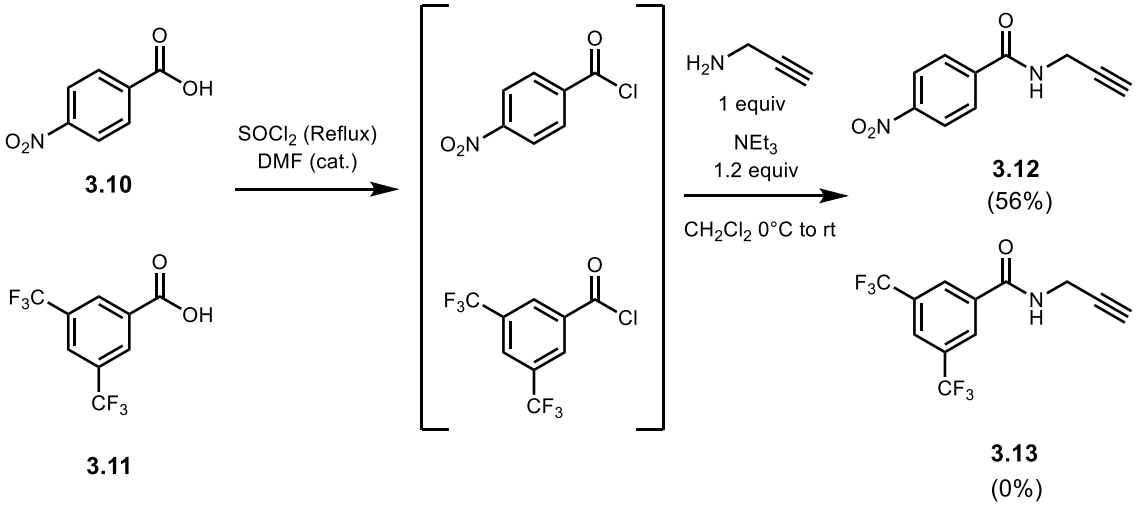

Figure 142 Synthesis of Electron-Deficient Benzamides

The synthetic approach above worked reasonably well for *p*-nitro substrate **3.10**. Crude material from a pair of reactions was combined and purified on silica with dichloromethane as the mobile phase. The compound was recovered as a yellow solid. The compound took a very long time to elute on the column (**3.12** was recovered from fractions 40-96), and in hindsight would have benefited from a more polar mobile phase, e.g. perhaps a 95:5 DCM:MeOH mixture.

The same synthesis did not work for 3,5-CF_3 benzoic acid **3.11**. Upon addition of propargyl and triethylamine, the reaction mixture turned black and seemingly degraded. Black particulates had to be filtered out of the reaction mixture during workup. Analysis of the material recovered from the organic layers after workup showed only degraded material.

With **3.12** in hand, it was submitted to typical kinetic conditions in both dichloromethane and methanol with **C1** used as the catalyst.

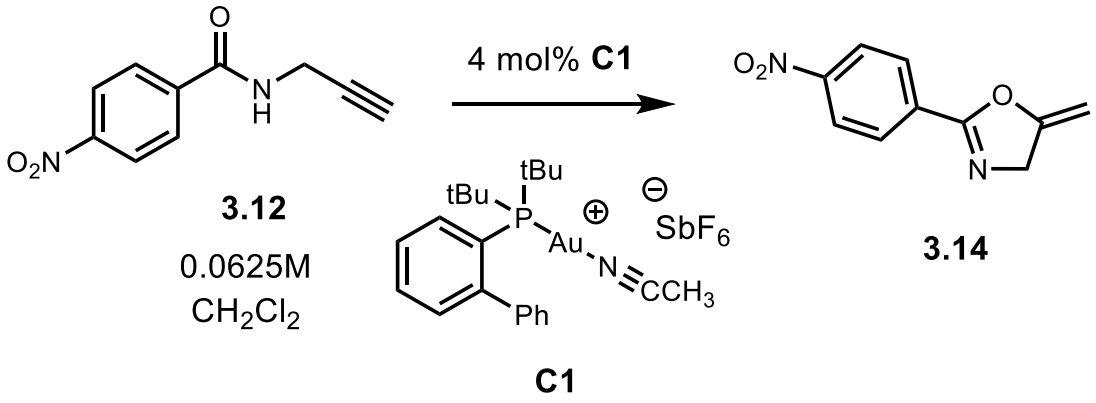

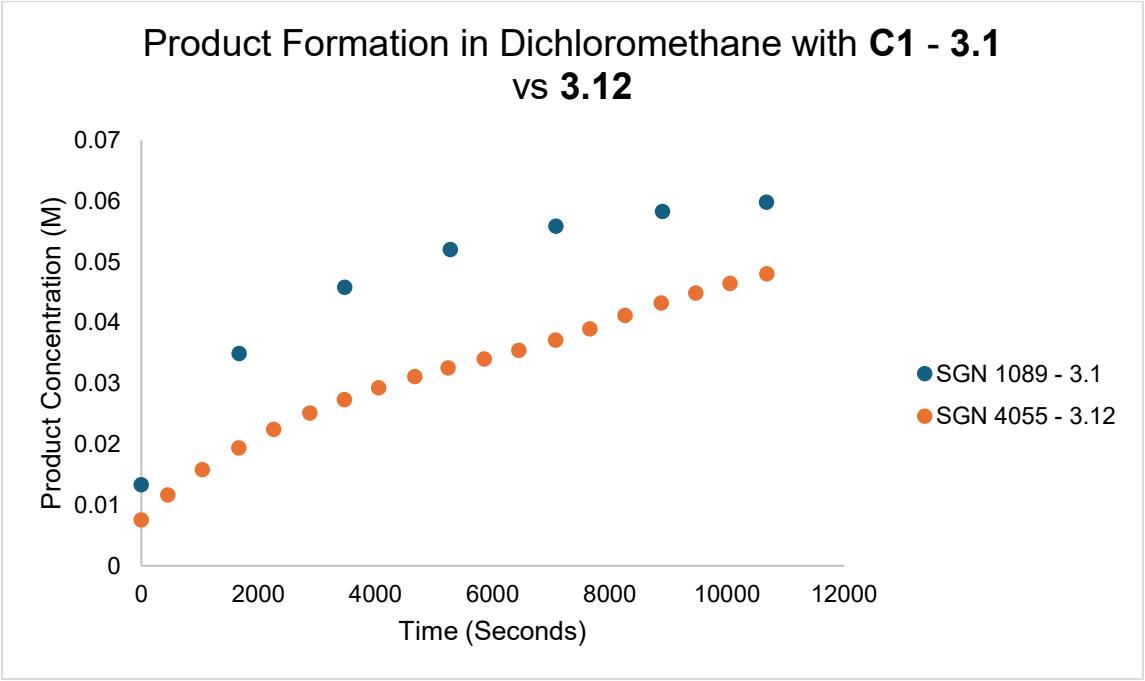

Figure 143 Comparative Product Formation in CH_2Cl_2 with 4 mol% **C1**

Cyclization occurs readily in dichloromethane for **3.12**, but an asterisk should be placed on the results obtained. The substrate is only sparingly soluble in CH_2Cl_2, meaning the concentration cannot be reliably measured over the entire reaction course. Once the NMR tube was collected the following morning, all substrate had gone into solution. Oxazoline **3.14** is therefore soluble in

dichloromethane, allowing for gradual dissolution of **3.12** over time. The observed rate is markedly slower than that of **3.1** (k_{rel} **3.10**/**3.1** = 0.38), but given the solubility issues, this is likely not the true rate.

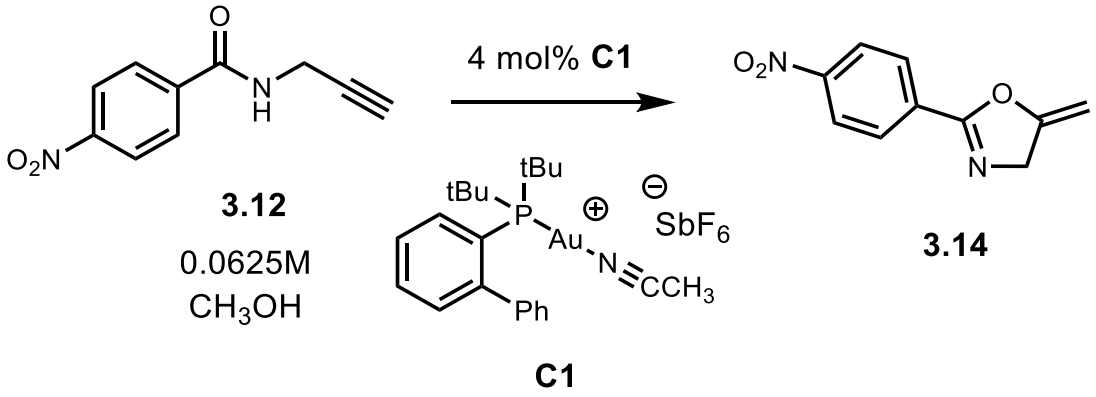

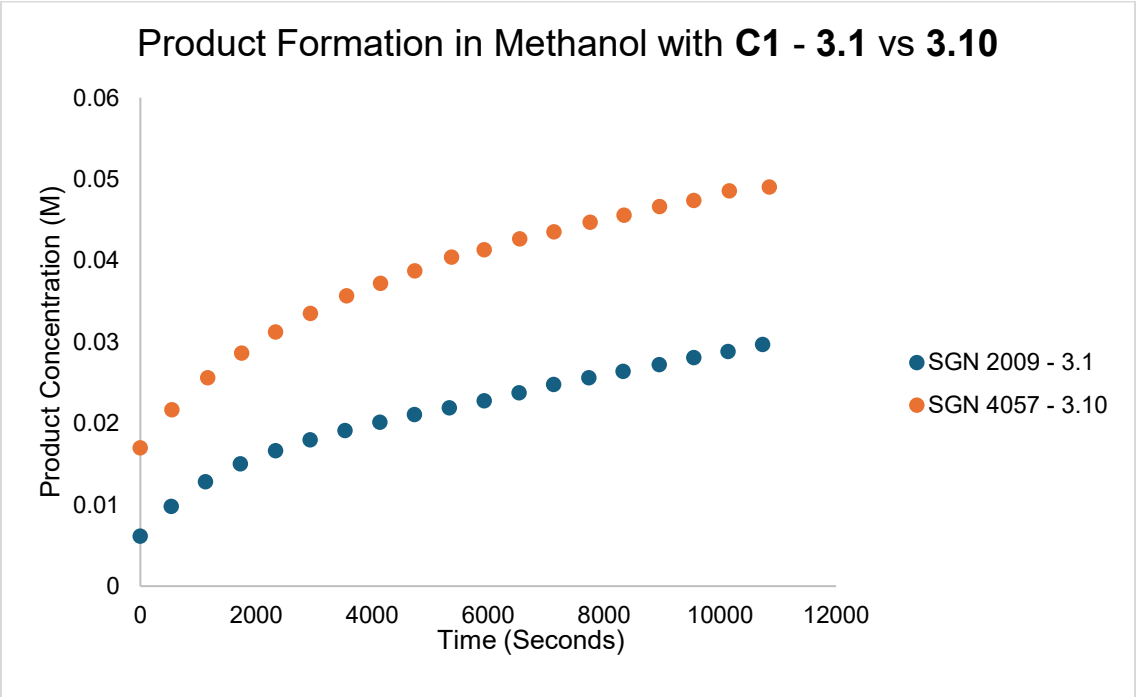

Figure 144 Formation of **3.14** in CH_3OH with 4 mol% **C1**

Contrary to the experiment in dichloromethane, in methanol, no solubility issues are observed. **3.12** is easily dissolved in methanol for catalysis by **C1**. Quite surprisingly, the observed rate is very rapid. Rather than being slowed in methanol,

3.12 gives a nearly identical rate to the **3.12** in dichloromethane (k_{rel} $CH_3OH:CH_2Cl_2$ = 0.94). Though again, the rate in dichloromethane should be treated skeptically. However, what can still be reasonably asserted from this result is that the addition of a nitro group at the para position of the ring results in a substrate which is virtually unimpacted by the change in solvent. Furthermore, rather than the rate of **3.12** in methanol being slower than that of **3.1**, it is instead 32% faster (k_{rel} **3.12**/**3.1** = 1.32).

Ultimately, the results obtained for this substrate are quite unexpected and initially inconclusive. Follow-up solvent and isotopic labeling studies for **3.12** could potentially help to elucidate the potential reasons for its unexpected performance.

Conclusion

As has been described above, the discrepant rates between dichloromethane and methanol described in chapter 2 are attributable to enhanced decomposition of the catalyst in methanol, not just a change in the rate-determining step. Reaction mixtures in dichloromethane show largely intact catalyst at the end of the reaction period, while mixtures in methanol show an array of decay products. Addition of triethylamine to reaction mixtures allows for identification of many of the degradation products as mono or digold acetylides formed from the alkyne substrate. Stunningly, the vinylgold species frequently referenced in literature as the catalyst resting state is completely unobserved in any of the above reactions. Isolation of a phosphine vinylgold derived from the propargyl benzamide substrate fails completely, despite successful reports of NHC-ligated vinylgolds in the

literature. Additionally, high loadings of base result in formation of an alkylgold aromatic tautomer, not the vinylgold traditionally expected.

These observations further cloud the understanding for this oft-utilized benchmark reaction. Protodeauration has long been held as rate-limiting, but experiments described here show that this can be perturbed heavily by solvent.

When carbamates are instead used as the substrate, the foremost issue with catalysis becomes decay of the gold by formation of digold acetylides, stemming from the enhanced basicity of the substrate carbonyl. Johnphos-ligated **C1** seemingly fails to perform any meaningful cyclization for these substrates, while the more Lewis acidic PPh_3-ligated **C6** does achieve cyclization for *tert*-butyl carbamate **3.4**, but cleavage of the *t*-butyl group gives an oxazolidinone product.

Electron-deficient nitro benzamide **3.12** cyclizes 60% slower than **3.1** in dichloromethane but cyclizes 32% faster than **3.1** in methanol. The methanol result notably contrasts with expectations from the isotopic labeling studies discussed in chapter 2. Having such a potent electron-withdrawing group on the ring may perturb the rate-limiting step again, explaining why **3.12** seems entirely unfazed by the change between solvents. The zwitterion character of the nitro group may also impact hydrogen bonding, which is known to be highly relevant for this transformation.

It therefore becomes clear that both acidity and basicity of the substrate must be carefully considered for this, and potentially other, cyclizations. When terminal alkynes are used as substrates, π-complexation by the catalyst will

increase their acidity. If the solvent, e.g. methanol, is appropriately basic, the alkyne can be deprotonated to form a gold acetylide. Capture of the acetylide by another mole of catalyst results in a digold species, the stability of which can hinder or stop catalysis. Alternatively, as shown in the carbamate experiments, a particularly basic substrate can itself nullify the catalyst by acting as the base even in non-basic solvents such as dichloromethane.

These observed trends perhaps serve to contextualize the conflicting literature reports for the gold-catalyzed cyclization of N-propargyl benzamide. While the reaction is taken to be simple at face value, there are clearly lurking variables which may help to explain the conflicting reports seen in both computational and experimental reports in the field.

Chapter 4 Synthesis and Kinetics of Bisbiphenyl Phosphine Ligands

Introduction

Results published by the group in 2020 described the enhanced stability of Au(I) π-complexes with ligands bearing multiple biphenyls.[115] These published results used only unsubstituted biphenyls, with no electronic or steric variation. In follow-up work, it became desirous to see how various substituents on the rings may impact catalyst stability and subsequent catalytic activity. The ease of tunability for the scaffold allows for the study of electronic and steric effects in isolation or in tandem.

Synthesis of a *p*-N,N-Dimethylamino Bisbiphenyl Ligand

The first successfully synthesized bisbiphenyl ligand was the N,N-dimethylamino variant, **4.1**.

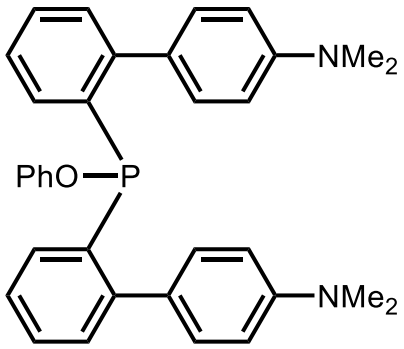

4.1

Figure 145 N,N-Dimethylamino Bisbiphenyl Ligand

The two varying groups on the central phosphorus atom electronically contrast, with the phenoxy group acting as a potent electron-withdrawing group.

Conversely, the biphenyl groups are more electron rich due to strong donation from the amine groups.

4.1 was synthesized in two steps starting from 1,2-Iodobromobenze and 4-(Dimethylamino)phenylboronic acid. A Suzuki coupling was first performed to form the ortho bromo biphenyl. The crude biphenyl was purified on silica with 2% ethyl acetate and 98% hexanes as the mobile phase, affording pure biphenyl in 84% yield. The biphenyl was lithiated with n-butyllithium and quenched with half an equivalent of triphenylphosphite. Recrystallization in 1:2 EtOAc:Hexanes afforded **4.1** in 69% yield.

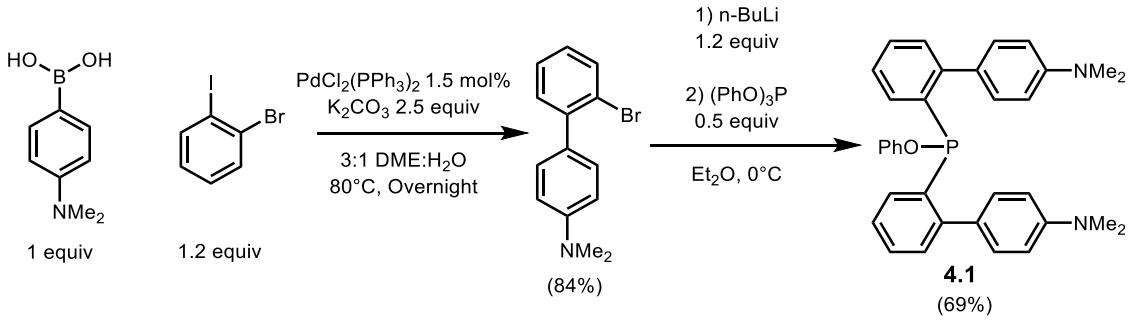

Figure 146 Synthesis of Dimethylamino Ligand **4.1**

Ligand **4.1** was then submitted to typical gold chloride synthetic conditions. Recrystallization of the crude material in 1:2 DCM:Hexanes afforded gold chloride **4.2** in 93% yield.

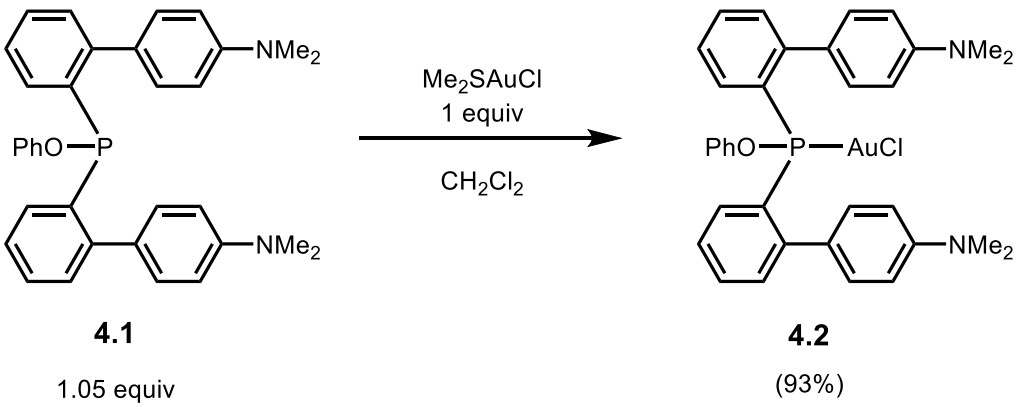

4.1

1.05 equiv

4.2

(93%)

Figure 147 Synthesis of Gold Chloride **4.2**

The first halide abstraction reaction attempted for **4.2** was treatment with silver triflate in dichloromethane. When analyzed by NMR, the crude material showed extremely broad peaks in both the ^{1}H and ^{31}P spectra, a phenomenon never observed when synthesizing the various Johnphos-ligated catalysts, nor other catalysts synthesized in the group bearing unsubstituted bisbiphenyl groups. The initial hypothesis was that abstraction of chloride and replacement by the weaker ligand resulted in decomposition.

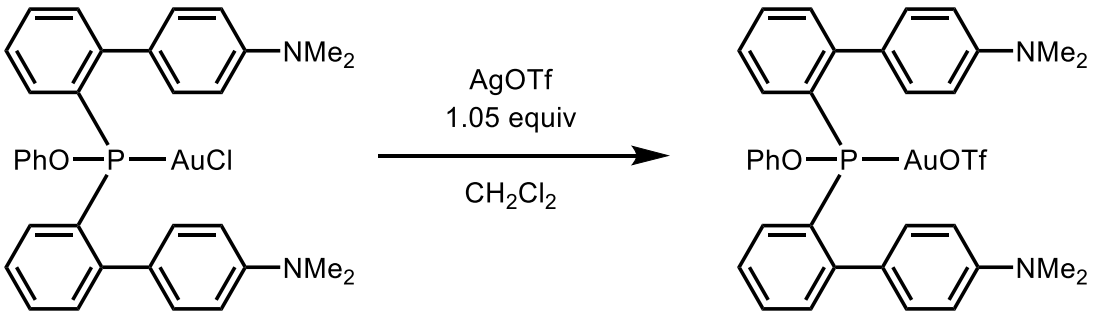

4.2

1 equiv

4.3

Figure 148 Synthesis of Gold Triflate **4.3**

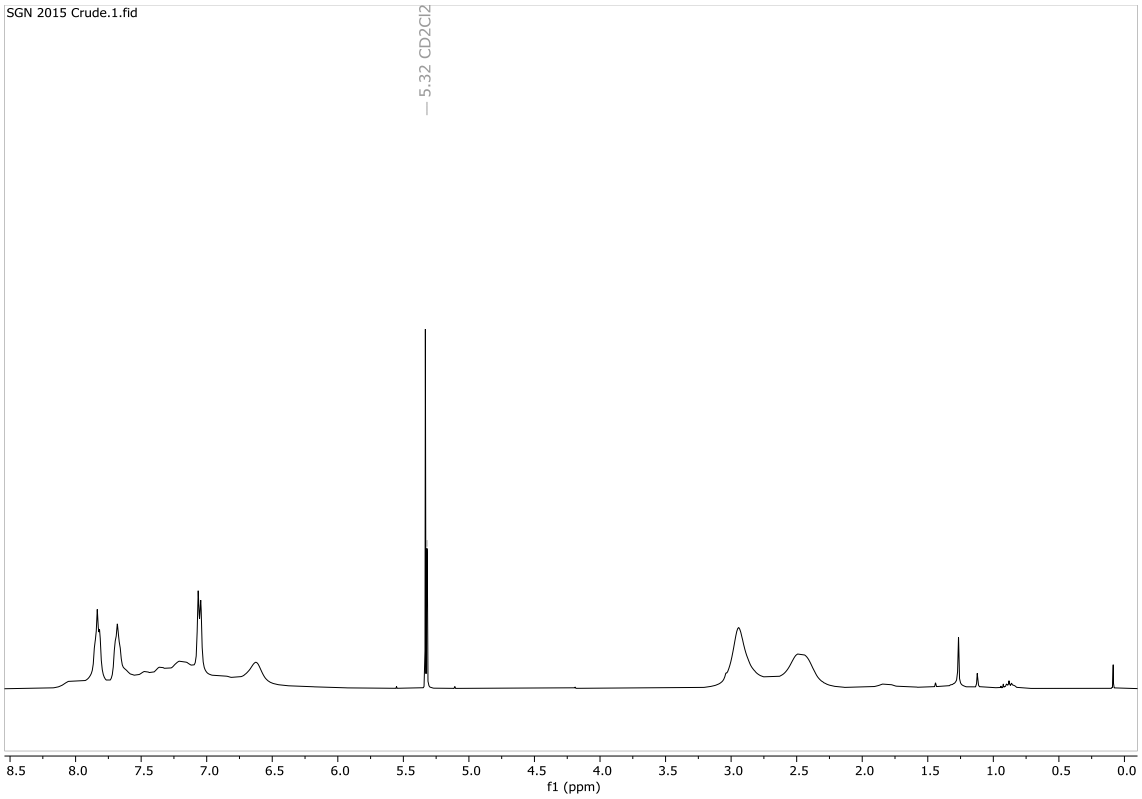

Figure 149 ^{1}H Spectrum of Crude Gold Triflate **4.3** in Dichloromethane

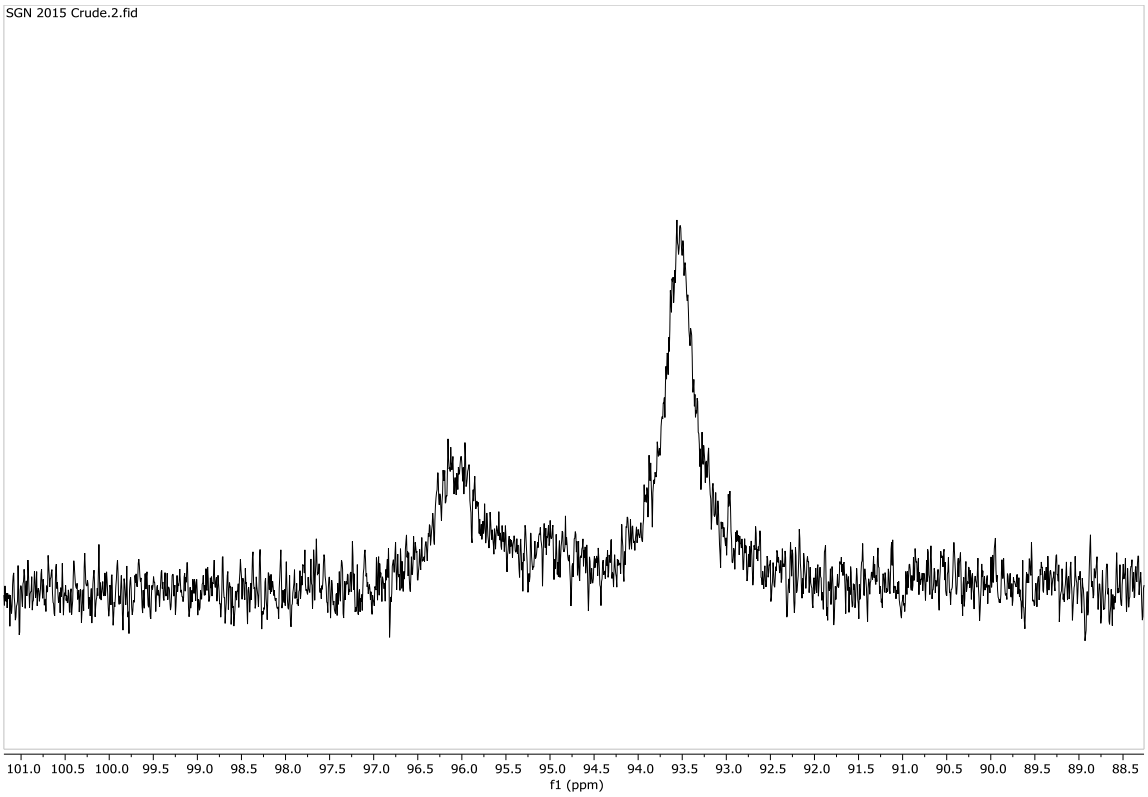

Figure 150 ^{31}P Spectrum of Crude Gold Triflate **4.3** in Dichloromethane

Typical recrystallization conditions of 1:2 DCM:Hexane failed to improve the spectra, with all subsequent spectra showing the same broad resonances. Hypothesizing other solvents may improve resolution, an attempt was made to collect a spectrum in CD_3OD, but this caused degradation of the material. Efforts were then directed towards synthesis of the gold triflimide, **4.4**, instead.

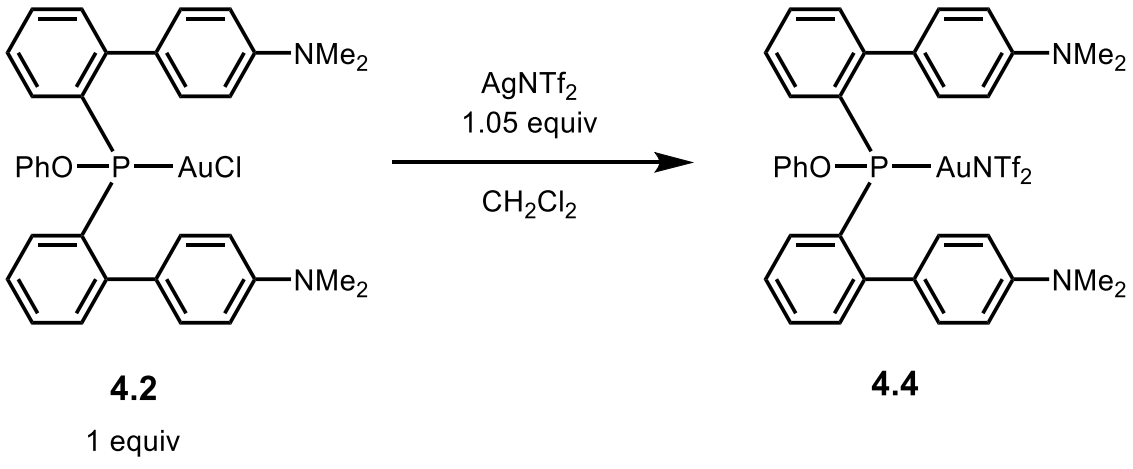

4.2

1 equiv

4.4

Figure 151 Synthesis of Gold Triflimide **4.4**

When **4.4** was synthesized according to the same procedure as **4.3**, the same issue of broad NMR spectra was observed. Also like **4.4**, recrystallization did not improve the appearance of the spectra. While the gold chloride of **4.2** is quite stable, once the chloride ligand is abstracted, the products initially appeared to degrade. Further inspection of spectra collected for **4.4** showed a potentially more promising result. Similar to **4.3**, the ^{1}H spectrum shows what appears to be multiple resonances for the methyl groups despite their symmetry in the precursor gold chloride and the proposed structure for **4.3**. The ^{31}P still showed a pair of broad signals, but a ^{19}F spectrum revealed a single, sharp resonance at -79ppm. The single peak in the fluorine spectrum prompted a suspicion that, rather than the multiple methyl peaks resulting from degradation and the formation of multiple species, the broad peaks are instead resulting from dynamic effects where the dimethylamino groups are no longer freely rotating. This hindered rotation presumably stems from coordination to the cationic gold upon abstraction of the chloride ligand. σ coordination by the dimethylamino groups would hinder the rotation of the bond to the phenyl ring, rendering the methyls on the nitrogen

diastereotopic. The additional resonances observed for the methyl groups can be rationalized by hindered rotations due to the proximity of two large ligands near each other in space. The prevailing hypothesis therefore became that, upon chloride abstraction, the catalyst dimerizes by coordination between gold and the nitrogen of another mole of catalyst.

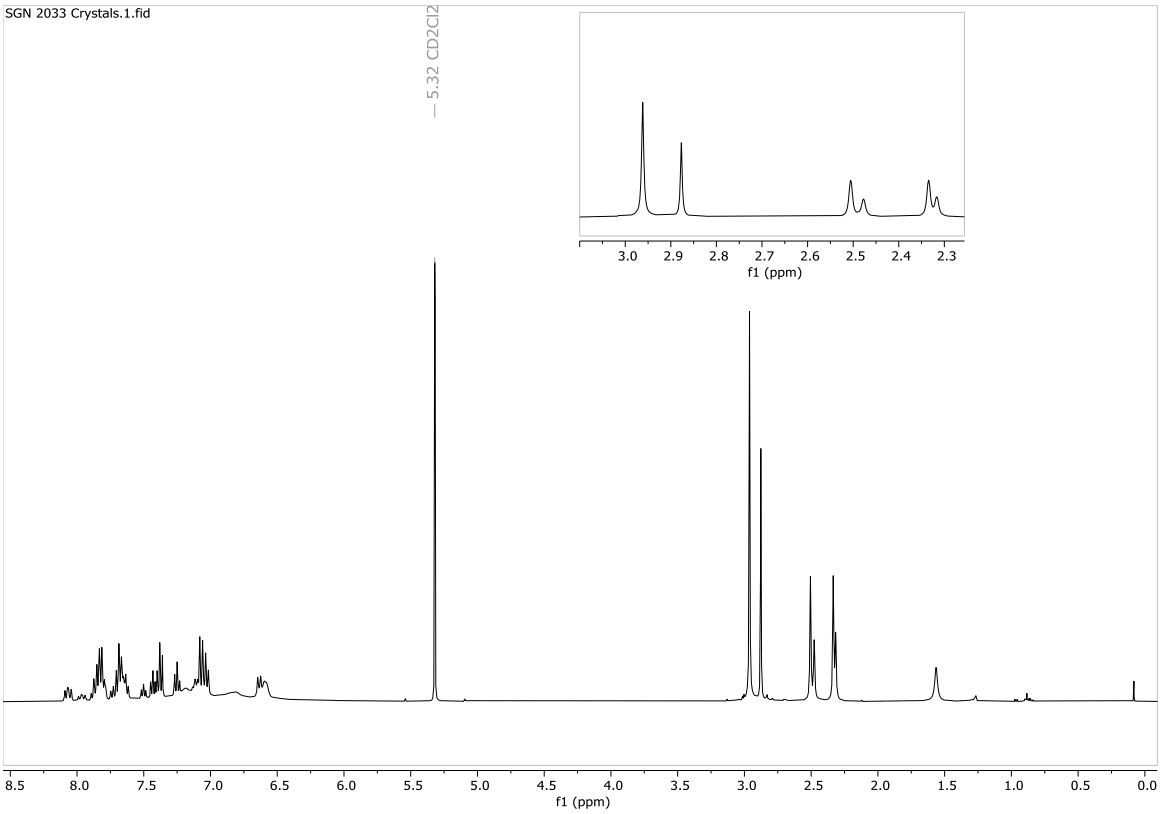

Figure 152 ^{1}H Spectrum of **4.4** Dimer in Dichloromethane

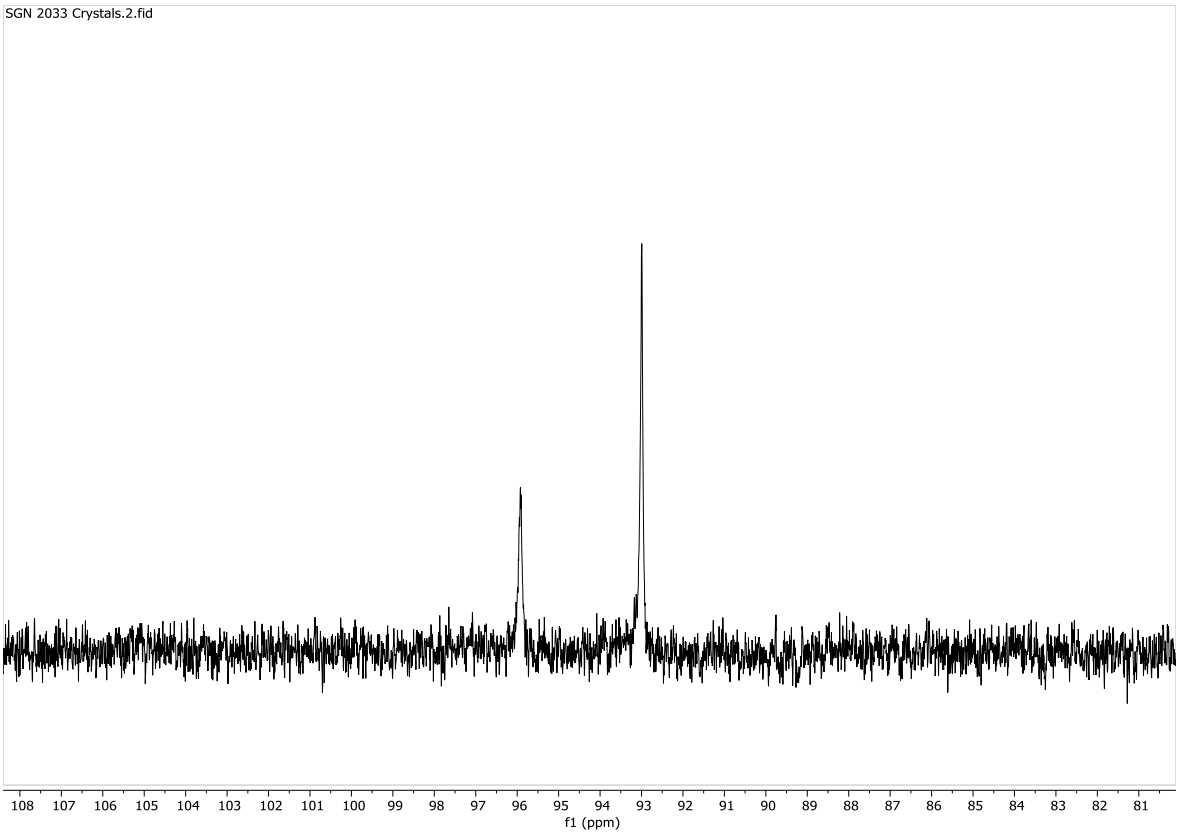

Figure 153 ^{31}P Spectrum of **4.4** Dimer in Dichloromethane

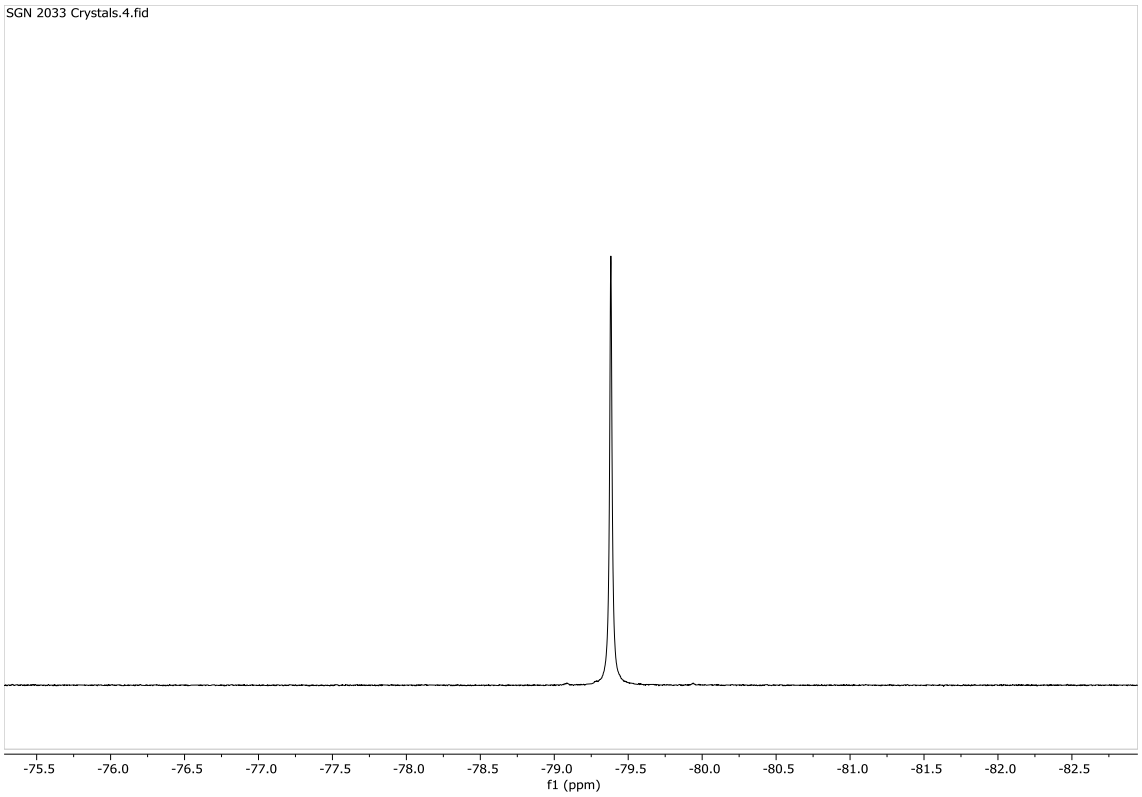

Figure 154 ^{19}**F** Spectrum of **4.4** Dimer in Dichloromethane

Now suspecting the poor spectra resulted from dimerization, other NMR solvents were surveyed to see if the peaks for **4.4** might sharpen. Spectra collected in toluene and benzene showed no improvement, indicating potential π-stacking with the solvent was not enough to break up any dimer. A spectrum collected in acetone also did not provide better resolution. When spectra were collected in acetonitrile, every peak in the spectrum sharpened. The ^{1}H spectrum gave signals much more consistent with the expected structure for **4.4**. The ^{31}P spectrum no longer showed a pair of peaks and instead gave a single broad signal. The sharpening of the spectra are very likely owed to σ-coordination by the solvent nitrogen to gold, which breaks up any dimers to give **4.4-ACN** as a singular species.

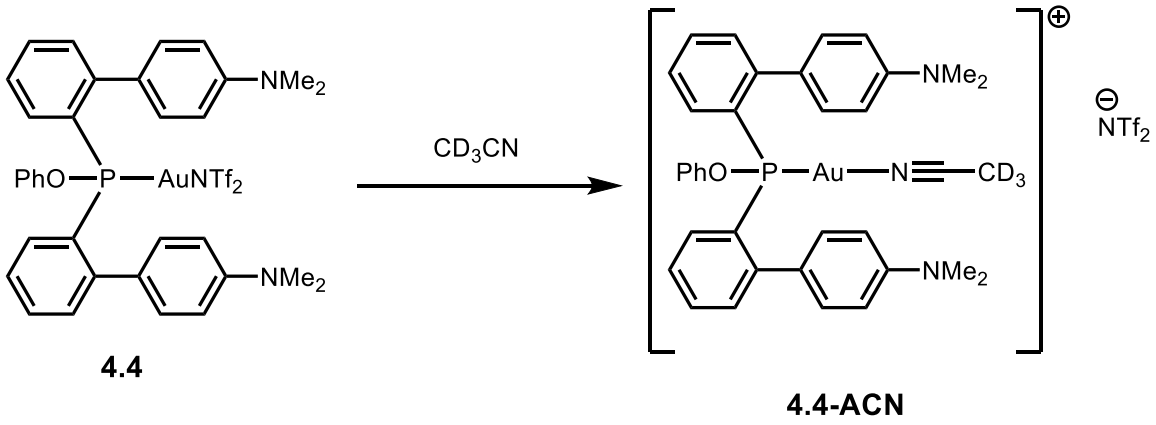

4.4 **4.4-ACN**

Figure 155 Formation of **4.4-ACN**

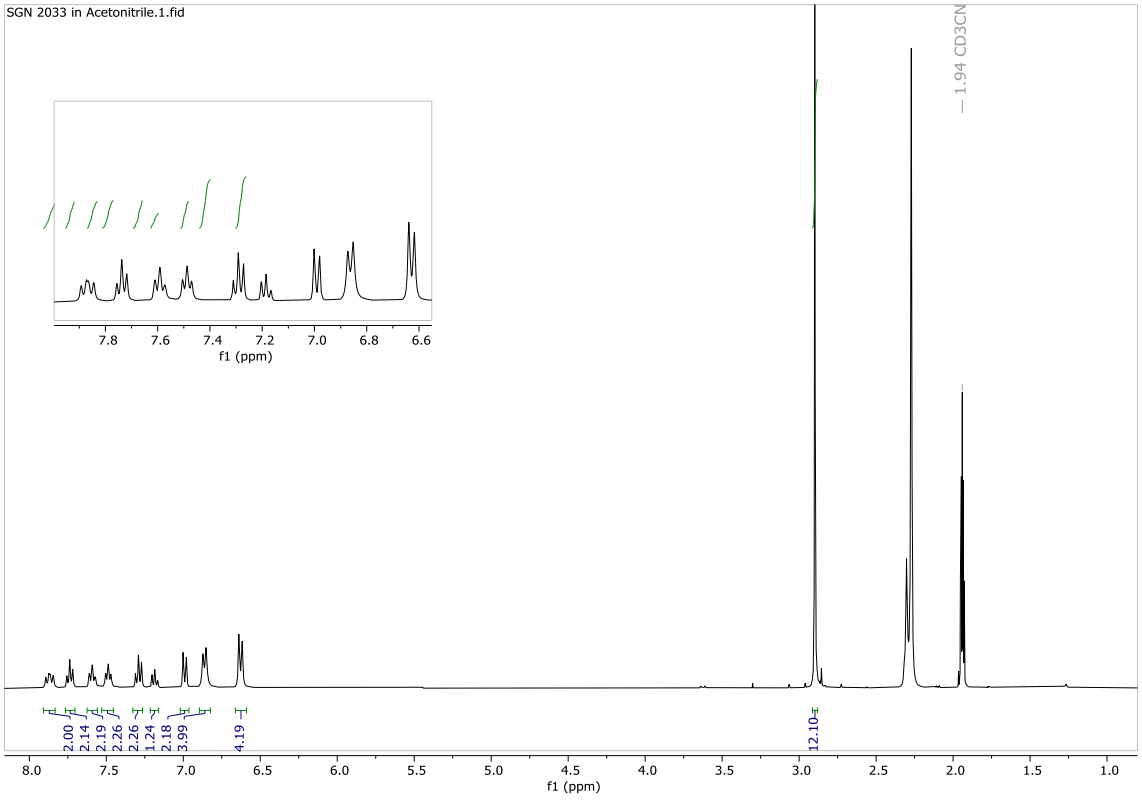

Figure 156 ^{1}H Spectrum of **4.4-ACN** in CD3CN

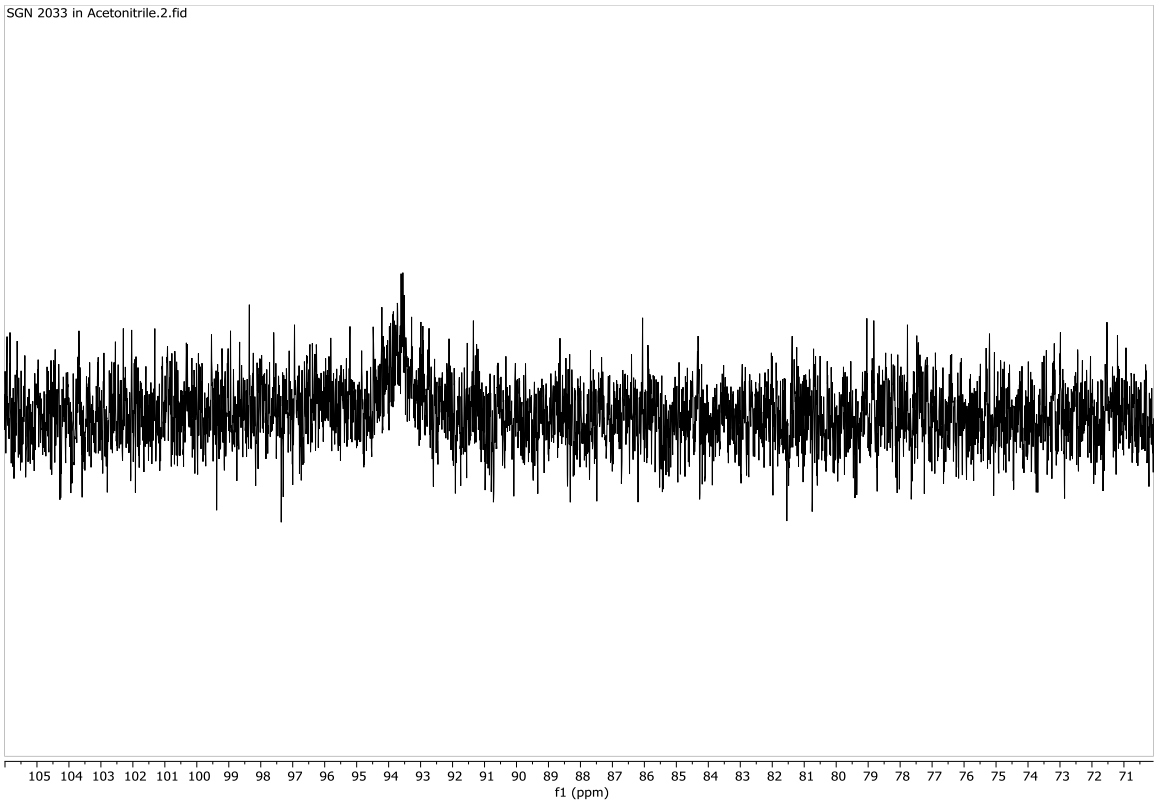

Figure 157 ^{31}P Spectrum of **4.4-ACN** in CD3CN

Having seen complexation by acetonitrile for gold triflimide **4.4**, NMR spectra of gold triflate **4.3** were also collected in acetonitrile. The same sharpening of peaks were observed, confirming formation of **4.3-ACN**.

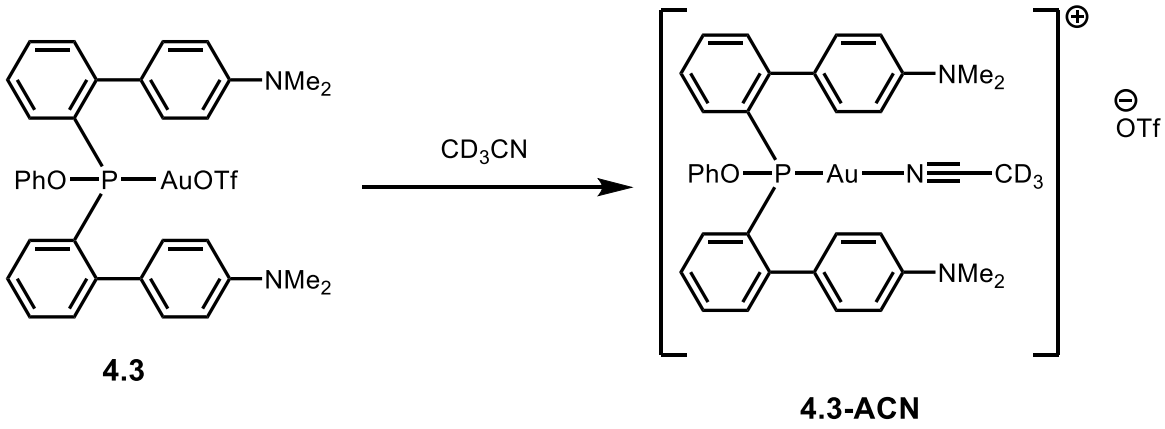

Figure 158 Formation of **4.3-ACN**

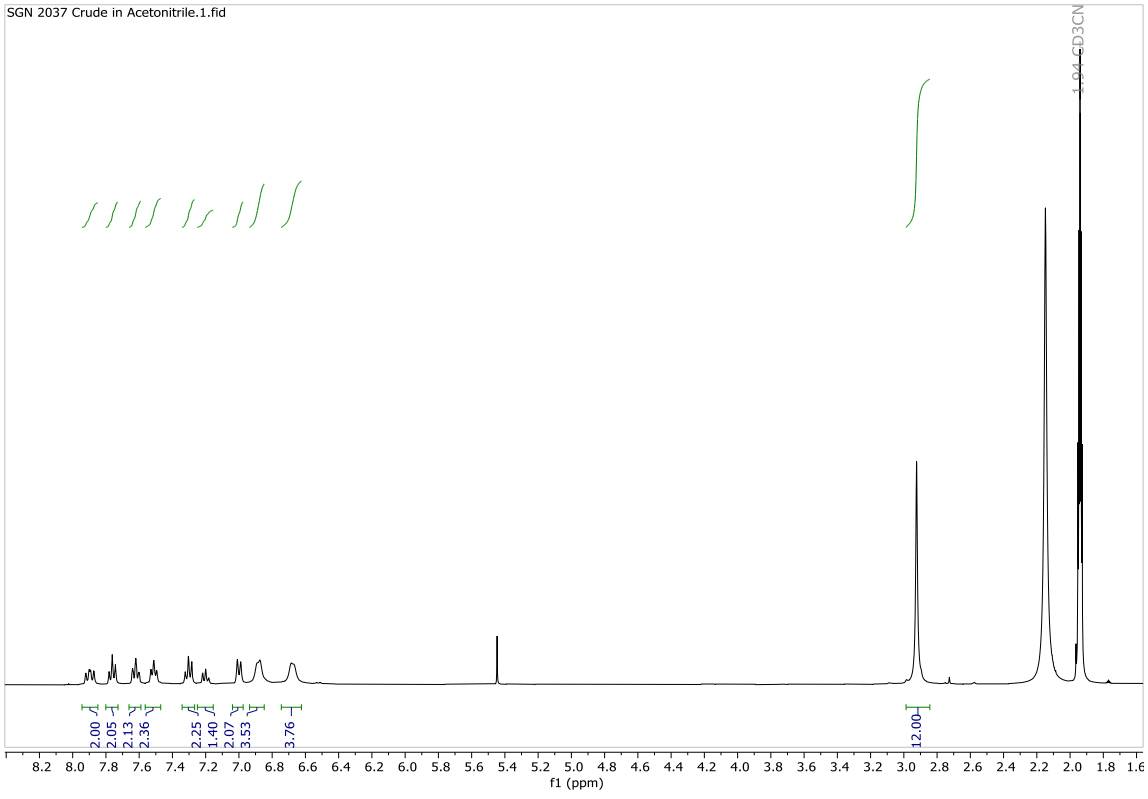

Figure 159 ^{1}H Spectrum of **4.3-ACN** in CD3CN

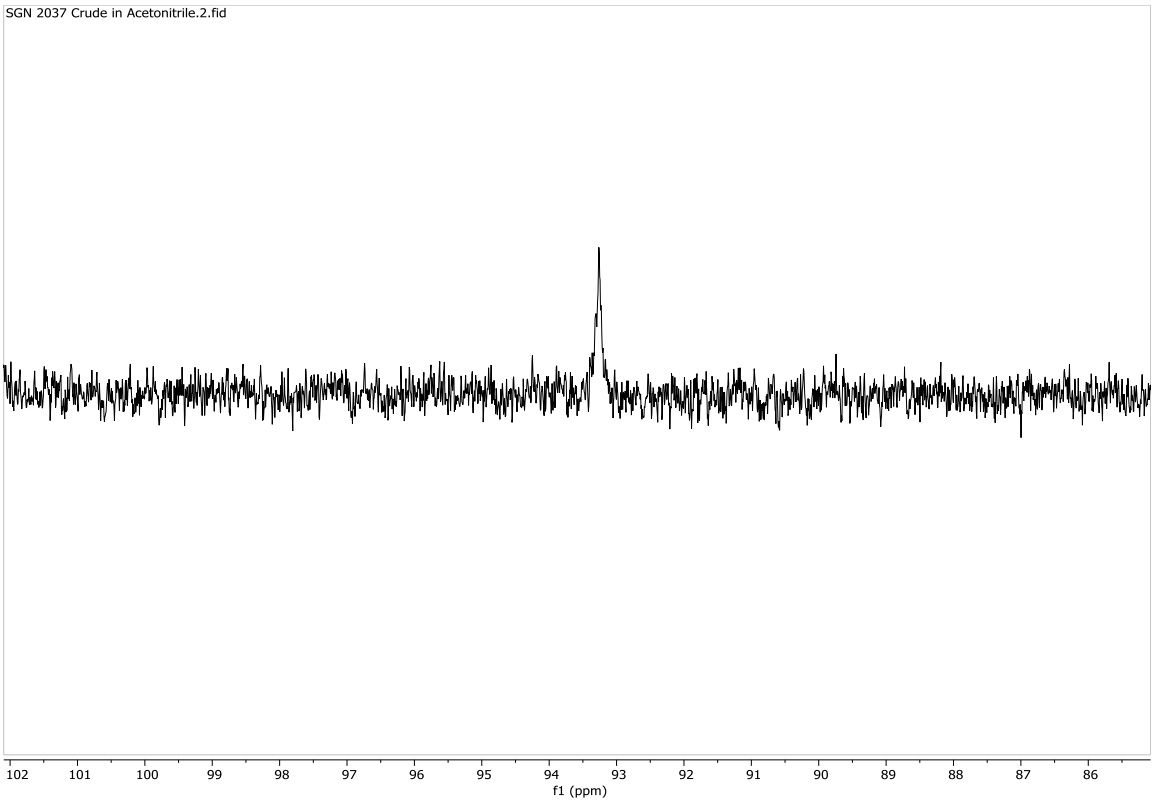

Figure 160 ^{31}P Spectrum of **4.3-ACN** in CD3CN

Knowing **4.3** and **4.4** exist as dimers in solution, it was hypothesized that the dimers may still be able to act as viable catalysts. Catalysis was never performed with **4.3**, but **4.4** was used successfully in the cyclization of N-propargyl benzamide (see discussion of its kinetic behavior as **C8** in chapter 2). When in the presence of a substrate with which to bind, **4.4** also sharpens to a single peak at ~95ppm when used as the catalyst for benzamide cyclization. This indicates the presence of an alkyne π system seems sufficient to break apart the dimer into a single species, halting dynamic effects.

Catalytic Behavior of 4.4 in the Cyclization of Pent-3-yn-1-ol

The catalytic behavior of **4.4** in the cyclization of N-propargyl benzamide was discussed in chapter 2. Its remarkable stability relative to other catalysts surveyed in the same transformation was discussed in chapter 3. To gain further understanding of its catalytic behavior, **4.4** was used in the catalysis of alcohol **4.5** to form dihydrofuran **4.6**.

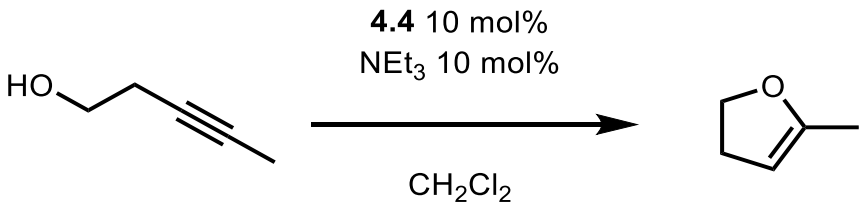

Figure 161 Au-Catalyzed Cyclization of Pent-3-yn-1-ol

The mechanism for the cyclization is essentially identical to that for the benzamide cyclization discussed in earlier chapters. The addition of triethylamine is necessary to poison the catalyst, as otherwise the reaction occurs too quickly to capture a rate by ^{1}H NMR. The triethylamine forms a sigma complex with gold just as the acetonitrile does in figures shown above.

In the case of this reaction, the internal positioning of the alkyne renders the formation of gold acetylides of the type discussed in chapter 3 impossible. Degradation is still possible, however, through the formation of the geminal digold species **4.6-Au-2** stemming from slow protodeauration.

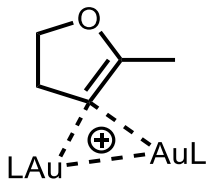

4.6-Au-2

Figure 162 Gem-digold **4.6-Au-2**

Just as discussed with the degradation pathways for the benzamide cyclization, formation of a gem-digold for this cyclization leads to irreversible catalyst decay, subsequently reducing the rate of cyclization. Having observed remarkable stability for **4.4** in the benzamide cyclization, it was additionally surveyed here.

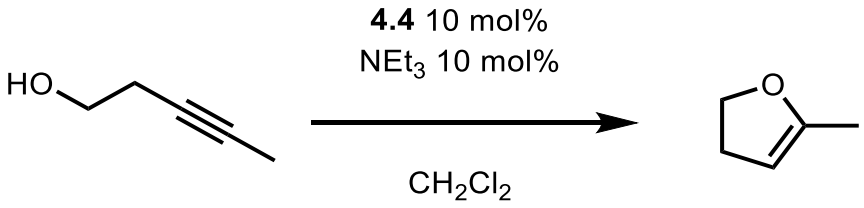

4.5 **4.6**

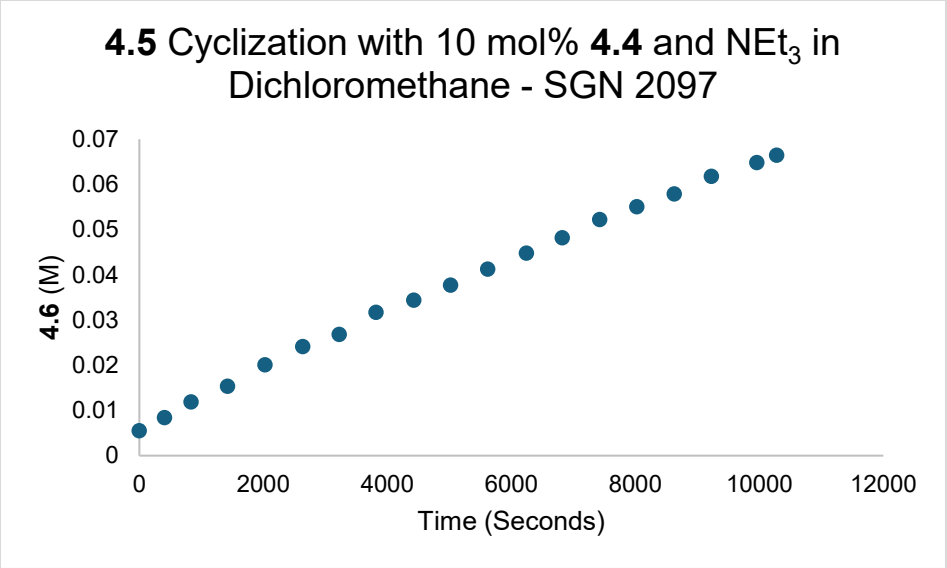

Figure 163 Formation of **4.6** in the Presence of **4.4**

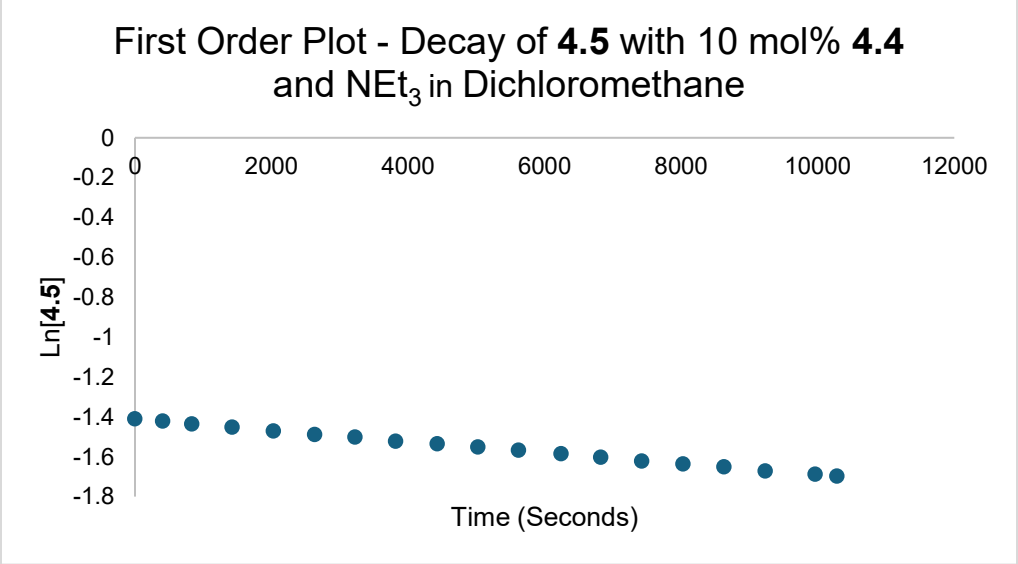

Figure 164 First Order Decay of **4.**5 in the Presence of **4.4**

The cyclization of **4.5** with 10 mol% **4.4** and triethylamine is extremely slow, reaching less than 50% conversion in three hours. This stands largely in contrast to the rates observed with other catalysts. To illustrate the slow rate, the graphs above are repeated below with values from catalysis with **C1** plotted on the same graph.

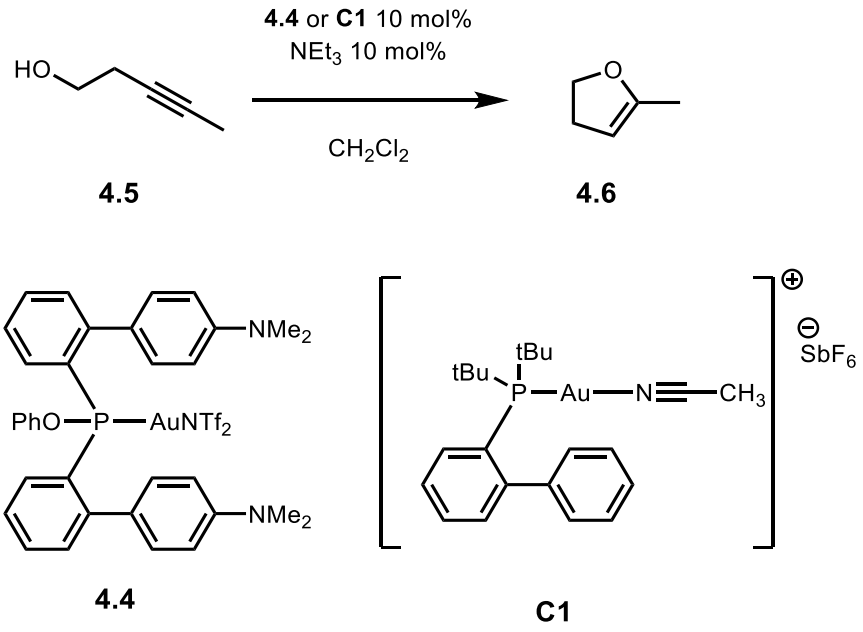

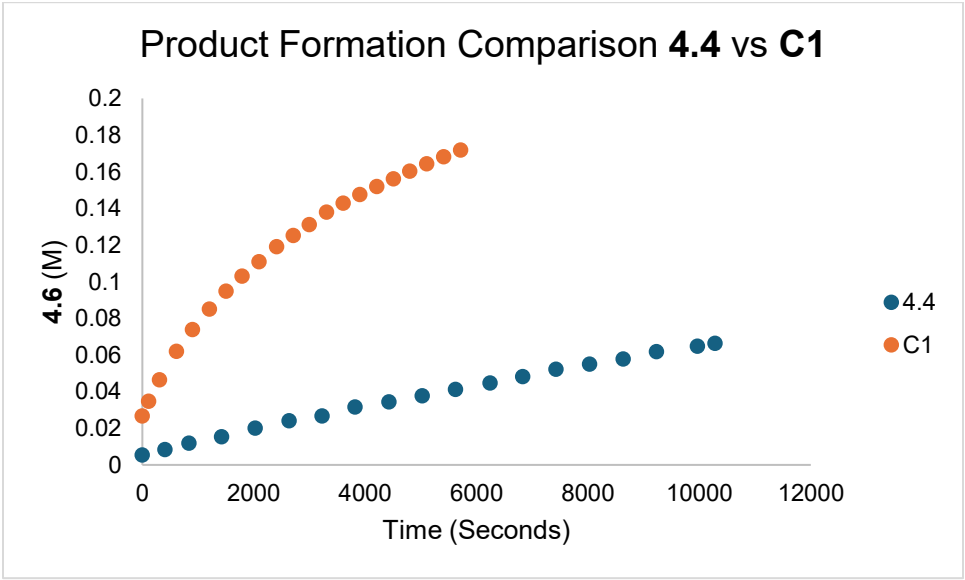

Figure 165 Comparative Product Formation - **4.4** vs **C1**

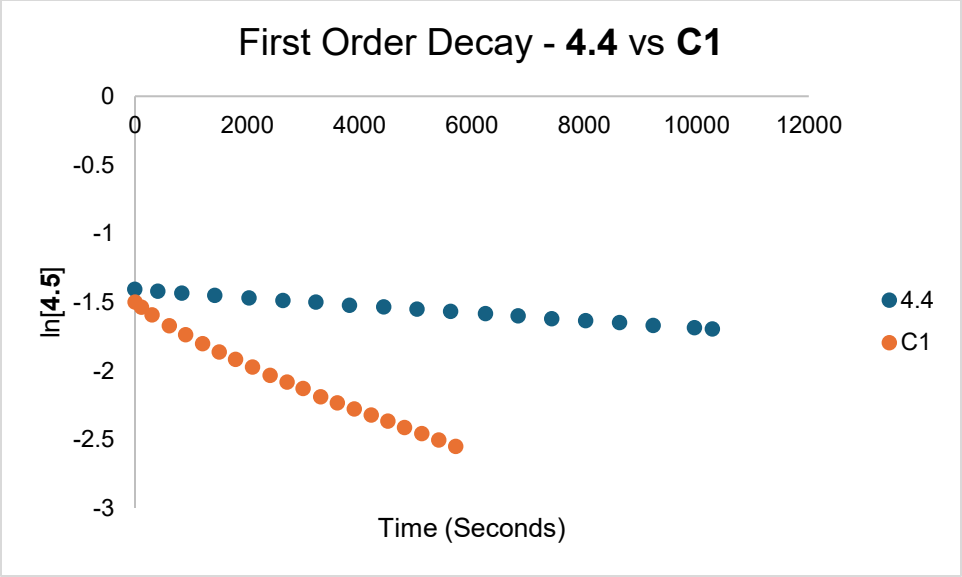

Figure 166 Comparative First Order Decay **– 4.4** vs **C1**

4.4 performs much more slowly than **C1** in the transformation (k_{rel} **C1**/**4.4** = 6.15). The result is surprising given cyclization for the substrate is typically fast. The result is particularly intriguing when the ^{31}P spectra for the reaction are analyzed. During the three hour reaction course, the catalyst does not degrade at all. A single peak is observed at ~99ppm for the entirety of the three hours.

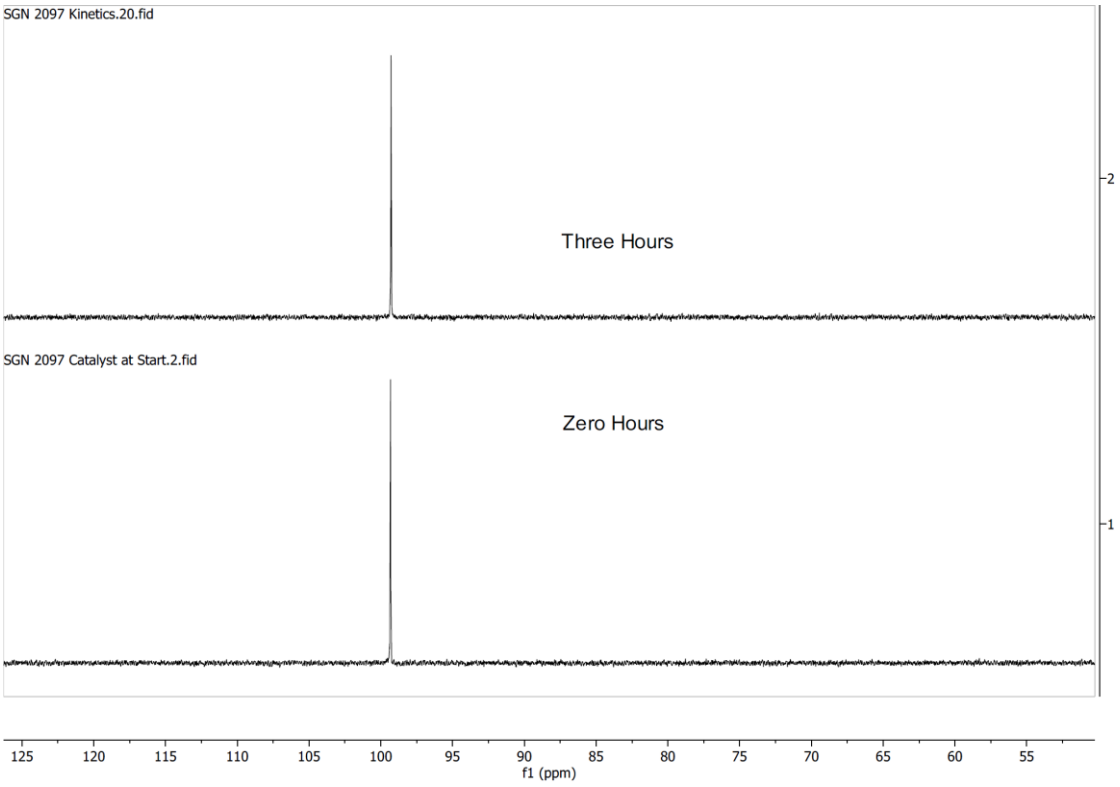

Figure 167 ^{31}P NMR for **4.5** Cyclization with **4.4** at Zero and Three Hours

Two days later, the NMR tube used for the experiment did show some degree of metal plating, so the catalyst will eventually degrade if left in solution for a time. However, the stability of the catalyst stands in stark contrast to what is observed for **C1** in the same reaction. At only two hours of reaction time, **C1** has partially degraded into one major off-cycle product, with minor degradation products also visible.

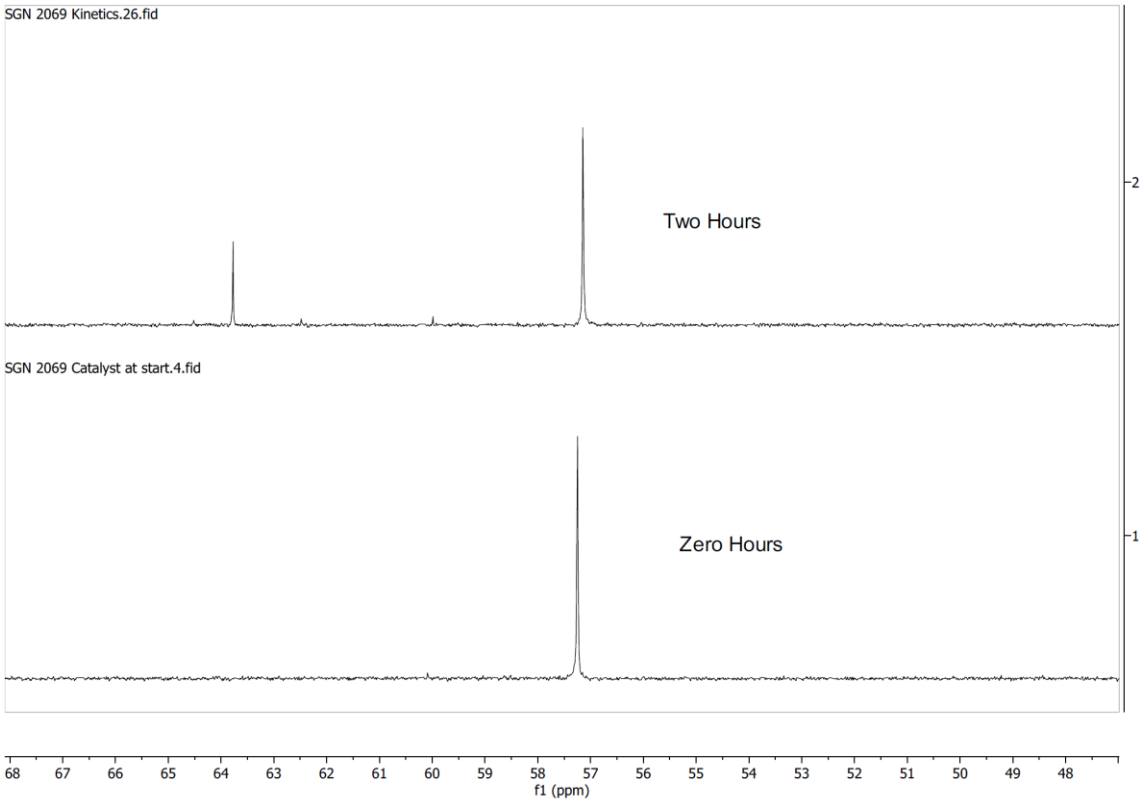

Figure 168 ^{31}P NMR for 4.5 Cyclization with **C1** at Zero and Two Hours

This is the exact opposite of what one would likely expect to observe when analyzing the phosphorus spectra for these two reactions. **C1**, the faster catalyst of the two, catalyzes the reaction at more than six times the rate of **4.4**, but shows multiple peaks in its phosphorus spectrum in only two hours. **4.4**, the slower catalyst, shows absolutely no degradation at 150% the reaction time. In the time of a typical kinetics experiment, **4.4** is entirely exempt from any degradation pathways. Much of the conceit for the initial synthesis of bisbiphenyl ligands was specifically to enhance catalyst stability, which has clearly been successful in its case. The stability presumably cannot be owed entirely to sterics, as similarly bulky ligands such as Jackiephos still degrade in both this cyclization and that of the propargyl benzamide. **4.4** perhaps lands at exactly the right balance of electronics

and sterics to avoid any rapid degradation, but the reason is ultimately not currently clear.

Synthesis of a *p*-Methoxy Bisbiphenyl Ligand

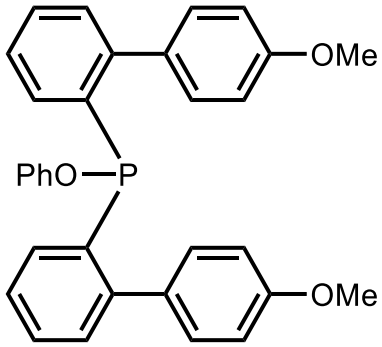

4.7

Figure 169 p-Methoxy Bisbiphenyl Ligand

Ligand **4.7** was chosen as a second synthetic target. Similar behavior to **4.1** was expected due to the retention of the phenoxy ligand and the replacement of the dimethylamino groups with methoxy groups, which should be similarly electron-donating. **4.7** was successfully synthesized according to the scheme below.

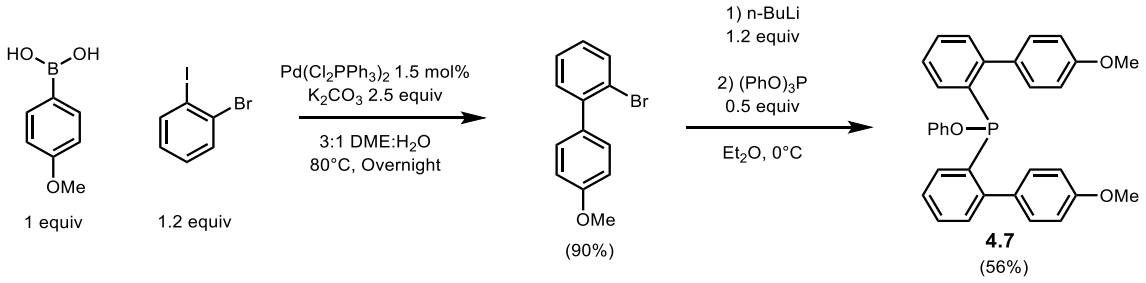

Figure 170 Synthesis of p-methoxy ligand **4.7**

First, Suzuki coupling between *p*-methoxy boronic acid and 1,2-iodobromobenzene gave the precursor bromobiphenyl in 90% yield. **4.7** was then

synthesized by lithiation and quenching with triphenylphosphite, with a 66% pure yield recovered.

Conversion to the gold chloride went less smoothly than is typical, with **4.8** being difficult to recrystallize away from residual impurities.

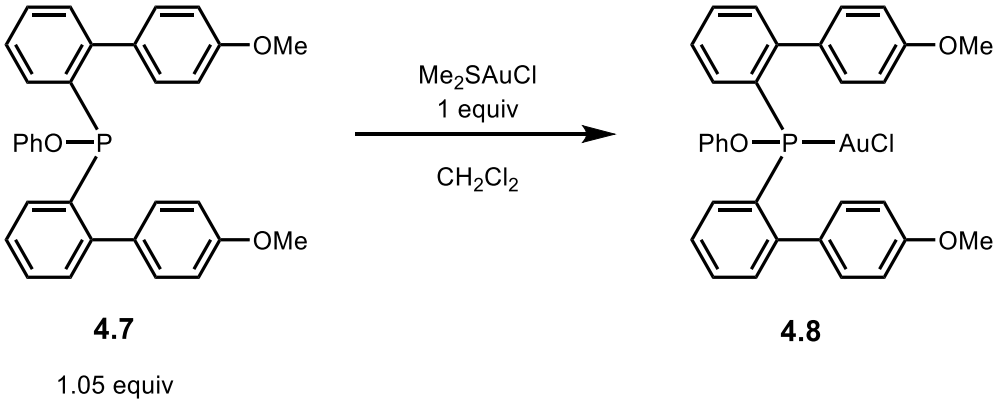

Figure 171 Synthesis of Gold Chloride **4.8**

Unfortunately, conversion to the gold triflimide was problematic. Multiple attempts were made with different stoichiometries and recrystallization conditions, but gold triflate **4.9** was never successfully recovered.

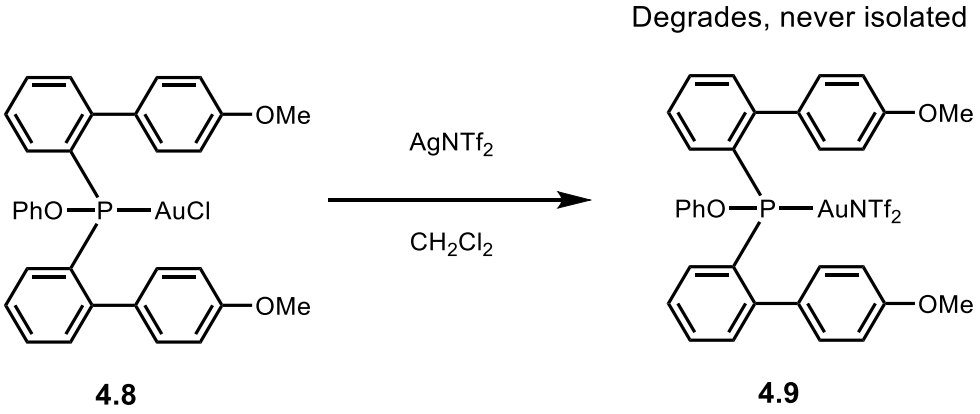

Figure 172 Unsuccessful Synthesis of Gold Triflimide **4.9**

The reason for the instability of the methoxy ligand relative to the amino isn't immediately clear. A likely explanation is the dimerization of **4.3** and **4.4** gives rise to a more stable gold center after abstraction of the chloride ligand. The pendant methoxy groups of **4.9** are presumably less prone to this behavior, causing **4.9** to rapidly degrade.

Conclusion

The successful synthesis of the dimethylamino-based ligand and its use in catalysis indicate promise for the bisbiphenyl motif as a ligand scaffold. **4.4** is remarkably stable in the cyclization of both N-propargyl benzamide and pentynol **4.5**. Its pace in the benzamide cyclization is reasonably fast (see discussion in chapter two), and it shows no degradation after hours of reaction time. For the cyclization of alcohol **4.5**, the rate observed is much slower. However, it displays the same stability for this cyclization as well, showing no degradation after three hours whereas catalyst **C1** shows significant degradation after merely two.

The methoxy-based scaffold was never successfully converted to an active catalyst. The reason for its instability is not known. The results seen for the amino ligand indicate that further studies with varied substituents on the bisbiphenyl rings could lead to the discovery of more catalysts with the same notable stability, potentially alleviating the issue of low turnover rates for Au(I) catalysts.

Chapter 5: Summary and Outlook

As revealed by experiments detailed in previous chapters, the Au(I)-Catalyzed cyclization of N-propargyl benzamide features much more mechanistic complexity than is currently reported. Vinylgolds are posited as key intermediates and catalyst resting states, yet all experiments described above have failed both to capture them or observe them as an intermediate. The rate-limiting step of the reaction, typically proposed to be protodeauration, has been shown to have a solvent-dependent switch, changing from protodeauration to cyclization when the solvent is changed from dichloromethane to methanol. A significant cause of the deleterious rates in methanol is catalyst decomposition, as the formation of mono and digold acetylides is much more prevalent in methanol than in dichloromethane, a more frequently-used solvent for gold-catalyzed transformations. A bisbiphenyl ligand was discovered to be effectively immune to decomposition on a typical reaction timescale for the cyclization of both the benzamide and an analogous transformation of pent-3-yn-1-ol. Further exploration of this and other ligands may yield catalysts less prone to these degradation pathways.

Given the immense popularity of the benzamide cyclization as a test reaction for many gold systems, the results described above serve to recontextualize many of the reports in which it appears. The abundance of its use in the literature is likely for two reasons. First, it is commercially available, or can be synthesized easily in one step from other commercial reagents. Second, the frequency with which it appears in the literature has given rise to an overwhelming consensus about the rate-limiting nature of protodeauration. As a result, when the

reaction is used to test new gold systems, whether those systems involve ligands, additives, or co-catalysts, the results and conclusions are made with rate-limiting deauration in mind. Some of the contrasting trends observed in literature may possibly be explained when re-examined with an eye towards a switchable rate-limiting step.

Much of the gold(I) catalysis literature also shows a substantial bias towards halogenated solvents. Chloroform and dichloromethane are perhaps the most common solvents used in optimized conditions. This bias is potentially fraught when considering recent efforts made by the EPA to diminish the use of dichloromethane in both industrial and academic synthesis. A greater understanding of gold's performance in other solvents will become a necessity as chlorinated solvents are phased out. If this common benchmark reaction shows such an enormous dependency on solvent for its performance, the various catalyst systems it has been used to study are likely to behave very differently or perhaps fail outright when they are utilized in other media.

The study of acetylides in the work above should also be noted. Alkynes are perhaps the functional group most associated with gold(I) catalysis, and understanding such a potentially common intermediate is therefore vital to understanding much of gold's reactivity. The experiments with carbamates are especially noteworthy. The substrates are self-deactivating, as the basicity of the carbonyl in tandem with the enhanced acidity of the alkyne leads to quantitative deactivation of the gold by the formation of mono and digold acetylides. The benzamide cyclization seemingly sits on something of a knife's edge. An overly

nucleophilic carbonyl is also overly basic, irreversibly degrading the catalyst. Too electron-poor a carbonyl, however, may not cyclize at all. This is particularly of concern when cyclization instead becomes rate-limiting. Benzamides are reactive, but carbamates are not. Given the prevalence of terminal alkynes as substrates for activation by gold, an understanding of the exact tipping point at which acetylides formation outcompetes π-activation is critical to optimizing the performance of gold catalysts.

Future Experiments

For the benzamide cyclization, the obvious sensitivity to solvent invites a survey of other solvent systems. One experiment not detailed above was a cyclization performed in 1,4-dioxane, which returned a rate between that of dichloromethane and methanol. The growing abundance of literature in gold catalysis and elsewhere describing the utility of hexafluoroisopropanol makes it another exciting candidate for study.

The intricacies of the mechanism pertaining to acetylide formation can also be further probed. Analysis of base-treated reaction mixtures detailed in chapter 3 showed the alkylgold oxazole formation is likely formed entirely in a pathway involving the acetylide. The presence of triethylamine and concurrent generation of acid clouds the mechanistic step by which this transformation may occur. Issues of triethylamine and a co-generated acid in the mixture can be remedied by formal synthesis and isolation of the monogold acetylide. This could be achieved by quantitative deprotonation with n-butyllithium followed by quenching with

stoichiometric gold. The acetylide formed could then be placed into NMR solvent and studied to see if it will cyclize to the alkylgold and/or the oxazole.

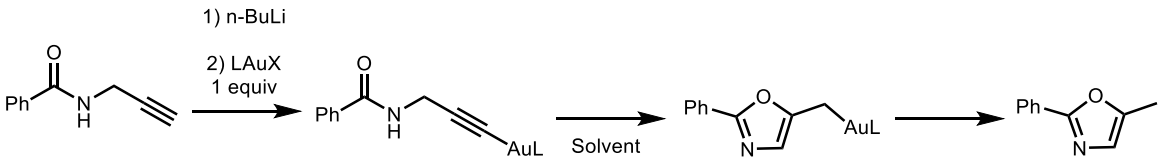

Varying the substituents on the appended phenyl ring also provides another interesting avenue of study. The *p*-nitro variant discussed in chapter 3 quite conspicuously is unaffected by the solvent switch from dichloromethane to methanol. A possible reason for this may be the charged nature of the nitro group. Recall from chapter 1 that Hammond and Xu saw an enormous rate increase for the benzamide cyclization when pyridine-N-oxide was used as an H-bonding additive. The zwitterionic state of the nitro group could possibly be acting as an H-bonding site, easing proton transfer for the various steps of the reaction. To assess this possibility, non-ionic withdrawing groups could be surveyed in the same transformation, e.g. *p*-cyano, or *p*-fluoro, among others. Electron-donating substituents were not attempted to avoid the potential of an overly-basic carbonyl as observed in the carbamate experiments, but this is less likely to occur with electron-rich aryl substituents than direct heteroatom sigma donors.

In conclusion, while the view of the N-propargyl benzamide cyclization in the field of gold catalysis may be an overly simple one, its true utility is perhaps yet unrealized. The greater mechanistic complexity discovered in these experiments indicate it may prove to be an even more fruitful scaffold with which to study gold mechanisms than previously thought. The generation of multiple intermediates of

interest, as well as the modularity of the substrate, indicates its highest potential may be as a tool for mechanistic study, rather than as a simple benchmark. As has been shown, the true complexity of the reaction has been hidden for more than twenty years.

References

(1) Schmidbaur, H. Gold-Chemie: Ein Eldorado. *Naturwissenschaftliche Rundsch.* **1995**, *48* (12), 443–451.

(2) Teles, J. H.; Brode, S.; Chabanas, M. Cationic Gold(I) Complexes: Highly Efficient Catalysts for the Addition of Alcohols to Alkynes. *Angew. Chem. Int. Ed.* **1998**, *37* (10), 1415–1418. https://doi.org/10.1002/(SICI)1521-3773(19980605)37:10<1415::AID-ANIE1415>3.0.CO;2-N.

(3) Dyker, G. An Eldorado for Homogeneous Catalysis? *Angew. Chem. Int. Ed.* **2000**, *39* (23), 4237–4239. https://doi.org/10.1002/1521-3773(20001201)39:23<4237::AID-ANIE4237>3.0.CO;2-A.

(4) Hashmi, A. S. K. Gold-Catalyzed Organic Reactions. *Chem. Rev.* **2007**, *107* (7), 3180–3211. https://doi.org/10.1021/cr000436x.

(5) Li, Z.; Brouwer, C.; He, C. Gold-Catalyzed Organic Transformations. *Chem. Rev.* **2008**, *108* (8), 3239–3265. https://doi.org/10.1021/cr068434l.

(6) Zheng, Z.; Ma, X.; Cheng, X.; Zhao, K.; Gutman, K.; Li, T.; Zhang, L. Homogeneous Gold-Catalyzed Oxidation Reactions. *Chem. Rev.* **2021**, *121* (14), 8979–9038. https://doi.org/10.1021/acs.chemrev.0c00774.

(7) Stylianakis, I.; Kolocouris, A. Comprehensive Overview of Homogeneous Gold-Catalyzed Transformations of π-Systems for Application Scientists. *Catalysts* **2023**, *13* (6), 921. https://doi.org/10.3390/catal13060921.

(8) Roth, K. E.; Blum, S. A. Relative Kinetic Basicities of Organogold Compounds. *Organometallics* **2010**, *29* (7), 1712–1716. https://doi.org/10.1021/om901101f.

(9) Campeau, D.; León Rayo, D. F.; Mansour, A.; Muratov, K.; Gagosz, F. Gold-Catalyzed Reactions of Specially Activated Alkynes, Allenes, and Alkenes. *Chem. Rev.* **2021**, *121* (14), 8756–8867. https://doi.org/10.1021/acs.chemrev.0c00788.

(10) Fukuda, Y.; Utimoto, K. Effective Transformation of Unactivated Alkynes into Ketones or Acetals with a Gold(III) Catalyst. *J. Org. Chem.* **1991**, *56* (11), 3729–3731. https://doi.org/10.1021/jo00011a058.

(11) Fukuda, Y.; Utimoto, K. Efficient Transformation of Methyl Propargyl Ethers into α,β-Unsaturated Ketones. *Bull. Chem. Soc. Jpn.* **1991**, *64* (6), 2013–2015. https://doi.org/10.1246/bcsj.64.2013.

(12) Genin, E.; Toullec, P. Y.; Antoniotti, S.; Brancour, C.; Genêt, J.-P.; Michelet, V. Room Temperature Au(I)-Catalyzed Exo-Selective Cycloisomerization of

Acetylenic Acids: An Entry to Functionalized γ-Lactones. *J. Am. Chem. Soc.* **2006**, *128* (10), 3112–3113. https://doi.org/10.1021/ja056857j.

(13) Liu, L.-P.; Xu, B.; Mashuta, M. S.; Hammond, G. B. Synthesis and Structural Characterization of Stable Organogold(I) Compounds. Evidence for the Mechanism of Gold-Catalyzed Cyclizations. *J. Am. Chem. Soc.* **2008**, *130* (52), 17642–17643. https://doi.org/10.1021/ja806685j.

(14) Hashmi, A. S. K.; Schuster, A. M.; Rominger, F. Gold Catalysis: Isolation of Vinylgold Complexes Derived from Alkynes. *Angew. Chem. Int. Ed.* **2009**, *48* (44), 8247–8249. https://doi.org/10.1002/anie.200903134.

(15) Hashmi, A. S. K.; Ramamurthi, T. D.; Rominger, F. On the Trapping of Vinylgold Intermediates. *Adv. Synth. Catal.* **2010**, *352* (6), 971–975. https://doi.org/10.1002/adsc.201000011.

(16) Dubé, P.; Toste, F. D. Synthesis of Indenyl Ethers by Gold(I)-Catalyzed Intramolecular Carboalkoxylation of Alkynes. *J. Am. Chem. Soc.* **2006**, *128* (37), 12062–12063. https://doi.org/10.1021/ja064209+.

(17) Luzung, M. R.; Mauleón, P.; Toste, F. D. Gold(I)-Catalyzed [2 + 2]-Cycloaddition of Allenenes. *J. Am. Chem. Soc.* **2007**, *129* (41), 12402–12403. https://doi.org/10.1021/ja075412n.

(18) Shi, Y.; Roth, K. E.; Ramgren, S. D.; Blum, S. A. Catalyzed Catalysis Using Carbophilic Lewis Acidic Gold and Lewis Basic Palladium: Synthesis of Substituted Butenolides and Isocoumarins. *J. Am. Chem. Soc.* **2009**, *131* (50), 18022–18023. https://doi.org/10.1021/ja9068497.

(19) Huang, L.; Rudolph, M.; Rominger, F.; Hashmi, A. S. K. Photosensitizer-Free Visible-Light-Mediated Gold-Catalyzed 1,2-Difunctionalization of Alkynes. *Angew. Chem. Int. Ed.* **2016**, *55* (15), 4808–4813. https://doi.org/10.1002/anie.201511487.

(20) Xie, J.; Shi, S.; Zhang, T.; Mehrkens, N.; Rudolph, M.; Hashmi, A. S. K. A Highly Efficient Gold-Catalyzed Photoredox α-C(Sp3)□H Alkynylation of Tertiary Aliphatic Amines with Sunlight. *Angew. Chem. Int. Ed.* **2015**, *54* (20), 6046–6050. https://doi.org/10.1002/anie.201412399.

(21) Taschinski, S.; Döpp, R.; Ackermann, M.; Rominger, F.; de Vries, F.; Menger, M. F. S. J.; Rudolph, M.; Hashmi, A. S. K.; Klein, J. E. M. N. Light-Induced Mechanistic Divergence in Gold(I) Catalysis: Revisiting the Reactivity of Diazonium Salts. *Angew. Chem. Int. Ed.* **2019**, *58* (47), 16988–16993. https://doi.org/10.1002/anie.201908268.

(22) Brown, T. J.; Widenhoefer, R. A. Cationic Gold(I) π-Complexes of Terminal Alkynes and Their Conversion to Dinuclear σ,π-Acetylide Complexes. *Organometallics* **2011**, *30* (21), 6003–6009. https://doi.org/10.1021/om200840g.

(23) Bucher, J.; Wurm, T.; Taschinski, S.; Sachs, E.; Ascough, D.; Rudolph, M.; Rominger, F.; Hashmi, A. S. K. Dual Gold Catalysis: Synthesis of Fluorene Derivatives from Diynes. *Adv. Synth. Catal.* **2017**, *359* (2), 225–233. https://doi.org/10.1002/adsc.201600987.

(24) Graf, K.; Hindenberg, P. D.; Tokimizu, Y.; Naoe, S.; Rudolph, M.; Rominger, F.; Ohno, H.; Hashmi, A. S. K. The Role of Acetylides in Dual Gold Catalysis: A Mechanistic Investigation of the Selectivity Difference in the Naphthalene Synthesis from Diynes. *ChemCatChem* **2014**, *6* (1), 199–204. https://doi.org/10.1002/cctc.201300820.

(25) Hansmann, M. M.; Rudolph, M.; Rominger, F.; Hashmi, A. S. K. Mechanistic Switch in Dual Gold Catalysis of Diynes: C(Sp3)–H Activation through Bifurcation—Vinylidene versus Carbene Pathways. *Angew. Chem. Int. Ed.* **2013**, *52* (9), 2593–2598. https://doi.org/10.1002/anie.201208777.

(26) Hashmi, A. S. K.; Lauterbach, T.; Nösel, P.; Vilhelmsen, M. H.; Rudolph, M.; Rominger, F. Dual Gold Catalysis: σ,π-Propyne Acetylide and Hydroxyl-Bridged Digold Complexes as Easy-To-Prepare and Easy-To-Handle Precatalysts. *Chem. – Eur. J.* **2013**, *19* (3), 1058–1065. https://doi.org/10.1002/chem.201203010.

(27) Larsen, M. H.; Houk, K. N.; Hashmi, A. S. K. Dual Gold Catalysis: Stepwise Catalyst Transfer via Dinuclear Clusters. *J. Am. Chem. Soc.* **2015**, *137* (33), 10668–10676. https://doi.org/10.1021/jacs.5b05773.

(28) Tokimizu, Y.; Wieteck, M.; Rudolph, M.; Oishi, S.; Fujii, N.; Hashmi, A. S. K.; Ohno, H. Dual Gold Catalysis: A Novel Synthesis of Bicyclic and Tricyclic Pyrroles from N-Propargyl Ynamides. *Org. Lett.* **2015**, *17* (3), 604–607. https://doi.org/10.1021/ol503623m.

(29) Tšupova, S.; Hansmann, M. M.; Rudolph, M.; Rominger, F.; Hashmi, A. S. K. New Pathways for the Dual Gold-Catalyzed Cyclization of Diynes. *Chem. – Eur. J.* **2016**, *22* (45), 16286–16291. https://doi.org/10.1002/chem.201602873.

(30) Vreeken, V.; Broere, D. L. J.; Jans, A. C. H.; Lankelma, M.; Reek, J. N. H.; Siegler, M. A.; van der Vlugt, J. I. Well-Defined Dinuclear Gold Complexes for Preorganization-Induced Selective Dual Gold Catalysis. *Angew. Chem. Int. Ed.* **2016**, *55* (34), 10042–10046. https://doi.org/10.1002/anie.201603938.

(31) Cheong, P. H.-Y.; Morganelli, P.; Luzung, M. R.; Houk, K. N.; Toste, F. D. Gold-Catalyzed Cycloisomerization of 1,5-Allenynes via Dual Activation of an Ene Reaction. *J. Am. Chem. Soc.* **2008**, *130* (13), 4517–4526. https://doi.org/10.1021/ja711058f.

(32) Braun, I.; Asiri, A. M.; Hashmi, A. S. K. Gold Catalysis 2.0. *ACS Catal.* **2013**, *3* (8), 1902–1907. https://doi.org/10.1021/cs400437s.

(33) Odabachian, Y.; Le Goff, X. F.; Gagosz, F. An Unusual Access to Medium Sized Cycloalkynes by a New Gold(I)-Catalysed Cycloisomerisation of Diynes. *Chem. – Eur. J.* **2009**, *15* (36), 8966–8970. https://doi.org/10.1002/chem.200901312.

(34) Hashmi, A. S. K.; Braun, I.; Rudolph, M.; Rominger, F. The Role of Gold Acetylides as a Selectivity Trigger and the Importance of Gem-Diaurated Species in the Gold-Catalyzed Hydroarylating-Aromatization of Arene-Diynes. *Organometallics* **2012**, *31* (2), 644–661. https://doi.org/10.1021/om200946m.

(35) Hashmi, A. S. K.; Wieteck, M.; Braun, I.; Nösel, P.; Jongbloed, L.; Rudolph, M.; Rominger, F. Gold-Catalyzed Synthesis of Dibenzopentalenes – Evidence for Gold Vinylidenes. *Adv. Synth. Catal.* **2012**, *354* (4), 555–562. https://doi.org/10.1002/adsc.201200086.

(36) Hansmann, M. M.; Tšupova, S.; Rudolph, M.; Rominger, F.; Hashmi, A. S. K. Gold-Catalyzed Cyclization of Diynes: Controlling the Mode of 5-Endo versus 6-Endo Cyclization—An Experimental and Theoretical Study by Utilizing Diethynylthiophenes. *Chem. – Eur. J.* **2014**, *20* (8), 2215–2223. https://doi.org/10.1002/chem.201302967.

(37) Rudolph, M.; Hashmi, A. S. K. Gold Catalysis in Total Synthesis—an Update. *Chem. Soc. Rev.* **2012**, *41* (6), 2448–2462. https://doi.org/10.1039/C1CS15279C.

(38) Schmidbaur, H. The Aurophilicity Phenomenon: A Decade of Experimental Findings, Theoretical Concepts and Emerging Applications. *Gold Bull.* **2000**, *33* (1), 3–10. https://doi.org/10.1007/BF03215477.

(39) Schmidbaur, H.; Schier, A. A Briefing on Aurophilicity. *Chem. Soc. Rev.* **2008**, *37* (9), 1931–1951. https://doi.org/10.1039/B708845K.

(40) Schmidbaur, H.; Schier, A. Aurophilic Interactions as a Subject of Current Research: An up-Date. *Chem. Soc. Rev.* **2011**, *41* (1), 370–412. https://doi.org/10.1039/C1CS15182G.

(41) Raubenheimer, H. G.; Schmidbaur, H. Gold Chemistry Guided by the Isolobality Concept†. *Organometallics* **2012**, *31* (7), 2507–2522. https://doi.org/10.1021/om2010113.

(42) Weber, D.; Tarselli, M. A.; Gagné, M. R. Mechanistic Surprises in the Gold(I)-Catalyzed Intramolecular Hydroarylation of Allenes. *Angew. Chem.* **2009**, *121* (31), 5843–5846. https://doi.org/10.1002/ange.200902049.

(43) Weber, D.; Jones, T. D.; Adduci, L. L.; Gagné, M. R. Strong Electronic and Counterion Effects on Geminal Digold Formation and Reactivity as Revealed by Gold(I)–Aryl Model Complexes. *Angew. Chem. Int. Ed.* **2012**, *51* (10), 2452–2456. https://doi.org/10.1002/anie.201107659.

(44) Zhdanko, A.; Maier, M. E. Quantitative Evaluation of the Stability of Gem-Diaurated Species in Reactions with Nucleophiles. *Organometallics* **2013**, *32* (6), 2000–2006. https://doi.org/10.1021/om400083f.

(45) Hashmi, A. S. K.; Weyrauch, J. P.; Frey, W.; Bats, J. W. Gold Catalysis: Mild Conditions for the Synthesis of Oxazoles from N-Propargylcarboxamides and Mechanistic Aspects. *Org. Lett.* **2004**, *6* (23), 4391–4394. https://doi.org/10.1021/ol0480067.

(46) Weyrauch, J. P.; Hashmi, A. S. K.; Schuster, A.; Hengst, T.; Schetter, S.; Littmann, A.; Rudolph, M.; Hamzic, M.; Visus, J.; Rominger, F.; Frey, W.; Bats, J. W. Cyclization of Propargylic Amides: Mild Access to Oxazole Derivatives. *Chem. – Eur. J.* **2010**, *16* (3), 956–963. https://doi.org/10.1002/chem.200902472.

(47) Wang, W.; Hammond, G. B.; Xu, B. Ligand Effects and Ligand Design in Homogeneous Gold(I) Catalysis. *J. Am. Chem. Soc.* **2012**, *134* (12), 5697–5705. https://doi.org/10.1021/ja3011397.

(48) Doherty, S.; Knight, J. G.; Hashmi, A. S. K.; Smyth, C. H.; Ward, N. A. B.; Robson, K. J.; Tweedley, S.; Harrington, R. W.; Clegg, W. Efficient Cycloisomerization of Propargyl Amides by Electrophilic Gold(I) Complexes of KITPHOS Monophosphines: A Comparative Study. *Organometallics* **2010**, *29* (18), 4139–4147. https://doi.org/10.1021/om1006769.

(49) Bárta, O.; Císařová, I.; Schulz, J.; Štěpnička, P. Assessing the Influence of Phosphine Substituents on the Catalytic Properties of Self-Stabilised Digold(I) Complexes with Supporting Ferrocene Phosphinonitrile Ligands. *New J. Chem.* **2019**, *43* (28), 11258–11262. https://doi.org/10.1039/C9NJ02555C.

(50) Lu, Z.; Han, J.; Okoromoba, O. E.; Shimizu, N.; Amii, H.; Tormena, C. F.; Hammond, G. B.; Xu, B. Predicting Counterion Effects Using a Gold Affinity Index and a Hydrogen Bonding Basicity Index. *Org. Lett.* **2017**, *19* (21), 5848–5851. https://doi.org/10.1021/acs.orglett.7b02829.

(51) Biasiolo, L.; Del Zotto, A.; Zuccaccia, D. Toward Optimizing the Performance of Homogeneous L-Au-X Catalysts through Appropriate Matching of the Ligand (L) and Counterion (X–). *Organometallics* **2015**, *34* (9), 1759–1765. https://doi.org/10.1021/acs.organomet.5b00308.

(52) Seidel, G.; Lehmann, C. W.; Fürstner, A. Elementary Steps in Gold Catalysis: The Significance of Gem-Diauration. *Angew. Chem. Int. Ed.* **2010**, *49* (45), 8466–8470. https://doi.org/10.1002/anie.201003349.

(53) Segato, J.; Baratta, W.; Belanzoni, P.; Belpassi, L.; Del Zotto, A.; Zuccaccia, D. Experimental and Theoretical Investigation of the Cycloisomerization of *N*-Propargylcarboxamide Catalyzed by NHC-Au-X in

Green Solvents. *Inorganica Chim. Acta* **2021**, *522*, 120372. https://doi.org/10.1016/j.ica.2021.120372.

(54) Wang, W.; Kumar, M.; Hammond, G. B.; Xu, B. Enhanced Reactivity in Homogeneous Gold Catalysis through Hydrogen Bonding. *Org. Lett.* **2014**, *16* (2), 636–639. https://doi.org/10.1021/ol403584e.

(55) Barrio, P.; Kumar, M.; Lu, Z.; Han, J.; Xu, B.; Hammond, G. B. Acidic Co-Catalysts in Cationic Gold Catalysis. *Chem. – Eur. J.* **2016**, *22* (46), 16410–16414. https://doi.org/10.1002/chem.201603478.

(56) Stein, P. M.; Rudolph, M.; Hashmi, A. S. K. Water Can Accelerate Homogeneous Gold Catalysis. *Adv. Synth. Catal.* **2021**, *363* (17), 4264–4271. https://doi.org/10.1002/adsc.202100729.

(57) Seppänen, O.; Aikonen, S.; Muuronen, M.; Alamillo-Ferrer, C.; Burés, J.; Helaja, J. Dual H-Bond Activation of NHC–Au(I)–Cl Complexes with Amide Functionalized Side-Arms Assisted by H-Bond Donor Substrates or Acid Additives. *Chem. Commun.* **2020**, *56* (93), 14697–14700. https://doi.org/10.1039/D0CC05999D.

(58) Han, J.; Lu, Z.; Wang, W.; Hammond, G. B.; Xu, B. Potassium Tris(Triflyl)Methide (KCTf3): A Broadly Applicable Promoter for Cationic Metal Catalysis. *Chem. Commun.* **2015**, *51* (72), 13740–13743. https://doi.org/10.1039/C5CC05306D.

(59) Jia, M.; Bandini, M. Counterion Effects in Homogeneous Gold Catalysis. *ACS Catal.* **2015**, *5* (3), 1638–1652. https://doi.org/10.1021/cs501902v.

(60) Homs, A.; Escofet, I.; Echavarren, A. M. On the Silver Effect and the Formation of Chloride-Bridged Digold Complexes. *Org. Lett.* **2013**, *15* (22), 5782–5785. https://doi.org/10.1021/ol402825v.

(61) Lu, Z.; Han, J.; Hammond, G. B.; Xu, B. Revisiting the Influence of Silver in Cationic Gold Catalysis: A Practical Guide. *Org. Lett.* **2015**, *17* (18), 4534–4537. https://doi.org/10.1021/acs.orglett.5b02224.

(62) Wang, D.; Cai, R.; Sharma, S.; Jirak, J.; Thummanapelli, S. K.; Akhmedov, N. G.; Zhang, H.; Liu, X.; Petersen, J. L.; Shi, X. “Silver Effect” in Gold(I) Catalysis: An Overlooked Important Factor. *J. Am. Chem. Soc.* **2012**, *134* (21), 9012–9019. https://doi.org/10.1021/ja303862z.

(63) Weber, D.; Gagné, M. R. Dinuclear Gold−Silver Resting States May Explain Silver Effects in Gold(I)-Catalysis. *Org. Lett.* **2009**, *11* (21), 4962–4965. https://doi.org/10.1021/ol902116b.

(64) Zhdanko, A.; Maier, M. E. Explanation of “Silver Effects” in Gold(I)-Catalyzed Hydroalkoxylation of Alkynes. *ACS Catal.* **2015**, *5* (10), 5994–6004. https://doi.org/10.1021/acscatal.5b01493.

(65) Boelke, A.; Kuczmera, T. J.; Lork, E.; Nachtsheim, B. J. N-Heterocyclic Iod(Az)Olium Salts – Potent Halogen-Bond Donors in Organocatalysis. *Chem. – Eur. J.* **2021**, *27* (52), 13128–13134. https://doi.org/10.1002/chem.202101961.

(66) Elías-Rodríguez, P.; Matador, E.; Benítez, M.; Tejero, T.; Díez, E.; Fernández, R.; Merino, P.; Monge, D.; Lassaletta, J. M. Silver-Free Gold-Catalyzed Heterocyclizations through Intermolecular H-Bonding Activation. *J. Org. Chem.* **2023**, *88* (4), 2487–2492. https://doi.org/10.1021/acs.joc.2c02932.

(67) Motiwala, H. F.; Armaly, A. M.; Cacioppo, J. G.; Coombs, T. C.; Koehn, K. R. K.; Norwood, V. M. I.; Aubé, J. HFIP in Organic Synthesis. *Chem. Rev.* **2022**, *122* (15), 12544–12747. https://doi.org/10.1021/acs.chemrev.1c00749.

(68) Tzouras, N. V.; Gobbo, A.; Pozsoni, N. B.; Chalkidis, S. G.; Bhandary, S.; Hecke, K. V.; Vougioukalakis, G. C.; Nolan, S. P. Hydrogen Bonding-Enabled Gold Catalysis: Ligand Effects in Gold-Catalyzed Cycloisomerizations in Hexafluoroisopropanol (HFIP). *Chem. Commun.* **2022**, *58* (61), 8516–8519. https://doi.org/10.1039/D2CC03056J.

(69) Tzouras, N. V.; Zorba, L. P.; Kaplanai, E.; Tsoureas, N.; Nelson, D. J.; Nolan, S. P.; Vougioukalakis, G. C. Hexafluoroisopropanol (HFIP) as a Multifunctional Agent in Gold-Catalyzed Cycloisomerizations and Sequential Transformations. *ACS Catal.* **2023**, *13* (13), 8845–8860. https://doi.org/10.1021/acscatal.3c01660.

(70) Hashmi, A. S. K.; Blanco Jaimes, M. C.; Schuster, A. M.; Rominger, F. From Propargylic Amides to Functionalized Oxazoles: Domino Gold Catalysis/Oxidation by Dioxygen. *J. Org. Chem.* **2012**, *77* (15), 6394–6408. https://doi.org/10.1021/jo301288w.

(71) Peng, H.; Akhmedov, N. G.; Liang, Y.-F.; Jiao, N.; Shi, X. Synergistic Gold and Iron Dual Catalysis: Preferred Radical Addition toward Vinyl–Gold Intermediate over Alkene. *J. Am. Chem. Soc.* **2015**, *137* (28), 8912–8915. https://doi.org/10.1021/jacs.5b05415.

(72) Mai, S.; Rao, C.; Chen, M.; Su, J.; Du, J.; Song, Q. Merging Gold Catalysis, Organocatalytic Oxidation, and Lewis Acid Catalysis for Chemodivergent Synthesis of Functionalized Oxazoles from N-Propargylamides. *Chem. Commun.* **2017**, *53* (75), 10366–10369. https://doi.org/10.1039/C7CC05746F.

(73) Witzel, S.; Hashmi, A. S. K.; Xie, J. Light in Gold Catalysis. *Chem. Rev.* **2021**, *121* (14), 8868–8925. https://doi.org/10.1021/acs.chemrev.0c00841.

(74) Liu, Y.; Shi, Y.; Wei, L.; Zhao, K.; Zhao, J.; Zhang, P.; Xu, X.; Li, P. Gold-Catalyzed One-Pot Synthesis of Polyfluoroalkylated Oxazoles from N-Propargylamides Under Visible-Light Irradiation. *Chem. – Asian J.* **2021**, *16* (17), 2417–2420. https://doi.org/10.1002/asia.202100614.

(75) Nalivela, K. S.; Rudolph, M.; Baeissa, E. S.; Alhogbi, B. G.; Mkhalid, I. A. I.; Hashmi, A. S. K. Sequential Au/Cu Catalysis: A Two Catalyst One-Pot Protocol for the Enantioselective Synthesis of Oxazole α-Hydroxy Esters via Intramolecular Cyclization/Intermolecular Alder-Ene Reaction. *Adv. Synth. Catal.* **2018**, *360* (11), 2183–2190. https://doi.org/10.1002/adsc.201800246.

(76) Dong, G.; Bao, M.; Xie, X.; Jia, S.; Hu, W.; Xu, X. Asymmetric Allylation by Chiral Organocatalyst-Promoted Formal Hetero-Ene Reactions of Alkylgold Intermediates. *Angew. Chem. Int. Ed.* **2021**, *60* (4), 1992–1999. https://doi.org/10.1002/anie.202012678.

(77) Bao, M.; Zhou, Y.; Yuan, H.; Dong, G.; Li, C.; Xie, X.; Chen, K.; Hong, K.; Yu, Z.-X.; Xu, X. Catalytic (4+2) Annulation via Regio- and Enantioselective Interception of in-Situ Generated Alkylgold Intermediate. *Angew. Chem. Int. Ed.* **2024**, *63* (31), e202401557. https://doi.org/10.1002/anie.202401557.

(78) Hashmi, A. S. K.; Weyrauch, J. P.; Frey, W.; Bats, J. W. Gold Catalysis: Mild Conditions for the Synthesis of Oxazoles from N-Propargylcarboxamides and Mechanistic Aspects. *Org. Lett.* **2004**, *6* (23), 4391–4394. https://doi.org/10.1021/ol0480067.

(79) Doherty, S.; Knight, J. G.; Hashmi, A. S. K.; Smyth, C. H.; Ward, N. A. B.; Robson, K. J.; Tweedley, S.; Harrington, R. W.; Clegg, W. Efficient Cycloisomerization of Propargyl Amides by Electrophilic Gold(I) Complexes of KITPHOS Monophosphines: A Comparative Study. *Organometallics* **2010**, *29* (18), 4139–4147. https://doi.org/10.1021/om1006769.

(80) Hashmi, A. S. K.; Yu, Y.; Rominger, F. Efficient One-Pot Synthesis of Unsymmetrical Gold(I) N-Heterocyclic Carbene Complexes and Their Use as Catalysts. *Organometallics* **2012**, *31* (3), 895–904. https://doi.org/10.1021/om2008919.

(81) Orbisaglia, S.; Jacques, B.; Braunstein, P.; Hueber, D.; Pale, P.; Blanc, A.; de Frémont, P. Synthesis, Characterization, and Catalytic Activity of Cationic NHC Gold(III) Pyridine Complexes. *Organometallics* **2013**, *32* (15), 4153–4164. https://doi.org/10.1021/om400338k.

(82) Hettmanczyk, L.; Manck, S.; Hoyer, C.; Hohloch, S.; Sarkar, B. Heterobimetallic Complexes with Redox-Active Mesoionic Carbenes as Metalloligands: Electrochemical Properties, Electronic Structures and Catalysis. *Chem. Commun.* **2015**, *51* (54), 10949–10952. https://doi.org/10.1039/C5CC01578B.

(83) Doherty, S.; Knight, J. G.; Perry, D. O.; Ward, N. A. B.; Bittner, D. M.; McFarlane, W.; Wills, C.; Probert, M. R. Triaryl-Like MONO-, BIS-, and TRISKITPHOS Phosphines: Synthesis, Solution NMR Studies, and a Comparison in Gold-Catalyzed Carbon–Heteroatom Bond Forming 5-Exo-Dig and 6-Endo-Dig Cyclizations. *Organometallics* **2016**, *35* (9), 1265–1278. https://doi.org/10.1021/acs.organomet.6b00146.

(84) Hettmanczyk, L.; Schulze, D.; Suntrup, L.; Sarkar, B. Mono- and Digold(I) Complexes with Mesoionic Carbenes: Structural Characterization and Use in Catalytic Silver-Free Oxazoline Formation. *Organometallics* **2016**, *35* (22), 3828–3836. https://doi.org/10.1021/acs.organomet.6b00675.

(85) Rigo, M.; Hettmanczyk, L.; Heutz, F. J. L.; Hohloch, S.; Lutz, M.; Sarkar, B.; Müller, C. Phosphinines versus Mesoionic Carbenes: A Comparison of Structurally Related Ligands in Au(I)-Catalysis. *Dalton Trans.* **2016**, *46* (1), 86–95. https://doi.org/10.1039/C6DT03766F.

(86) Cervantes-Reyes, A.; Rominger, F.; Rudolph, M.; Hashmi, A. S. K. Gold(I) Complexes Stabilized by Nine- and Ten-Membered N-Heterocyclic Carbene Ligands. *Chem. – Eur. J.* **2019**, *25* (50), 11745–11757. https://doi.org/10.1002/chem.201902458.

(87) Cervantes-Reyes, A.; Rominger, F.; Rudolph, M.; Hashmi, A. S. K. Gold(I) Complexes with Eight-Membered NHC Ligands: Synthesis, Structures and Catalytic Activity. *Adv. Synth. Catal.* **2020**, *362* (12), 2523–2533. https://doi.org/10.1002/adsc.202000281.

(88) Seppänen, O.; Aikonen, S.; Muuronen, M.; Alamillo-Ferrer, C.; Burés, J.; Helaja, J. Dual H-Bond Activation of NHC–Au(I)–Cl Complexes with Amide Functionalized Side-Arms Assisted by H-Bond Donor Substrates or Acid Additives. *Chem. Commun.* **2020**, *56* (93), 14697–14700. https://doi.org/10.1039/D0CC05999D.

(89) Franchino, A.; Martí, À.; Nejrotti, S.; Echavarren, A. M. Silver-Free Au(I) Catalysis Enabled by Bifunctional Urea- and Squaramide-Phosphine Ligands via H-Bonding. *Chem. – Eur. J.* **2021**, *27* (46), 11989–11996. https://doi.org/10.1002/chem.202101751.

(90) Rendón-Nava, D.; Álvarez-Hernández, A.; Mendoza-Espinosa, D. Synthesis and Catalytic Applications of Multinuclear Gold(I)-1,2,3-Triazolylidene Complexes. *Eur. J. Inorg. Chem.* **2021**, *2021* (9), 840–847. https://doi.org/10.1002/ejic.202001022.

(91) Zhang, J.; Liu, T.; Zhang, G.; Cai, J.; Wang, Y.; Tong, J.; Ma, Y.; Szostak, R.; Szostak, M. Indazolin-3-Ylidenes (Indy*): Easily Accessible, Sterically-Hindered Indazole-Derived N-Heterocyclic Carbenes and Their Application in

Gold Catalysis. *Dalton Trans.* **2024**, *53* (9), 4260–4265. https://doi.org/10.1039/D4DT00287C.

(92) Kaplanai, E.; Tzouras, N. V.; Tsoureas, N.; Pozsoni, N. B.; Bhandary, S.; Hecke, K. V.; Nolan, S. P.; Vougioukalakis, G. C. Synthesis of N-Heterocyclic Carbene (NHC)-Au/Ag/Cu Benzotriazolyl Complexes and Their Catalytic Activity in Propargylamide Cycloisomerization and Carbonyl Hydrosilylation Reactions. *Dalton Trans.* **2024**, *53* (26), 11001–11008. https://doi.org/10.1039/D4DT01414F.

(93) Wegener, M.; Huber, F.; Bolli, C.; Jenne, C.; Kirsch, S. F. Silver-Free Activation of Ligated Gold(I) Chlorides: The Use of [Me3NB12Cl11]− as a Weakly Coordinating Anion in Homogeneous Gold Catalysis. *Chem. – Eur. J.* **2015**, *21* (3), 1328–1336. https://doi.org/10.1002/chem.201404487.

(94) Zeng, X.; Liu, S.; Xu, B. Stable yet Reactive Cationic Gold Catalysts with Carbon Based Counterions. *RSC Adv.* **2016**, *6* (81), 77830–77833. https://doi.org/10.1039/C6RA19064B.

(95) Schießl, J.; Schulmeister, J.; Doppiu, A.; Wörner, E.; Rudolph, M.; Karch, R.; Hashmi, A. S. K. An Industrial Perspective on Counter Anions in Gold Catalysis: On Alternative Counter Anions. *Adv. Synth. Catal.* **2018**, *360* (20), 3949–3959. https://doi.org/10.1002/adsc.201800629.

(96) Schießl, J.; Schulmeister, J.; Doppiu, A.; Wörner, E.; Rudolph, M.; Karch, R.; Hashmi, A. S. K. An Industrial Perspective on Counter Anions in Gold Catalysis: Underestimated with Respect to “Ligand Effects.” *Adv. Synth. Catal.* **2018**, *360* (13), 2493–2502. https://doi.org/10.1002/adsc.201800233.

(97) Campagnolo, F.; Bevilacqua, M.; Baron, M.; Tubaro, C.; Biffis, A.; Zuccaccia, D. Insights on the Anion Effect in N-Heterocyclic Carbene Based Dinuclear Gold(I) Catalysts. *ChemPlusChem* **2024**, *89* (3), e202300421. https://doi.org/10.1002/cplu.202300421.

(98) Han, J.; Shimizu, N.; Lu, Z.; Amii, H.; Hammond, G. B.; Xu, B. Efficient Generation and Increased Reactivity in Cationic Gold via Brønsted Acid or Lewis Acid Assisted Activation of an Imidogold Precatalyst. *Org. Lett.* **2014**, *16* (13), 3500–3503. https://doi.org/10.1021/ol501443m.

(99) Kumar, M.; Hammond, G. B.; Xu, B. Cationic Gold Catalyst Poisoning and Reactivation. *Org. Lett.* **2014**, *16* (13), 3452–3455. https://doi.org/10.1021/ol501663f.

(100) Wolf, J.; Huber, F.; Erochok, N.; Heinen, F.; Guérin, V.; Legault, C. Y.; Kirsch, S. F.; Huber, S. M. Activation of a Metal-Halogen Bond by Halogen Bonding. *Angew. Chem. Int. Ed.* **2020**, *59* (38), 16496–16500. https://doi.org/10.1002/anie.202005214.

(101) Elías-Rodríguez, P.; Matador, E.; Benítez, M.; Tejero, T.; Díez, E.; Fernández, R.; Merino, P.; Monge, D.; Lassaletta, J. M. Silver-Free Gold-Catalyzed Heterocyclizations through Intermolecular H-Bonding Activation. *J. Org. Chem.* **2023**, *88* (4), 2487–2492. https://doi.org/10.1021/acs.joc.2c02932.

(102) Segato, J.; Baratta, W.; Belanzoni, P.; Belpassi, L.; Del Zotto, A.; Zuccaccia, D. Experimental and Theoretical Investigation of the Cycloisomerization of *N*-Propargylcarboxamide Catalyzed by NHC-Au-X in Green Solvents. *Inorganica Chim. Acta* **2021**, *522*, 120372. https://doi.org/10.1016/j.ica.2021.120372.

(103) Wang, W.; Hammond, G. B.; Xu, B. Ligand Effects and Ligand Design in Homogeneous Gold(I) Catalysis. *J. Am. Chem. Soc.* **2012**, *134* (12), 5697–5705. https://doi.org/10.1021/ja3011397.

(104) Ma, Y.; Ali, H. S.; Hussein, A. A. A Mechanistic Study on the Gold(I)-Catalyzed Cyclization of Propargylic Amide: Revealing the Impact of Expanded-Ring N-Heterocyclic Carbenes. *Catal. Sci. Technol.* **2022**, *12* (2), 674–685. https://doi.org/10.1039/D1CY01617B.

(105) Ali, H. S.; Hussein, A. A.; Obies, M. Impact of Counteranions on N-Heterocyclic Carbene Gold(I)-Catalyzed Cyclization of Propargylic Amide. *RSC Adv.* **2023**, *13* (5), 2896–2902. https://doi.org/10.1039/D2RA06210K.

(106) Hashmi, A. S. K.; Schuster, A. M.; Rominger, F. Gold Catalysis: Isolation of Vinylgold Complexes Derived from Alkynes. *Angew. Chem. Int. Ed.* **2009**, *48* (44), 8247–8249. https://doi.org/10.1002/anie.200903134.

(107) Liu, L.-P.; Xu, B.; Mashuta, M. S.; Hammond, G. B. Synthesis and Structural Characterization of Stable Organogold(I) Compounds. Evidence for the Mechanism of Gold-Catalyzed Cyclizations. *J. Am. Chem. Soc.* **2008**, *130* (52), 17642–17643. https://doi.org/10.1021/ja806685j.

(108) Wang, W.; Kumar, M.; Hammond, G. B.; Xu, B. Enhanced Reactivity in Homogeneous Gold Catalysis through Hydrogen Bonding. *Org. Lett.* **2014**, *16* (2), 636–639. https://doi.org/10.1021/ol403584e.

(109) Brooner, R. E. M.; Brown, T. J.; Widenhoefer, R. A. Synthesis and Study of Cationic, Two-Coordinate Triphenylphosphine– Gold–π Complexes. *Chem. – Eur. J.* **2013**, *19* (25), 8276–8284. https://doi.org/10.1002/chem.201204564.

(110) Lan, R.; Yager, B.; Jee, Y.; Day, C. S.; Jones, A. C. Ligand Effects, Solvent Cooperation, and Large Kinetic Solvent Deuterium Isotope Effects in Gold(I)-Catalyzed Intramolecular Alkene Hydroamination. *Beilstein J. Org. Chem.* **2024**, *20*, 479–496. https://doi.org/10.3762/bjoc.20.43.

(111) Griebel, C.; Hodges, D. D.; Yager, B. R.; Liu, F. L.; Zhou, W.; Makaravage, K. J.; Zhu, Y.; Norman, S. G.; Lan, R.; Day, C. S.; Jones, A. C. Bisbiphenyl

Phosphines: Structure and Synthesis of Gold(I) Alkene π-Complexes with Variable Phosphine Donicity and Enhanced Stability. *Organometallics* **2020**, *39* (14), 2665–2671. https://doi.org/10.1021/acs.organomet.0c00278.

(112) Peng, H.; Akhmedov, N. G.; Liang, Y.-F.; Jiao, N.; Shi, X. Synergistic Gold and Iron Dual Catalysis: Preferred Radical Addition toward Vinyl–Gold Intermediate over Alkene. *J. Am. Chem. Soc.* **2015**, *137* (28), 8912–8915. https://doi.org/10.1021/jacs.5b05415.

(113) Grirrane, A.; Garcia, H.; Corma, A.; Álvarez, E. Intermolecular [2 + 2] Cycloaddition of Alkyne-Alkene Catalyzed by Au(I) Complexes. What Are the Catalytic Sites Involved? *ACS Catal.* **2011**, *1* (12), 1647–1653. https://doi.org/10.1021/cs2004278.

(114) Hashmi, A. S. K.; Schuster, A. M.; Gaillard, S.; Cavallo, L.; Poater, A.; Nolan, S. P. Selectivity Switch in the Synthesis of Vinylgold(I) Intermediates. *Organometallics* **2011**, *30* (22), 6328–6337. https://doi.org/10.1021/om2009556.

(115) Griebel, C.; Hodges, D. D.; Yager, B. R.; Liu, F. L.; Zhou, W.; Makaravage, K. J.; Zhu, Y.; Norman, S. G.; Lan, R.; Day, C. S.; Jones, A. C. Bisbiphenyl Phosphines: Structure and Synthesis of Gold(I) Alkene π-Complexes with Variable Phosphine Donicity and Enhanced Stability. *Organometallics* **2020**, *39* (14), 2665–2671. https://doi.org/10.1021/acs.organomet.0c00278.

Experimental Section

General Experimental

Unless otherwise noted commercial materials were used without further purification. Complexes were prepared in an oxygen-free, moisture-free glovebox or under Argon using Schlenk techniques. Deuterated solvents were purchased from Cambridge Isotope Laboratories. Unless otherwise stated, the deuterated solvents for kinetics experiments were used as received. All other solvents were purchased anhydrous. NMR spectra were obtained on Bruker spectrometers operating at a proton frequency of either 300, 400 or 500 MHz. Unless otherwise noted, spectra were collected at 25 °C. Structural assignments were made with additional information from gCOSY, gHSQC, and gHMBC experiments. For kinetic plots, the total concentrations of alkyne starting material and cyclized product were normalized, assuming that the sum of the signals for each were constant.

Observed rates and corresponding errors for individual experiments were calculated using the LINEST function in EXCEL. Where multiple trials were conducted, standard deviation on the average was calculated.

Kinetic Procedures

Representative Kinetic Procedure

Catalyst **C1** (1.54mg, 0.002mmol, 4 mol %) of catalyst was dissolved in 0.8mL of solvent and added to a vial containing N-propargyl benzamide (7.96mg, 0,05mmol). The mixture was mixed briefly by pipet, transferred to an NMR tube,

then transferred to the NMR spectrometer. ^{1}H NMR spectra were collected immediately and then every 10 min for 3 h.

Experimental Procedure for Methanol Titration Experiments

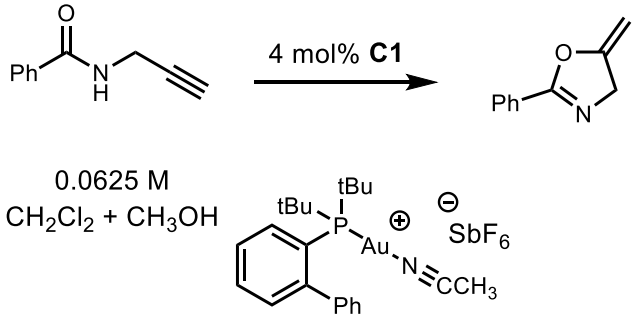

C1

In all cases, 7.96mg (0.05mmol) of benzamide and 1.54mg of catalyst **C1** (0.002mmol, 4mol%) were carried to the NMR room in separate vials. Catalyst was dissolved in CH_2Cl_2, after which the corresponding volume of CH_3OH would be added. This solution would then be transferred to the vial containing substrate and mixed with a pipette. The total solvent volume between methanol and dichloromethane was adjusted for each experiment such that the overall volume would always be 0.8mL (0.0625M respective to substrate). The solution would then be transferred to the NMR spectrometer. ^{1}H NMR would be taken at regular intervals.

Experimental Procedure for Isotopically Labeled Kinetics Experiments

Experimental Procedure for Deuterated Methanol Titration Experiments

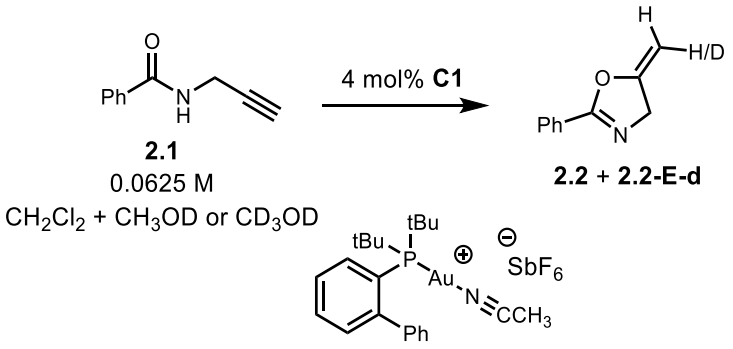

In all cases, 7.96mg (0.05mmol) of benzamide and 1.54mg of catalyst **C1** (0.002mmol, 4mol%) were carried to the NMR room in separate vials. Catalyst was dissolved in CH_2Cl_2, after which the corresponding volume of methanol-d_1 or d_4 would be added. This solution would then be transferred to the vial containing substrate and mixed with a pipette. The total solvent volume between methanol and dichloromethane was adjusted for each experiment such that the overall volume would always be 0.8mL (0.0625M respective to substrate). The solution would then be transferred to the NMR spectrometer. ^{1}H NMR would be taken at regular intervals.

Experimental Procedure for Cyclization of **2.1-C-d**

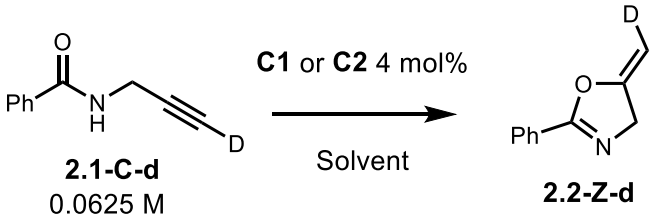

2.1-C-d
0.0625 M

2.2-Z-d

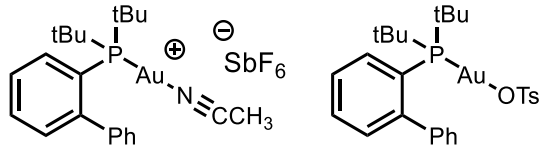

C1 **C2**

Separate vials containing 8mg benzamide (0.05mmol) and 1.54mg of catalyst **C1** (0.002mmol, 4mol%) OR 1.3mg of catalyst **C2** (0.002mmol, 4mol%) were brought to the NMR room. Catalyst was dissolved in 0.8mL of CH_2Cl_2, CD_2Cl_2, or CH_3OH depending on the experiment. This solution was then transferred to the vial containing the benzamide substrate. Solution containing substrate and catalyst was mixed by pipette, then transferred to the NMR spectrometer. ^1H NMR spectra were collected at regular intervals.

Cyclization of Benzamide 3.1 Under Basic Conditions for Identification of Intermediates

General Experimental Procedure for Cyclization in Basic Conditions

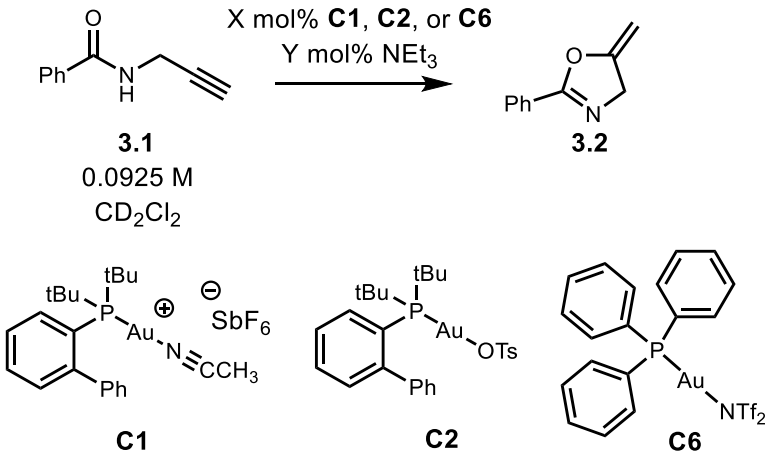

Triethylamine was added to dry catalyst **C1**, **C2**, or **C6**. The catalyst and triethylamine mixture were then dissolved in 0.8mL of CD_2Cl_2. The resulting CD_2Cl_2 solution of catalyst and triethylamine was then used to dissolve 11.72mg (0.074mmols) of benzamide, after which the reaction mixture was transferred to an NMR tube for analysis. Amounts of catalyst and triethylamine used were varied on a case-by-case basis to match the experimental schemes in the chapter above.

General Procedure for Kinetic Analysis of Carbamates 3.4 and 3.9

0.8mL of a 0.0625M solution of **3.4** or **3.9** (0.05mmols of carbamate) would be used to dissolve 0.002mmols (4 mol%) of solid catalyst. This mixture would then be transferred immediately to the NMR spectrometer, with ^{1}H and ^{31}P spectra being collected at regular intervals.

General Kinetics Experimental Procedure for Cyclization of 3.12

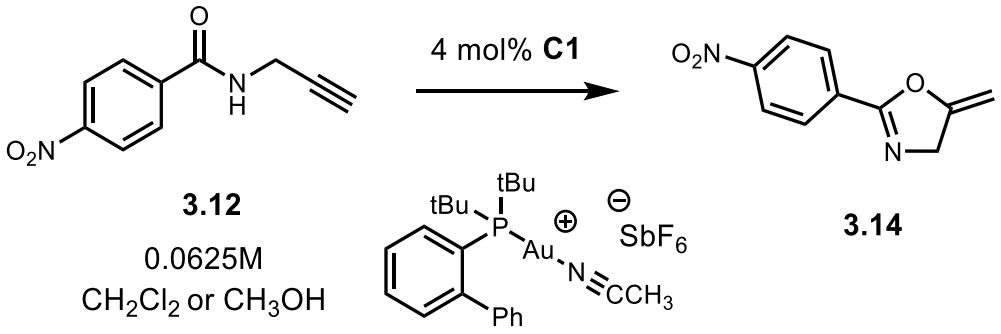

Separate vials containing 10.51mg (0.05mmol) of **3.12** and 1.54mg (0.002mmol) of **C1** were carried to the NMR room. They were dissolved together in CH_2Cl_2 and transferred to the NMR spectrometer. ^1H spectra were collected at regular intervals. **Note: 3.12** is poorly soluble in dichloromethane, so the reported concentration of 0.0625M is likely erroneous for the cyclization in dichloromethane. The observed rate should be treated as an approximation of the actual rate.

Synthetic Procedures

Experimental Procedure for Synthesis of **C6**.

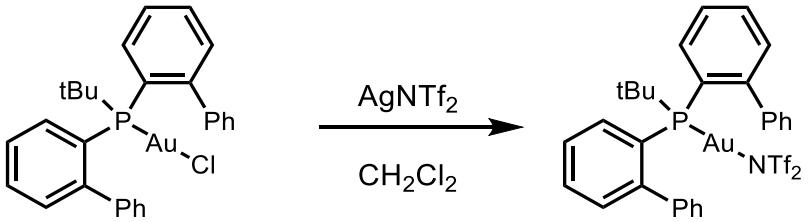

50mg (0.08mmol, 1 equiv) of precursor gold chloride was weighed into a scintillation vial and brought into a glovebox. 32.5mg (0.084mmol, 1.05 equiv) of

$AgNTf_2$ was then added to the to the vial containing the gold chloride. The vial containing the two compounds was sealed with a rubber septum and removed from the glovebox. 5mL of anhydrous dichloromethane were added to the vial under inert atmosphere. The mixture was then sonicated at room temperature for six minutes. Following sonication, the mixture became white and cloudy from precipation of silver chloride as a byproduct. The mixture was filtered through a column of celite into another scintillation vial. The resulting liquid was clear following filtration. The sample was then concentrated *in vacuo*, affording crude C6 as a white powder. To remove residual impurities, recrystallization was performed overnight in a freezer in a 1:2 mixture of dichloromethane:hexanes. Pure C6 was recovered as a white powder in 87% yield.

The precursor gold chloride was prepared according to published procedures.[111]

Experimental Procedure for Synthesis of N-Deuterated Benzamide **2.1-*N*-d**

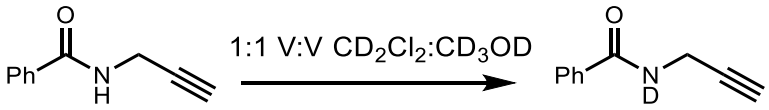

2.1 **2.1-N-d**

50mg (0.314mmol) of benzamide was dissolved in 1mL of a 1:1 volume:volume mixture of CD_2Cl_2:CD_3OD and stirred at room-temperature overnight. The mixture was concentrated *in vacuo*, affording N-deuterated benzamide in 95% yield. D incorporation was determined by ^1H NMR to be ~99%.

Experimental Procedure for Synthesis of Bis-Deuterated Benzamide **2.1-d2**

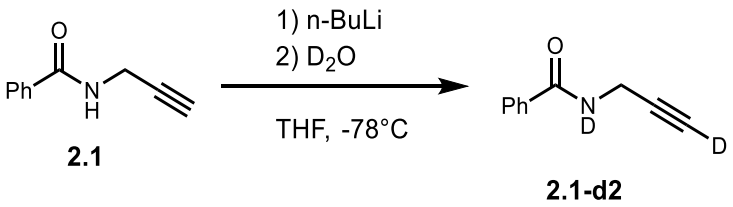

2.1 **2.1-d2**

50mg (0.314mmol) of benzamide was placed in a flame-dried round-bottom flask with a stir bar. The flask was vacuumed and refilled with N_2 three times. The solid was then dissolved in 1.5mL of anhydrous tetrahydrofuran and chilled to -78°C in a bath of dry ice and acetone. 0.35mL of a 2.5M n-butyllithium solution (0.875mmol, 2.8 equivalents) was added, at which point the mixture turned a deep, reddish purple. The mixture was allowed to stir at reduced temperature for approximately 30 minutes, at which point 3mL of D_2O was added to quench the reaction. Upon addition of D_2O, the mixture returned to a yellow, off-white color. The mixture was allowed to warm to room temperature, after which it was extracted with 3x5mL portions of anhydrous CH_2Cl_2. Organic layers were combined, dried with Na_2SO_4, and concentrated *in vacuo*. Bis-deuterated product was obtained in 50% yield. By ^1H NMR, deuterium incorporation at nitrogen was determined to be 93%, and incorporation at alkyne was determined to be 92%.

Experimental Procedure for Synthesis of C-Deuterated Benzamide **2.1-C-d**

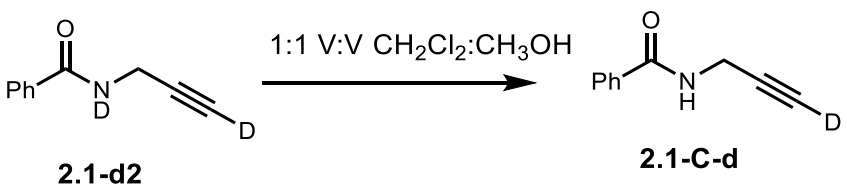

2.1-d2 **2.1-C-d**

50mg of bis-deuterated benzamide was placed in 2ml of a 1:1 volume:volume mixture of CH_2Cl_2 and CH_3OH and stirred at room temperature for four hours. Solvent was then removed *in vacuo*, affording the C-deuterated substrate in 98% yield, with no loss of alkyne deuterium label.

Synthesis of Carbamate **3.4**

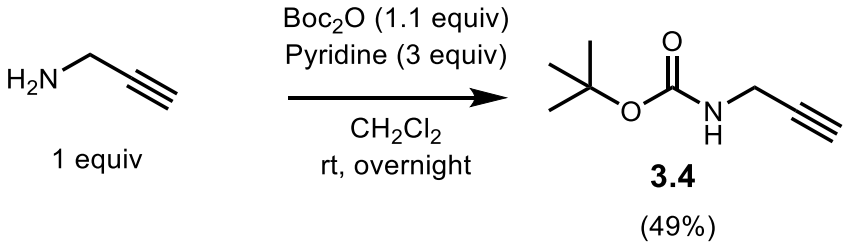

3.4

(49%)

110mg of propargyl amine (0.12mL, 2mmol, 1 equiv), 480mg of Boc_2O (0.5mL, 2.2mmol, 1.1 equiv), and 469mg of pyridine (0.48mL, 6mmol, 3 equiv) were dissolved in 6mL of anhydrous dichloromethane and left to stir overnight. The following day, the reaction was diluted with 6mL of H_2O and extracted with 3x10mL of diethyl ether. Organic layers were combined, brine washed, dried with Na_2SO_4, and concentrated *in vacuo*. The crude mixture was then purified on silica using 10% ethyl acetate and 90% hexanes as the mobile phase. $KMnO_4$ solution was used as a stain to visualize spots by TLC. Pure product was obtained in fractions 7-20 in 49% yield.

Synthesis of Carbamate **3.9**

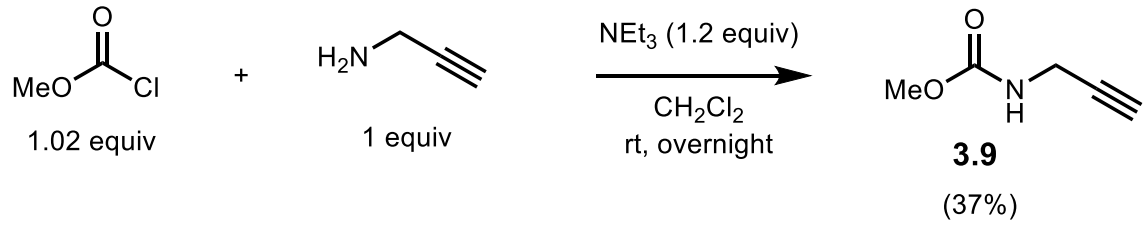

164mg of propargylamine (0.19mL, 3mmol, 1 equiv) and 363mg of triethylamine (0.5mL, 3.6mmol, 1.2 equiv) were dissolved together in anhydrous dichloromethane, then cooled to 0°C in an ice water bath. 289mg of methyl chloroformate (0.24mL, 3.02mmol, 1.02 equiv) was slowly added, after which the ice bath was removed. The mixture was left to stir overnight. No aqueous workup was performed. The crude mixture was concentrated *in vacuo* on a rotary evaporator. Purification was done on silica using dichloromethane as the mobile phase. $KMnO_4$ solution was used as a stain to visualize spots by TLC. Pure product was obtained in 37% yield.

Synthetic Procedure for Preparation of **3.12**

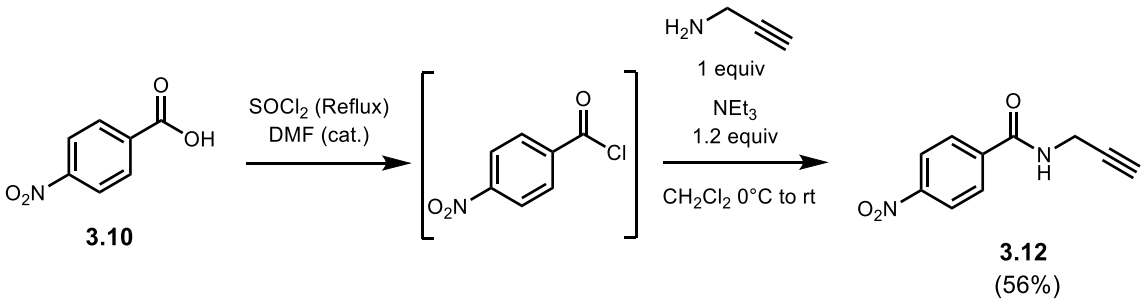

234mg (2mmol, 1.02 equiv) of para-nitrobenzoic acid **3.10** was placed in a dry 10mL round-bottom flask with a stir bar. 0.5mL (820mg, 6.67mmol, 3.3 equiv) was added to dissolve **3.10**. A few drops of anhydrous N,N-dimethylformamide

were added to the solution, which was then heated at reflux for five hours. After this time, 5mL of anhydrous dichloromethane was added, and the mixture was cooled to 0°C in an ice bath. Propargylamine (108mg, 0.13mL, 1.96mmol, 1 equiv) and triethylamine (239mg, 0.34mL, 2.4mmol, 1.2 equiv) were then slowly added to the solution. The solution immediately turned a dark brown and was warm to the touch, even in an ice bath. The mixture was left to stir overnight.

The following day, the reaction was diluted with 15mL of H_2O and extracted with 3x12mL of CH_2Cl_2. An insoluble black precipitate was removed by Buchner filtration. The organic layers were combined and washed with saturated ammonium chloride, dried over Na_2SO_4, and concentrated *in vacuo*. Purification was performed on silica using dichloromethane as the mobile phase. Elution under these conditions was extremely slow, and it is recommended in the future to use a methanol:dichloromethane mixture as the mobile phase instead. Pure **3.12** was recovered in fractions 40-96 in 56% overall yield.

Synthesis of 2'-bromo-N,N-dimethyl-[1,1'-biphenyl]-4-amine

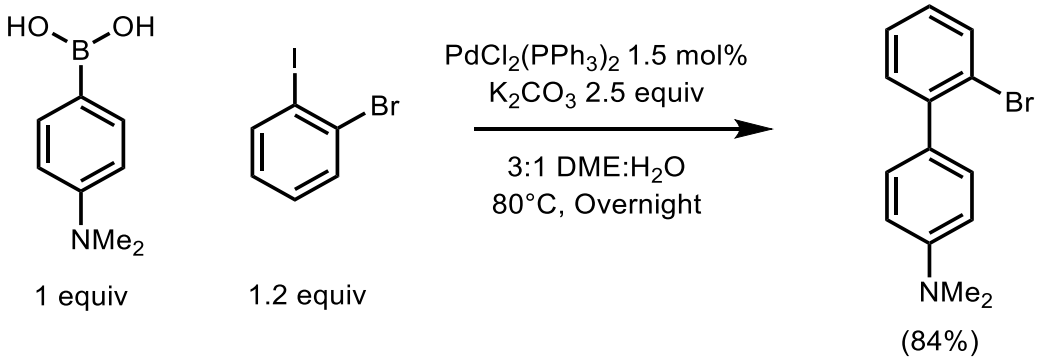

1.5g (9mmol, 1 equiv) of boronic acid, 3.1g (22.5mmol, 2.5 equiv) of potassium carbonate, and 95mg (0.135mmol, 1.5 mol%) of $PdCl_2(PPh_3)_2$ were

placed into a dry round-bottom flask with a stir bar. The solids were then dissolved in 36mL of a 3:1 mixture of 1,2-dimethoxyethane (DME) and water. 1.35mL (3.05g, 10.8mmol, 1.2equiv) of 1,2-Iodobromobenze was then added to the mixture. The solution was heated to 80°C in a silicon oil bath and left to stir overnight. The following day, the flask was connected to a rotary evaporator and the DME was removed. The remaining aqueous mixture was diluted with an additional 60mL of water and extracted with 3x40mL of diethyl ether. The organic layers were then combined, brine washed, dried over Na_2SO_4, and concentrated *in vacuo*. The crude material was purified on silica using 2% ethyl acetate and 98% hexanes as the mobile phase. The product was first recovered as an oil, which was placed in the freezer overnight. Following overnight storage in the freezer, the desired biphenyl was recovered as a solid in 84% pure yield.

Synthesis of 2-bromo-4'-methoxy-1,1'-biphenyl

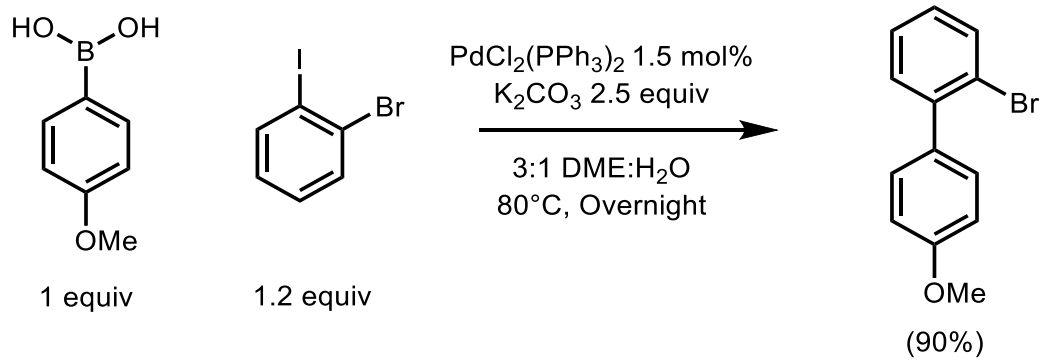

1.37g (9mmol, 1 equiv) of boronic acid, 3.1g (22.5mmol, 2.5 equiv) of potassium carbonate, and 95mg (0.135mmol, 1.5 mol%) of $PdCl_2(PPh_3)_2$ were placed into a dry round-bottom flask with a stir bar. The solids were then dissolved in 36mL of a 3:1 mixture of 1,2-dimethoxyethane (DME) and water. 1.35mL (3.05g, 10.8mmol, 1.2equiv) of 1,2-Iodobromobenze was then added to the mixture. The solution was heated to 80°C in a silicon oil bath and left to stir overnight. The following day, the flask was connected to a rotary evaporator and the DME was removed. The remaining aqueous mixture was diluted with an additional 60mL of water and extracted with 3x40mL of diethyl ether. The organic layers were then combined, brine washed, dried over Na_2SO_4, and concentrated *in vacuo*. The crude material was purified on silica at first using hexanes as the mobile phase. Fractions were analyzed by TLC until residual iodobromobenzene had been eluted. Following that, the mobile phase was changed to 2% ethyl acetate and 98% hexanes. The desired biphenyl was recovered as a solid in 90% yield.

Synthesis of Dimethylamino Ligand **4.1**

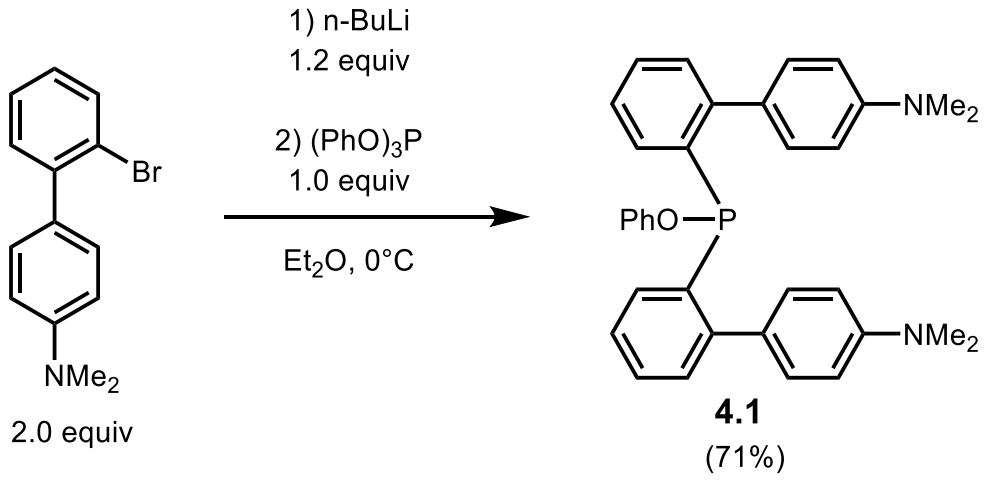

828mg (3mmol, 2 equiv) of 2'-bromo-N,N-dimethyl-[1,1'-biphenyl]-4-amine was placed into an oven-dried round-bottom-flask with a stir bar. The flask was vacuumed and refilled with inert gas three times. The biphenyl was then dissolved in 12mL of anhydrous diethyl ether with stirring and cooled to 0°C in an ice bath. 1.5mL (3.6mmol, 2.4 equiv) of a 2.5M solution of n-butyllithium in hexane was slowly added to the solution and left to stir for 15 minutes. After this time, a thick, off-white suspension had formed in the flask. 0.4mL (462mg, 1.5mmol, 1 equiv) of triphenylphosphite was added to the flask, after which the suspension rapidly fell back into solution. The mixture was then left to stir overnight.

The following day, the reaction mixture was diluted with 24mL of water. The organic ether layer was then separated into a separate flask. The remaining aqueous layer was then extracted 3x12mL with dichloromethane. The ether and the collected dichloromethane fractions were then combined and brine washed. The organic layers were then dried over Na_2SO_4 and concentrated *in vacuo*. The resulting crude solid was recrystallized overnight in a freezer in a 1:2

volume:volume mixture of ethyl acetate and hexanes. **4.1** was recovered as a yellowish solid in 71% pure yield.

Synthesis of Dimethoxy Ligand **4.7**

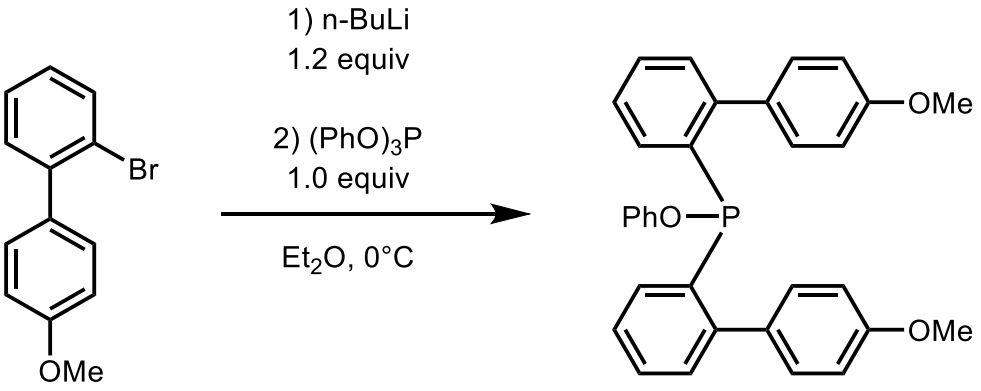

263 (1mmol, 2 equiv) of 2-bromo-4'-methoxy-1,1'-biphenyl was placed into an oven-dried round-bottom-flask with a stir bar. The flask was vacuumed and refilled with inert gas three times. The biphenyl was then dissolved in 6mL of anhydrous diethyl ether with stirring and cooled to 0°C in an ice bath. 0.5mL (1.2mmol, 1.2 equiv) of a 2.5M solution of n-butyllithium in hexane was slowly added to the solution and left to stir for 15 minutes. After this time, a thick, off-white suspension had formed in the flask. 0.13mL (154mg, 0.5mmol, 1 equiv) of triphenylphosphite was added to the flask, after which the suspension rapidly fell back into solution. The mixture was then left to stir overnight.

The following day, the reaction mixture was diluted with 12mL of water. The organic ether layer was then separated into a separate flask. The remaining aqueous layer was then extracted 3x6mL with dichloromethane. The ether and the collected

dichloromethane fractions were then combined and brine washed. The organic layers were then dried over Na_2SO_4 and concentrated *in vacuo*. The resulting crude solid was recrystallized overnight in a freezer in a 1:2 volume:volume mixture of ethyl acetate and hexanes. **4.7** was recovered as a white solid in 56% pure yield.

Synthesis of Gold Chloride **4.2**

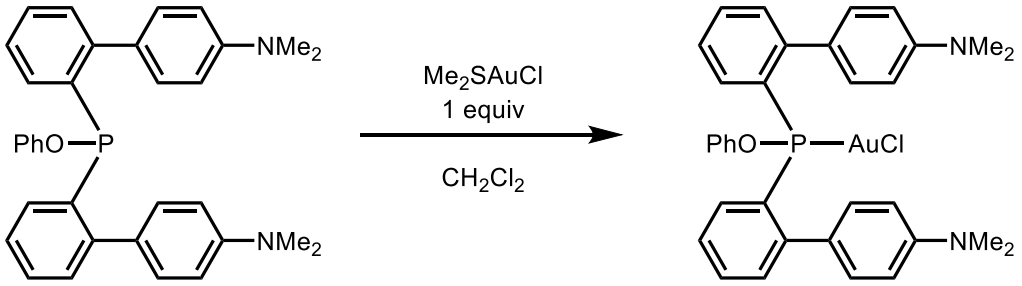

4.1

1.05 equiv

4.2

(93%)

50mg (0.097mmol, 1.05 equiv) of **4.1** was placed in a round-bottom flask with 27mg (0.092mmol, 1 equiv) of dimethylsulfide gold(I) chloride. The reagents were dissolved in 6mL of dichloromethane and swirled by hand for approximately one minute. The solvent was removed *in vacuo* and the resulting powder was recrystallized overnight in a freezer in a 1:2 volume:volume mixture of dichloromethane and hexanes. **4.2** was recovered as a white solid in 93% pure yield.

Synthesis of Gold Triflate **4.3**

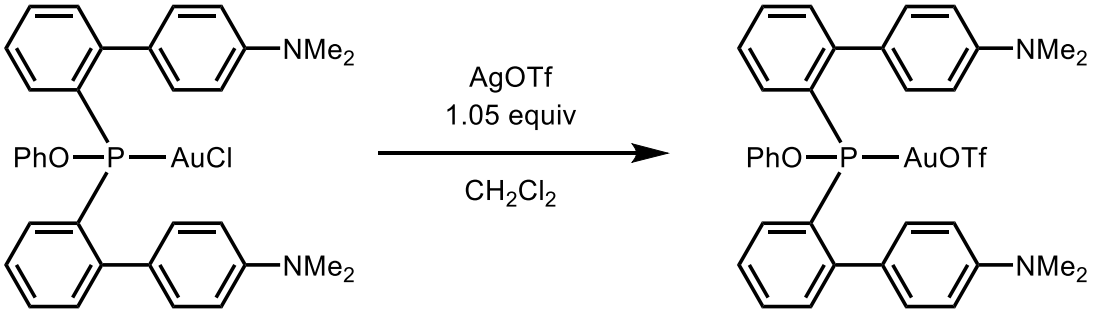

4.2
1 equiv

4.3
(92% Crude Yield)

47mg (0.06mmol, 1 equiv) of **4.2** was weighed into a scintillation vial and brought into a glovebox. 16.8mg (0.7mmol, 1.05 equiv) of silver triflate was added to the vial, which was then sealed with a septum. The sealed vial was removed from the glovebox and the solids were dissolved in 5mL of anhydrous dichloromethane and sonicated at room temperature for ten minutes. The resulting mixture was filtered through celite and concentrated *in vacuo*. The dimerization of the resulting compound make it difficult to assess the purity of **4.3** by NMR, and likewise difficult to assess the yield. The crude yield was 92%.

Synthesis of Gold Triflimide **4.4**

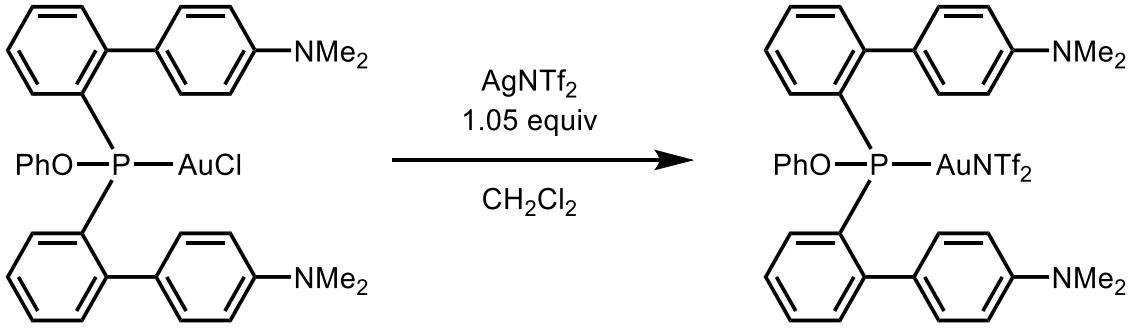

4.2
1 equiv

4.4
(82% Crude Yield)

50mg (0.067mmol, 1 equiv) of **4.2** was weighed into a scintillation vial and brought into a glovebox. 27.2mg (0.7mmol, 1.05 equiv) of silver triflate was added to the vial, which was then sealed with a septum. The sealed vial was removed from the glovebox and the solids were dissolved in 5mL of anhydrous dichloromethane and sonicated at room temperature for ten minutes. The resulting mixture was filtered through celite and concentrated *in vacuo*. The dimerization of the resulting compound make it difficult to assess the purity of **4.3** by NMR, and likewise difficult to assess the yield. The crude yield was 82%.

Catalyst Survey Rates in Dichloromethane (Table III)

Raw plots of **2.1** cyclization (0.0625 M) in 0.8 mL of CD_2Cl_2 with 0.002 mmol **C1** (4 mol%) and corresponding first order plots.

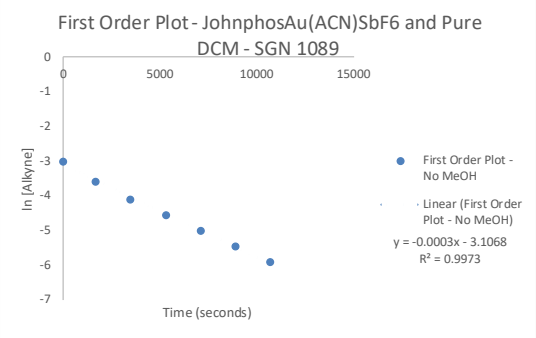

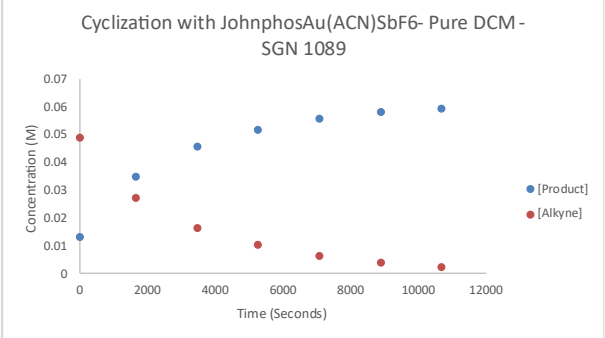

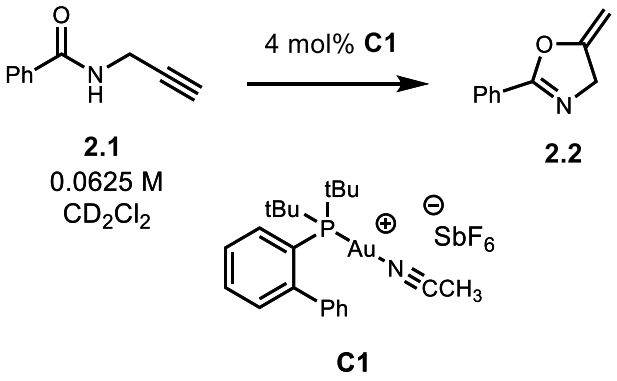

	CD_2Cl_2	Catalyst Amount	Catalyst Loading	k_{obs}/s^{-1}
SGN 1089	0.8 mL	0.002 mmol	4 mol%	$2.68 \times 10^{-4} \pm 6.25 \times 10^{-6}$

Raw plots of **2.1** cyclization (0.0625 M) in 0.8 mL of CD_2Cl_2 with 0.002 mmol **C2** (4 mol%) and corresponding first order plots.

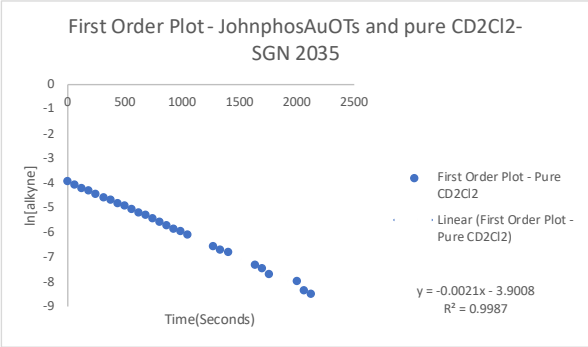

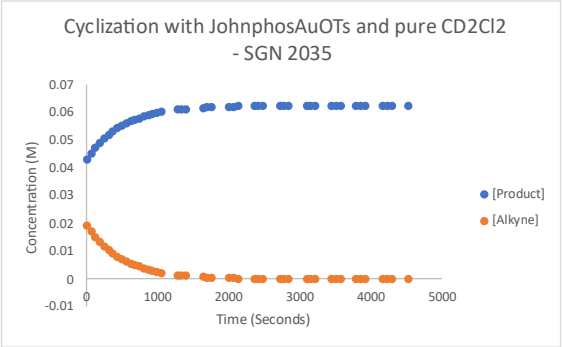

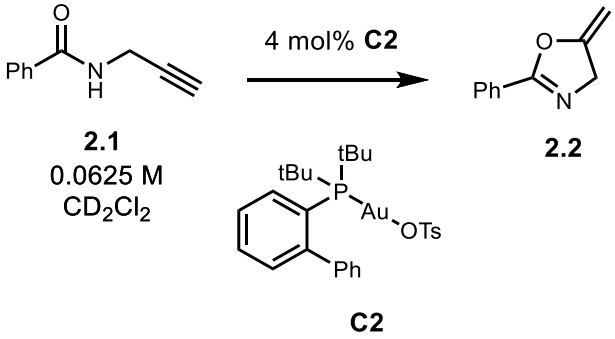

	CD_2Cl_2	Catalyst Amount	Catalyst Loading	k_{obs}/s^{-1}
SGN 2035	0.8 mL	0.002 mmol	4 mol%	$2.11 \times 10^{-3} \pm 1.55 \times 10^{-5}$

Raw plots of **2.1** cyclization (0.0625 M) in 0.8 mL of CD_2Cl_2 with 0.002 mmol **C3** (4 mol%) and corresponding first order plots.

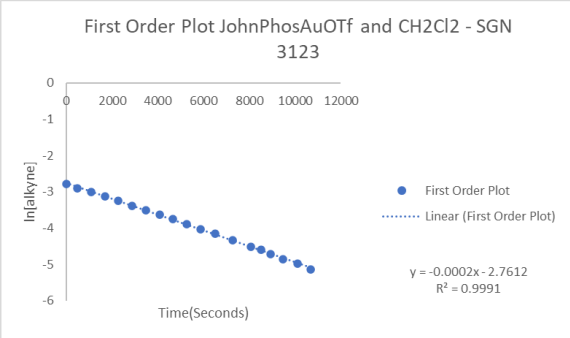

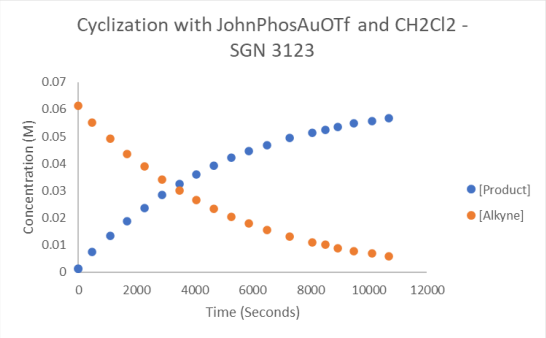

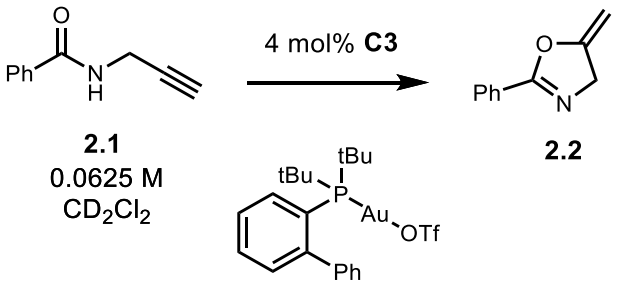

2.1
0.0625 M
CD_2Cl_2

2.2

C3

	CH_2Cl_2	**Catalyst Amount**	**Catalyst Loading**	**k_{obs}/s^{-1}**
SGN 3123	0.8 mL	0.002 mmol	4 mol%	$2.18 \times 10^{-4} \pm 1.56 \times 10^{-6}$

Raw plots of **2.1** cyclization (0.0625 M) in 0.8 mL of CD_2Cl_2 with 0.002 mmol **C4** (4 mol%) and corresponding first order plots.

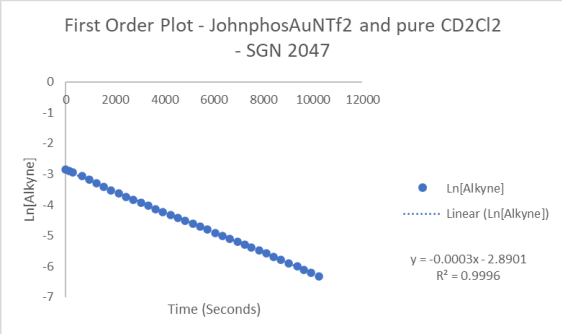

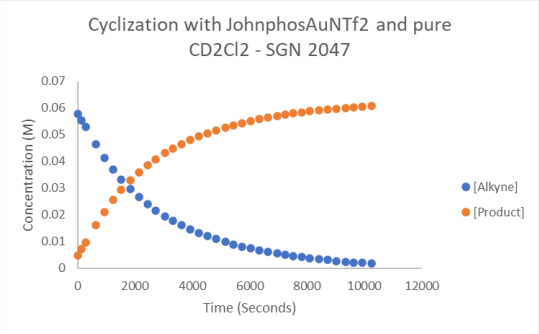

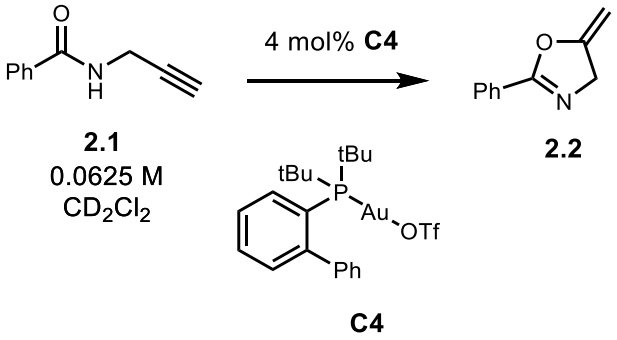

2.1
0.0625 M
CD_2Cl_2

2.2

C4

	CD_2Cl_2	**Catalyst Amount**	**Catalyst Loading**	**k_{obs}/s^{-1}**
SGN 2047	0.8 mL	0.002 mmol	4 mol%	$3.34 \times 10^{-4} \pm 1.14 \times 10^{-6}$

Raw plots of **2.1** cyclization (0.0625 M) in 0.8 mL of CD_2Cl_2 with 0.002 mmol **C5** (4 mol%) and corresponding first order plots.

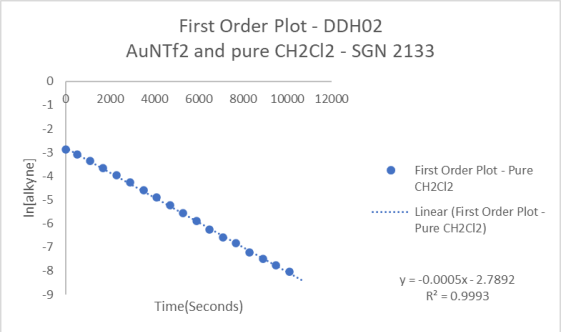

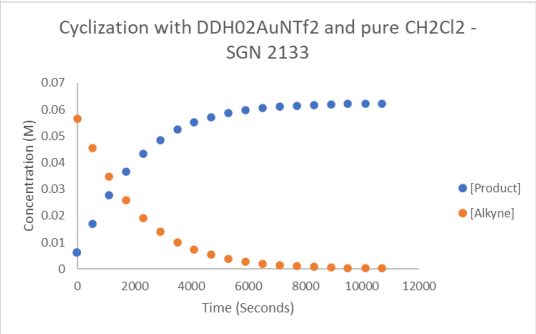

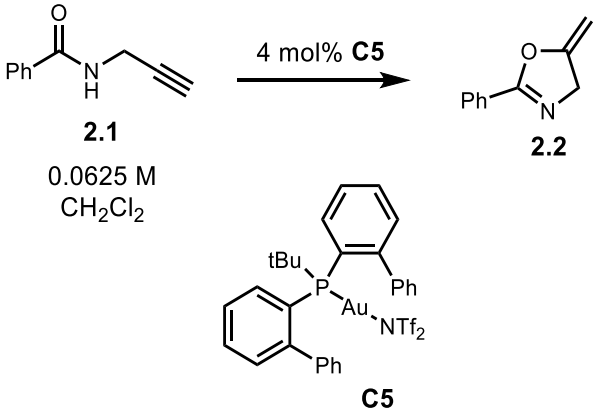

2.1

0.0625 M
CH_2Cl_2

2.2

C5

	CH_2Cl_2	**Catalyst Amount**	**Catalyst Loading**	**k_{obs}/s^{-1}**
SGN 2133	0.8 mL	0.002 mmol	4 mol%	$5.25 \times 10^{-4} \pm 3.47 \times 10^{-6}$

Raw plots of **2.1** cyclization (0.0625 M) in 0.8 mL of CD_2Cl_2 with 0.002 mmol **C6** (4 mol%) and corresponding first order plots.

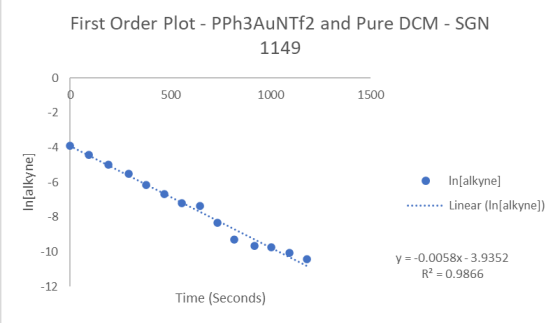

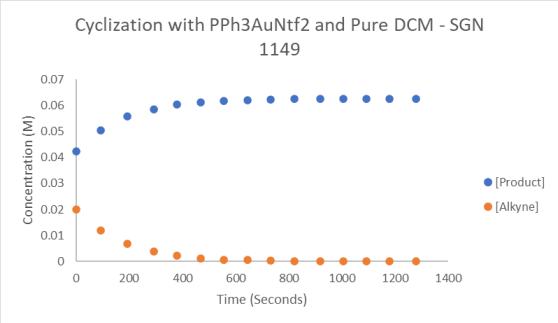

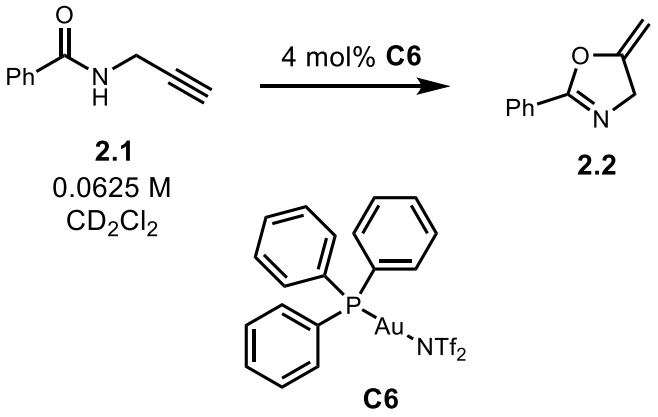

	CD_2Cl_2	Catalyst Amount	Catalyst Loading	k_{obs}/s^{-1}
SGN 1149	0.8 mL	0.002 mmol	4 mol%	$5.58 \times 10^{-3} \pm 1.96 \times 10^{-4}$

Raw plots of **2.1** cyclization (0.0625 M) in 0.8 mL of CD_2Cl_2 with 0.002 mmol **C7** (4 mol%) and corresponding first order plots.

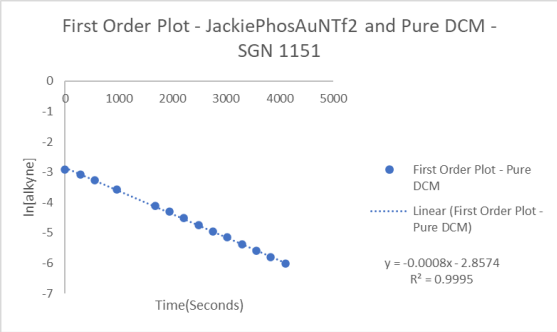

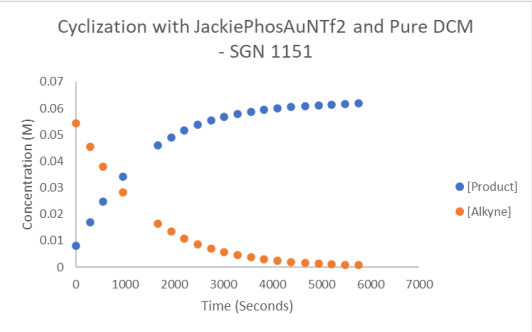

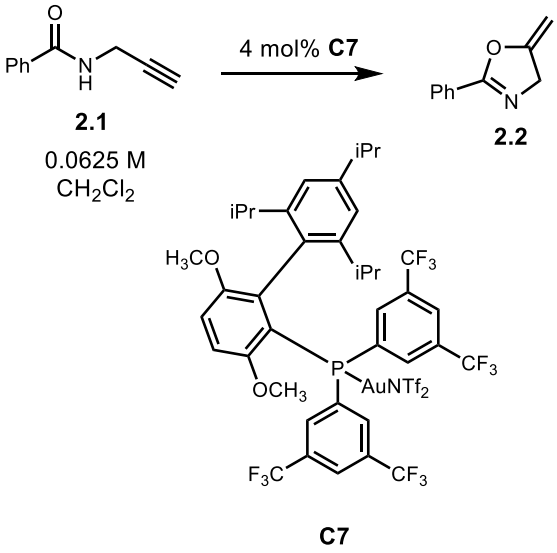

	CH_2Cl_2	Catalyst Amount	Catalyst Loading	$k_{obs/S}^{-1}$
SGN 1151	0.8 mL	0.002 mmol	4 mol%	$7.67 \times 10^{-4} \pm 5.14 \times 10^{-6}$

Raw plots of **2.1** cyclization (0.0625 M) in 0.8 mL of CD_2Cl_2 with 0.002 mmol **C8** (4 mol%) and corresponding first order plots.

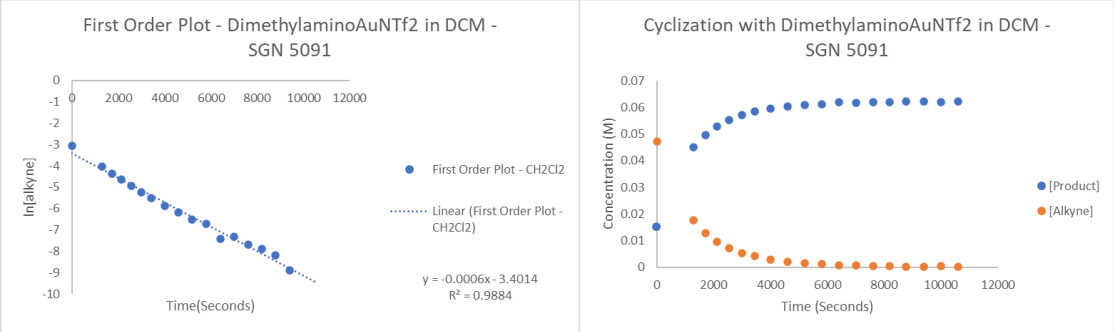

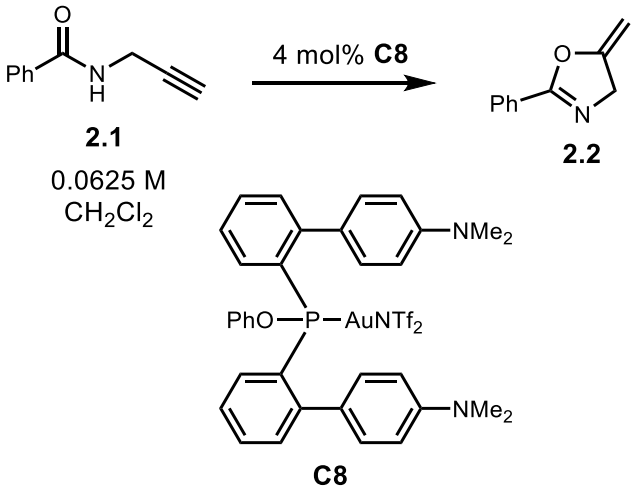

	CH_2Cl_2	Catalyst Amount	Catalyst Loading	$k_{obs/S}^{-1}$
SGN 5091	0.8 mL	0.002 mmol	4 mol%	$7.41 \times 10^{-4} \pm 1.14 \times 10^{-5}$

Catalyst Survey Rates in Methanol (Table V)

Raw plots of **2.1** cyclization (0.0625 M) in 0.8 mL of CH_3OH with 0.002 mmol **C1** (4 mol%) and corresponding first order plots.

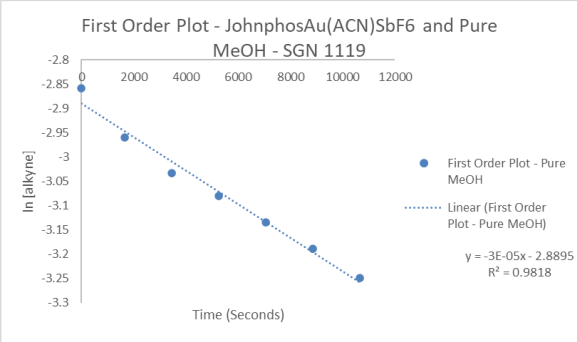

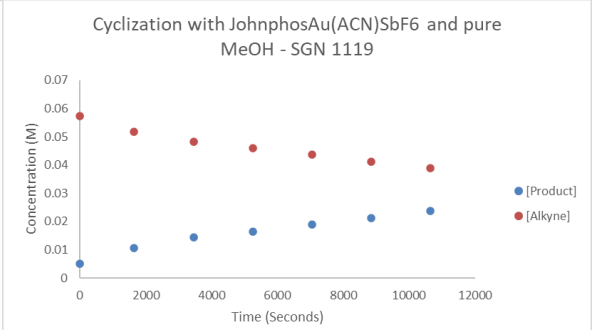

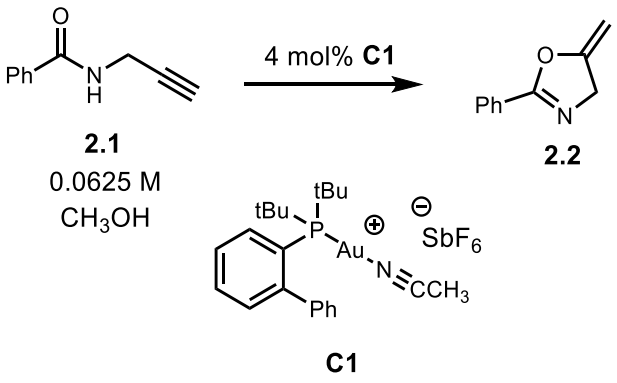

	CH_3OH	Catalyst Amount	Catalyst Loading	k_{obs}/s^{-1}
SGN 1119	0.8 mL	0.002 mmol	4 mol%	$3.45 \times 10^{-5} \pm 2.10 \times 10^{-6}$

Raw plots of **2.1** cyclization (0.0625 M) in 0.8 mL of CH_3OH with 0.002 mmol **C2** (4 mol%) and corresponding first order plots.

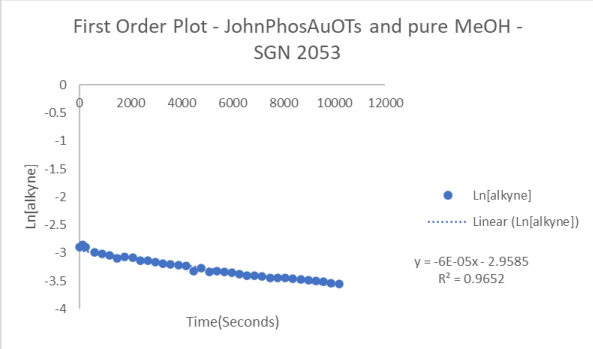

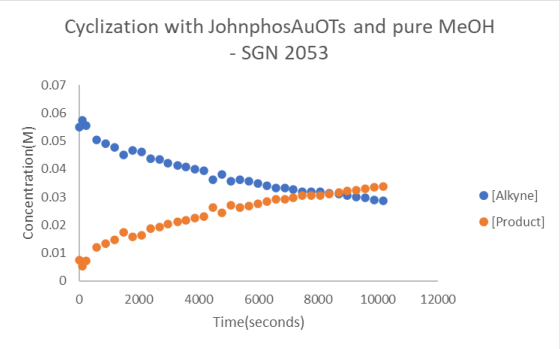

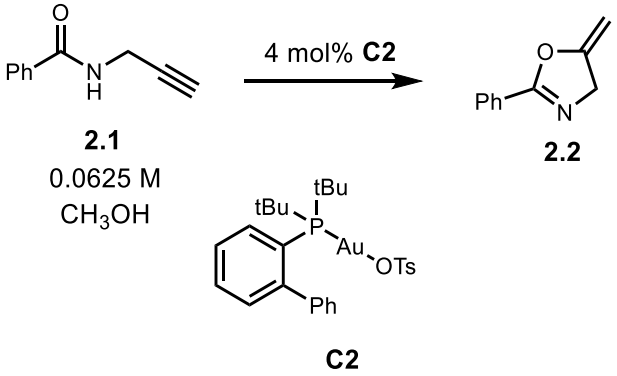

	CH_3OH	**Catalyst Amount**	**Catalyst Loading**	**k_{obs}/s^{-1}**
SGN 2053	0.8 mL	0.002 mmol	4 mol%	$6.26 \times 10^{-5} \pm 2.03 \times 10^{-6}$

Raw plots of **2.1** cyclization (0.0625 M) in 0.8 mL of CH_3OH with 0.002 mmol **C3** (4 mol%) and corresponding first order plots.

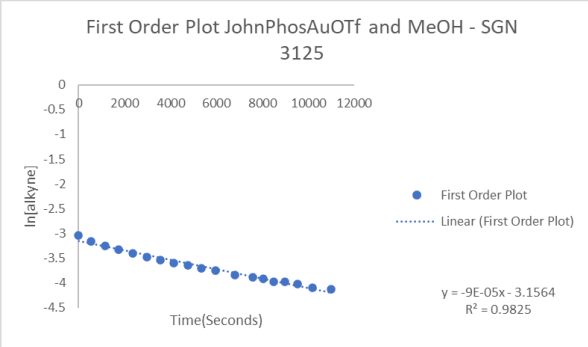

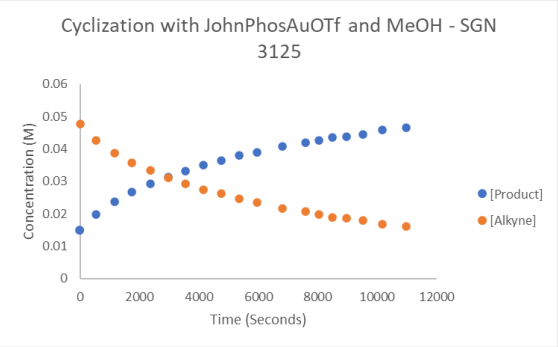

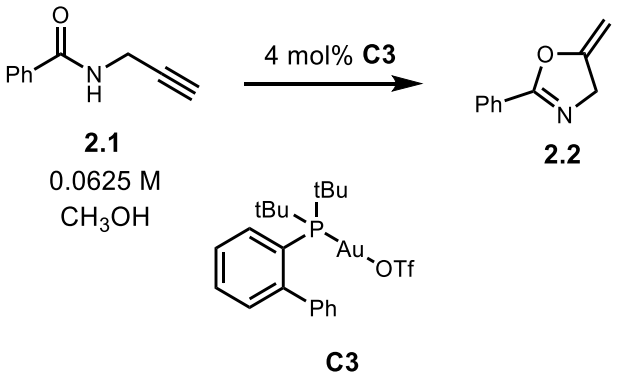

2.1
0.0625 M
CH_3OH

2.2

C3

	CH_3OH	**Catalyst Amount**	**Catalyst Loading**	**k_{obs}/s^{-1}**
SGN 3125	0.8 mL	0.002 mmol	4 mol%	$9.43 \times 10^{-5} \pm 3.05 \times 10^{-6}$

Raw plots of **2.1** cyclization (0.0625 M) in 0.8 mL of CH_3OH with 0.002 mmol **C4** (4 mol%) and corresponding first order plots.

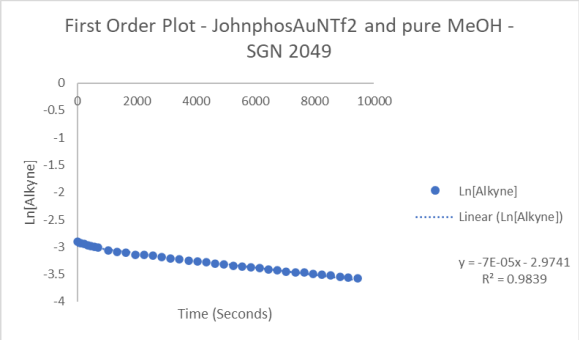

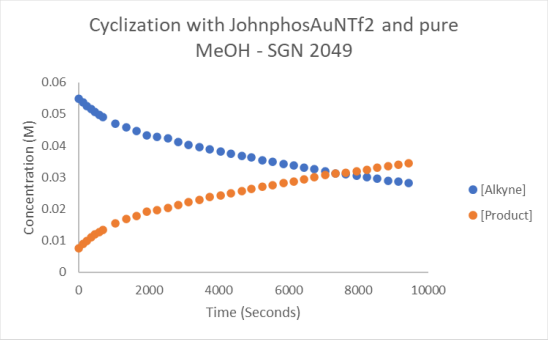

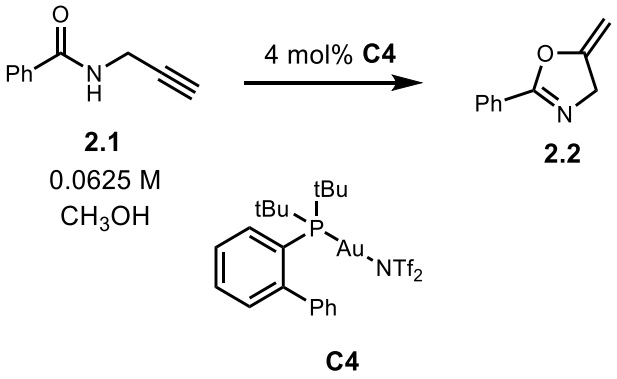

2.1
0.0625 M
CH_3OH

2.2

C4

	CH_3OH	**Catalyst Amount**	**Catalyst Loading**	**k_{obs}/s^{-1}**
SGN 2049	0.8 mL	0.002 mmol	4 mol%	$6.65 \times 10^{-5} \pm 1.46 \times 10^{-6}$

Raw plots of **2.1** cyclization (0.0625 M) in 0.8 mL of CH_3OH with 0.002 mmol **C5** (4 mol%) and corresponding first order plots.

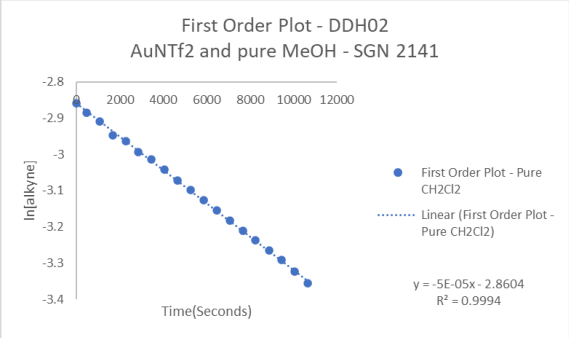

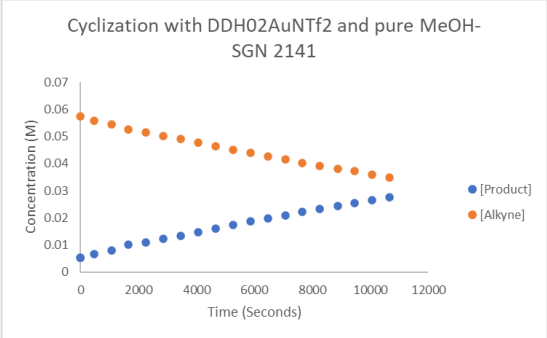

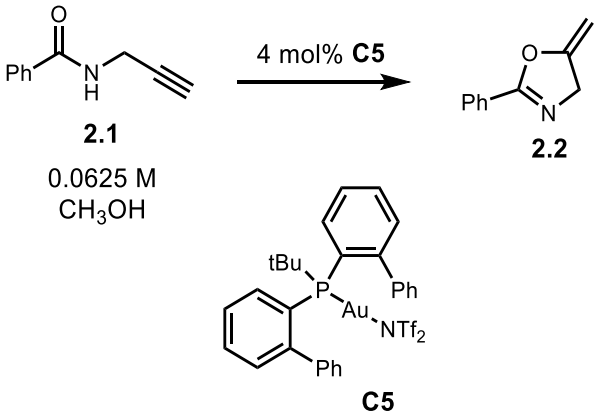

	CH_3OH	**Catalyst Amount**	**Catalyst Loading**	**k_{obs}/s^{-1}**
SGN 2141	0.8 mL	0.002 mmol	4 mol%	$4.58 \times 10^{-4} \pm 2.77 \times 10^{-7}$

Raw plots of **2.1** cyclization (0.0625 M) in 0.8 mL of CH_3OH with 0.002 mmol **C6** (4 mol%) and corresponding first order plots.

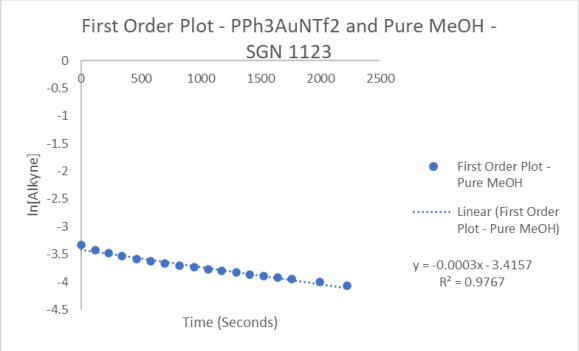

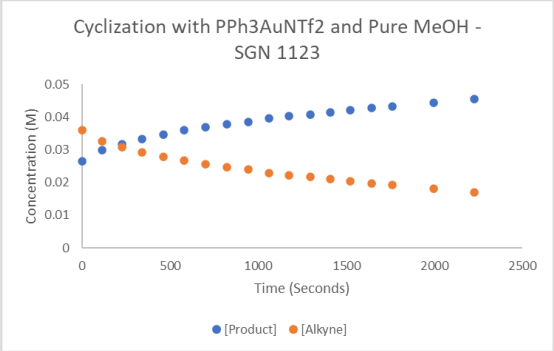

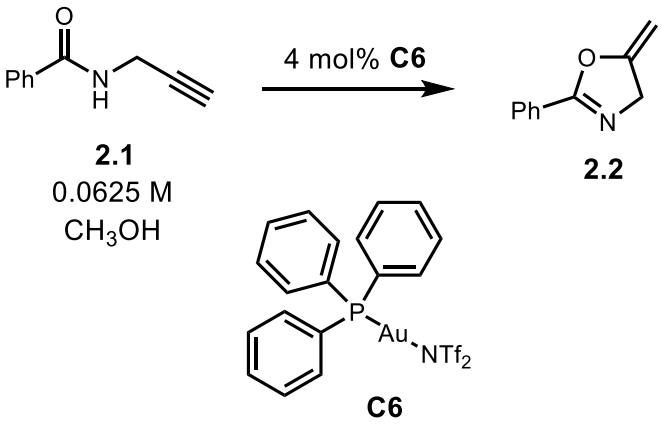

	CH_3OH	**Catalyst Amount**	**Catalyst Loading**	**k_{obs}/s^{-1}**
SGN 1123	0.8 mL	0.002 mmol	4 mol%	$3.11 \times 10^{-4} \pm 1.20 \times 10^{-5}$

Raw plots of **2.1** cyclization (0.0625 M) in 0.8 mL of CH_3OH with 0.002 mmol **C7** (4 mol%) and corresponding first order plots.

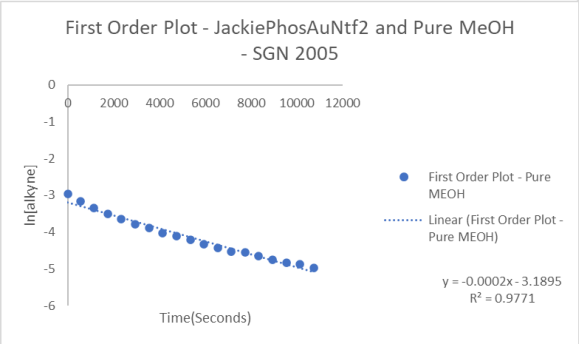

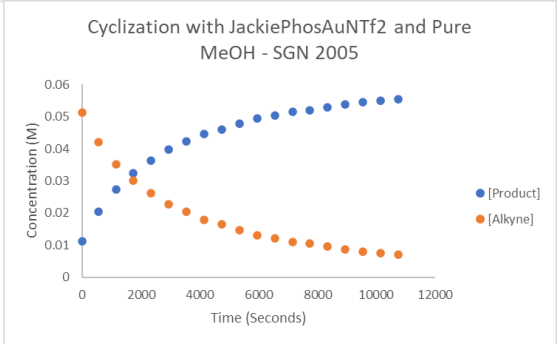

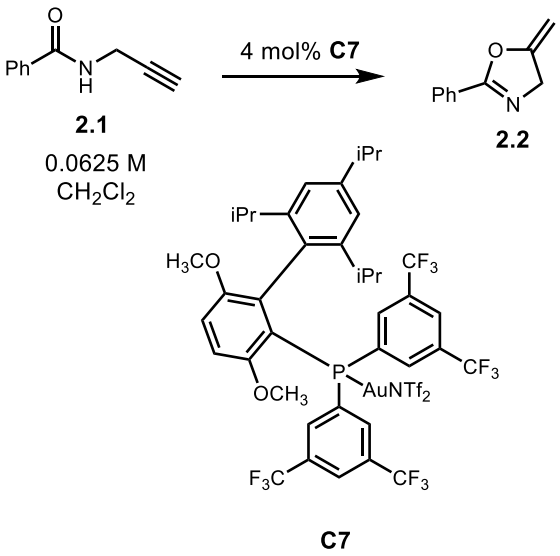

	CH_3OH	**Catalyst Amount**	**Catalyst Loading**	**$k_{obs/S}^{-1}$**
SGN 2005	0.8 mL	0.002 mmol	4 mol%	$1.78 \times 10^{-4} \pm 6.57 \times 10^{-6}$

Raw plots of **2.1** cyclization (0.0625 M) in 0.8 mL of CH_3OH with 0.002 mmol **C8** (4 mol%) and corresponding first order plots.

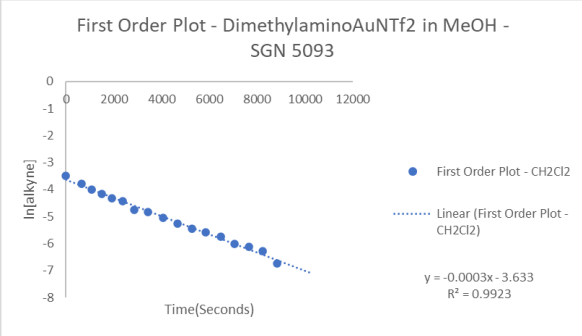

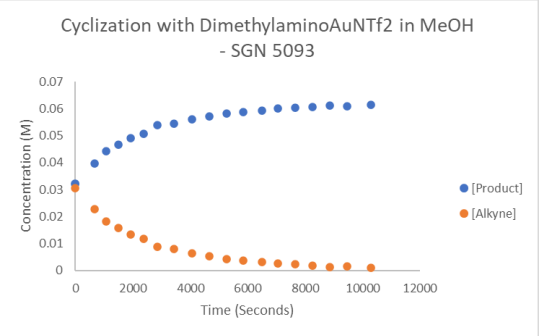

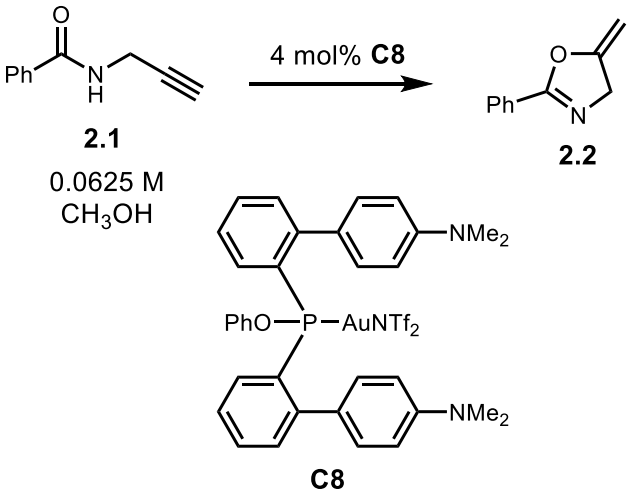

	CH_2Cl_2	Catalyst Amount	Catalyst Loading	k_{obs}/s^{-1}
SGN 5093	0.8 mL	0.002 mmol	4 mol%	$4.36 \times 10^{-4} \pm 1.81 \times 10^{-5}$

Rate of Cyclization in Dichloromethane with CH_3OH Titrations

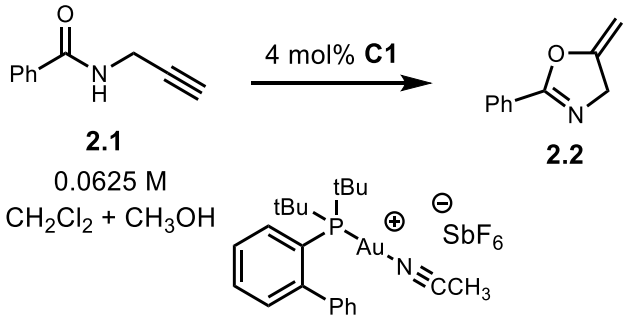

2.1

0.0625 M

CH_2Cl_2 + CH_3OH

2.2

C1

Comparison plots of CH_3OH Titration into CH_2Cl_2

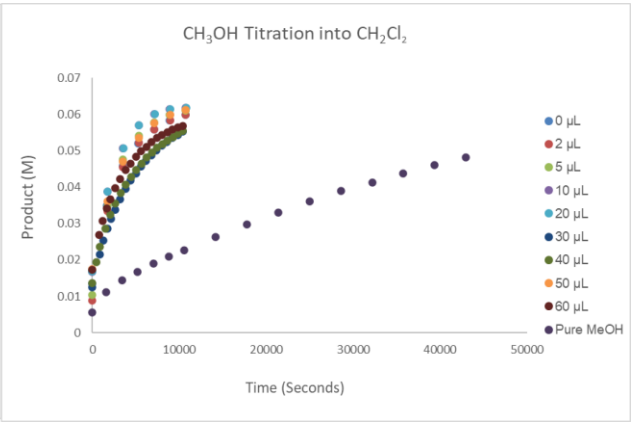

	CH_3OH Volume (µL)	Catalyst Amount	Catalyst Loading	$k_{obs/S}^{-1}$
SGN 1089	0	0.002 mmol	4 mol%	$2.68 \times 10^{-4} \pm 6.25 \times 10^{-6}$
SGN 1103	2	0.002 mmol	4 mol%	$2.76 \times 10^{-4} \pm 7.55 \times 10^{-6}$
SGN 1107	5	0.002 mmol	4 mol%	$3.23 \times 10^{-4} \pm 3.49 \times 10^{-6}$
SGN 1111	10	0.002 mmol	4 mol%	$2.97 \times 10^{-4} \pm 3.14 \times 10^{-6}$
SGN 1101	20	0.002 mmol	4 mol%	$4.0 \times 10^{-4} \pm 7.03 \times 10^{-6}$
SGN 4139	30	0.002 mmol	4 mol%	$1.8 \times 10^{-4} \pm 1.68 \times 10^{-6}$

SGN 4143	40	0.002mmol	4 mol%	$1.79 \times 10^{-4} \pm 2.44 \times 10^{-6}$
SGN 1113	50	0.002 mmol	4 mol%	$3.25 \times 10^{-4} \pm 6.01 \times 10^{-6}$
SGN 4147	60	0.002 mmol	4 mol%	$1.96 \times 10^{-4} \pm 3.83 \times 10^{-6}$
SGN 1127	Pure MeOH	0.002mmol	4mol%	$2.96 \times 10^{-5} \pm 4.25 \times 10^{-6}$

Rate of Cyclization in Dichloromethane with Methanol-d titrations

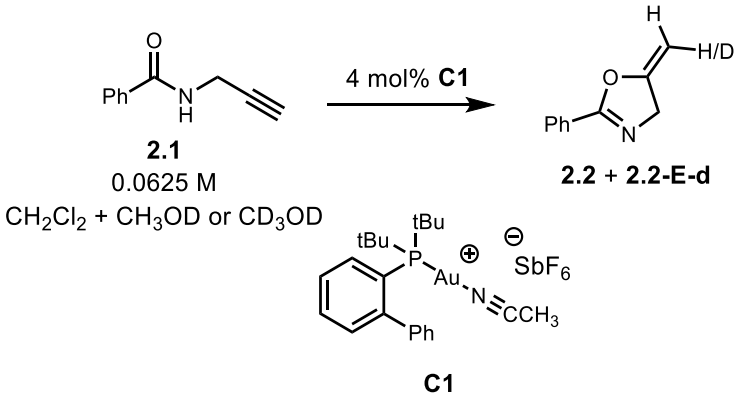

Comparison Plots for Methanol-d titration into CH2Cl2

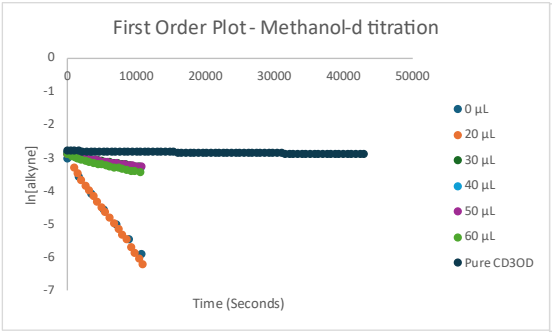

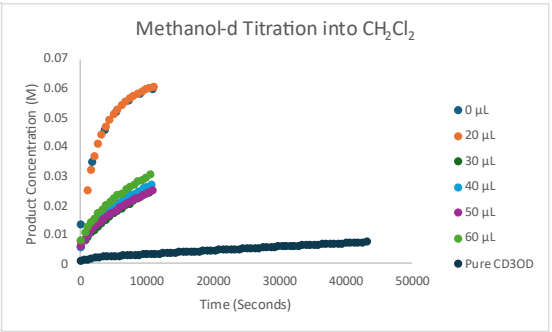

	Methanol-d volume (µL)	Catalyst Amount	Catalyst Loading	k_{obs}/S^{-1}
SGN 3029	20	0.002 mmol	4 mol%	$2.92 \times 10^{-4} \pm 3.10 \times 10^{-6}$
SGN 4141	30	0.002 mmol	4 mol%	$3.80 \times 10^{-5} \pm 9.32 \times 10^{-7}$

SGN 4145	40	0.002 mmol	4mol%	$4.29 \times 10^{-5} \pm 1.43 \times 10^{-6}$
SGN 3031	50	0.002 mmol	4 mol%	$3.62 \times 10^{-5} \pm 1.13 \times 10^{-6}$
SGN 4149	60	0.002 mmol	4 mol%	$4.87 \times 10^{-5} \pm 1.38 \times 10^{-6}$
SGN 3017	Pure CD_3OD	0.002mmol	4mol%	$2.32 \times 10^{-6} \pm 2.64 \times 10^{-8}$

Supporting Data for Kinetic Isotope Effects

Raw plots of 2.1 cyclization (0.0625 M) in 0.8 mL of CH3OH with 0.002 mmol C1 (4 mol%) and corresponding first order plots for determination of kinetic isotope effects.

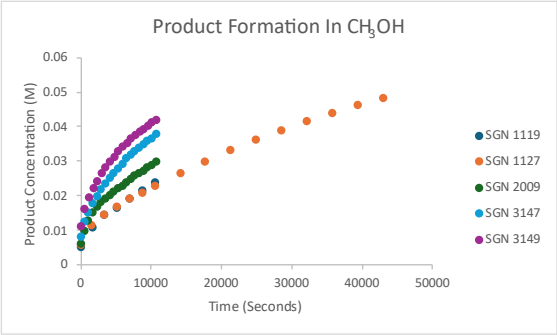

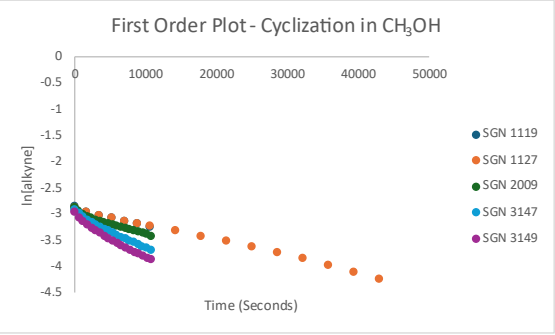

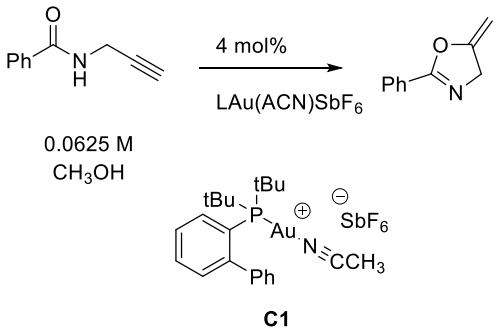

C1

	Solvent	Catalyst Amount	Catalyst Loading	k_{obs}/s^{-1}
SGN 1119	0.8 mL CH_3OH	0.002 mmol	4 mol%	$3.45 \times 10^{-5} \pm 2.1 \times 10^{-6}$

SGN 1127	0.8 mL CH_3OH	0.002 mmol	4 mol%	$2.96 \times 10^{-5} \pm 4.25 \times 10^{-7}$
SGN 2009	0.8 mL CH_3OH	0.002mmol	4 mol%	$4.5 \times 10^{-5} \pm 1.81 \times 10^{-6}$
SGN 3147	0.8 mL CH_3OH	0.002 mmol	4 mol%	$6.91 \times 10^{-5} \pm 1.64 \times 10^{-6}$
SGN 3149	0.8 mL CH_3OH	0.002 mmol	4 mol%	$8.01 \times 10^{-5} \pm 2.27 \times 10^{-6}$
Average Rate				$5.17 \times 10^{-5} \pm 1.65 \times 10^{-6}$

Raw plots of 2.1 cyclization (0.0625 M) in 0.8 mL of CH_3OH with 0.002 mmol C2 (4 mol%) and corresponding first order plots for determination of kinetic isotope effects.

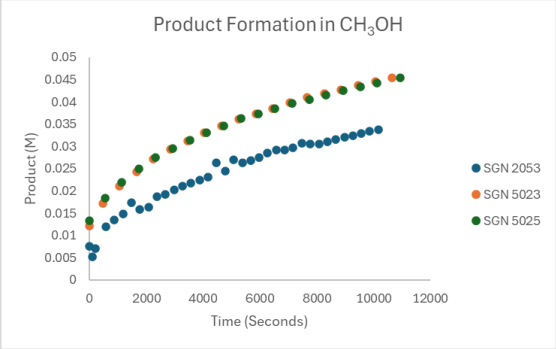

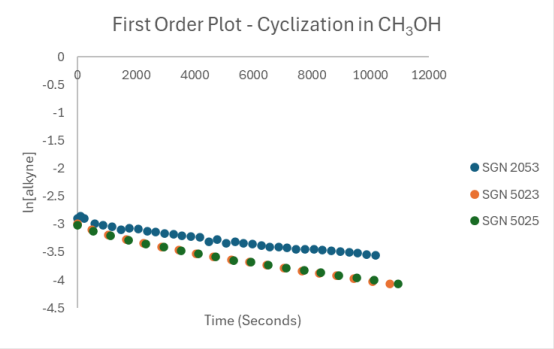

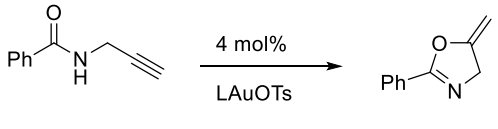

0.0625 M
CH_3OH

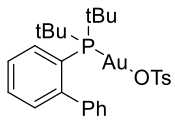

C2

	Solvent	**Catalyst Amount**	**Catalyst Loading**	$k_{obs/S}^{-1}$
SGN 2053	0.8 mL CH_3OH	0.002 mmol	4 mol%	$6.26 \times 10^{-5} \pm 2.03 \times 10^{-6}$
SGN 5023	0.8 mL CH_3OH	0.002 mmol	4 mol%	$9.55 \times 10^{-5} \pm 2.83 \times 10^{-6}$
SGN 5025	0.8 mL CH_3OH	0.002 mmol	4 mol%	$9.12 \times 10^{-5} \pm 2.63 \times 10^{-6}$
Average Rate				$8.31 \times 10^{-5} \pm 2.50 \times 10^{-6}$

Raw plots of **2.1-C-d** benzamide decay (0.0625 M) in 0.8 mL of DCM with 0.002 mmol **C1** (4 mol%) and corresponding first order plots.

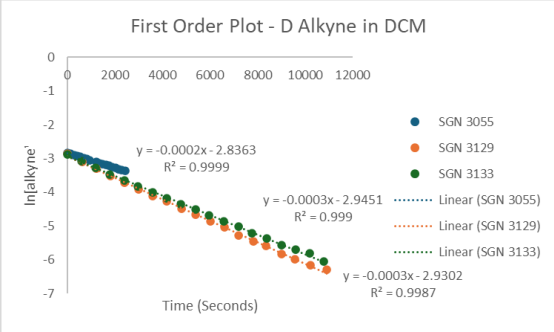

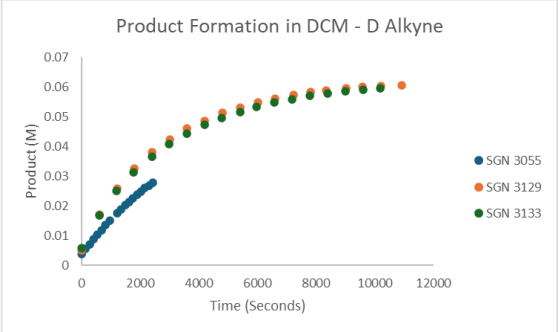

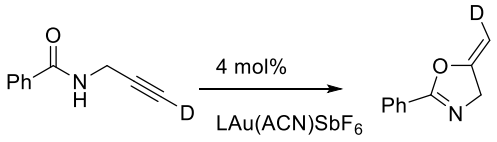

0.0625 M
CH_2Cl_2 or CD_2Cl_2

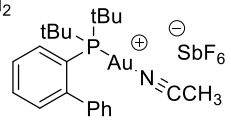

C1

	Solvent	Catalyst Amount	Catalyst Loading	$k_{obs/S}^{-1}$
SGN 3055	0.8 mL CD-$_2Cl_2$	0.002 mmol	4 mol%	2.19 x 10^{-4}±6.4. x 10^{-7}
SGN 3129	0.8mL CH_2Cl2	0.002 mmol	4 mol%	3.18 x 10^{-4}±2.80 x 10^{-6}
SGN 3133	0.8mL CH_2Cl_2	0.002mmol	4 mol%	2.88 x 10^{-4}±2.20 x 10^{-6}
Average Rate – D Alkyne				2.75 x 10^{-4}±5.64 x 10^{-6}
Average Rate – H Alkyne				3.0 x 10^{-4}±4.35 x 10^{-6}

Raw plots of **2.1-C-d** benzamide decay (0.0625 M) in 0.8 mL of DCM with 0.002 mmol **C2** (4 mol%) and corresponding first order plots.

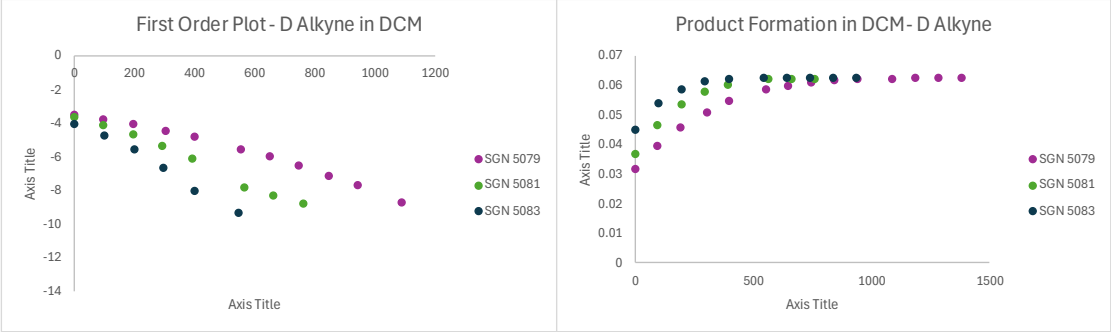

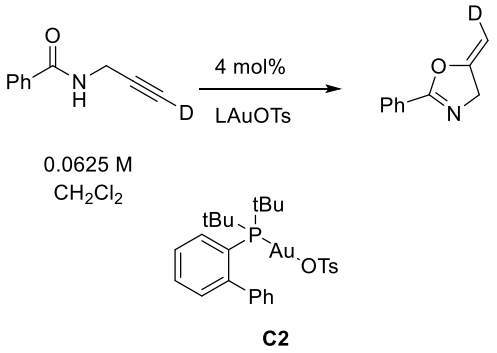

	Solvent	Catalyst Amount	Catalyst Loading	k_{obs}/s^{-1}
SGN 5079	0.8 mL CH_2Cl_2	0.002 mmol	4 mol%	$4.76 \times 10^{-3} \pm 2.15 \times 10^{-4}$
SGN 5081	0.8mL CH_2Cl2	0.002 mmol	4 mol%	$7.20 \times 10^{-3} \pm 2.68 \times 10^{-4}$
SGN 5083	0.8mL CH_2Cl_2	0.002mmol	4 mol%	$1.01 \times 10^{-2} \pm 4.56 \times 10^{-4}$
Average Rate – D Alkyne				$7.35 \times 10^{-3} \pm 3.13 \times 10^{-4}$
Average Rate – H Alkyne				$6.89 \times 10^{-3} \pm 2.69 \times 10^{-4}$

Raw plots for determination of N-deuterated primary kinetic isotope effect with catalyst **C1** in benzamide cyclization by way of methanol-d titration into dichloromethane.

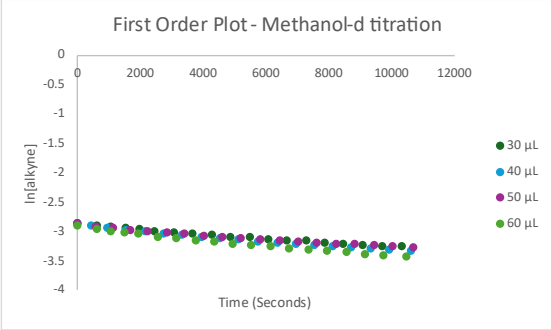

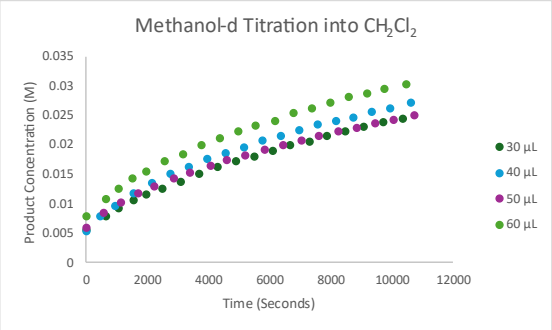

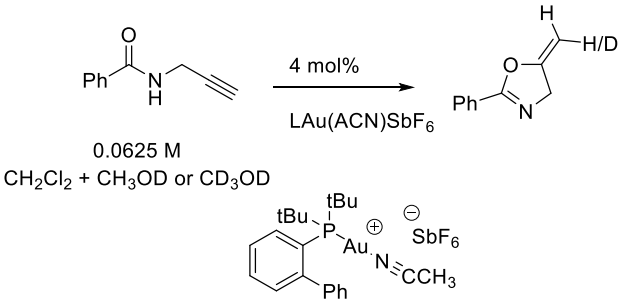

C1

	Methanol-d volume (µL)	**Catalyst Amount**	**Catalyst Loading**	$k_{obs/S}^{-1}$
SGN 4141	30	0.002 mmol	4 mol%	$3.80 \times 10^{-5} \pm 9.32 \times 10^{-7}$
SGN 4145	40	0.002 mmol	4mol%	$4.29 \times 10^{-5} \pm 1.43 \times 10^{-6}$
SGN 3031	50	0.002 mmol	4 mol%	$3.62 \times 10^{-5} \pm 1.13 \times 10^{-6}$
SGN 4149	60	0.002 mmol	4 mol%	$4.87 \times 10^{-5} \pm 1.38 \times 10^{-6}$
Average Rate – MeOD Titration				$4.13 \times 10^{-5} \pm 1.22 \times 10^{-6}$
Average Rate – Pure DCM				$3.0 \times 10^{-4} \pm 4.35 \times 10^{-6}$
Primary kH/kD = 7.26				

Raw plots for determination of N-deuterated primary kinetic isotope effect with catalyst **C2** in benzamide cyclization by way of methanol-d titration into dichloromethane.

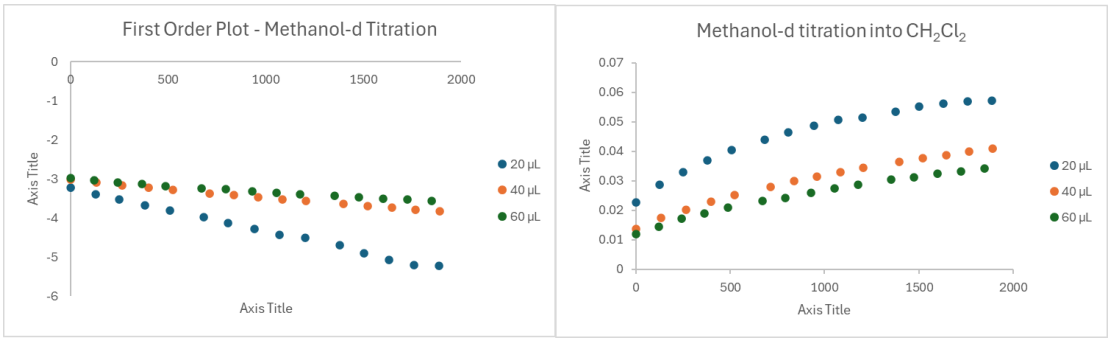

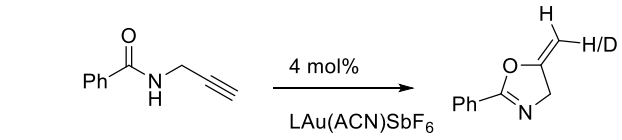

0.0625 M
CH_2Cl_2 + CH_3OD or CD_3OD

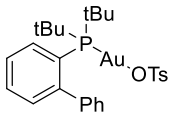

C2

	Methanol-d volume (µL)	**Catalyst Amount**	**Catalyst Loading**	$k_{obs/S}^{-1}$
SGN 5041	20	0.002 mmol	4mol%	$1.09 \times 10^{-3} \pm 1.53 \times 10^{-5}$
SGN 5043	40	0.002 mmol	4 mol%	$4.22 \times 10^{-4} \pm 6.81 \times 10^{-6}$
SGN 5045	60	0.002 mmol	4mol%	$3.07 \times 10^{-4} \pm 6.19 \times 10^{-6}$
Average Rate – MeOD Titration				$6.06 \times 10^{-4} \pm 9.43 \times 10^{-6}$
Average Rate – MeOH Titration				$2.54 \times 10^{-3} \pm 3.72 \times 10^{-4}$
Primary kH/kD = 4.19				

Raw plots for determination of inverse secondary kinetic isotope effect with **2.1-C-d** (0.0625M) in CH_3OH with 4 mol% **C1**.

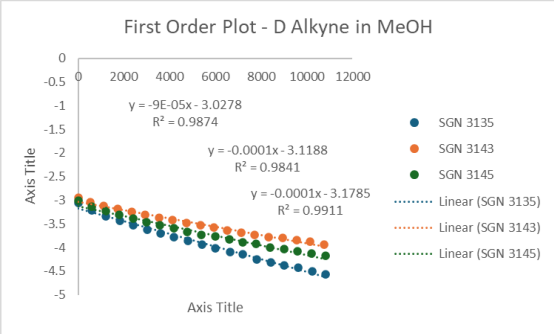

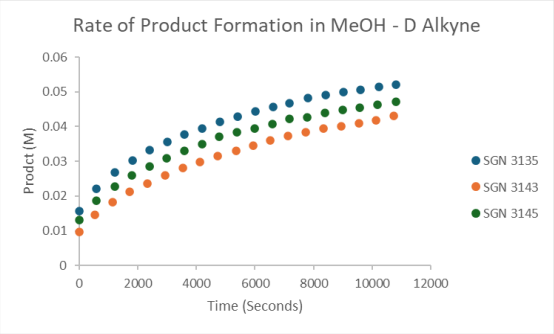

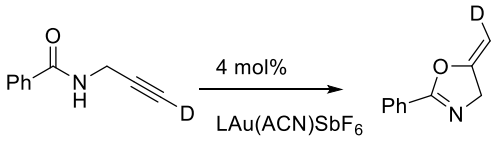

0.0625 M
CH_3OH

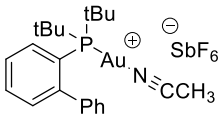

C1

	Solvent	**Catalyst Amount**	**Catalyst Loading**	k_{obs}/s^{-1}
SGN 3135	0.8 mL CH_3OH	0.002 mmol	4 mol%	$1.33 \times 10^{-4} \pm 3.06 \times 10^{-7}$
SGN 3143	0.8 mL CH_3OH	0.002 mmol	4 mol%	$8.82 \times 10^{-5} \pm 2.42 \times 10^{-6}$
SGN 3145	0.8 mL CH_3OH	0.002mmol	4 mol%	$1.03 \times 10^{-4} \pm 3.18 \times 10^{-6}$
Average Rate – D Alkyne				$1.08 \times 10^{-4} \pm 3.92 \times 10^{-6}$
Average Rate – H Alkyne				$5.17 \times 10^{-5} \pm 1.65 \times 10^{-6}$
Inverse Secondary kH/kD = 0.479				

Raw plots for determination of inverse secondary kinetic isotope effect with **2.1-C-d** (0.0625M) in CH_3OH with 4 mol% **C2**.

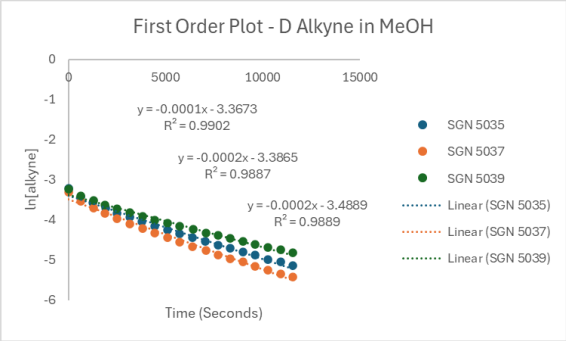

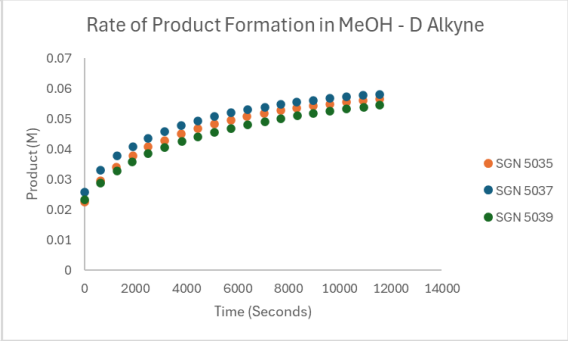

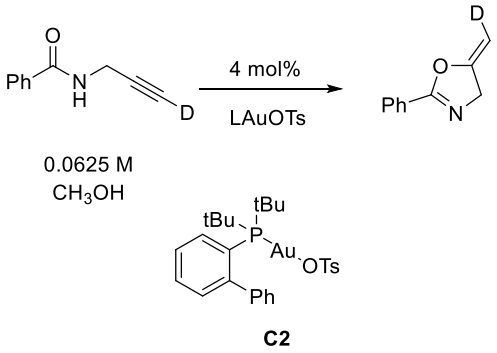

	Solvent	**Catalyst Amount**	**Catalyst Loading**	k_{obs}/s^{-1}
SGN 5035	0.8 mL CH_3OH	0.002 mmol	4 mol%	$1.58 \times 10^{-4} \pm 4.1 \times 10^{-6}$
SGN 5037	0.8 mL CH_3OH	0.002 mmol	4 mol%	$1.75 \times 10^{-4} \pm 4.48 \times 10^{-6}$
SGN 5039	0.8 mL CH_3OH	0.002mmol	4 mol%	$1.30 \times 10^{-4} \pm 3.14 \times 10^{-6}$
Average Rate – D Alkyne				$1.54 \times 10^{-4} \pm 3.91 \times 10^{-6}$
Average Rate – H Alkyne				$8.31 \times 10^{-5} \pm 2.50 \times 10^{-6}$
Inverse Secondary kH/kD = 0.54				

Supporting Data for Base-Treated Kinetics

Raw plots of **3.1** cyclization (0.0625 M) in 0.8 mL of CD_2Cl_2 with 0.004 mmol **C1** (8 mol%) and 13 mol% Triethylamine with corresponding first order plot.

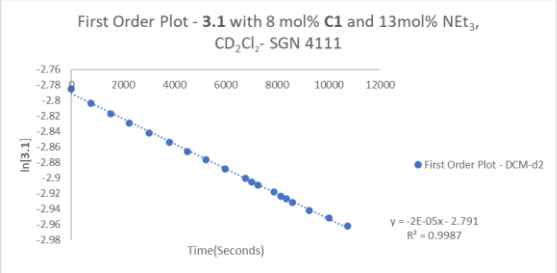

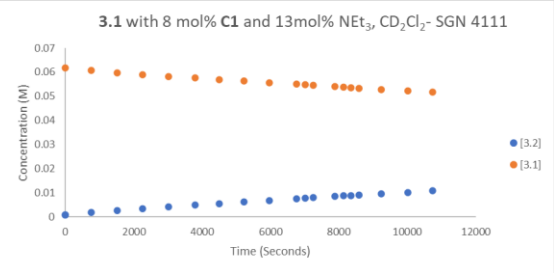

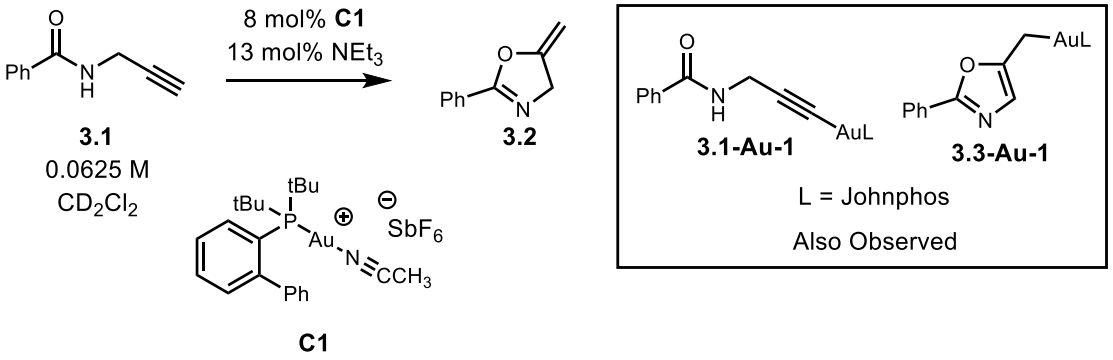

	CD_2Cl_2	Catalyst Amount	Catalyst Loading	$k_{obs/S}^{-1}$
SGN 4111	0.8 mL	0.004 mmol	8 mol%	$1.62 \times 10^{-5} \pm 1.41 \times 10^{-7}$

Raw plots of **3.1** cyclization (0.0625 M) in 0.8 mL of CD_2Cl_2 with 0.004 mmol **C1** (8 mol%) and 7.2 mol% Triethylamine with corresponding first order plot.

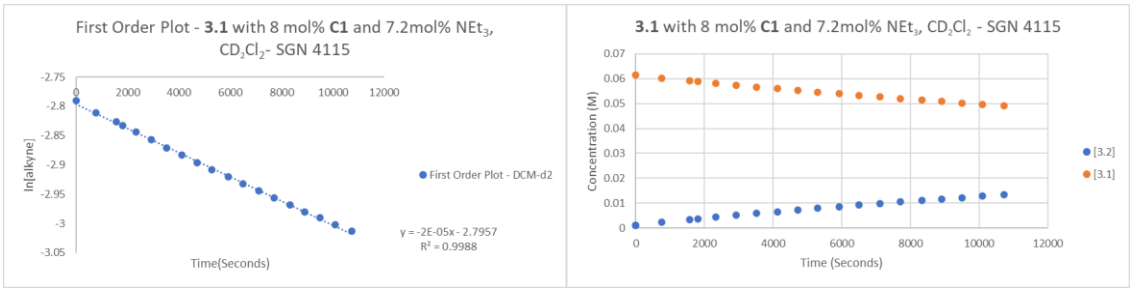

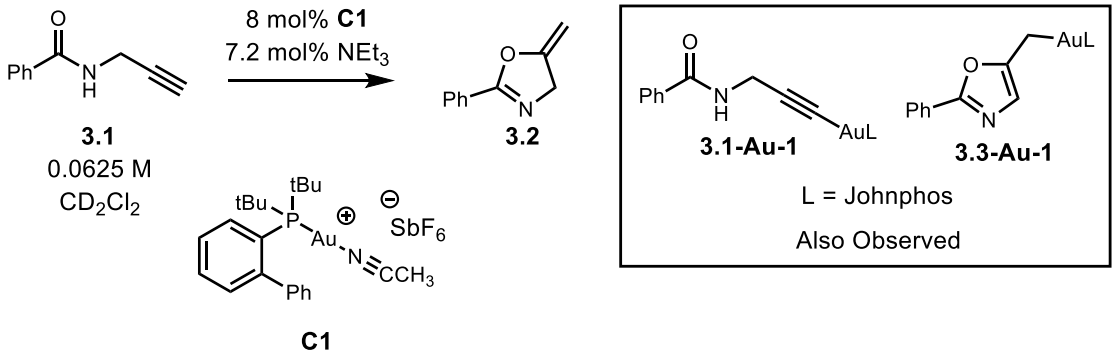

	CD_2Cl_2	Catalyst Amount	Catalyst Loading	k_{obs}/s^{-1}
SGN 4115	0.8 mL	0.004 mmol	8 mol%	$2.07 \times 10^{-5} \pm 1.77 \times 10^{-7}$

Raw plots of **3.1** cyclization (0.0625 M) in 0.8 mL of CD_2Cl_2 with 0.004 mmol **C6** (8 mol%) and 13 mol% Triethylamine with corresponding first order plot.

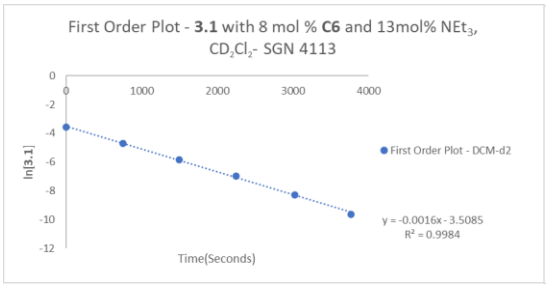

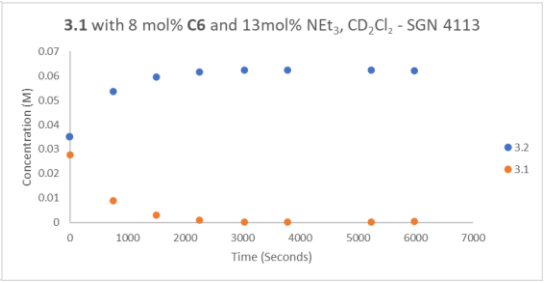

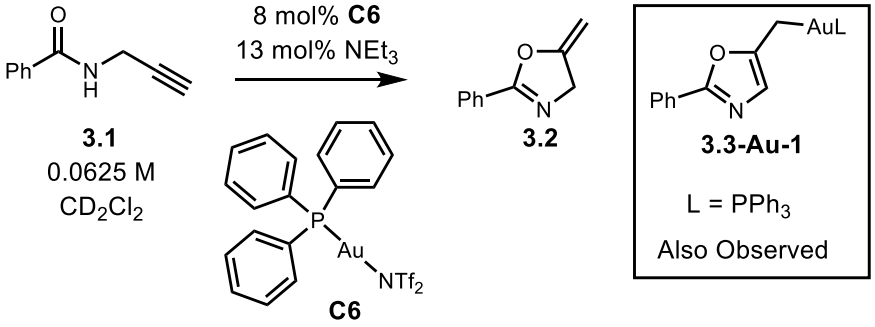

	CD_2Cl_2	Catalyst Amount	Catalyst Loading	$k_{obs/S}^{-1}$
SGN 4113	0.8 mL	0.004 mmol	8 mol%	$1.6 \times 10^{-3} \pm 3.22 \times 10^{-5}$

Raw plots of **3.1** cyclization (0.0625 M) in 0.8 mL of CD_2Cl_2 with 0.004 mmol **C6** (8 mol%) and 7.2 mol% Triethylamine with corresponding first order plot.

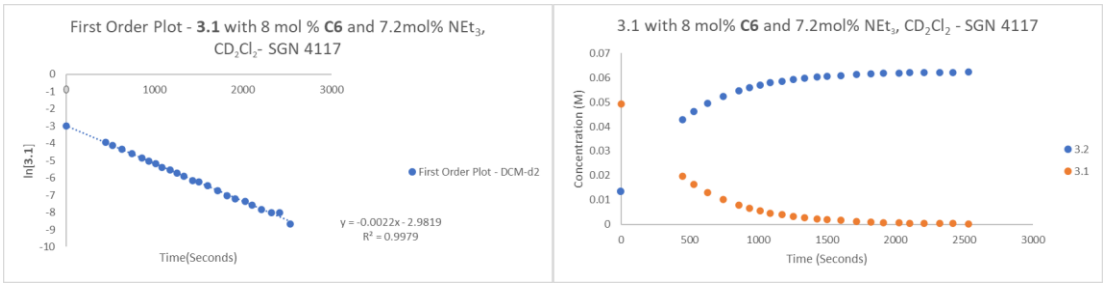

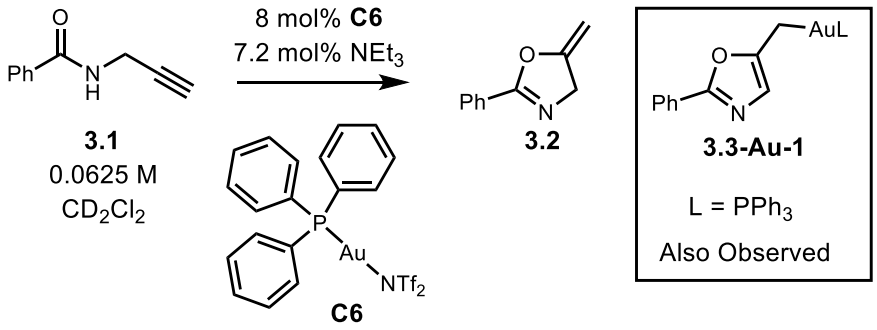

	CD_2Cl_2	Catalyst Amount	Catalyst Loading	k_{obs}/s^{-1}
SGN 4117	0.8 mL	0.004 mmol	8 mol%	$2.2 \times 10^{-3} \pm 2.13 \times 10^{-5}$

Kinetic Analysis of Nitro Benzamide 3.12

Raw plot of **3.12** cyclization (0.0625 M) in 0.8 mL of CH_2Cl_2 with 0.002 mmol **C1** (5 mol%) with corresponding first order plot.

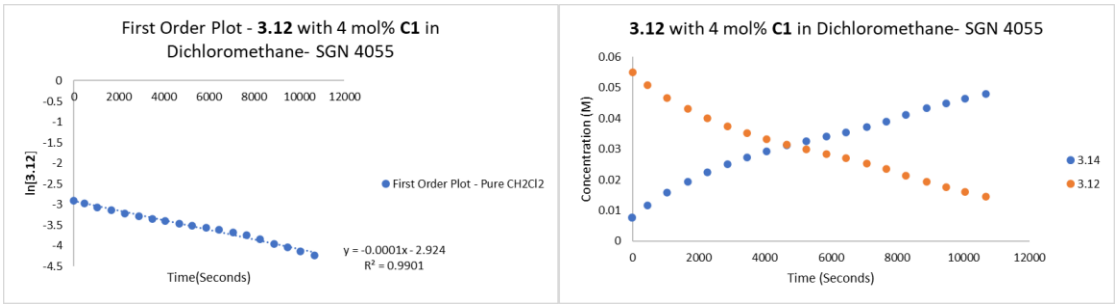

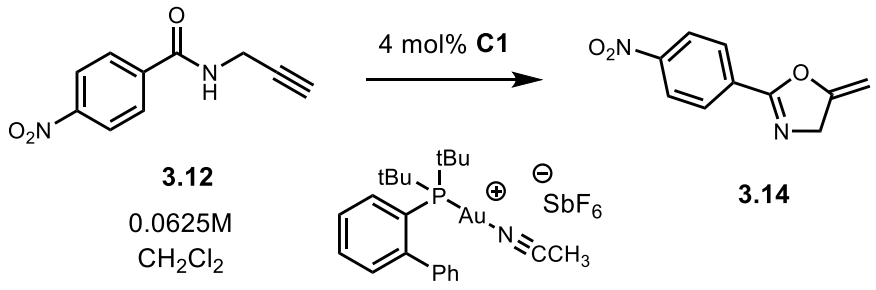

	CH_2Cl_2	Catalyst Amount	Catalyst Loading	$k_{obs/S}^{-1}$
SGN 4055	0.8 mL	0.004 mmol	8 mol%	$1.2 \times 10^{-4} \pm 2.8 \times 10^{-6}$

Raw plot of **3.12** cyclization (0.0625 M) in 0.8 mL of CH_3OH with 0.002 mmol **C1** (5 mol%) with corresponding first order plot.

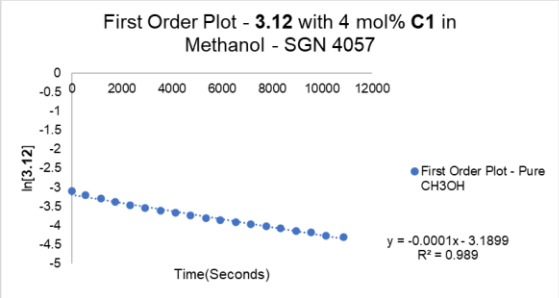

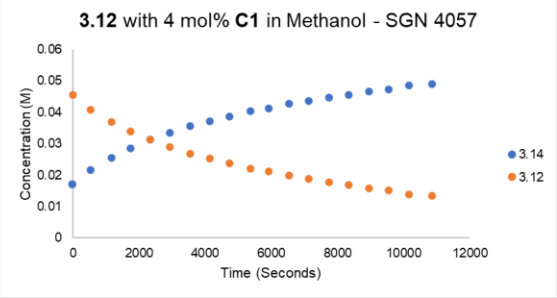

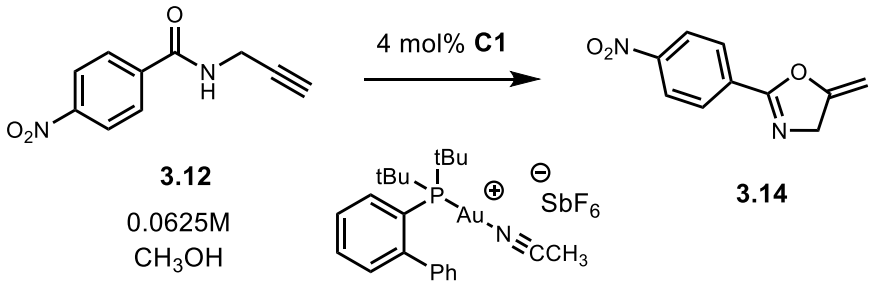

	CH₃OH	Catalyst Amount	Catalyst Loading	k_{obs}/s^{-1}
SGN 4057	0.8 mL	0.004 mmol	8 mol%	$1.1 \times 10^{-4} \pm 2.76 \times 10^{-6}$

Spectroscopic Data of Kinetics Reaction Mixtures

Formation of 3.1-Au-1 and 3.3-Au-1 where L = Johnphos

^{1}H Spectrum of **3.1-Au-1** where L = Johnphos

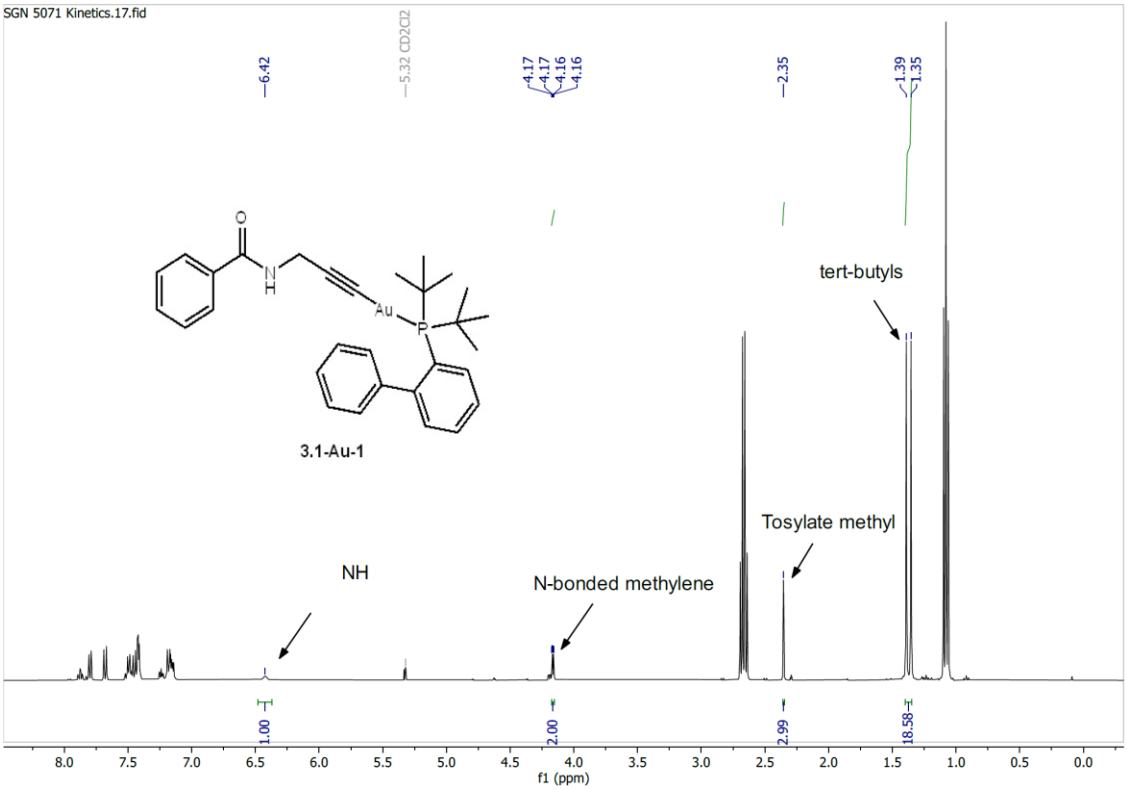

^{1}H NMR (400 MHz, Methylene Chloride-d_2) δ 6.42 (s, 1H), 4.16 (dd, J = 4.9, 1.7 Hz, 2H), 2.35 (s, 3H), 1.37 (d, J = 14.9 Hz, 18H).

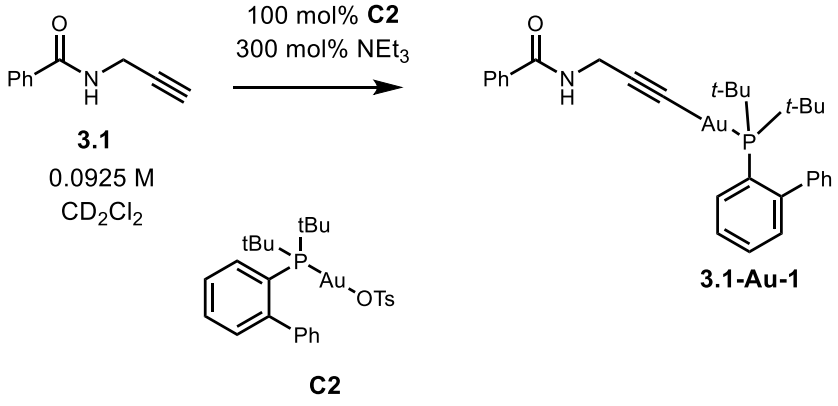

^{13}C Spectrum of **3.1-Au-1** where L = Johnphos

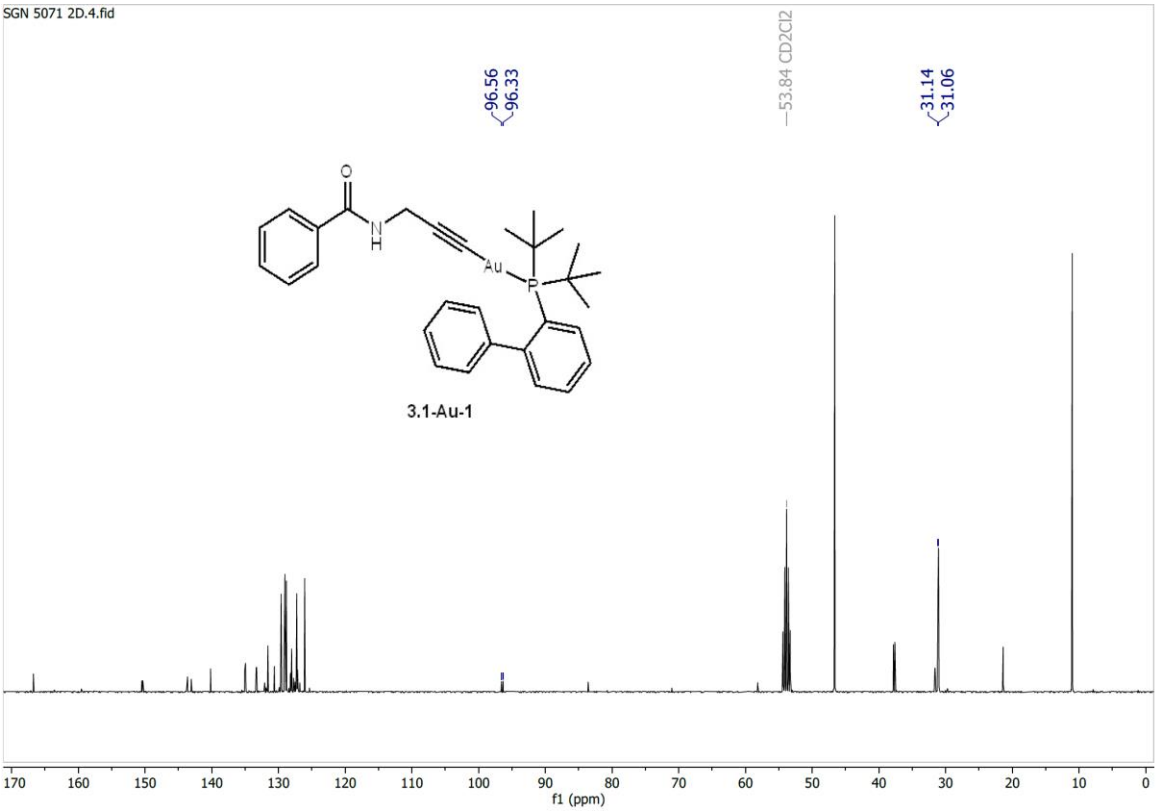

$^{13}C\{^{1}H\}$ NMR (101 MHz, CD_2Cl_2) δ 96.7, 96.5, 31.3, 31.2.

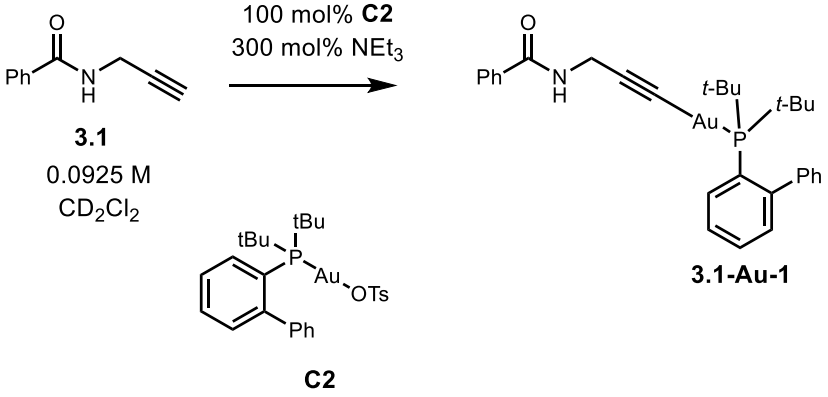

^{31}P Spectrum of **3.1-Au-1** where L = Johnphos

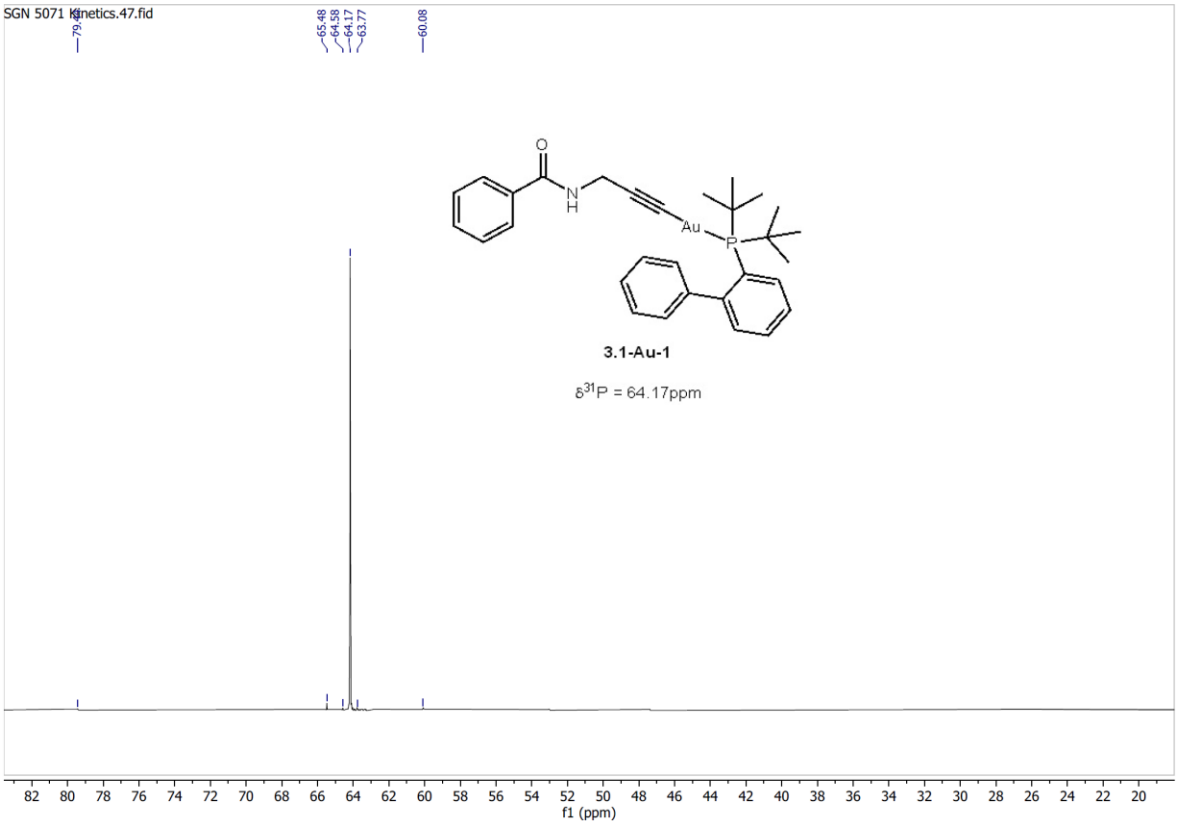

^{31}P{^{1}H} NMR (162 MHz, CD_2Cl_2) δ 79.44, 65.48, 64.58, 64.17, 60.08.

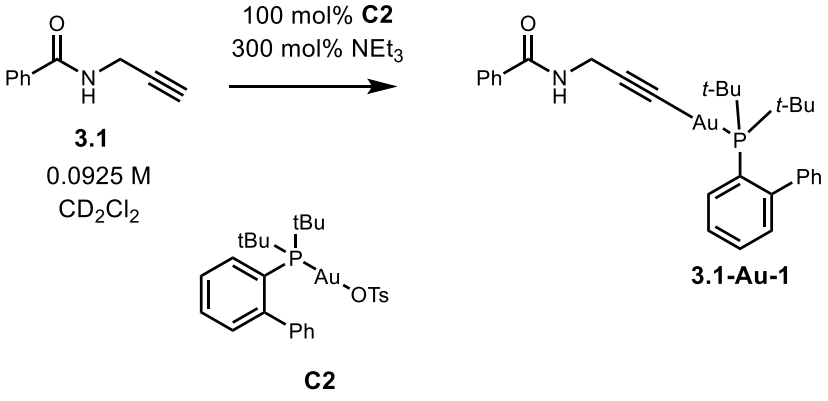

HSQC Spectrum of **3.1-Au-1** where L = Johnphos

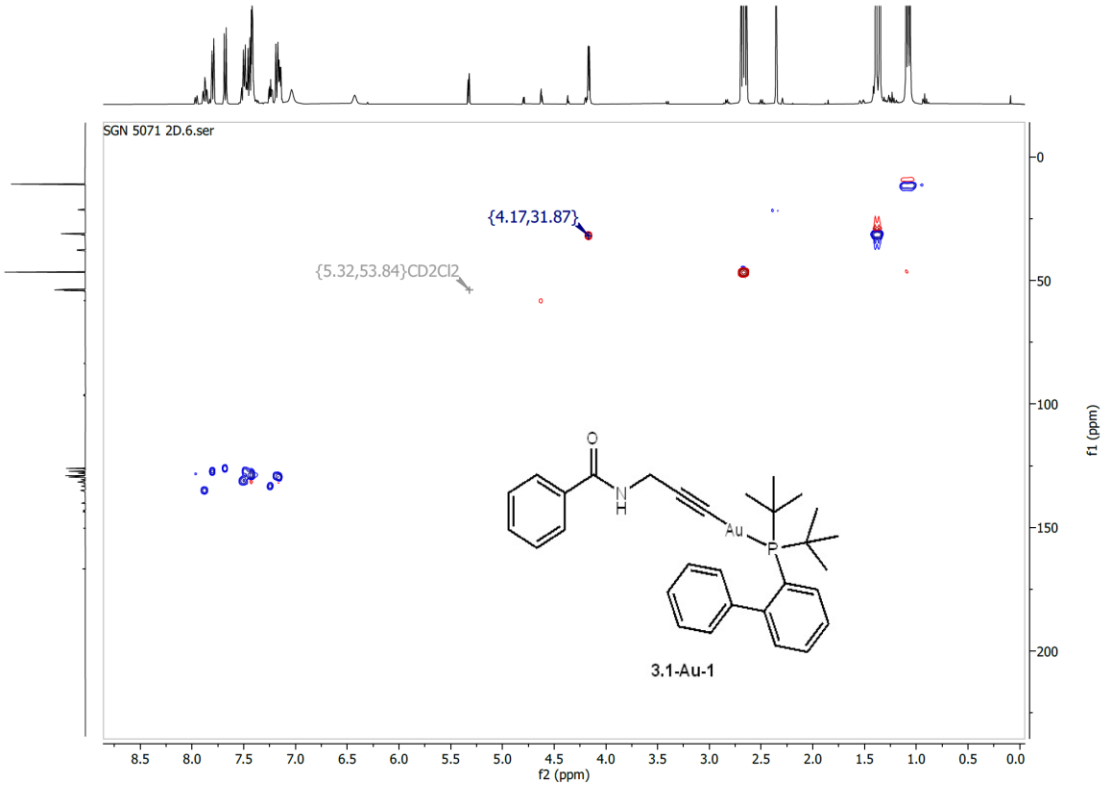

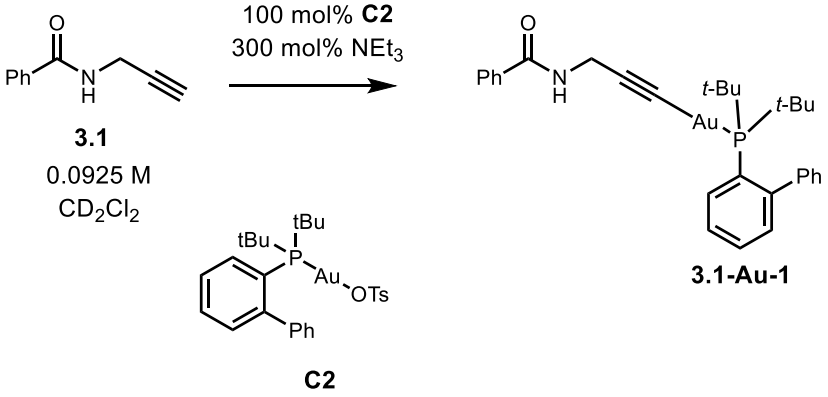

HMBC of **3.1-Au-1** where L = Johnphos

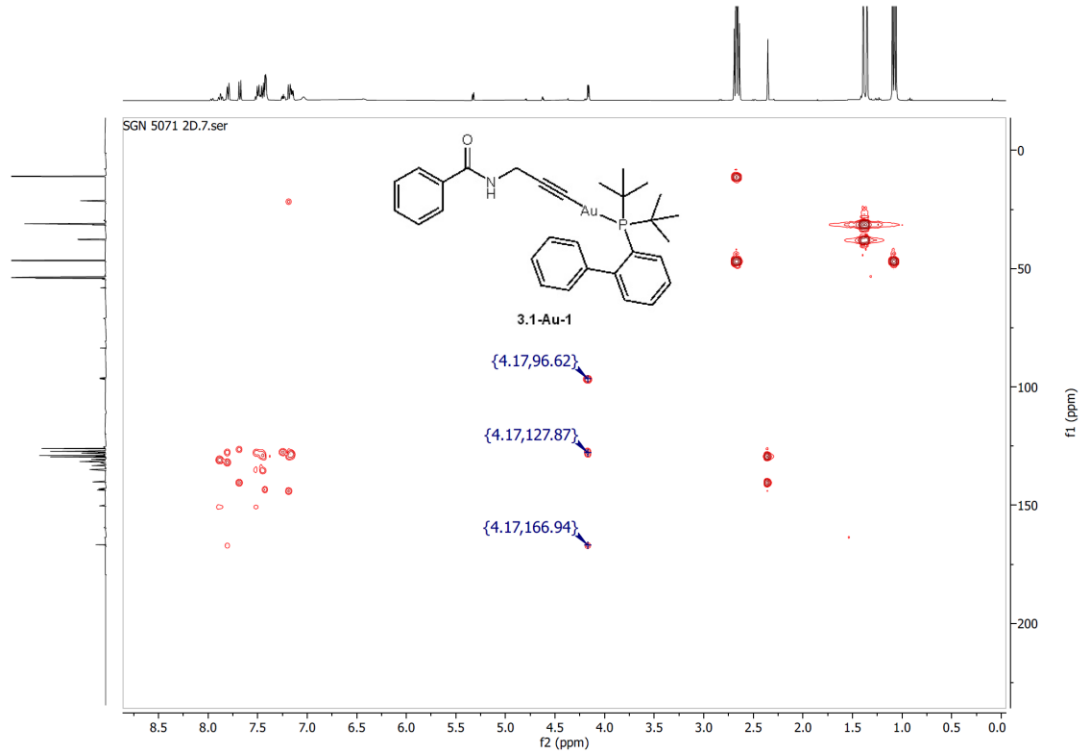

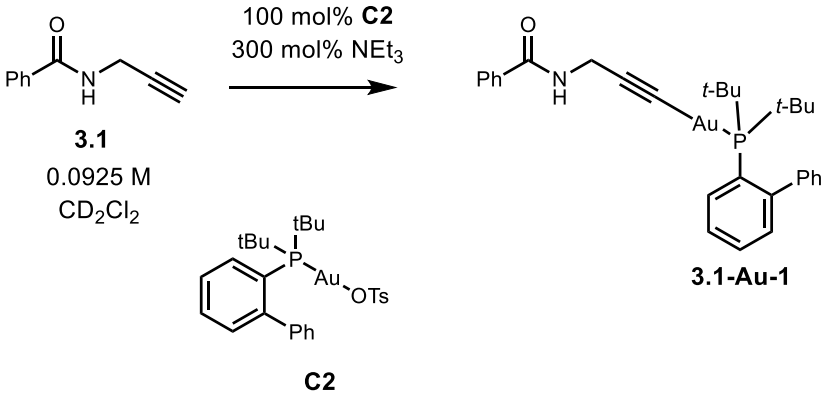

^{1}H Spectrum of **3.3-Au-1** where L = Johnphos

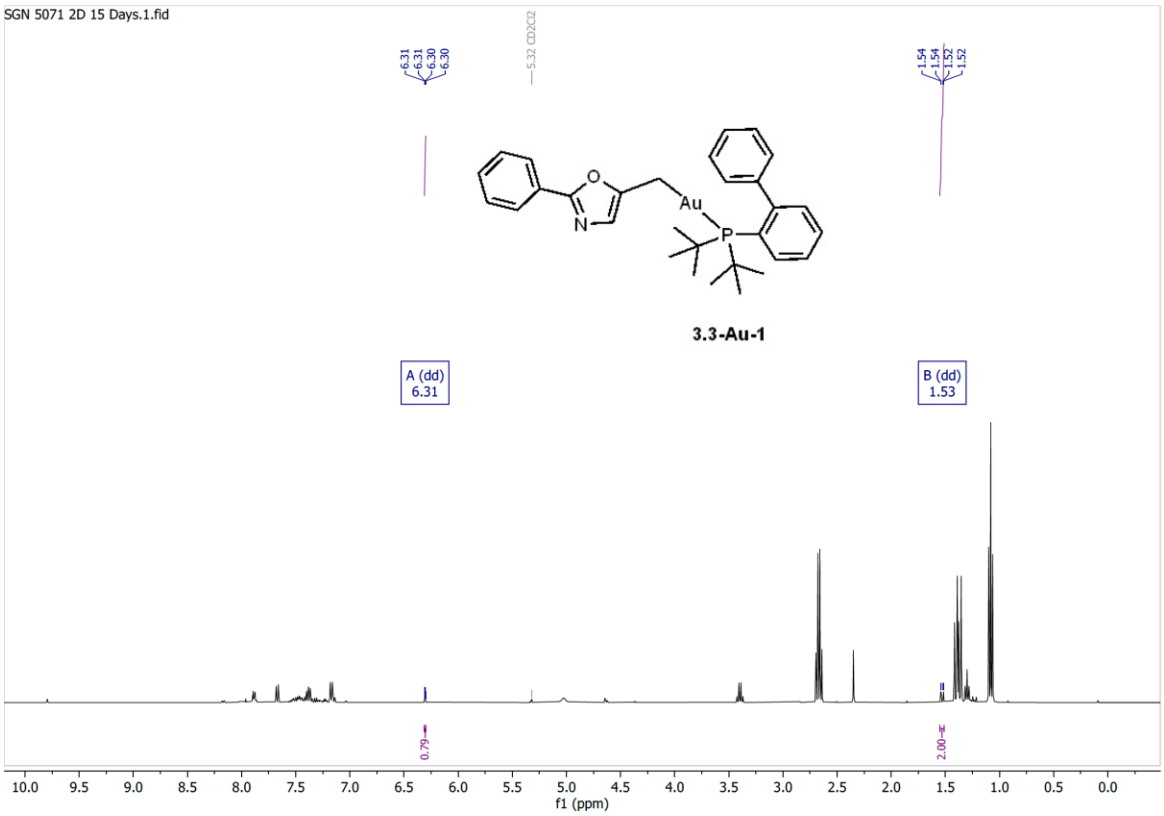

^{1}H NMR (400 MHz, Methylene Chloride-d_2) δ 6.30 (dd, J = 1.2 Hz, 1H), 1.53 (dd, J = 9.1, 1.1 Hz, 2H).

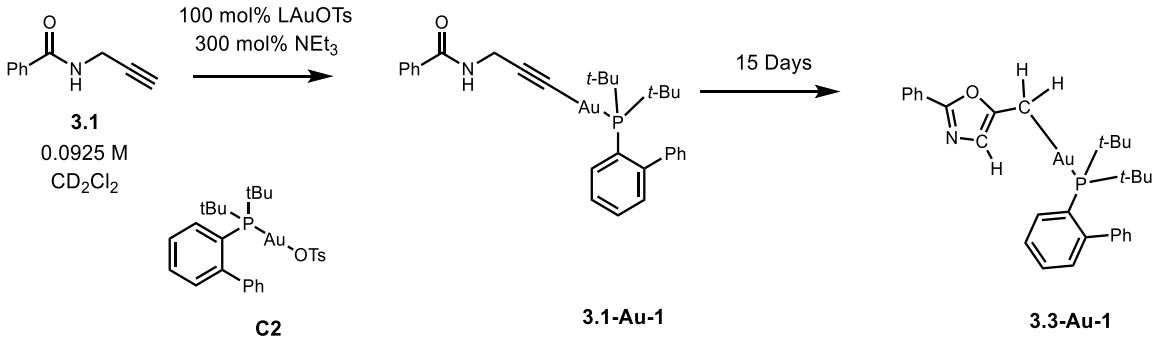

^{13}C Spectrum of **3.3-Au-1** where L = Johnphos

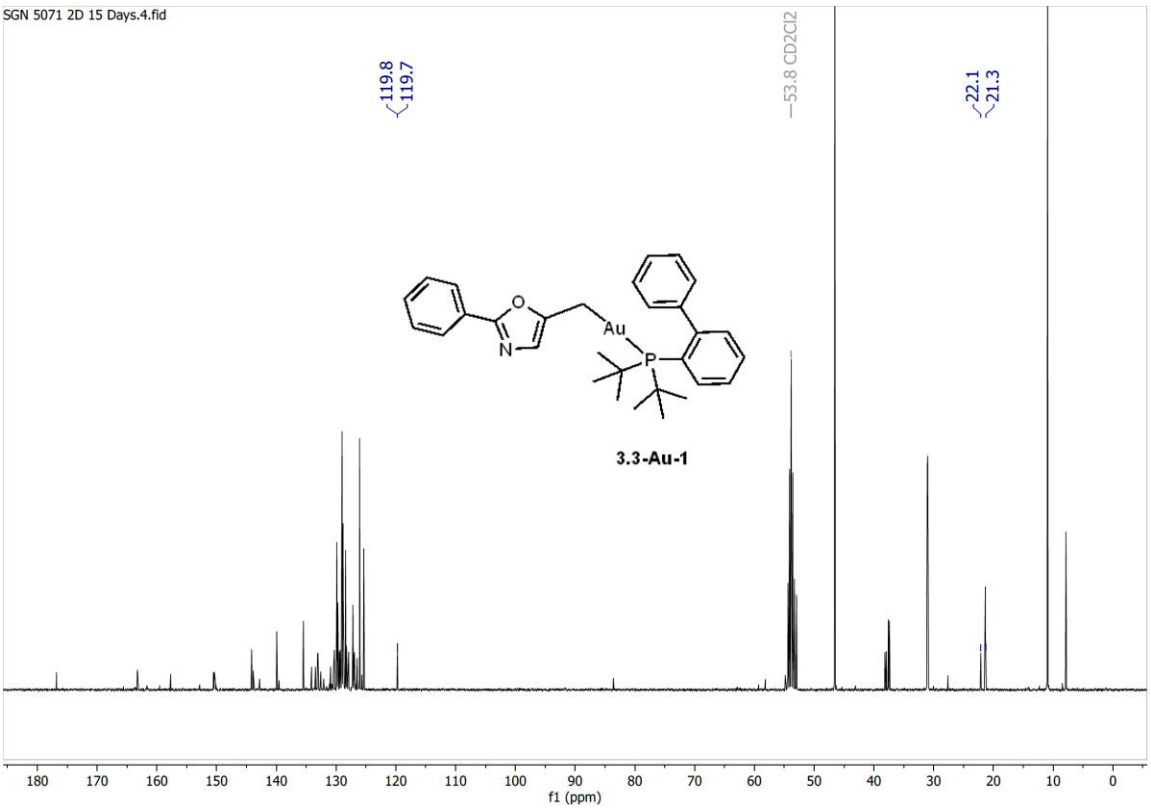

^{13}C NMR (101 MHz, CD_2Cl_2) δ 119.8, 119.7, 22.1, 21.3. Chemical shifts listed are proposed to be two individual signals both split into doublets by ^{31}P coupling. For the resonance at ~119ppm, J^5_{HP} = 3.4Hz. For the resonance at ~21-22ppm, J^2_{HP} = 85Hz.

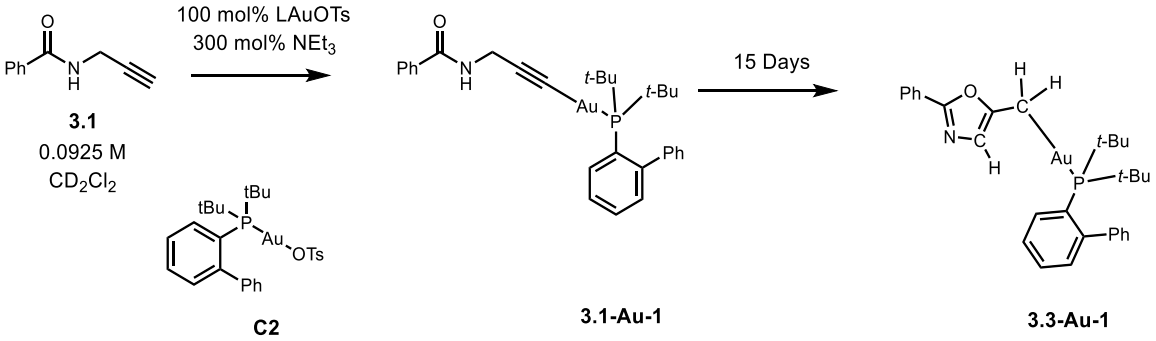

^{31}P Spectrum of **3.2-Au-2** where L = Johnphos

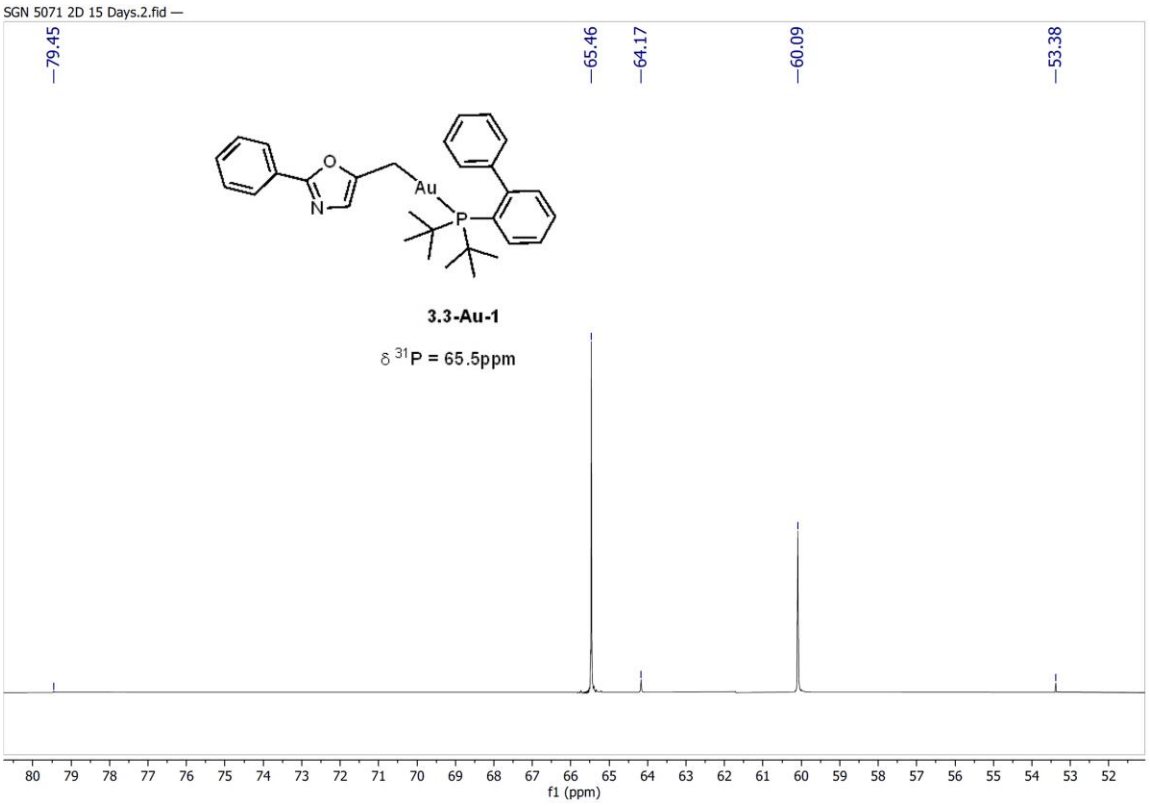

$^{31}P\{^{1}H\}$ NMR (162 MHz, CD_2Cl_2) δ 79.45, 65.46, 64.17, 60.09, 53.38.

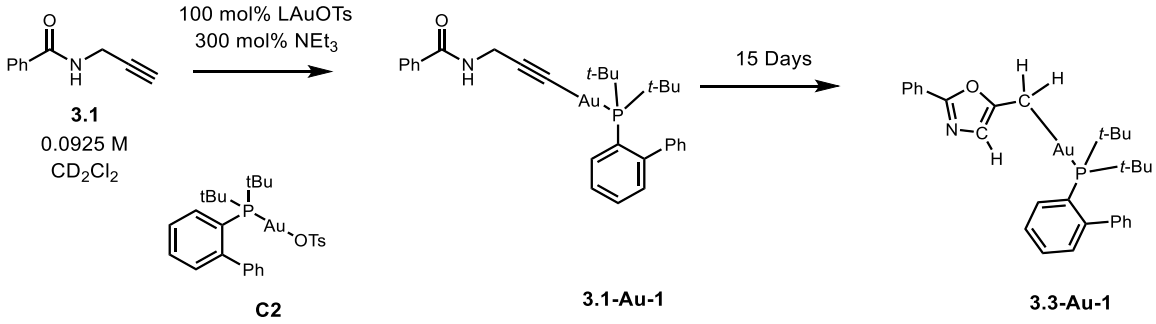

COSY Spectrum of **3.2-Au-2** where L = Johnphos

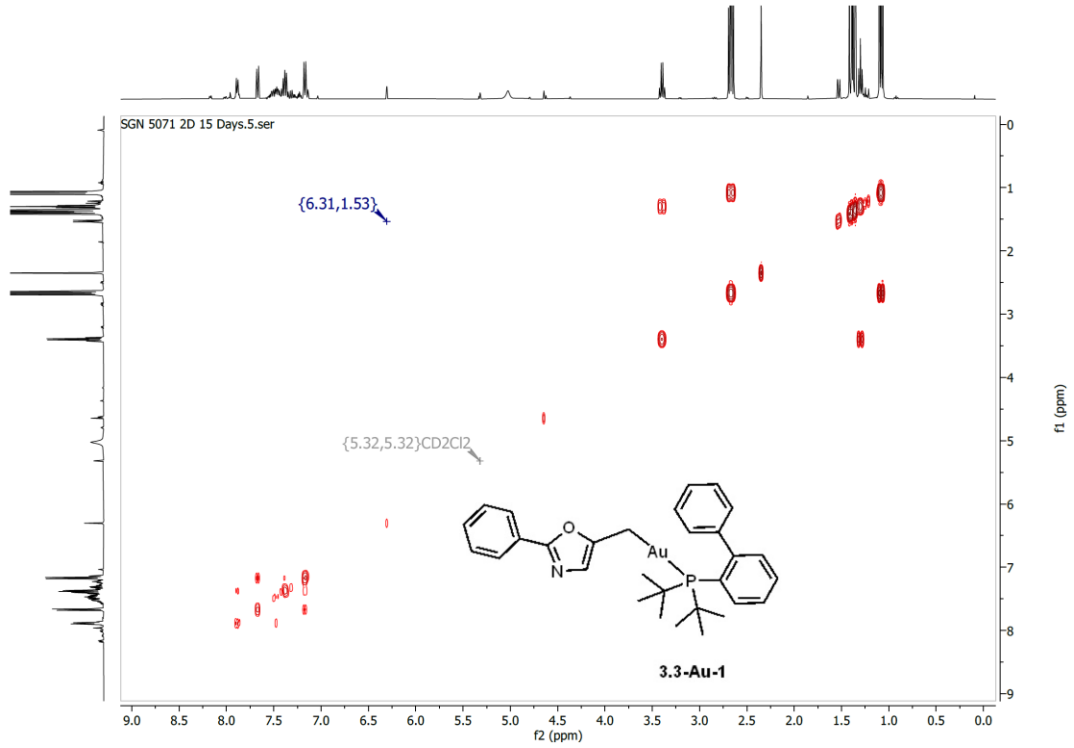

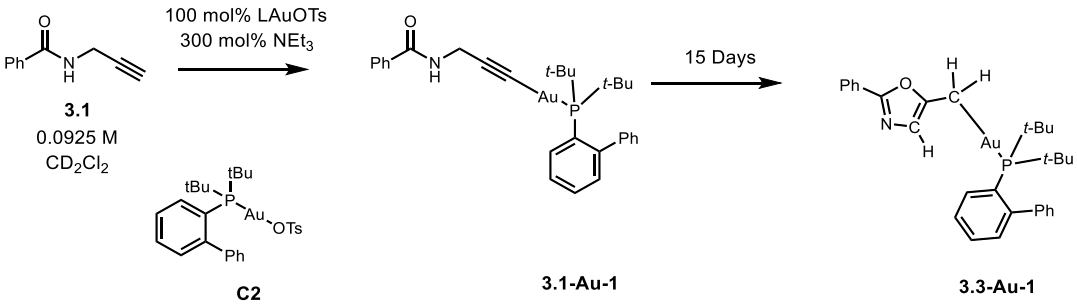

HSQC Spectrum of **3.2-Au-1** where L = Johnphos

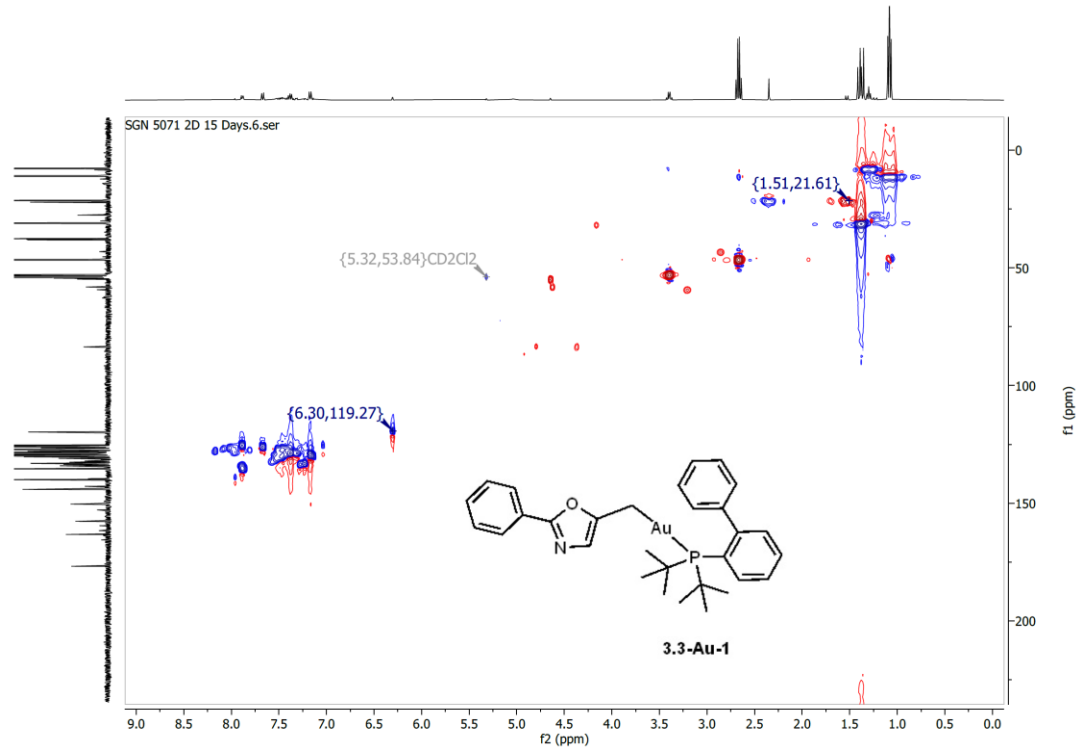

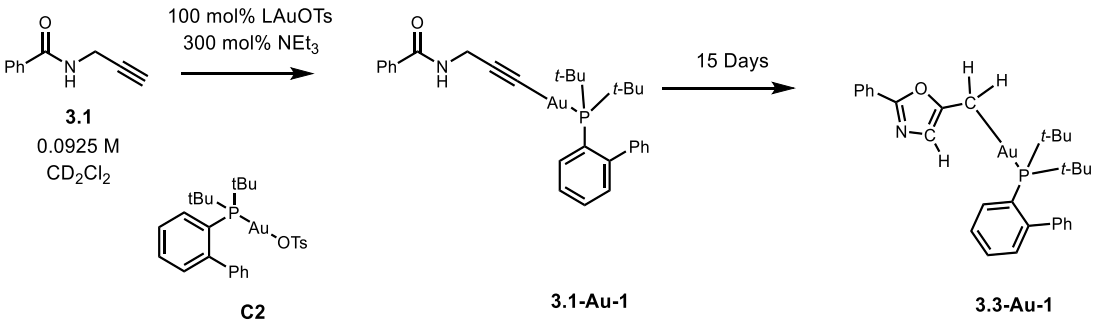

HMBC Spectrum of **3.2-Au-2** where L = Johnphos

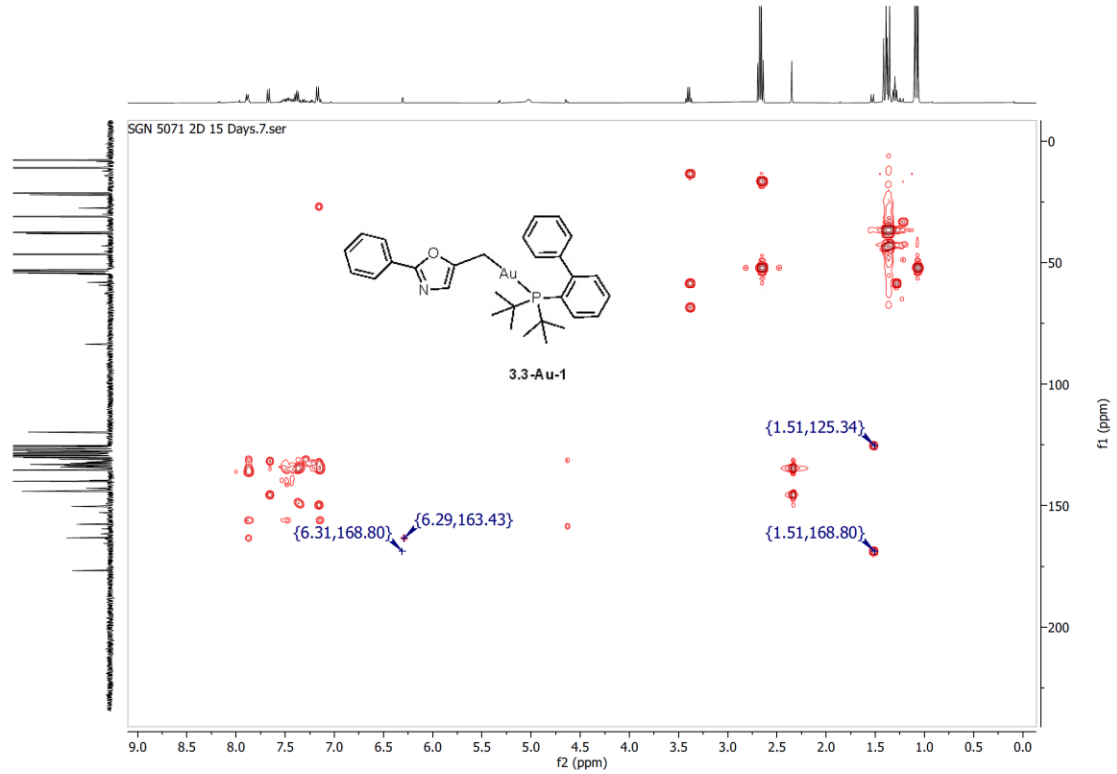

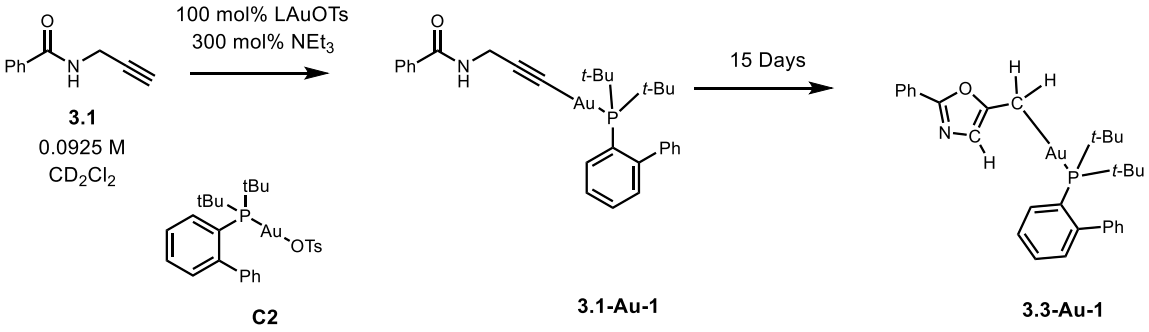

Formation of Keto-amide 3.4

HSQC Spectrum of Keto-amide **3.4**

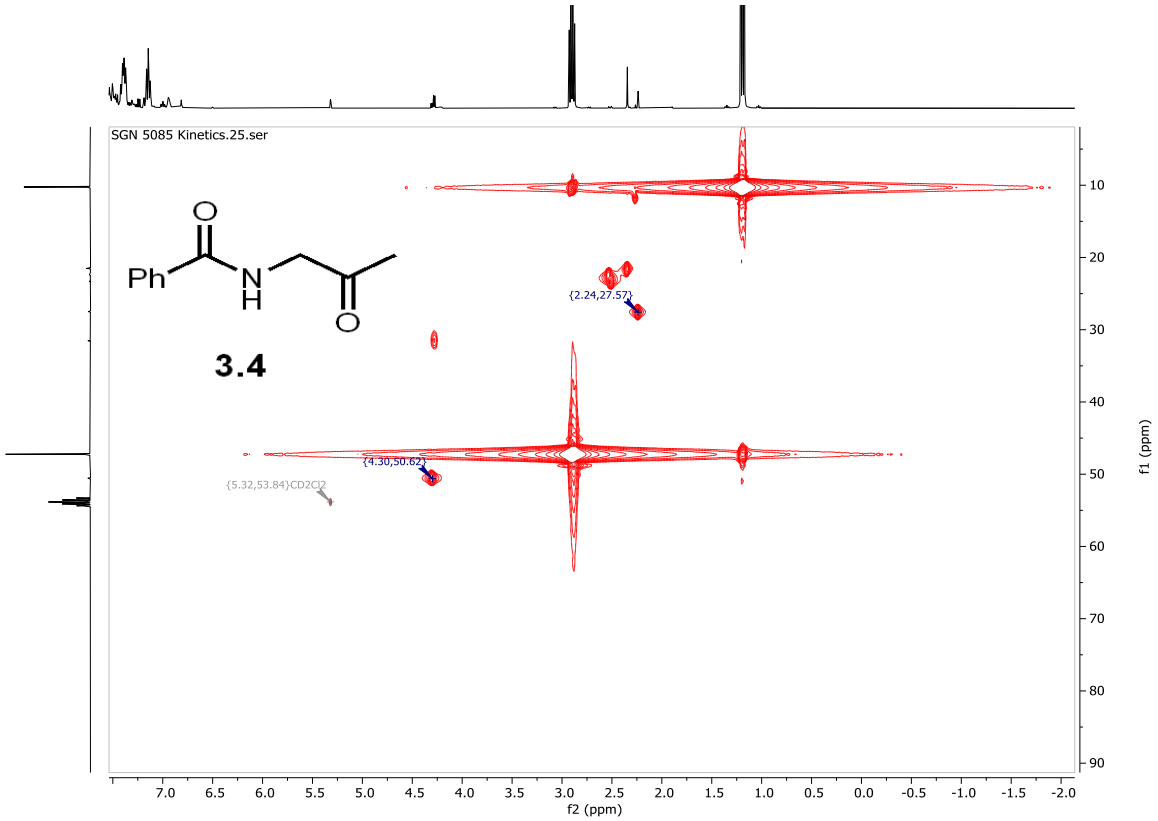

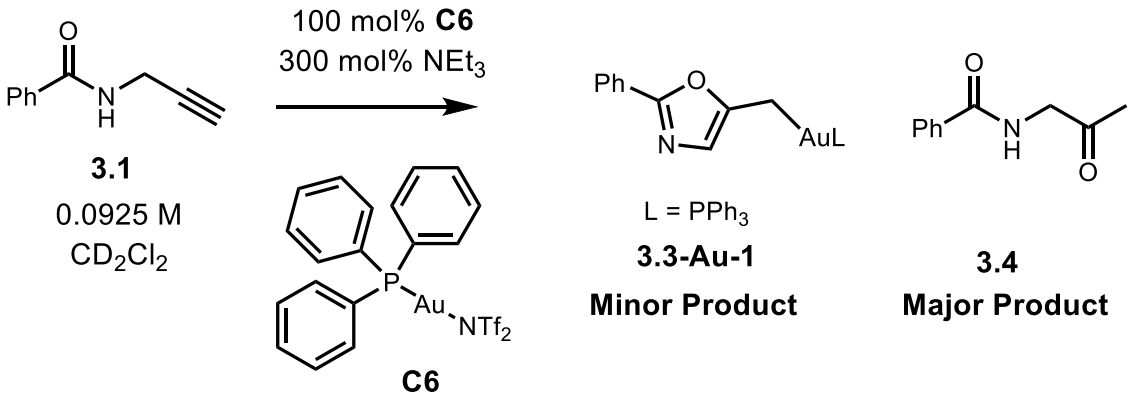

HMBC Spectrum of Keto-amide **3.4**

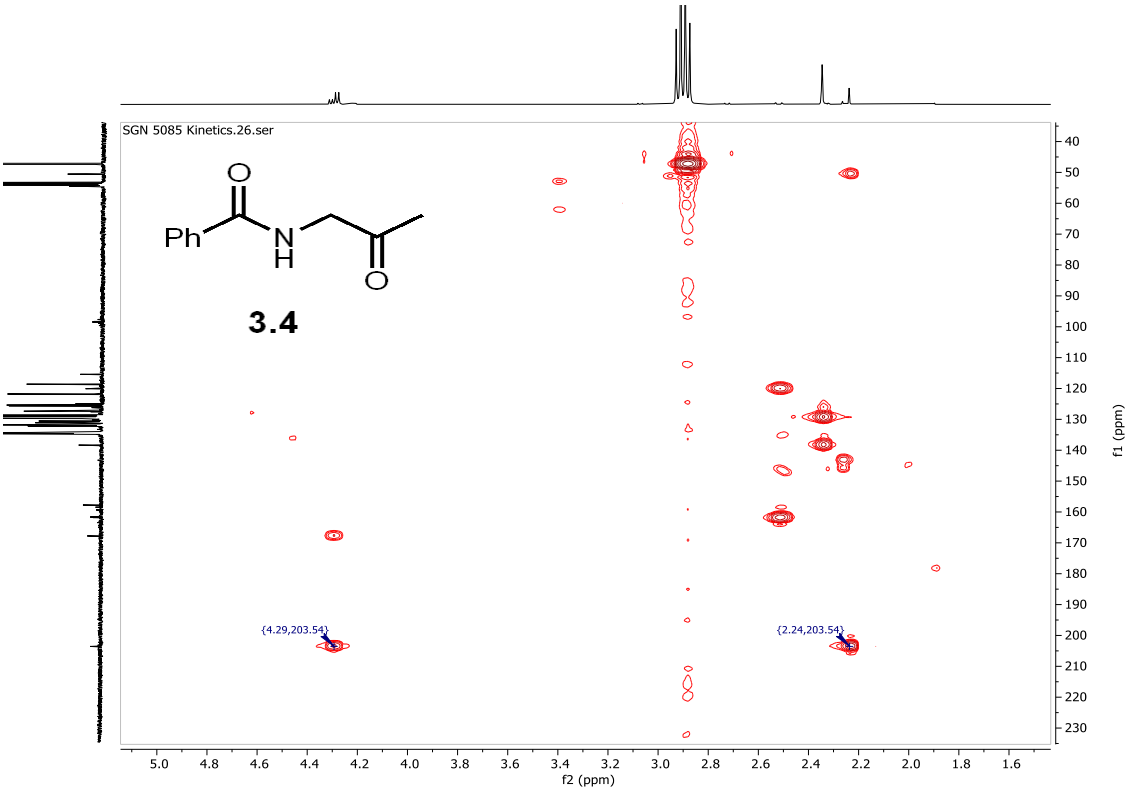

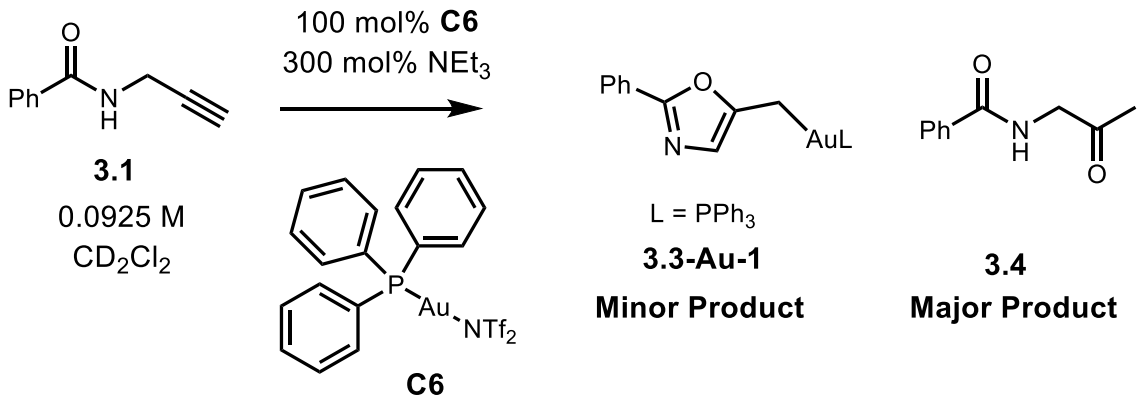

Reaction Analysis of Carbamate 3.4

General Procedure for Kinetic Analysis of Carbamates **3.4** and **3.9**

0.8mL of a 0.0625M solution of **3.4** or **3.9** (0.05mmols of carbamate) would be used to dissolve 0.002mmols (4 mol%) of solid catalyst. This mixture would then

be transferred immediately to the NMR spectrometer, with ^{1}H and ^{31}P spectra being collected at regular intervals.

^{31}P Spectrum of **3.4-Au-2**

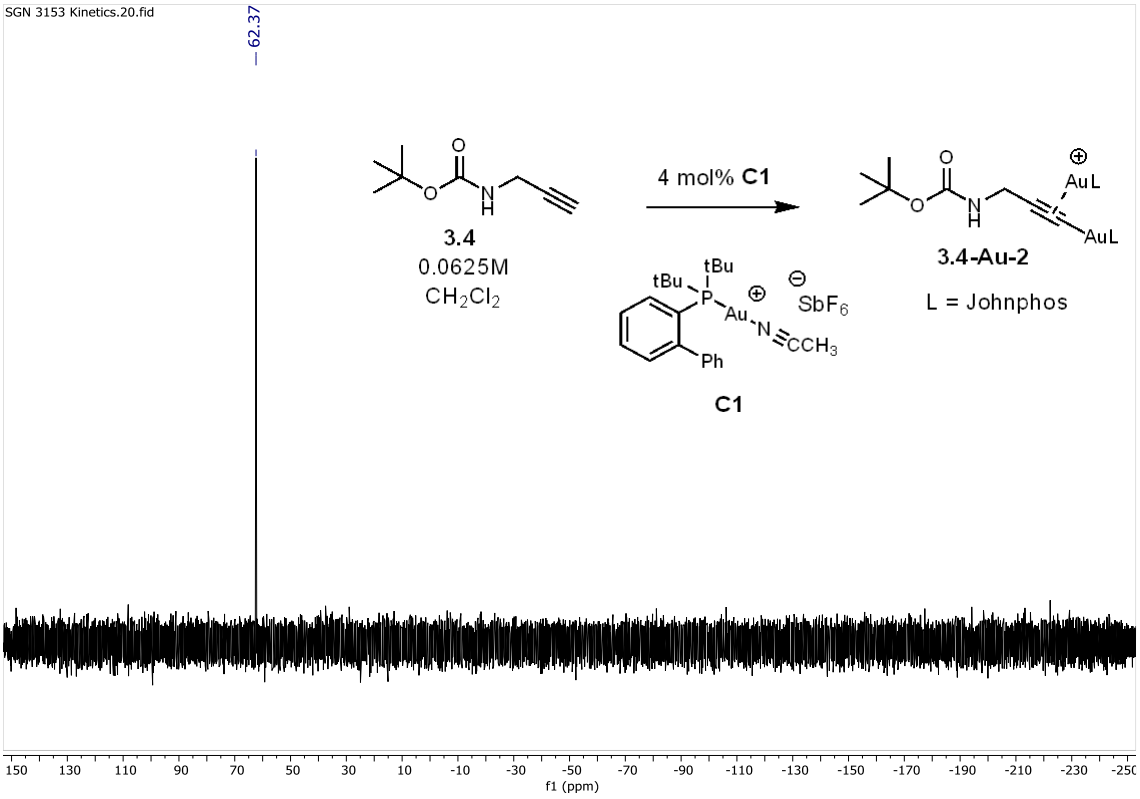

^{1}H NMR of Mixture Formed from Reaction of **3.4** and 4 mol% **C6**

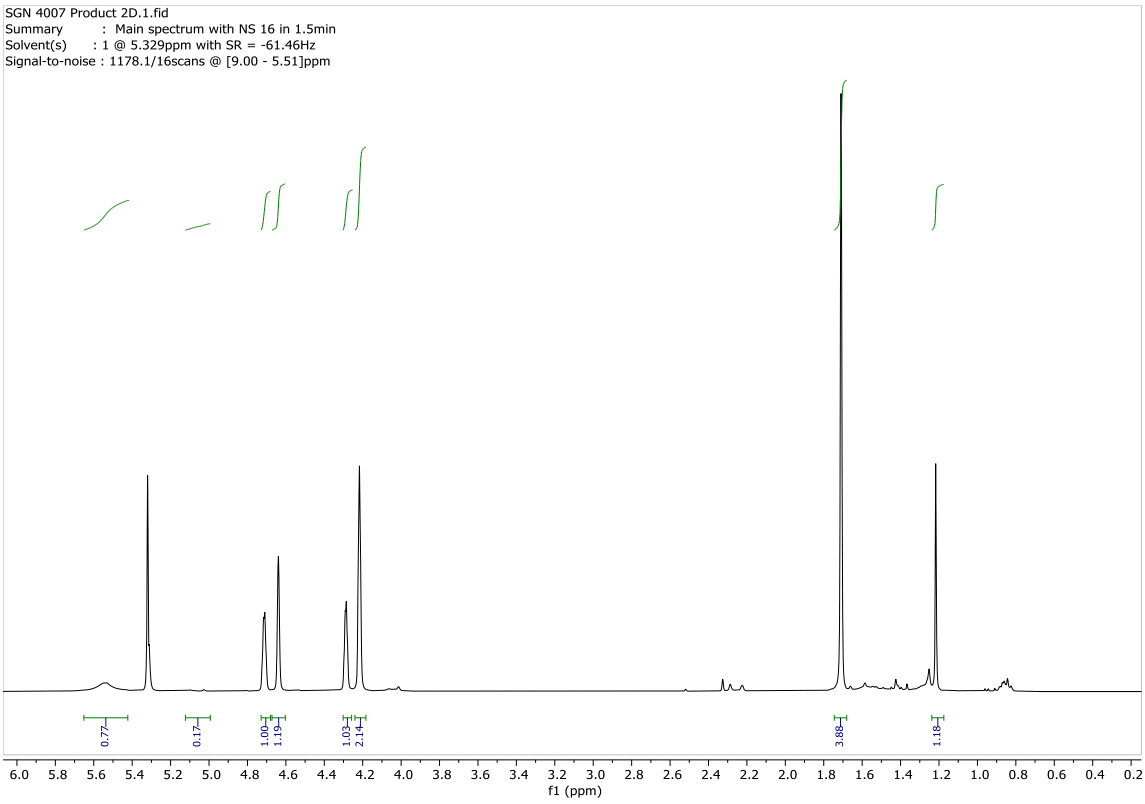

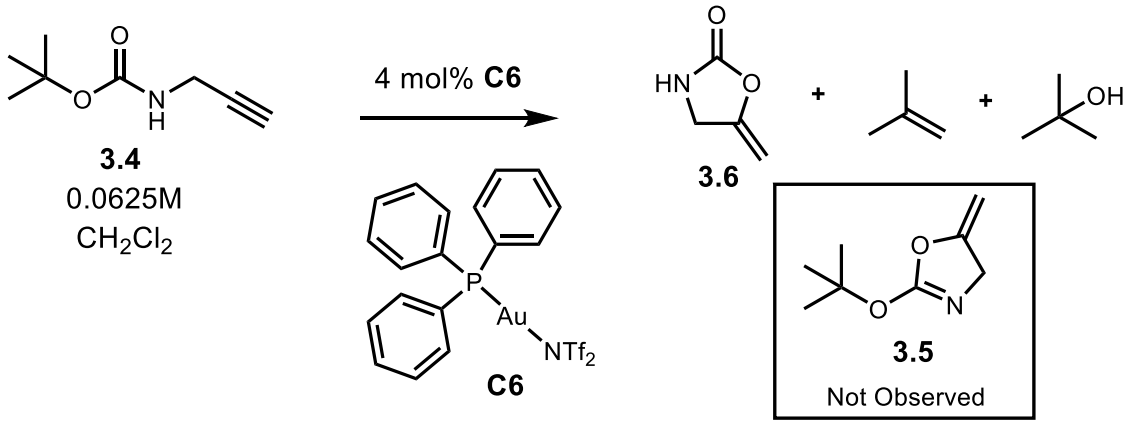

HSQC Spectrum of Mixture Formed from Reaction of **3.4** and 4 mol% **C6**

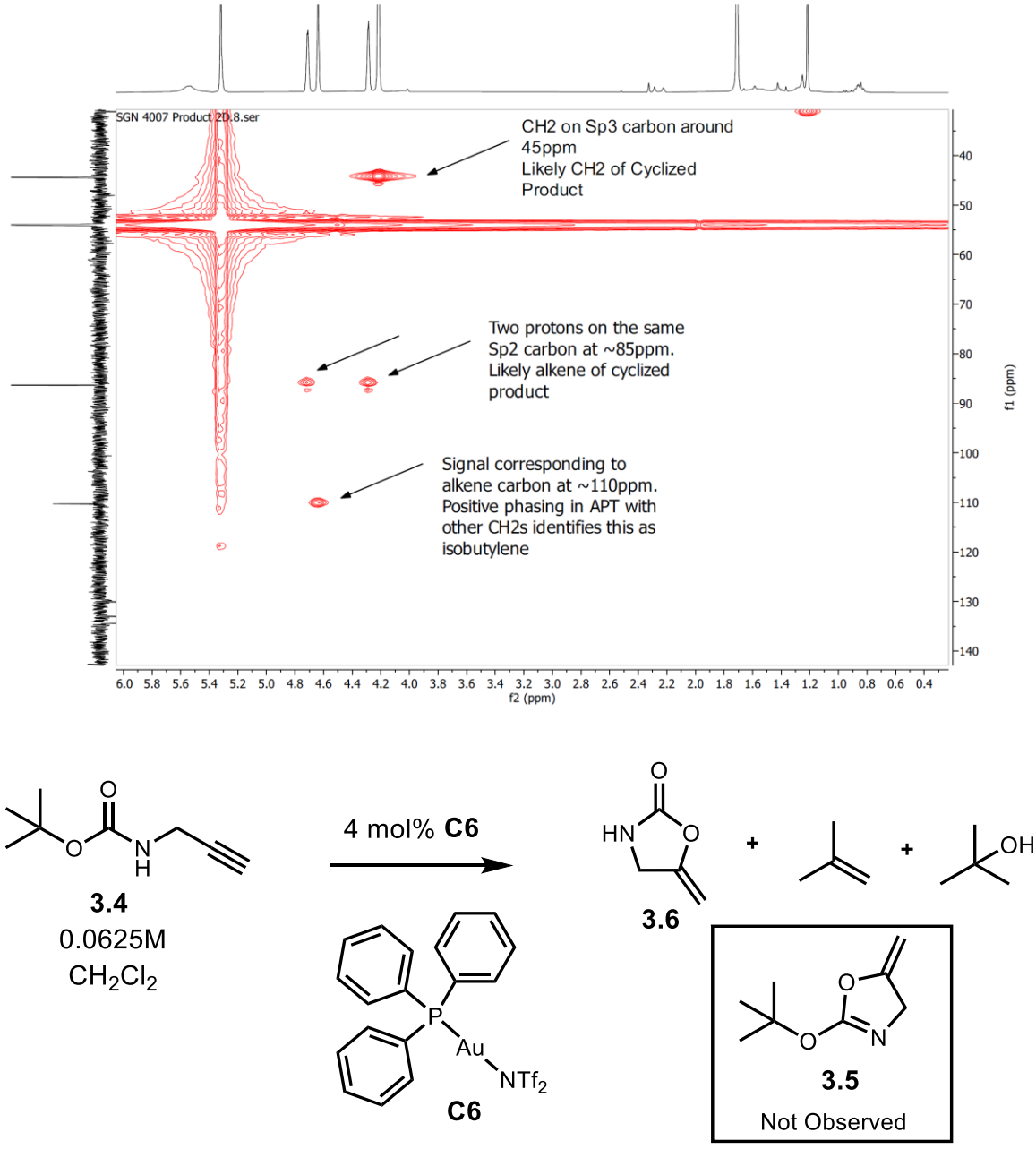

COSY Spectrum of Mixture Formed from Reaction of **3.4** and 4 mol% **C6**

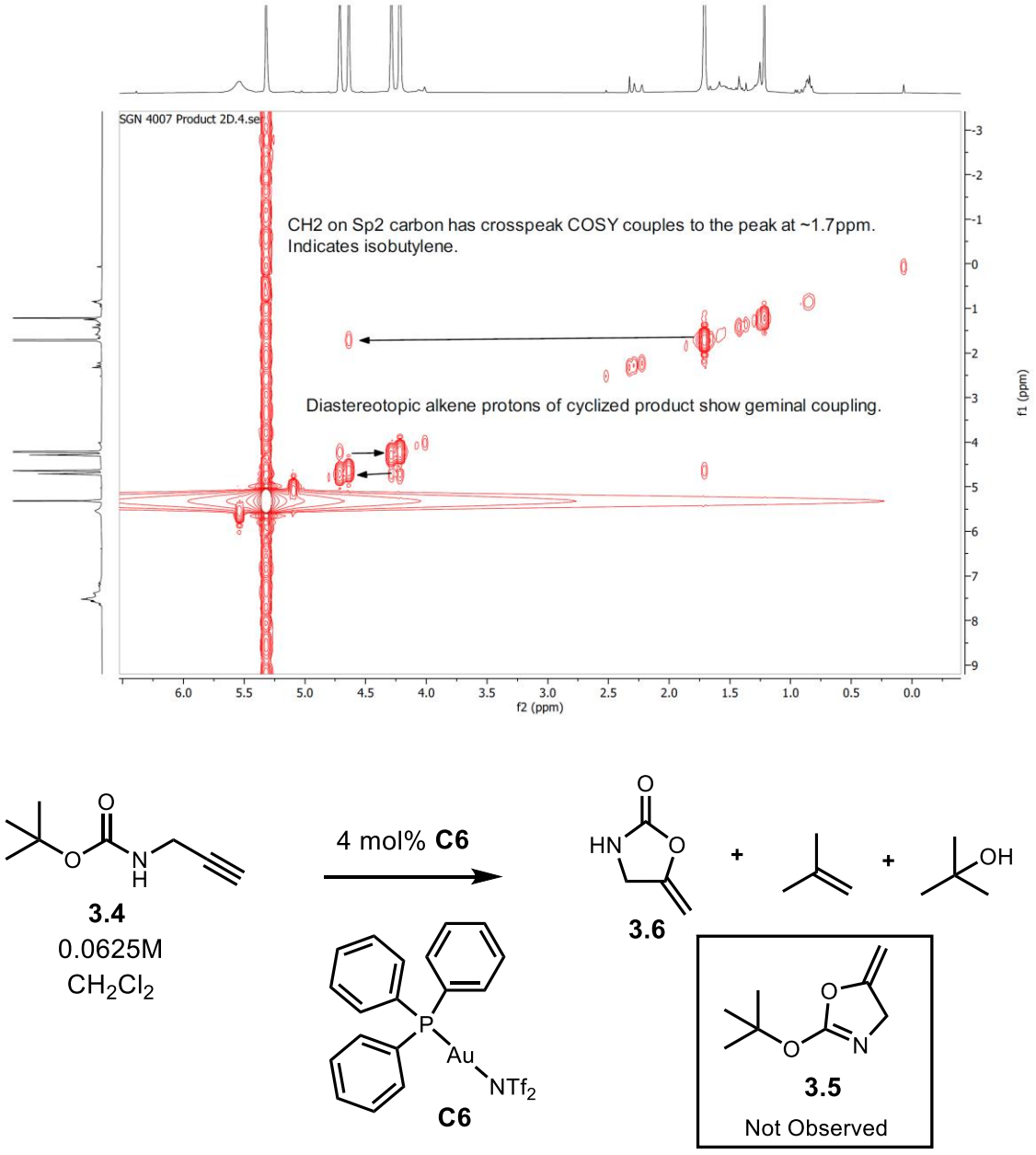

HMBC Spectrum of Mixture Formed from Reaction of **3.4** and 4 mol% **C6**

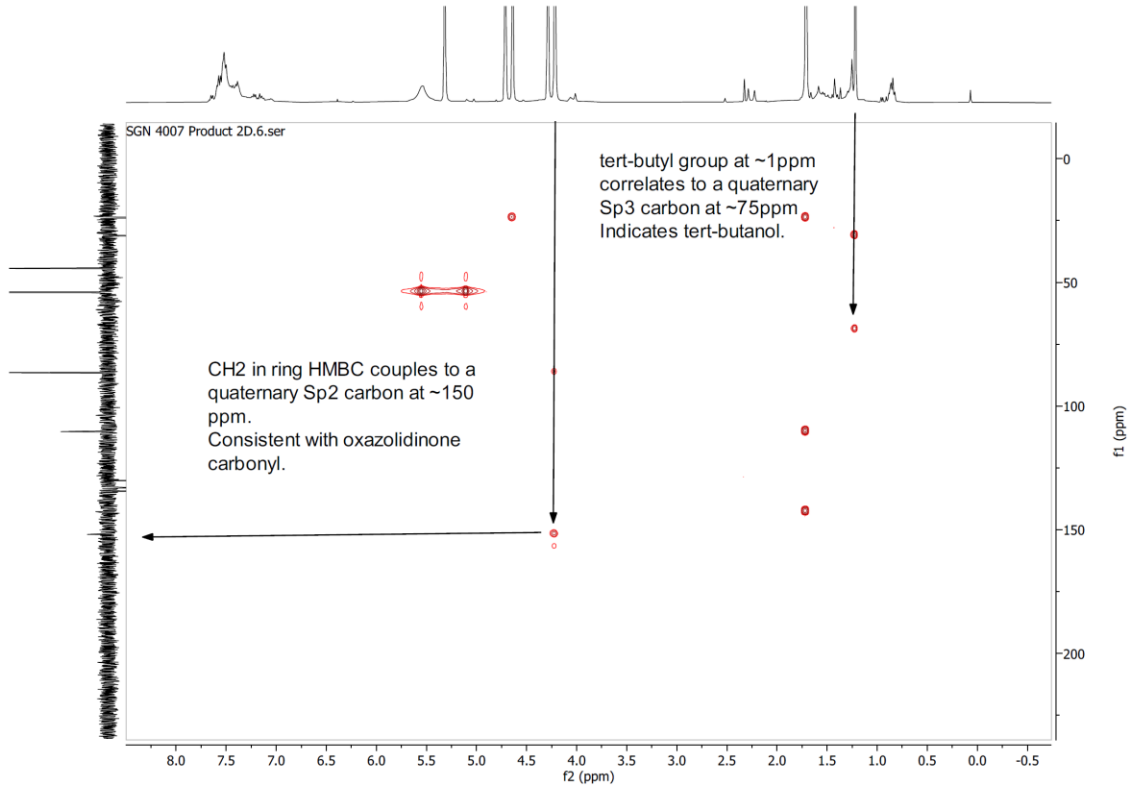

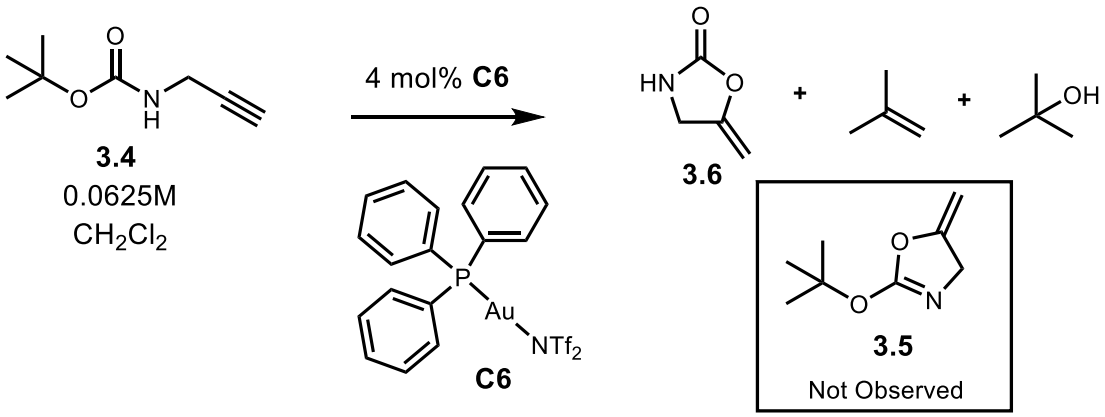

NMR Spectra for Compounds Synthesized

1H NMR Spectrum of C6

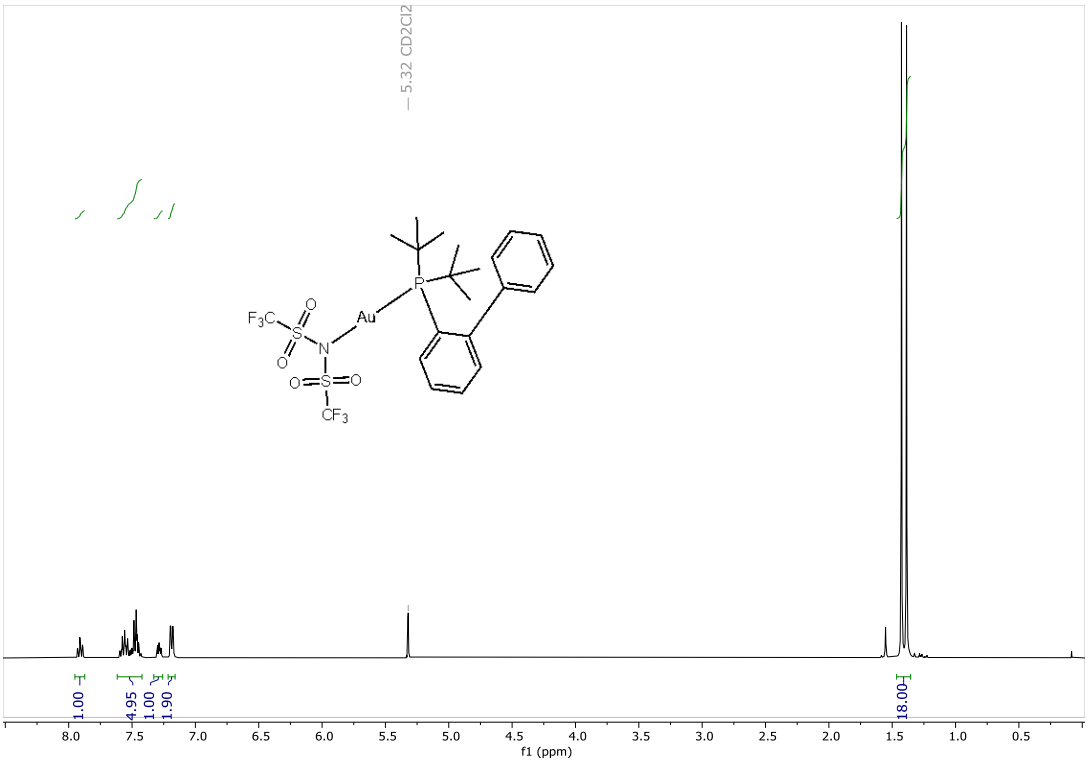

1H NMR (400 MHz, CH_2Cl_2) δ 7.60 (t, *J* = 9.2 Hz, 1H), 7.54 (t, *J* = 1.5 Hz, 2H), 7.44 (t, *J* = 1.8 Hz, 2H), 7.30 (t, *J* = 7.3 Hz, 2H), 7.12 (dd, *J* = 7.6, 1.4 Hz, 2H), 1.28 (d, *J* = 16.9 Hz, 9H).

^{13}C NMR Spectrum of Catalyst **C6**

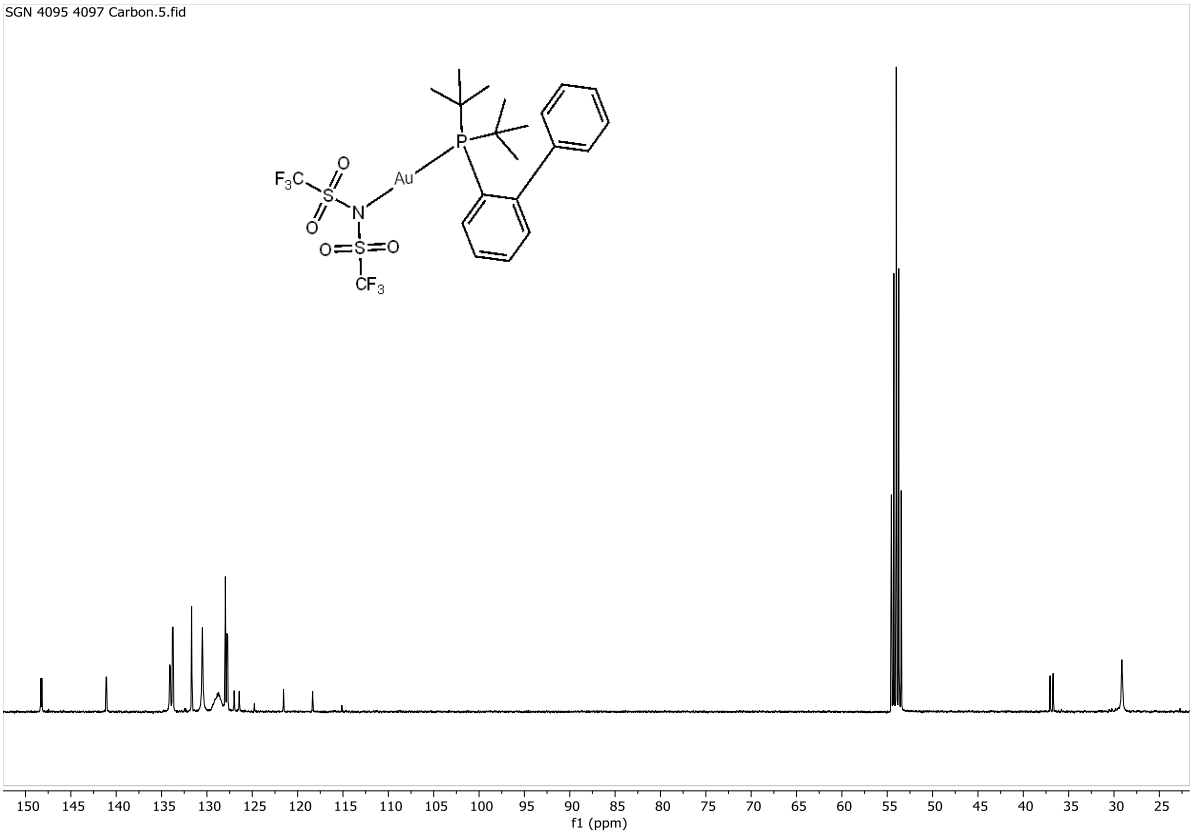

^{13}C{^{1}H} NMR (101 MHz, CD_2Cl_2) δ 148.09 (d, J_{CP} = 11.1 Hz), 140.93 (d, J_{CP} = 5.0 Hz), 133.90 (d, J_{CP} = 6.5 Hz), 133.60 (d, J_{CP} = 8.2 Hz), 131.52 (d, J_{CP} = 2.4 Hz), 130.34, 128.63, 127.81, 127.59 (d, J = 8.9 Hz), 126.56 (d, ^{1}J = 56.1 Hz), 119.79 (q, $^{1}J_{CF}$ = 323.4 Hz), 36.72 (d, $^{1}J_{CP}$ = 34.0 Hz), 28.96.

^{31}P NMR Spectrum of Catalyst C6

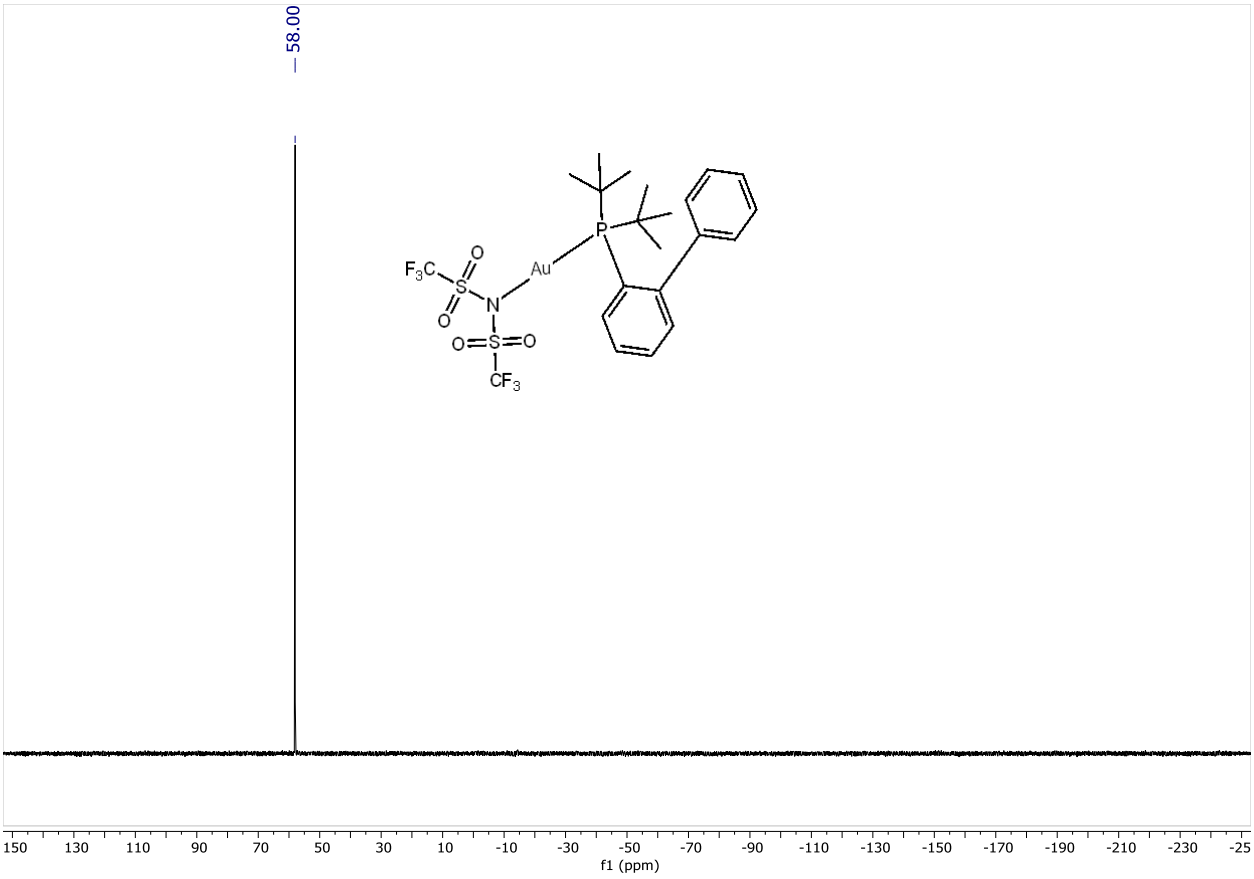

^{31}P{^{1}H} NMR (162 MHz, CD_2Cl_2) δ 28.42.

^{1}H NMR Spectrum of Ligand **4.1**

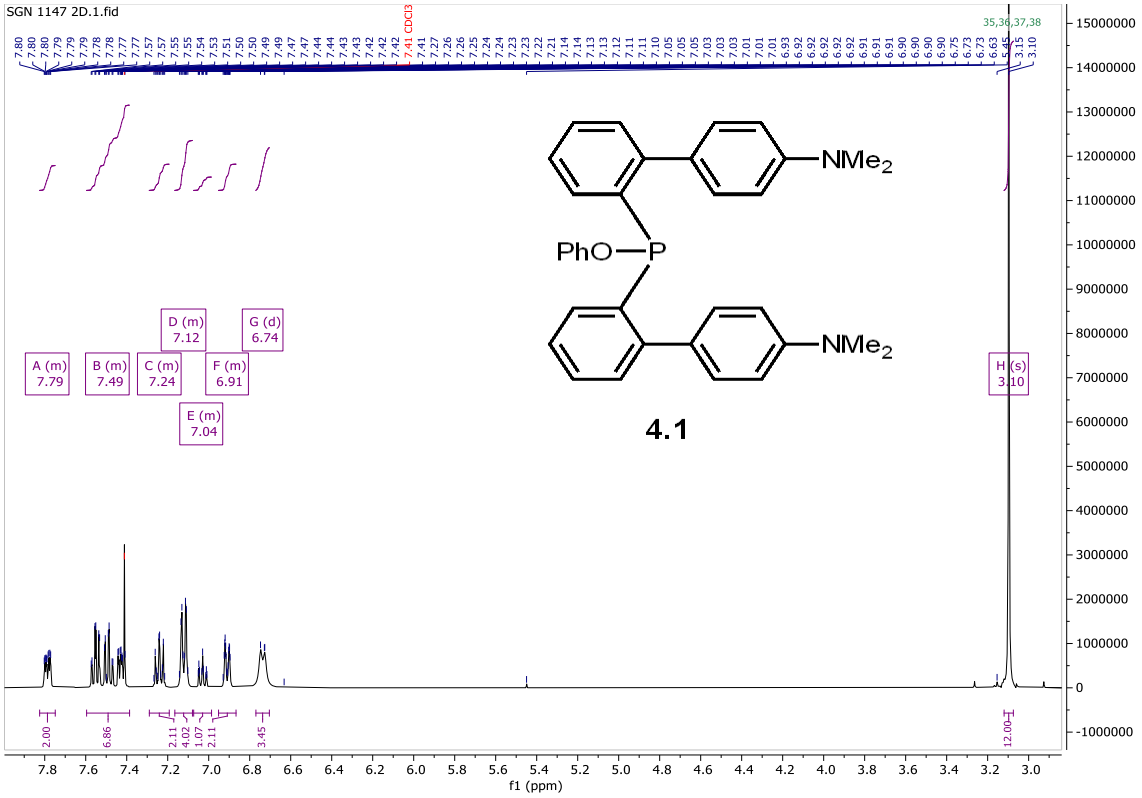

^{1}H NMR (400 MHz, $CDCl_3$) δ 7.82 – 7.75 (m, 2H), 7.60 – 7.39 (m, 7H), 7.29 – 7.19 (m, 2H), 7.17 – 7.08 (m, 4H), 7.07 – 6.99 (m, 1H), 6.95 – 6.87 (m, 2H), 6.74 (d, *J* = 8.3 Hz, 3H), 3.10 (s, 12H).

^{31}P NMR Spectrum of Ligand **4.1**

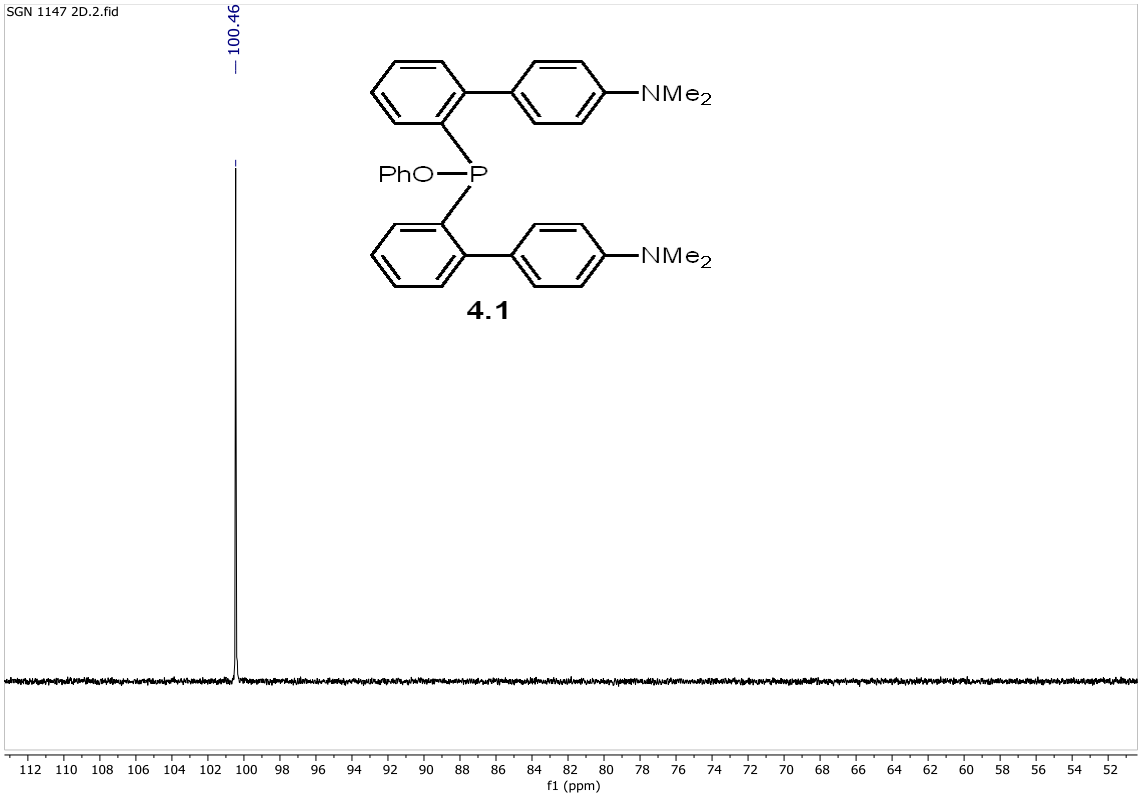

^{31}P{^{1}H} NMR (162 MHz, $CDCl_3$) δ 100.46.

^{13}C NMR Spectrum of Ligand **4.1**

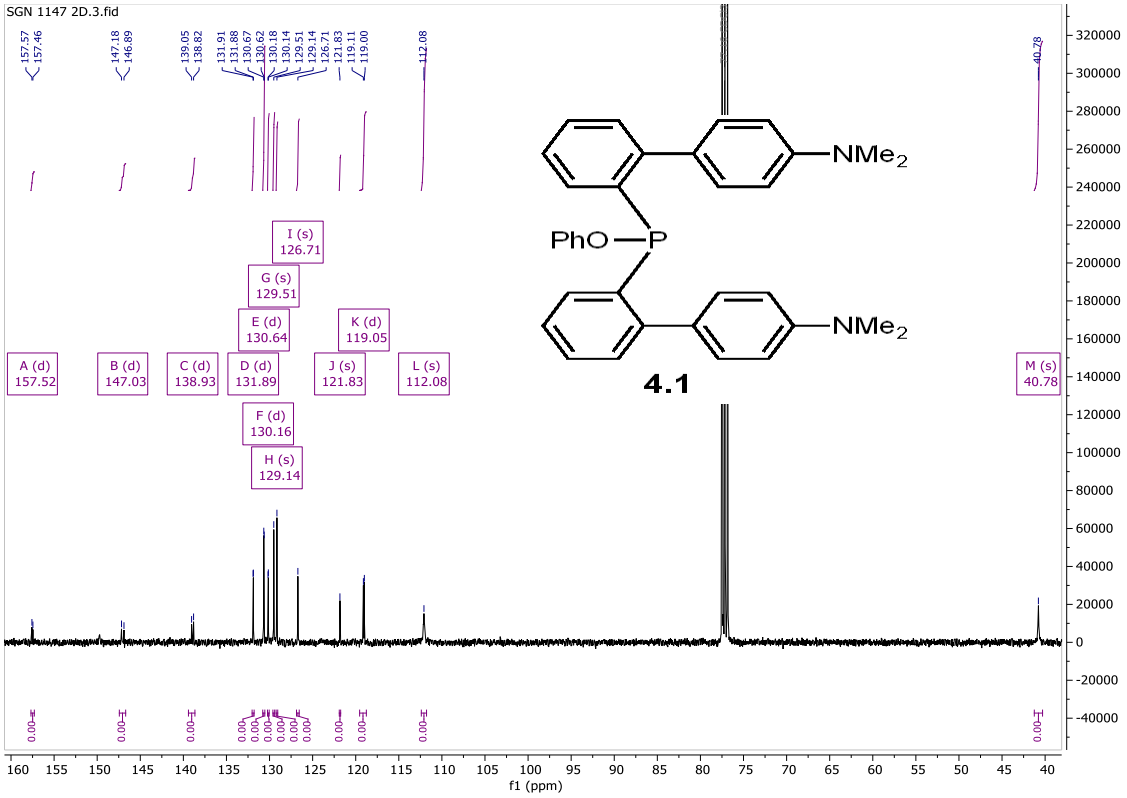

^{13}C{^{1}H} NMR (101 MHz, $CDCl_3$) δ 157.52 (d, *J* = 11.5 Hz), 147.03 (d, *J* = 28.7 Hz), 138.93 (d, *J* = 23.2 Hz), 131.89 (d, *J* = 3.0 Hz), 130.64 (d, *J* = 4.7 Hz), 130.16 (d, *J* = 3.8 Hz), 129.51, 129.14, 126.71, 121.83, 119.05 (d, *J* = 11.1 Hz), 112.08, 40.78.

^{1}H Spectrum of Gold Chloride **4.2**

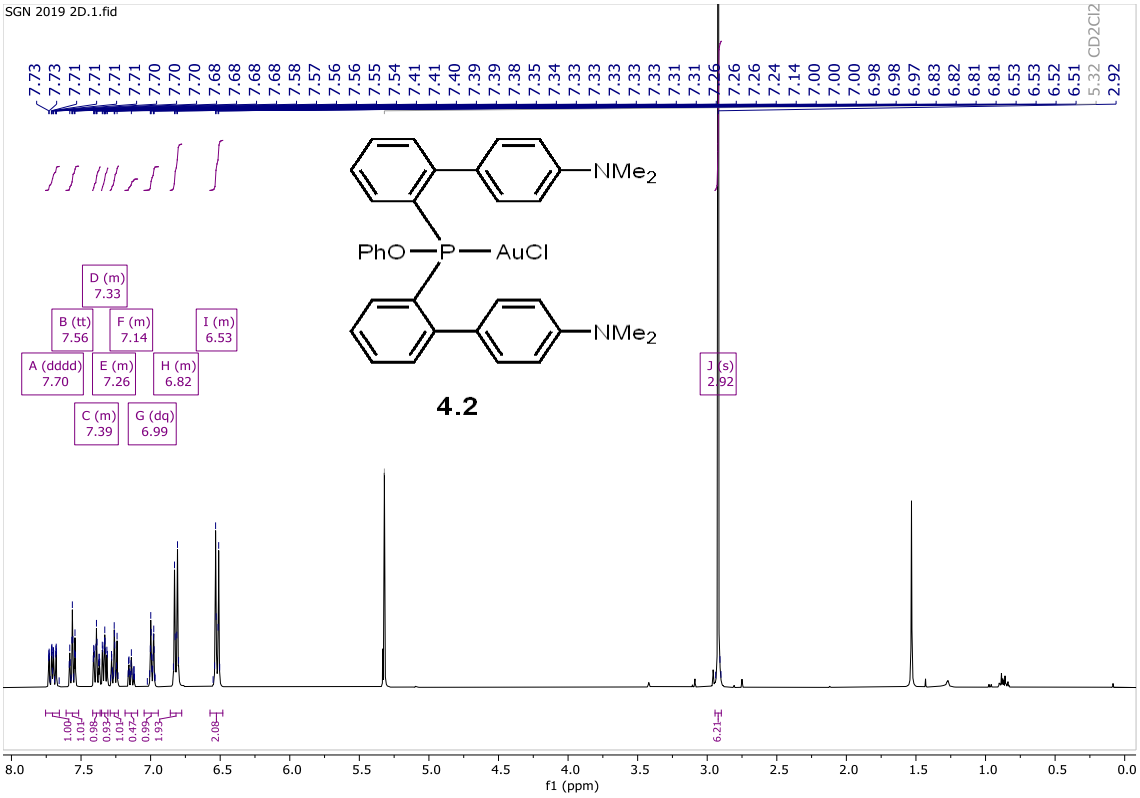

^{1}H NMR (400 MHz, CD_2Cl_2) δ 7.70 (dddd, *J* = 12.5, 7.9, 1.4, 0.5 Hz, 1H), 7.56 (tt, *J* = 7.5, 1.5 Hz, 1H), 7.42 – 7.36 (m, 1H), 7.35 – 7.31 (m, 1H), 7.29 – 7.23 (m, 1H), 7.18 – 7.09 (m, 0H), 6.99 (dq, *J* = 7.6, 1.1 Hz, 1H), 6.86 – 6.78 (m, 2H), 6.57 – 6.48 (m, 2H), 2.92 (s, 12H).

^{31}P NMR Spectrum of Gold Chloride **4.2**

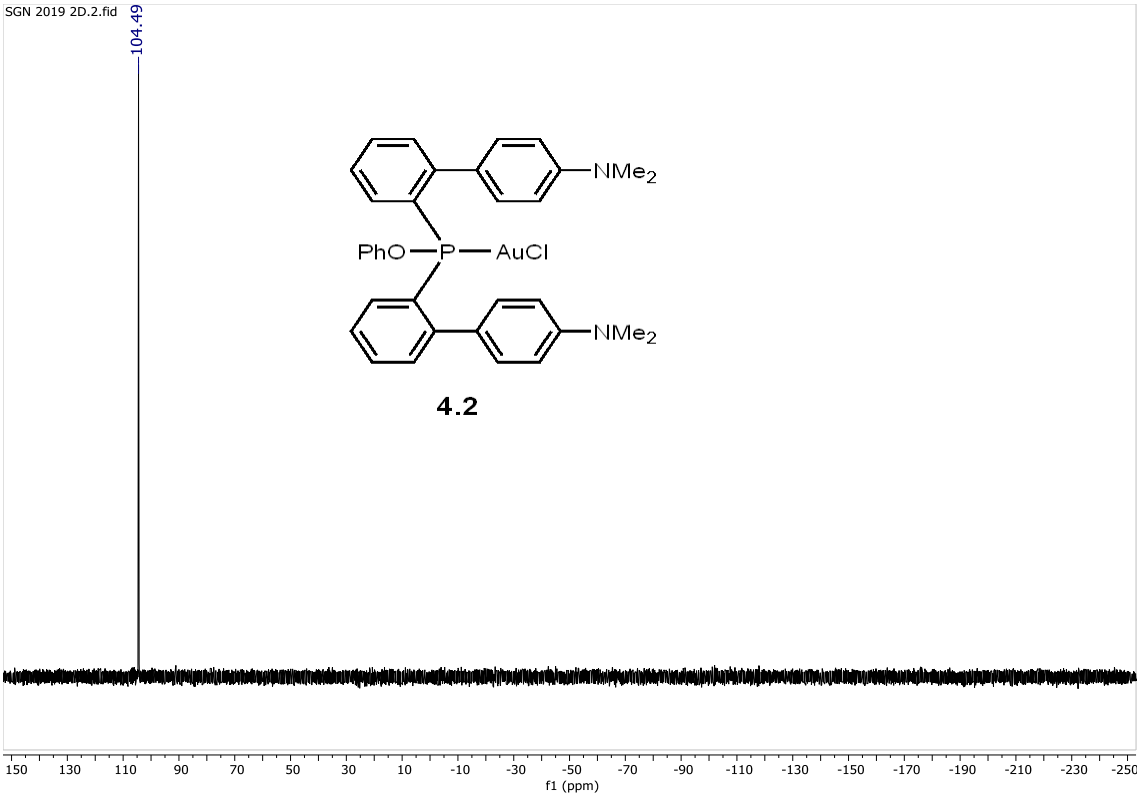

^{31}P{^{1}H} NMR (162 MHz, CD_2Cl_2) δ 104.49.

^{13}C NMR Spectrum of Gold Chloride **4.2**

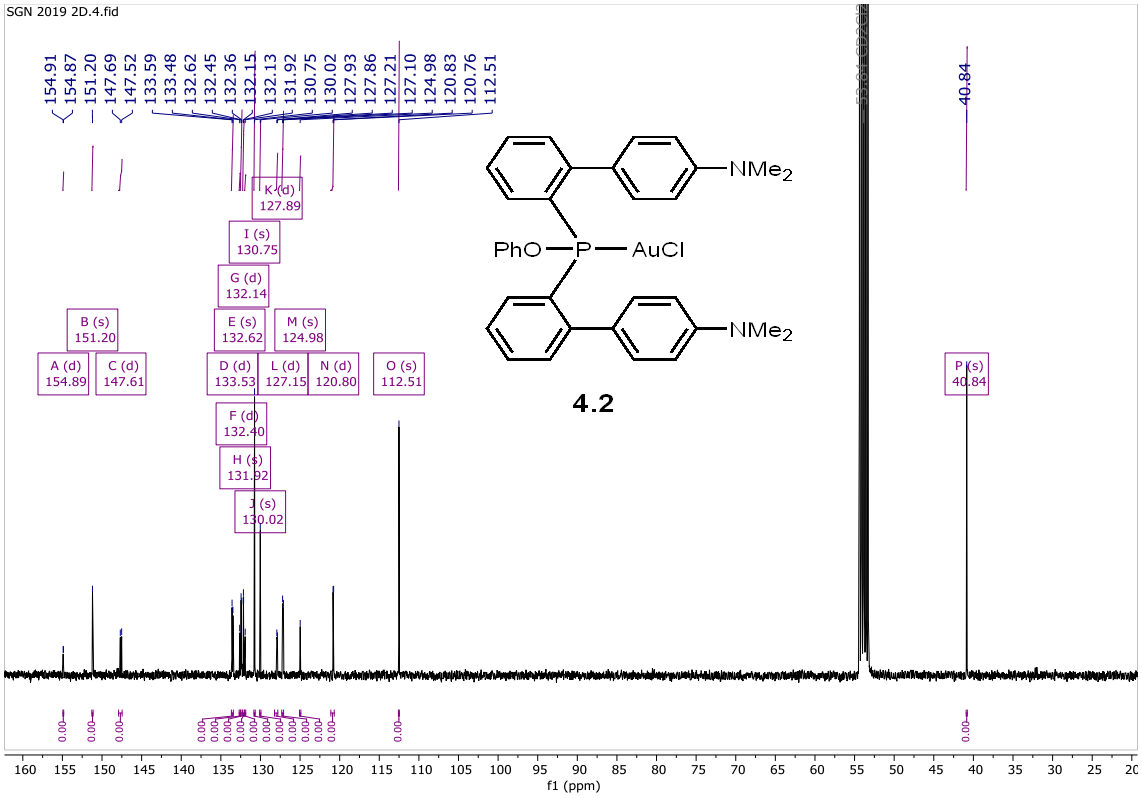

^{13}C{^{1}H} NMR (101 MHz, CD_2Cl_2) δ 154.89 (d, *J* = 4.4 Hz), 151.20, 147.61 (d, *J* = 17.1 Hz), 133.53 (d, *J* = 10.8 Hz), 132.62, 132.40 (d, *J* = 8.6 Hz), 132.14 (d, *J* = 2.2 Hz), 131.92, 130.75, 130.02, 127.89 (d, *J* = 7.1 Hz), 127.15 (d, *J* = 10.3 Hz), 124.98, 120.80 (d, *J* = 7.6 Hz), 112.51, 40.84.

^{1}H Spectrum of Ligand **4.7**

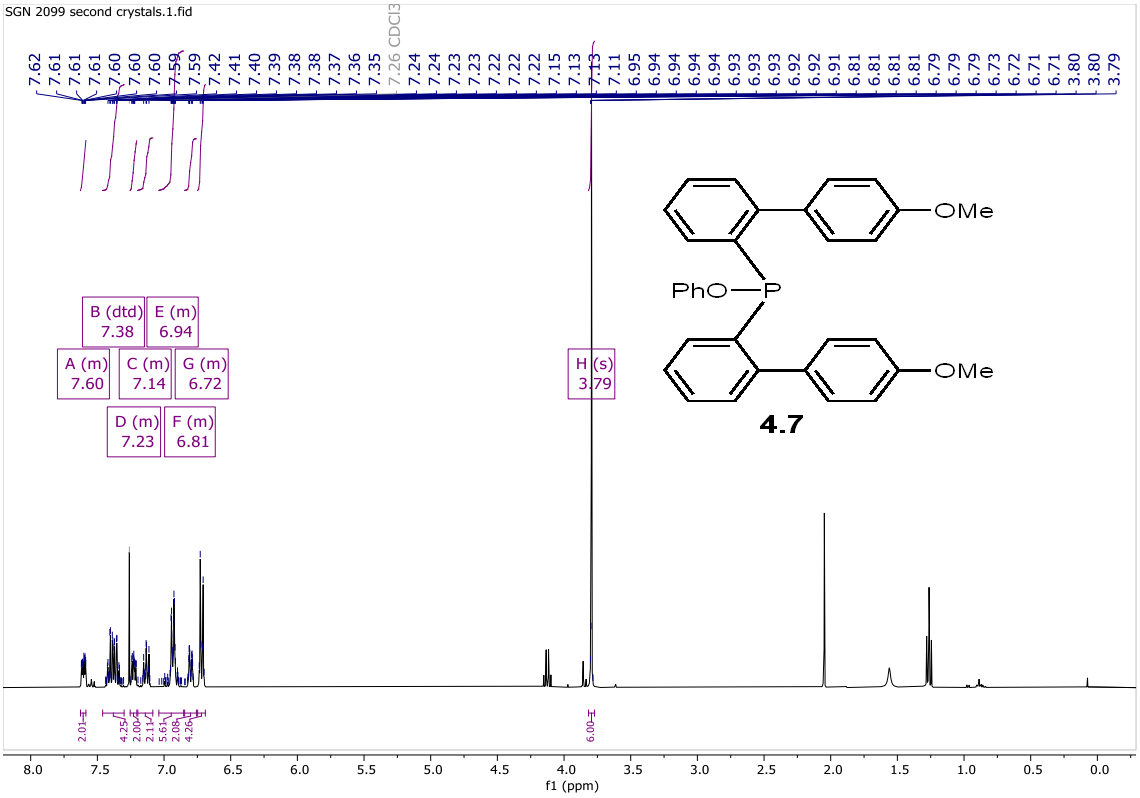

^{1}H NMR (400 MHz, $CDCl_3$) δ 7.63 – 7.59 (m, 2H), 7.38 (dtd, *J* = 19.6, 7.4, 1.6 Hz, 4H), 7.25 – 7.20 (m, 2H), 7.20 – 7.08 (m, 2H), 7.04 – 6.85 (m, 6H), 6.85 – 6.76 (m, 2H), 6.75 – 6.69 (m, 4H), 3.79 (s, 6H).

^{31}P NMR Spectrum of Ligand **4.8**

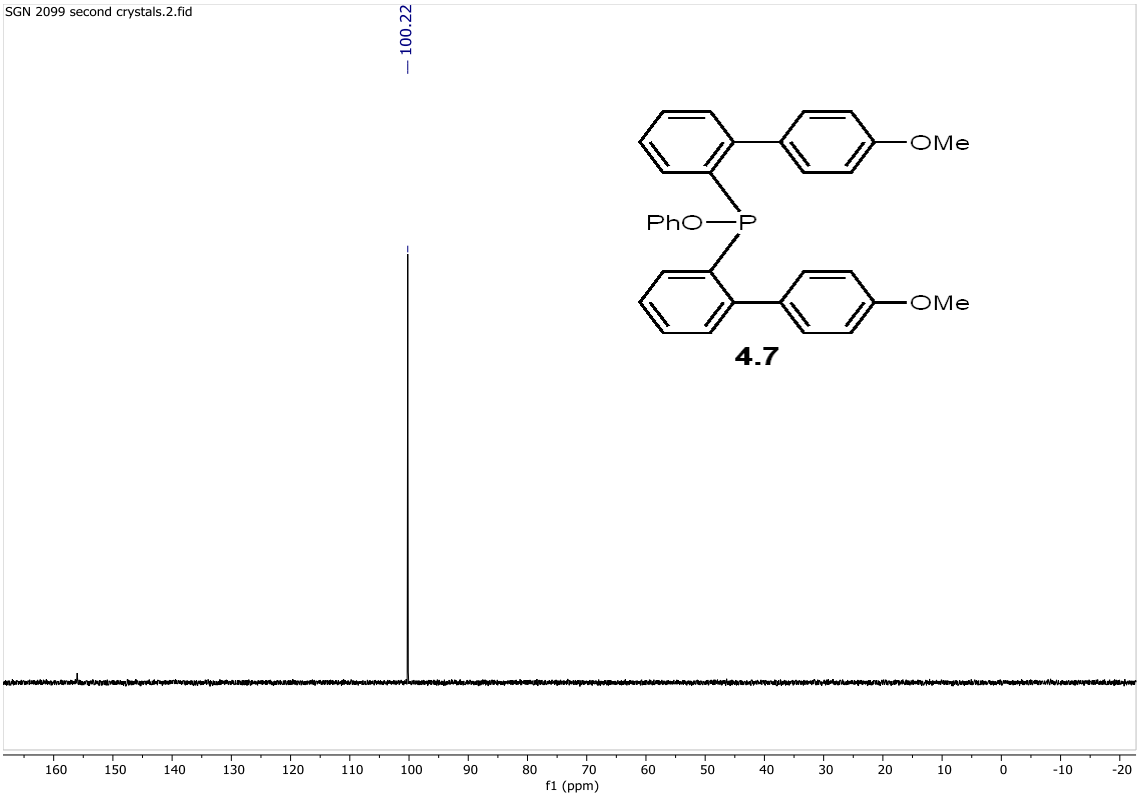

^{31}P{^{1}H} NMR (162 MHz, $CDCl_3$) δ 100.22.

Curriculum Vitae

Skylar Norman

Education

Ph.D in Organic Chemistry| August 2025 | Wake Forest University

- Advisor: Professor Amanda C. Jones
- Committee Members: Professor Bruce King and Professor Ulrich Bierbach
- *Mechanistic and kinetic analysis of Au(I)-catalyzed reactions by NMR spectroscopy*
- *Synthesis and characterization of bisbiphenyl phosphine ligands for gold catalysis*
- *Determination of ligand impact on catalyst stability by synthesis of Au(I) π-complexes*

B.S. in Chemistry | December 2016 | The College of William and Mary

- Advisor: Professor Jonathan R. Scheerer
- *Synthesis of biologically active alkaloid natural products*

Additional Research Experience

Research Technician | Feb 2018-Aug 2019 | Wake Forest School of Medicine

- *Performed synthesis of ^{11}C* and *^{18}F radiotracers for in-vivo PET imaging of both animal and human models*
- *Verified identity of radiolabeled compounds by HPLC, GC, and MS*
- *Developed LC separation methods for radiotracers*
- *Performed cell culture and biodistribution assays*

Post-Baccalaureate Researcher | Jan 2017-May 2017 | Scheerer Lab, William and Mary

- *Performed early exploration of synthetic routes to a pyrrolodiketopiperazine core*

Publications

Norman, S. G., Jiao, L., Yi, J. Ding, W., Jones. A. C., Solvent-Dependent Change in the Rate-Determining Step of Au(I) Catalyzed N-Propargyl Benzamide Cyclization, *Accepted Submission to J. Org. Chem.*, **2025**. DOI: 10.1021/acs.joc.5c00787

Griebel, C., Hodges D. D., Yager, B. R., Liu, F. L., Zhou, W., Makaravage, K. J., Zhu, Y., **Norman, S. G.**, Lan, R., Day, C. S., Jones. A. C., Bisbiphenyl Phosphines: Structure and Synthesis of Gold(I) Alkene π-Complexes with Variable Phosphine Donicity and Enhanced Stability, *Organometallics.*, **2020**, 39, 2665-2671.

Dileep Kumar J. S., Prabhakaran J., Damuka N., Hines J. W., **Norman S. G**., Dodda M., John Mann J., Mintz A., Sai K. K. S. In vivo comparison of N-^{11}CH3 vs O-^{11}CH3 radiolabeled microtubule targeted PET ligands, *Bioorg . Med. Chem. Lett*. **2020,** 30, 2, 126785.

Solingapuram Sai K. K., Bashetti N., Chen X., **Norman S. G.**, Hines J. W., Meka O., Kumar J. V. S., Devanathan S., Deep G., Furdui C. M., Mintz A., Initial biological evaluations of ^{18}F-KS1, a novel ascorbate derivative to image oxidative stress in cancer. *EJNMMI Res.* **2019**, 1, 9, 43.

Kelley, E. W., **Norman, S. G.**, Scheerer, J.R. Synthesis of monoalkylidene diketopiperazines and application to the synthesis of barettin, *Org. Biomol. Chem.*, **2017**, *15*, 8634-8640.

Posters and Presentations

Norman, S. G. Skeletal Editing through Single Atom Changes. *Summer Synthesis Series*, Wake Forest University, July 11, **2024**. (Oral Presentation)

Norman, S. G.; Jones, A. C., Solvent Dependency on the Rate-Determining Step of Gold-Catalyzed N-Propargyl Benzamide Cyclization. Poster presented at the Division of Organic Chemistry Graduate Research Symposium, Bozeman, MT, July 20-23, **2023**.

Kelley, E. W.; **Norman, S. G.**; Scheerer, J. R. Synthesis of monoalkylidene diketopiperazines and application to the synthesis of barettin. Poster presented at the William and Mary Undergraduate Research Symposium, Williamsburg, VA, February 17, **2017**.

Academic and Professional Honors

2023 Wake Forest University Department of Chemistry Outstanding Teaching Assistant

2020 Wake Forest University Department of Chemistry Outstanding First-Year Graduate Student

2017 Alfred R. Armstrong Outstanding Teaching Assistant, William and Mary

2013 Smithfield Little Theatre Performing Arts and Education Scholarship

Teaching Experience

Various Substitute Lecturer, Wake Forest University

- *Served as substitute lecturer for first semester organic and first semester general chemistry lecture courses*
- *Gave lectures introducing Lewis structures (General Chemistry) and NMR Spectroscopy (Organic)*

2020-2025 Undergraduate Research Mentor, Wake Forest University

- *Mentored eight undergraduates on laboratory techniques, ligand synthesis, structure elucidation by NMR, and mechanistic kinetic experiments of Au(I) catalysts*

2019-2025 Laboratory Teaching Assistant, Wake Forest University

- *Supervised organic and general chemistry laboratory courses*
- *Assisted students individually and in small groups via office hours*
- *Graded practical and written exams*

2022-2025 Chemistry Center Teaching Assistant, Wake Forest University

- *Held recitation-style practice sessions for first and second semester organic students*
- *Guided students through newly-learned material from lecture by way of practice problems*
- *Wrote practice exams and held mock exam sessions for students ahead of in-class exams*

2015-2016 Laboratory Teaching Assistant, College of William and Mary

- *Supervised first and second semester organic chemistry courses*
- *Oversaw and graded sections of 22 students*